Radium, radon and inert gases in groundwaters and rocks as geochemical tracers.

Lee, D. J.

Award date:
1980

Awarding institution:
University of Bath

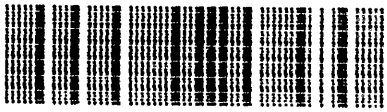

X

Author ....D.J. LEE.....(PhD thesis).... Date .1980...

Title Radium, Radon and Inert Gases in Groundwaters

and Hocks as Geochemical Tracers.

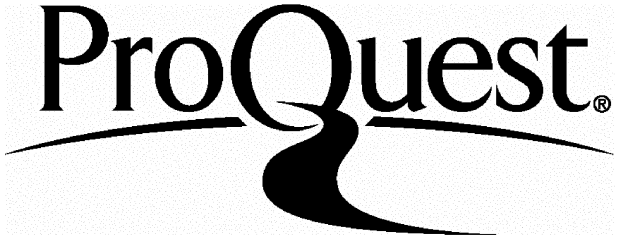

Declaration

I D. J. Lee hereby declare that the contents of this thesis are substantially my own unaided work and I am the joint author of the published papers included in Appendix 5.
The work was carried out whilst I was registered as a candidate for the Degree of Doctor of Philosophy at the University of Bath.

D. J. LEE

ABSTRACT

Natural radioelements and inert gases in solution in groundwaters have been applied to problems of groundwater flow and age measurement. The ^{4}He content of groundwaters generally increases with age and in the Bunter Sandstone, Nottinghamshire, the ^{4}He contents of groundwaters have been linearly related to ^{14}C ages. In the Lincolnshire Limestone, the ^{4}He contents of the groundwaters have been used to indicate mixing of recharge water and interstitial water. In the other study areas, ^{4}He and ^{40}Ar in groundwaters have been used as qualitative indicators of age. The ^{4}He contents of core samples have been related to the ^{4}He contents of the interstitial water and the formation depth. ^{4}He diffusion in confined and non-confined sedimentary structures has been discussed.

The amounts of non-radiogenic inert gases dissolved in groundwaters have been used to estimate groundwater recharge temperatures. In the Bunter Sandstone, these have been related to palaeoclimatic history by calibrating with the ^{14}C ages. Estimated recharge temperatures have also been related to seasonal recharge, changes in the altitude of recharge and to variations in the hydrogen and oxygen isotopic ratios.

Variation of the ^{222}Rn contents of groundwaters has been used as an indicator of aquifer variability. The relative importance of intergranular and fissure flow and the variation in efficiency of ^{222}Rn release into groundwaters has been investigated. The fraction of ^{222}Rn released from rocks has been determined and the mechanisms by which ^{222}Rn is released from

sandstone, limestone and granite rock fragments has been discussed. Variability of the ^{226}Ra contents of groundwaters has been explained in terms of the relative importance of the recoil and etch mechanisms of solution and the solubility of ^{226}Ra salts in groundwaters.

TABLE OF CONTENTS

APPENDIX 3. Mass spectrometry

3.1. Schematic arrangement of the MS10 mass spectrometer

3.2. Variation of positive ion current with electron voltage illustrating the difference in ionization potential of $^{40}Ar^{2+}$ and $^{20}Ne^{+}$

3.3. Variation in sensitivity (μAmp/torr) with trap current for the inert gases.

APPENDIX 4. The solubility of the inert gases as a function of temperature

4.1. Variation of the fresh water solubility of He with temperature at atmospheric partial pressure (5.2×10^{-6} atm.)

4.2. Variation of the fresh water solubility of Ne with temperature at atmospheric partial pressure (1.81×10^{-5} atm.)

4.3. Variation of the fresh water solubility of Ar with temperature at atmospheric partial pressure (9.56×10^{-3} atm.)

4.4. Variation of the fresh water solubility of Kr with temperature at atmospheric partial pressure (1.14×10^{-6} atm.)

4.5. Variation of the fresh water solubility of Xe with temperature at atmospheric partial pressure (8.06×10^{-8} atm.)

4.6. Variation of the fresh water solubility of radon with temperature at one atmosphere partial pressure.

APPENDIX 5. Publications

LIST OF FIGURES

CHAPTER 3.

CHAPTER 4.

CHAPTER 5.

LIST OF TABLES

CHAPTER 3.

CHAPTER 4.

CHAPTER 8.

CHAPTER 9.

CHAPTER 10.

CHAPTER 1

INTRODUCTION

1.1 THE NATURE OF RADIOACTIVITY

1.1.1. Introduction

Atoms consist of a small positively charged nucleus, containing nearly the entire mass of the atom, surrounded by a distribution of negatively charged electrons. The nucleus consists of positively charged particles, protons, and neutral particles, neutrons, which are of nearly equal mass. They are bound together by nuclear forces to form a nucleus with a diameter of the order of 10^{-12}cm. Electrons are bound to the nucleus by the electrostatic attraction of their negative charge to the positive charge of the nucleus, which results in an atomic diameter in the order 10^{-8}cm

The integral number of protons in the nucleus is termed the atomic number, Z, and the total number of nucleons (protons and neutrons) is termed the mass number, A. The mass of nuclear particles is expressed as "atomic mass units" (a.m.u.) and both the neutron and proton have a mass of approximately 1 a.m.u., whereas the mass of an electron or a beta particle is only $^1/_{1850}$ the mass of a proton. Nuclei with the same atomic number Z, but different atomic mass A, are different forms of the same element and are called isotopes.

1.1.2. Nuclear reactions

A nuclear reaction is a process in which a nucleus reacts with another nucleus, an elementary particle, or a photon to produce, in a time of the order of 10^{-12} seconds or less, one or more other nuclei (and possibly other particles). Such a reaction is usually written:

Target (projectile, product) residual

Nuclear reactions, like chemical reactions are always accompanied by release or absorption of energy, but a very important difference exists. In treating chemical reactions, macroscopic amounts of material undergoing reaction are considered, and, consequently, heats of reaction are usually expressed per mole of reactants. In the case of nuclear reactions, however, the energy involved is many orders of magnitude larger than that in any chemical reaction and the heats of reaction are given per nucleus transformed. For example, the reaction $^{14}N(\alpha,p)^{17}O$ releases 1.91×10^{-13} Joules. It is conventional in nuclear physics to express energy in the form of electron volts (ev), millions of electron volts (Mev) and billions (10^9) of electron volts (Bev), where an electron volt is the kinetic energy acquired by an electron falling through a potential difference of one volt and is equal to 1.602×10^{-19} Joules. Thus the energy released in the above reaction is 1.19 Mev, which compares with natural alpha-particle energies of several Mev, beta-particle energies from fractions of an ev to several Mev and natural gamma-ray energies of the order of 1 Mev. Energies of cosmic rays are of the order of Bev.

Typical chemical reactions have energies of the order of a few ev per molecule. For example, the combustion of graphite yields 393 kJ mol^{-1}.

$$C(\text{graphite}) + O_2(g) \longrightarrow CO_2(g) + 393 \text{ kJ mol}^{-1}$$

This is equivalent to an energy release of 4.1 eV/molecule. The solution of hydrogen chloride gas may be expressed as:

$$HCl(g) + H_2O \longrightarrow HCl(aq) + 75 \text{ kJ mol}^{-1}$$

This heat of reaction is equivalent to 0.78 eV/molecule.

1.1.3. Radioactive decay

Radioactive decay processes are spontaneous nuclear reactions which are characterised by the radiation emitted. They occur at random, and the exact time at which a given atom will decay cannot be predicted. However, in a large number of radioactive atoms, a certain fraction will decay in a given time. The fraction of the number of atoms transformed per unit time is called the decay constant, λ. The total number of radioactive decays per unit time depends on the fraction of atoms decaying, λ, and the total number of radioactive nuclei present, N, and is given by the product λN. The rate of change of N as a function of time, dN/dt, is therefore

given by

$$\frac{dN}{dt} = -\lambda N$$

This integrates to

$$N = No\, e^{-\lambda t} \qquad (1.1)$$

Where No is the number of radioactive nuclei present at a time $t = o$.

1.1.3. Radioactive decay.

Radioactive decay rates are commonly expressed in terms of the half-life, $t_{\frac{1}{2}}$, which is the time taken for one-half of a given amount of radioactive nuclide to decay. From equation (1.1), the half life is given by:

$$t_{\frac{1}{2}} = {}^{\ln 2}/_{\lambda}$$

Equation (1.1) may be solved for t if N, No and λ are known. It is the fundamental equation for nuclear age determination.

The most commonly used unit of radioactivity is the curie which is defined as the quantity of any radioactive nuclide in which the number of disintegrations per second is 3.70×10^{10}. Thus a curie of ^{226}Ra is approximately 1 g; a curie of ^{222}Rn is 0.66 mm^3 at standard temperature and pressure; and a curie of ^{238}U is about 3000 Kg. Because the levels of radioactivity found naturally are very much less than a curie, it is convenient to quote natural radiation in fractions of a curie. Thus a micro-curie, μCi, is 10^{-6}Ci; a nano-curie, nCi, is 10^{-9}Ci; and a pico-curie, pCi, is 10^{-12}Ci. The fundamental unit of radioactivity

is the becquerel. It is the S.I. unit of radioactivity and it is defined as the quantity of any radioactive nuclide in which the number of disintegrations per second is one.

1.1.4. Radioactive decay processes

α-decay

Almost all natural α-emitters are found among the heavy elements in the decay series of ^{238}U, ^{235}U and ^{232}Th. (appendix 1). The emission of an α-particle results in a reduction of 4 atomic mass units ($\Delta A = -4$) and two nuclear charge units ($\Delta Z = -2$). The energy of an α-particle is always discrete and isotopes can be identified by the characteristic energy of their α-particles.

The α-particle is a helium atom stripped of electrons, $^{4}He^{2+}$, travelling at a high velocity. When it is projected into matter, it collides with electrons, slows down to a point where it can capture them to form a helium atom, then is rapidly stopped. In air, for example, the range of α-particles is several centimetres, whereas in ordinary solids, the path length is a few tens of microns.

When a radionuclide decays by emission of an α-particle, it releases energy not only in the form of kinetic energy of the α-particle, but also as recoil energy of the product nucleus. Recoil energy can be calculated from the law of conservation of momentum and amounts to about 2% of the total energy released in α-decay. Although this energy represents only a small fraction of the nuclear energy released, its magnitude is amply sufficient to produce chemical and other effects.

The energy of the recoil nucleus is given by

$$E = P^2/_{2M}$$

Where E = recoil energy

M = mass of the recoil nucleus

For pure α-decay, $P = \sqrt{2E_\alpha M_\alpha}$

Therefore $E = \frac{E_\alpha M_\alpha}{M}$

Where E_α and M_α are the energy and mass, respectively, of the α-particle

α-Recoil is an important process in the hydrogeochemistry of uranium, radium and radon. When ^{238}U decays by α-emission, the product nucleus ^{234}Th may be energetically ejected into solution. ^{226}Ra, the product nucleus of the α-decay of ^{230}Th, and ^{222}Rn, the product nucleus of the α-decay ^{226}Ra, may be similarly recoiled into solution. The energy relationships of these nuclear reactions are given in Table 1.1

Table 1.1 Recoil- and α-energies in some hydrogeochemically important nuclear reactions.

Reaction	α-energy, E_α MeV	recoil mass, M a.m.u.	recoil energy, E MeV	%E of total energy released
$^{238}U \longrightarrow {}^{234}Th + \alpha$	4.2 (100%)	234	0.072	1.7%
$^{230}Th \longrightarrow {}^{226}Ra + \alpha$	4.615 (24%) 4.682 (76%)	226	0.082 (24%) 0.083 (76%)	1.7%
$^{226}Ra \longrightarrow {}^{222}Rn + \alpha$	4.589 (5.7%) 4.777 (94.3%)	222	0.083 (5.7%) 0.086(94.3%)	1.7%

β-decay

Any radioactive decay process in which the mass number of the nucleus remains unchanged, but the atomic number changes, is classed as beta-decay. The only type of beta-decay occurring among the natural radioactive series is called negatron (β^-) decay. This may be considered as a process by which a neutron is converted to a proton plus an electron resulting in an increase of the atomic number by one unit ($\Delta Z = +1$), for example:

$$^{234}_{90}Th \longrightarrow {}^{234}_{91}Pa + \beta^-$$

Positron (β^+) decay arises from the transformation of a proton to a neutron and is accompanied by a decrease in the atomic number of one unit ($\Delta Z = -1$). Alternatively, a nucleus may accomplish a decrease in Z of one unit with A remaining constant by capturing an orbital electron. As the K-electrons in an atom are, on average, closest to the nucleus, the capture probability is greatest for a K-electron. An example of K-capture is given by the decay of ^{40}K to ^{40}Ar (Figure 1.1).

When a radioactive nucleus decays by β-decay, a β-particle is emitted, together with a neutrino which allows for energy and angular momentum to be conserved. Because β-decay involves three particles (nucleus, β and neutrino), the β-particles are emitted with a continuous energy distribution extending from zero up to a maximum value.

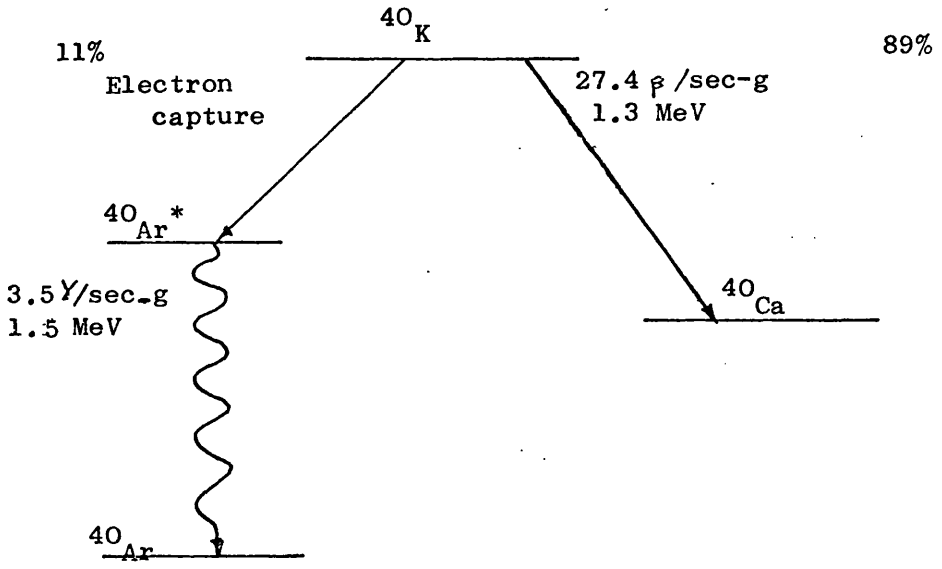

Figure 1.1. The decay scheme of ^{40}K

γ-transitions

Decay by α- or β-emission frequently leaves the product nucleus in an excited energetic state. A nucleus in an excited state may give up its excitation energy and return to the ground state in a variety of ways. The most common transition is by the emission of electromagnetic radiation. Such radiation is called γ-radiation and is emitted with a frequency which is determined by the energy transition involved. Gamma-ray emission may be accompanied, or even replaced, by the emission of internal conversion electrons. Thirdly, a nucleus may be de-excited by the formation of an electron-positron pair, provided that the energy available exceeds 1.02 Mev (equivalent to the rest mass of two electrons). The three processes described are known as gamma-transitions, although only in the first is the gamma-ray emitted by the nucleus. All are characterised by a change in energy without change in Z and A.

1.1.5. Radioactive Series

Some radionuclides decay to daughter nuclides which are also radioactive. The newly formed radioactive nuclei may themselves decay into other radioactive nuclei. This mechanism is known as series decay. Series decay is important in geochemistry as there are three naturally occurring decay series, ^{238}U, ^{235}U and ^{232}Th. (appendix 1). A series is said to be in radioactive equilibrium when for each decaying parent atom, one of each intermediate daughter atoms also decays (on the average). At equilibrium, the number of atoms of each intermediate daughter will be directly proportional to its half-life. The concentration of the ultimate stable daughter will continue to increase at a decreasing rate.

Natural decay series are usually old enough for radioactive equilibrium to have been established, but instances where the series are not in equilibrium are common. Disequilibrium is generally caused by the chemical fractionation of parent from daughter because of their different chemical properties. The nature and degree of disequilibrium may offer an indication of geochemical history.

1.1.6. The determination of geological age.

The use of radioactive decay as a basis of time determination relies on three basic assumptions.

(1) that a parent element decays at a known, constant rate into a daughter element, either directly or in a radioactive series,

(2) that the system is closed with respect to the radioactive species involved during the decay process, and

(3) that at the time at which the rock or mineral is formed, it must either be free of the ultimate daughter isotope or contain this isotope in a known ratio with other isotopes so that the original content of the decay product can be determined.

Geological age may be estimated by determining the amount a naturally occurring radionuclide has decayed either by measuring the amount of that nuclide remaining or the amount of daughter product that has accumulated.

Considering the case where the initial and final concentrations of the parent are determined. Let the number of parent atoms present at equilibrium be P_s. Let this nuclide be removed from the system in which it is in equilibrium. The nuclide will decay according to its decay constant, λ. The amount of the nuclide remaining is a function of elapsed time, t, and is given by:-

$$P(t) = P_s e^{-\lambda t} \qquad (1.2)$$

solving for t, gives $t = {}^{1}/_{\lambda} \ln {}^{P_s}/_{P}$ (1.3)

where P is the amount to which P_s has decayed. The mathematical limitations of this method are that if P is small compared with P_s, the error in determining P will become large. The maximum range is ten half-lives of the parent, by which time its activity has decayed to 0.1% of the original activity. Examples of the method are ^{14}C and ^{3}H dating.

For the case where measurement of the accumulation of a daughter product is made:-

The number of daughter atoms, D, present at time t is given by

$$D = P_o - P_t$$

where P_o and P_t are the numbers of atoms of parent present at t = o and t = t.

If, however, there were D_o atoms of daughter present initially in the system, then

$$D^* = D_{total} - D_o$$

where D^* = number of radiogenic daughter atoms

D_{total} = total number of daughter atoms present.

D^* is given by $D^* = P_o - P$

$$= P(e^{\lambda t} - 1) \qquad (1.4)$$

Solving for elapsed time,

$$t = {}^{1}/_{\lambda} \ln({}^{D^*}/_{P} + 1) \qquad (1.5)$$

If t is small compared with ${}^{1}/_{\lambda}$, then D^* is small compared with P and equation 1.5 approximates to:-

$$t \simeq \frac{D^*}{P}$$

Only ^{40}K, ^{87}Rb, ^{238}U, ^{235}U and ^{232}Th have been useful in geological age determination by this method.

The problems generally associated with absolute age determination of geological materials result from a breakdown of one or more of the basic assumptions. The validity of a final age determination must bear in mind the degree to which these assumptions hold. In many circumstances it is possible to date geological materials by more than one nuclear method. Often, the ages determined are discordant. An understanding of the reasons

for calculated ages disagreeing may lead to a better understanding of the geological processes involved and may ultimately lead to an absolute age. There are many factors which cause disagreement between measured geological ages. For example, gaseous decay products may diffuse out of the system being investigated and result in an artificially low production rate of the daughter isotope. This is a particularly important consideration in the $^{238}U/^{206}Pb$ method for geological age determination, where the radioactive daughter ^{222}Rn is gaseous; and in the $^{40}K/^{40}Ar$ method, where ^{40}Ar may diffuse away from its site of production. Renewed hydrothermal activity may lead to redistribution of the elements involved in a geological age determination and may be a serious source of error, particularly in the uranium/lead methods where uranium will be removed much more readily than lead. There may also be an unknown amount of daughter isotope present in the system when it was formed. This is particularly important in the Rb/Sr age method, but the contribution of the original daughter content may be determined, by an independent method to yield a true age.

1.2. THE GEOCHEMISTRY OF URANIUM AND THORIUM

The geochemical importance of uranium and thorium arises from their radioactivity and widespread distribution in the lithosphere. Uranium also occurs widely distributed in the hydrosphere because of its ability to form soluble complexes, unlike thorium which is readily hydrolysed in aqueous solution. Uranium occurs naturally as ^{238}U, ^{235}U and ^{234}U, ^{238}U being the most abundant isotope (99.27%) with a half-life of 4.5×10^9 years. ^{238}U decays by a series of α- and β-emissions to ^{206}Pb, producing, as it does so, several other radioactive daughters with shorter half-lives which are of geochemical importance: ^{234}U, ^{226}Ra, ^{222}Rn, ^{210}Pb. The radioactive decay schemes for ^{238}U and ^{235}U are given in appendix 1. ^{235}U and ^{234}U occur to the extent of 0.72% and 0.06% respectively in nature. The half-lives are 7.1×10^8 years and 2.4×10^5 years respectively. Thorium occurs naturally as ^{232}Th with a half-life of 1.41×10^{10} years. The decay scheme for ^{232}Th is given in appendix 1.3.

The geochemistry of thorium and uranium is characterised by their crystallochemical relationships to several elements with similar ionic radii (Table 1.2). Because of the similarity in size of their tetravalent ions uranium and thorium tend to accompany one another in nature.

Table 1.2. Ionic radii of selected ions

Ion	Radius, Å
Th^{4+}	1.10 [1]
Ca^{2+}	1.06 [1]
Ce^{3+}	1.18 [1]
Gd^{3+} to Lu^{3+}	1.11 - 0.99 [1]
U^{4+}	1.05 [1]
Ce^{4+}	1.02 [1]
Zr^{4+}	0.87 [2]
Y^{3+}	1.06 [1]

1.2.1. The Uranium and thorium content of igneous rocks

Thorium is strongly concentrated in acidic rocks (Table 1.3) during magmatic differentiation, resembling zirconium, yttrium, lanthanides and uranium, but differing from titanium.

Concentration of thorium continues during the pegmatitic stage after the close of crystallization because of its high valency and the fact that the Th^{4+} ion resembles the Ca^{2+} ion. There are only two independent thorium minerals into which thorium can crystallize, thorianite, $(Th, U)O_2$ and thorite, $Th[SiO_4]$. The latter is isomeric with zircon, $Zr[SiO_4]$ and thorium tends to be incorporated in zircon, because of the similarity in ionic sizes of thorium(IV) and zirconium(IV) (Table 1.2). Thorium is also concentrated in minerals of rare earths with similar ionic sizes, monazite and xenotime, and in cerium earth minerals (syenite, nepheline, syenite and pegmatites).

Like thorium, uranium forms mainly oxygen compounds and does not form sulphides, arsenides, tellurides, etc. in nature. It is strongly concentrated in the upper lithosphere, and becomes relatively enriched to thorium in acidic igneous rocks. During magmatic differentiation, uranium is often concentrated in granite and syenite pegmatites in which it may form a number of independent minerals. The U^{4+} ion, like Th^{4+} resembles Ca^{2+} in coordination, and it becomes enriched in residual

Table 1.3. Uranium and thorium contents of igneous rocks.

Rock type	U, ppm	Th, ppm
Basalt [3]	0.83	5.0
Diabase [3]	0.83	2.0
Granite [4]	3.96	13.45
Basic igneous rocks [3]	0.96	3.9
Intermediate igneous rocks [4]	2.61	9.97

Contents in parts per million (ppm)

solutions. However, the ionic radii of U^{4+} and Th^{4+} are too great to allow the admission of significant amounts of uranium into the common rock forming minerals.

Crystallization at high temperatures produces predominantly UO_2 minerals, which may be assumed to be of primary origin. The oxidation product, UO_3, is produced in all low temperature mineral assemblages [5]. The uranium rich minerals are formed during the late stages of deposition, the early crystallizing minerals, such as niobates and tantalates, in pegmatites, containing little uranium.

Pneumatolytic and hydrothermal stages concentrate uranium in the high temperature fractions in association with tin veins containing sulphides and sulpho salts of cobalt, nickel, bismuth and arsenic. Hydrothermal sulphide and arsenide veins containing cobalt, nickel, silver and bismuth minerals and formed at low temperatures and similar veins devoid of cobalt and nickel are also uraniferous. Uranium also accompanies zirconium and thorium in zircon, thorium and the rare earths in thorite, thorianite, monazite, xenotime and allanite, and titanium, niobium and tantalum in niobates and tantalates.

The most common chemical form of uranium in nature is UO_2 in the minerals pitchblende and uraninite. Uraninite is the richest uranium mineral (75 - 90% UO_2/UO_3) and associates with

pegmatites. Pitchblende associates with the hydrothermal sulphides and arsenides. Alteration of uraninite results in formation of hydroxides, phosphates, arsenates, vanadates, uranates, carbonates, silicates and sulphates of variable and complicated composition. These minerals are particularly numerous in hydrothermal veins in igneous and sedimentary rocks, and are frequently found in weathered parts of uraniferous ore bodies, e.g. becquerelite, $2UO_3\ 3H_2O$. Uranium as uranyl silicate or phosphate may also be incorporated in late hydrothermal minerals, e.g. in fluorite and opal.[6]

1.2.2. Uranium and thorium in sedimentary rocks

The uranium and thorium content of sedimentary rocks is generally lower than that of the igneous rocks from which they must ultimately have been derived. This is demonstrated for uranium in Table 1.4. Weathering of igneous, metamorphic (and sedimentary) rocks releases uranium which is later deposited syngenetically (and sometimes epigenetically) in many kinds of sediments. Pitchblende and uraninite in particular are easily altered to hydrated oxides, phosphates and silicates, and some uranium is leached, probably as soluble uranyl complexes.[8] Some uranium and thorium bearing minerals are not readily altered in place. Monazite, euxenite and samarskite, for example, are reduced by attrition during transportation with clastic sediments. Zircon is highly resistent to mechanical alteration and tends to accumulate in placers and the heavy

Table 1.4. Average uranium contents of various rocks [7]

Rock type	uranium content, ppm
Acid igneous	3.0
Intermediate igneous	1.5
Basic igneous	0.6
Ultrabasic igneous	0.03
Meteorites	0.003
Phosphate rock (Fla.)	120
Phosphate rock (N.Africa)	20-30
Bituminous shale (Tenn.)	50-80
Normal granite	4
Limestones	1.3
Other sedimentary rocks	1.2

mineral fraction of clastic sediments.[8] Most secondary minerals are readily susceptible to alteration and leaching and are quickly reduced during transportation.

Larson and Phair[9] identified regions in freshly formed igneous rocks from which up to 40% of the radioactivity may be leached.

(1) in metamict phases of primary silicates
(2) as interstitial material derived from late magmatic, deuteric or hydrothermal solutions,
(3) in certain non-metamict, partly soluble radioactive accessories, such as apatite, and
(4) as adsorbed ions in dessiminated weathering products such as iron oxide.

The uranium in solution may be redeposited or carried to the oceans. It is removed from solution by precipitation, adsorption and isomorphous substitution for Ca^{2+} (and possibly other elements). Usually, precipitation occurs in reducing environments, and uranium is deposited as uraninite. However, precipitation may occur in oxidising environments, when complex compounds such as torbernite-, autunite- and carnotite-type minerals are deposited. Adsorption occurs on the hydroxylate gel precipitates of iron, aluminium and manganese and on silica gel. Uranium may also be adsorbed by some clay minerals and by some organic compounds, for example, carbonaceous shales have greater uranium contents than other sedimentary rocks and most granites.

The presence of oxide and carbonate species in waters tends to preserve uranium in solution.

Thorium bearing minerals are resistent to weathering and tend to become concentrated in placers and in the heavy mineral resistate fraction of clastic sediments. Thorium, like uranium, is highly insoluble, but there is an important difference between them. Uranium, as the uranyl ion, is able to form complex compounds which are generally soluble. Some thorium is dissolved during the weathering of rocks, but it is easily hydrolysed in an oxidising environment, therefore much of it is deposited with hydrolyzate sediments, thus effecting separation of uranium and thorium. The remaining thorium in solution is carried into the oceans. The thorium content of some sedimentary rock types is given in Table 1.5.

Petroleum associated brines are always rich in uranium. Tomkeieff [5] found 100ppm uranium in water associated with an oil field. Asphaltiferous sandstones and asphaltites are also high in uranium content. The limited number of rich uranium deposits occur in sandstones and bituminous shales containing uranites, especially carnotite, the most important being uraninite and its alteration products found in hydrothermal deposits.

Table 1.5. Thorium content of sedimentary rocks

Rock type	Thorium content, ppm
Rocks of arenaceous origin [10]	5.4
Rocks of argillaceous origin [10]	12
Shales [11]	10.1
Limestones [3]	1.1

1.3. THE GEOCHEMISTRY OF RADIUM.

Radium occurs naturally as the isotopes ^{223}Ra, ^{224}Ra, ^{226}Ra and ^{228}Ra. The geochemical importance of the radium isotopes is largely determined by their half-lives rather than by their abundance. ^{224}Ra and ^{228}Ra are likely to be the most abundant isotopes because they are daughters of ^{232}Th and thorium is more abundant than uranium (appendix 1.3). But ^{226}Ra, a daughter of the ^{238}U decay series (appendix 1.1), is by far the most important isotope in geochemistry, because its half life of 1620 years permits it to be generally in equilibrium with its parent in rocks (Table 1.6). The age of the uranium occurrence and the degree to which the decay products are fractionated by geochemical processes determine the extent to which ^{226}Ra is in equilibrium with its parent ^{238}U [13], but these processes tend to occur on a time scale which is large compared with the time taken for equilibrium to be established (approximately 8000 years).

The chemistry of radium most closely resembles the chemistry of barium, reflecting its position as a member of group IIA of the Periodic Classification of the Elements (Table 1.7). Like uranium it is generally widely dispersed in nature in rocks of average radioactivity. A set of typical uranium, thorium and radium contents for rocks of average radioactivity is given in Table 1.6. Rocks with larger radium contents (above average radioactivity) may be divided into three categories:- [12]

Table 1.6. Average contents of U, Th and Ra in rocks [12]

Rock	U, ppm	Th, ppm	Ra, 10^{-6} ppm
Magmatic			
Acid	9.10	20.5	3.01
Median	6.20	16.4	2.57
Basic	3.20	5.6	1.28
Sedimentary			
Sandstone	4.20	6.00	1.50
Clay	4.50	13.0	1.30
Limestone	2.70	0.50	0.50

Table 1.7. Chemical properties of the group IIA elements

Property		Mg	Ca	Sr	Ba	Ra
Electronegativity [14]		1.56	1.22	1.10	1.02	(1.0)
Ionization potential, eV [15]	$M \longrightarrow M^+ + e$	7.646	6.113	5.695	5.212	5.229
	$M^+ \longrightarrow M^{2+} + e$	15.035	11.871	11.030	10.004	10.147
Ionic radius, Å (crystal radius)	Pauling [16]	0.65	0.99	1.13	1.35	(1.48)
	Stability ratio [17]	0.69	0.97	1.07	1.21	(1.30)
Heat of formation Kcalmol^{-1} [18]	MO	-145.8	-152	-141.2	-133.4	(-130)
	MCl_2	-151.0	-191.0	-197.6	-205.0	(-212)

(a) Increased, but uniformly dispersed ^{226}Ra content, as often found in shales, lignite, sandstone, peat and iron silicate rocks. The increased deposition is due to such processes as adsorption, ion exchange, co-precipitation and reduction.

(b) Ore concentrations of uranium and radium frequently found in hydrothermal zones of tectonic dislocation. Major processes are transport in solution in the presence of high CO_2 content and deposition as CO_2 is lost or by redox reactions especially with iron.

(c) Secondary concentrations of radium which are usually local formations, associated with adsorptive formations of radium in water conducting fissures, and in calcareous tuff and iron-manganese deposits.

During weathering of igneous, metamorphic and sedimentary rocks, equilibrium is often disrupted and radium may become separated from its precursors by geochemical cycles. In the ocean, for example, its concentration is limited by the low concentration of its immediate parent ^{230}Th in sea water. On the other hand, it may be concentrated by biological processes into calcareous shells and algae like Fucus [19].

Quartz sands and limestones often contain less than 0.1pCi g^{-1} of radium [20]. In the resistates, the average radium content is lower than the average for all igneous rocks. The radium content of limestones is lower, but more constant, than the radium content

of sandstones, but limestones containing admixed argillaceous material are higher in radium than are pure limestones.[1]

Like uranium, radium is found in high concentrations in brines associated with oil fields, but the radium content of crude oil is low. The high content of brines is explained by the fact that chloride rich waters readily dissolve radium from the surrounding rocks and oils by producing the highly soluble radium chloride[21]. Mazor[22] found radium contents as high as 1000 $\pm$ 200 pCi l^{-1} in brines associated with oil, gas and petroleum reservoirs.

The hydrochemistry of radium is complex and is neither well understood nor well documented.[23]

The radium content of groundwaters for example, is highly variable. Kenny et al[24] found that the radium content ranged from 0 - 4.7pCi l^{-1} in groundwaters from granitic and adjacent areas in Cornwall, Great Britain. The radium content of hot springs is usually much higher than that of groundwaters from the surrounding area. The radium content of the Bath Thermal Water for example was found to be 12.6 pCi l^{-1} [25] compared with 0.19 pCi l^{-1} in the proximate Carboniferous Limestone ground waters.

1.4. THE GEOCHEMISTRY OF RADON

There are three naturally occurring radioactive isotopes of radon; ^{219}Rn (actinon), ^{220}Rn (thoron) and ^{222}Rn (emanation). All have short half-lives: ^{222}Rn, 3.825 days; ^{219}Rn, 3.92 seconds; ^{220}Rn, 54.5 seconds, and are produced by the decay series of ^{238}U, ^{235}U and ^{232}Th respectively (appendix 1). Because of the relative half-lives, and the time taken for diffusion to occur, the most important isotope geochemically is ^{222}Rn.

The occurrence of ^{222}Rn is entirely dependent on its continual production by ^{226}Ra decay and it cannot accumulate to levels greater than radioactive secular equilibrium. Its presence is therefore determined by the occurrence of radium in subsurface materials and the mechanisms by which it is transferred. The migration of radon may be considered as

(a) the radioactive formation and recoil of a ^{222}Rn ion from ^{226}Ra,

(b) the diffusion of a neutral atom through the interior of a mineral grain, and

(c) the diffusion and transport of the neutral atom through permeable rock and soil. [26]

Relatively impervious radioactive minerals such as zircon lose very little of the radon generated in them, but open lattice structures such as carnotite may lose most of their radon under natural conditions. Migration of radon through permeable rock and soil may be by diffusion as a gas, or by transport in solution of geofluids. The migration of radon and deposition of its solid daughter products along fissures makes detection

of these features possible by their γ-radioactivity, providing that the soil covering is not too thick. If the soil covering is thick, the γ-radiation will not be detected, so radon migration offers an effective method of detecting concealed uranium ore deposits.

The radon content of soil air varies with atmospheric pressure, wind and moisture content of the soil. Frozen, snow covered soil, accumulates radon [27, 28] as do unventilated mines, including some with no visible uranium mineralisation. Radon is also a common occurrence in natural gases, and these have been studied in some detail [29, 30] in attempts to identify the source of high helium contents in some natural gases.

Because of its gaseous nature, and subsequent ease of transport by diffusion, an important aspect of the geochemistry of radon is its behaviour in the atmosphere. The average concentration in air is 10-30 x 10^{-14} Ci l^{-1} [31], but it varies considerably (Table 1.8). The daughter products of ^{222}Rn and ^{220}Rn are positively charged ions resulting from α-recoil and tend to attach themselves to the inert dusts that are normally present in the atmosphere. If the parent gases coexist with the dust in the same air mass for a sufficient period of time, radioactive equilibrium will be achieved. For ^{222}Rn, equilibrium will be established in about two hours, (neglecting the contribution to equilibrium of ^{210}Pb because of its long, 22 year, half-life).

Table 1.8. Geographical distribution of atmospheric radioactivity during 1957.[32]

Location	Activity, 10^{-14} Ci l^{-1}	
	^{222}Rn	^{220}Rn
Washington, D.C.	17.2	0.23
Yokosuka, Japan	5.4	0.048
Wales, Alaska	1.7	0.014
Kodiak, Alaska	0.7	0.0042
Little America, Antarctica	0.1	< 0.001

1.5. THE GEOCHEMISTRY OF THE INERT GASES

The inert gases appear to be normally abundant cosmically but rare terrestrially, because their chemical inertness did not allow them to be captured and retained in cosmic proportions during the formation of the earth's atmosphere. The inert gas content of the atmosphere is given in Table 1.9. Hollander et al [34] attributed the present composition of the terrestrial inert gases to several sources: the primeval gas captured and retained by the earth at the time of its formation, atoms formed subsequently by radioactive decay, loss to and gain from outer space, fission, cosmic radiation, and natural terrestrial nuclear reactions. Most inert gases present in the atmosphere are of primordial origin with the exception of the helium isotopes and ^{40}Ar.

In order to give a greater understanding of the mechanisms by which the earth and its atmosphere were formed, meteorites, and in particular the inert gas contents of meteorites, have been studied extensively. Meteorites contain both "trapped gases", which are generally primitive gases trapped and retained in the meteorite since its existence as a solid body, and radiogenic gases, produced in the meteorite by radioactive decay and by various induced nuclear reactions. Bogard [35] identified two major components of the trapped gases:

Table 1.9. Inert gas content of the atmosphere.[33]

Element	Volume per cent.	g cm^{-2} of Earth's surface
He	0.0005	0.0007
Ne	0.0018	0.012
Ar	0.93	12.9
Kr	0.0001	0.003
Xe	0.00001	0.00045
Rn	-	5×10^{-15} *

* Near the ground

(1) solar, or unfractionated, gases, and (2) planetary, or fractionated gases. Solar gases, which are present in only a small percentage of meteorites, represent a sampling of the solar wind that was imbedded in the surfaces of individual mineral grains. Planetary type gases are found in large concentrations in carbonaceous meteorites, and represent the minute remaining fraction of inert gases that existed in the planetary nebula when meteoritic bodies formed. As a consequence, planetary gases show elemental and isotopic fractionation.

Mazor et al [36] classified the elemental abundance ratios in meteorites: the He/Ne ratio is fairly constant within a given meteorite class, but varies among classes; the Ne/Ar ratio occurs in highly variable proportions; and the Ar/Kr and Kr/Xe ratios are constant. These ratios lead to the isotopic ratio $^{20}Ne/^{22}Ne$ being used to identify trapped planetary gas.

1.5.1. Helium

^{3}He and ^{4}He occur naturally in minerals, rocks and natural gases in highly variable proportions (Table 1.10). Some of the helium may be primordial, but most of it is produced by radioactive decay. ^{3}He is the daughter of tritium, the radioactive isotope of hydrogen. It is thought to be produced in rocks mainly

Table 1.10. Helium contents of some natural gases, minerals and rocks.[37]

Location	Material	$^3He/^4He \times 10^7$	He %
	Gases		
Stamford, Connecticut	Air	12.0	0.004
	"	13.0	
Rattlesnake field, Shiprock, New Mexico	Natural gas	0.5	7.7
Otis field, Kansas	"	2.0	1.6
Panhandle field, Amarillo, Texas	"	1.5	1
	Radioactive minerals		
Hitlero, Norway	Blomstrandite	0.2	
Bahai, Brazil	Monazite	0.2	
Great Bear Lake, Canada	Pitchblende	0.3	
Joachimsthal, Czechoslovakia	Uraninite	0.3	
	Non-radioactive minerals		$cm^3\ g^{-1}$
Lerhnäs, Kimito, Finland	Beryl	0.5	0.011
Keystone, South Dakota	"	1.2	0.022
West Rumney, New Hampshire	"	12	0.004
Cat Lake, Manitoba, Canada	Spodumene	24	0.01
Edison mine, So. Dakota	"	120	0.01
	Common rocks		
Guttenberg, N.J.	Palisade diabase	-	7.5×10^{-6}
Sudbury, Ontario, Canada	Gabbro	-	33×10^{-6}
Sudbury, Ontario, Canada	Murray granite	-	165×10^{-6}

by the reactions: ^{6}Li (n,α) ^{3}H [38]

^{7}Li $(\alpha, {}^{8}Be)$ ^{3}H

^{2}H (n,γ) ^{3}H [39]

then ^{3}H (β^{-}) ^{3}He

and in the atmosphere by the reactions:

^{14}N $(n, {}^{12}C)$ ^{3}H

^{14}N $(n, 3\alpha)$ ^{3}H

then ^{3}H (β^{-}) ^{3}He [40]

Both processes which generate ^{3}He in the atmosphere require one neutron. An ample supply of neutrons in the atmosphere is produced by cosmic rays, and the atmospheric ^{3}He content can be explained by this process, despite the uncertainty surrounding the quantity of ^{3}He lost from the atmosphere. The bulk of ^{3}He production in the earth is also by neutron reactions. Because the cosmic neutron density decreases very rapidly below the earth's surface, other sources of neutrons are required. Only relatively small numbers of neutrons are produced in the earth by spontaneous fission of uranium and by (α,n) reactions on light elements, so the ^{3}He generation rate is small.

The geological occurrence and distribution of ^{4}He is unique. It is continuously being formed by the radioactive decay of the uranium and thorium series. On the other hand, the crust is continuously losing helium at a rate less than its rate of formation, and there has been an increasing flow of helium to the surface throughout geological time in stable crustal areas. [41]

The possibility of using the amount of helium generated for geological age determination has led to the extensive investigation of the occurrence of helium. It was shown by Holmes [42] that acid rocks did not retain helium as well as basic rocks. Furthermore, Keevil [43] showed that the ferromagnesian minerals in the Cape Ann granite, Massachusetts, generally seemed to retain more helium than the feldspars and quartz, and acid felsitic and glassy rocks contained very little helium. Gerling [44] attributed high helium loss to the looseness of crystal packing of the bulk of rock forming minerals.

The helium driven into crystal structures of rock minerals may be considered as an interstitial solid solution, that is tightly held for the most part, except near radioactive concentrations, where the α-radiation damage permits helium to escape. The mobile ^{4}He content of ancient granites, for example, may approach a very high value. [41]

Helium will have opportunities to migrate to the surface along faults in areas undergoing metamorphism and faulting. Where these faults intersect the sedimentary cover, the possibility exists of helium being trapped in structures similar to those that form petroleum and natural gas reservoirs. The release of helium from rocks and minerals is also promoted by leaching with hydrogen, methane and its homologues, and by oxidation of rocks during weathering. These processes lead to the accumulation of helium in natural gases. The distribution of

helium in natural gas has been studied extensively and is well known. The helium content of natural gas ranges from 0 - 10%. The known deposits are enormous, but the precise geological origin of the gas remains obscure in most fields.

The ratio $^3He/^4He$ varies by more than two orders of magnitude (Table 1.9). Generally, the reasons for the variation are the preferential release of ^4He due to radiation damage and the retention of ^3He which is much more widely dispersed and held more tightly in relatively undisturbed lattice sites. Morrison and Pine [39] calculate the average ratio of $^3He/^4He$ for granitic rock as $(1 \pm 0.5) \times 10^{-7}$, then discuss, more specifically, events which may cause a change in this ratio in different types of helium occurrences.

(1) Gas-well helium. The $^3He/^4He$ ratio is close to that for average granitic rocks indicating that the gases have been formed by normal nuclear reactions in a large body of granite.

(2) Radioactive minerals. The production of ^4He by α-decay greatly exceeds the production of ^3He leading to a low $^3He/^4He$ ratio.

(3) Beryls. The high helium content, but relatively normal $^3He/^4He$ ratio is explained by the fact that helium is included in beryls at the time of crystallization. The effect is a physico-chemical effect, rather than a nuclear effect.

(4) Spodumene, a lithium mineral. The high lithium content causes a high production of ^{3}He, relative to ^{4}He, so the $^{3}He/^{4}He$ ratio is high.

(5) Meteorites. The high cosmic flux causes external nuclear reactions to be of greater importance. This leads to a very high $^{3}He/^{4}He$ ratio.

The relative magnitude of competing nuclear reactions offers an explanation for the variation of the crustal $^{3}He/^{4}He$ ratio. However, recent helium isotope studies on terrestrial samples have revealed the existence of a helium component which is clearly distinct from atmospheric helium and crustal helium. This helium component shows a high ^{3}He enrichment and is characterised by a $^{3}He/^{4}He$ ratio of approximately 10^{-5}, compared with 10^{-6} for atmospheric helium and around 10^{-7} for crustal helium.[45]

^{3}He enrichment has been found in the deep water of the oceans[46, 47] in the hot brines in the axial rift of the Red Sea[45], in natural gases[48,49] and in the glassy rims of submarine pillow basalts[50,51]. It has been identified as primordial gas which is still present in the earth's interior and is being added to the atmosphere by intrusion of mantle material into the crust. The presence of the other primordial inert gases in oceanic basalts has also been inferred[52,53], but identification of primordial components other than helium is difficult.

Identification of primordial helium is not easy, as trapped gases in deep sea basalts contain, in addition to possible atmospheric components, embodied during or after emplacement, both primordial and radiogenic components and possibly also "recycled" components from crustal subduction. The relative contributions of the various components will determine whether the primordial component will be observed.

Helium is present in mineral springs and oceans in generally minute quantities. The deep ocean derives its helium from the influx of radiogenic and primordial helium from the crustal rocks on the bottom of the ocean, and the elemental and isotopic composition of deep ocean water reflects the relative contribution of the two components. The helium content of mineral springs generally reflects the extremely low solubility of helium, but instances where the helium content is significantly higher than average are important in terms of uranium occurrences, geothermal occurrences and areas of faulting.

The helium content of the atmosphere represents a balance between the rate at which helium is being added to the atmosphere from nuclear reactions and crustal degassing, and the rate at which helium is being removed from the atmosphere by escape from the upper atmosphere. The rate of production of ^4He, $P(^4He)$ by radioactive decay in the crust has been estimated as $(1 - 3) \times 10^6$ atoms $cm^{-2} s^{-1}$ [54]. The rate of accumulation of

^{3}He, P(^{3}He), by accretion of solar and galactic cosmic ray ^{3}He nuclei and by the decay of tritium produced by cosmic ray interactions in the atmosphere is 0.5 - 5 atoms cm^{-2} s^{-1} [54]. A certain proportion of the helium produced enters the atmosphere to contribute to the atmospheric helium content

$$Q\ (^4He) = 1.13 \times 10^{20} \text{ atoms cm}^{-2}$$

$$Q\ (^3He) = 1.41 \times 10^{13} \text{ atoms cm}^{-2}$$

where Q(^{4}He) and Q(^{3}He)are the quantities of ^{4}He and ^{3}He present in the atmosphere. [54]

From the values computed for the thermal and non-thermal escape of helium from the atmosphere, it is uncertain whether the atmosphere is in equilibrium with respect to its helium content, but it is assumed to have a constant value of 5.2×10^{-6} ppm by volume. [55] It is probable that the atmosphere is continually acquiring helium at a greater rate than the rate at which it is losing helium.

1.5.2. Argon

Argon occurs in nature as the stable isotopes ^{36}Ar, ^{38}Ar and ^{40}Ar. The terrestrial abundance of ^{40}Ar has increased enormously compared with ^{36}Ar and ^{38}Ar because of its production by the radioactive decay of ^{40}K (Figure 1.1) ^{40}K comprises 0.0119% of natural potassium. It is radioactive and decays with a half-life of 1.3×10^9 years by β-emission to ^{40}Ca (89%) and by electron capture to ^{40}Ar (11%).

The presence of both radiogenic and non-radiogenic argon in potassium bearing minerals was first shown by Aldrich and Nier [56]. The distribution of potassium determines the initial distribution of ^{40}Ar. Migration of argon from its site of production will subsequently dictate its natural occurrence and argon is found in minerals and rocks, mineral waters, mine gases, volcanic emanations and petroligenic natural gas. The production of ^{40}Ar by ^{40}K decay is the basis of a method for the determination of geological age.

Accurate potassium/argon ages are given only by minerals which retain a high proportion of radiogenic argon (micas, plagioclases, amphiboles). Minerals which do not quantitatively retain argon (potassium-feldspars, glauconites) will give low ages.

The $^{36}Ar/^{38}Ar$ ratio has been found to be low, compared with the atmospheric ratio, in some pitchblendes [57]. This has been attributed to the production of ^{38}Ar by nuclear reactions involving ^{35}Cl, present as an impurity in the pitchblende.

$$^{35}Cl \quad (\alpha, p) \quad ^{38}Ar$$

$$\text{or} \quad ^{35}Cl \quad (\alpha, n) \quad ^{38}K$$

$$\text{then} \quad ^{38}K \quad (\beta^{+}) \quad ^{38}Ar$$

Similar nuclear reactions are responsible for the production of small amounts of ^{36}Ar.

The origin of the argon content of the atmosphere has caused controversy. It is not fully understood whether it has been derived entirely by radioactive decay within the crust or much of it was present when the earth's atmosphere was formed. Damon and Kulp [58] argue that most of the ^{40}Ar now on the surface of the earth was probably introduced from the mantle during the first one billion years of earth history. Subsequent lesser additions have occurred through the weathering of surface rocks and the growth of continents.

However, calculation of the age of the earth from the ^{40}Ar content of the atmosphere by Shillibeer and Russell [59] supports the view that the ^{40}Ar content of the earth has been almost entirely produced by the continuous radioactive decay of ^{40}K in the crust and subsequent release of radiogenic argon by the crustal rocks as they are built into the continental masses. This model assumes that radiogenic argon is completely lost from the lithosphere, but it is known that some minerals retain a high proportion of the radiogenic argon produced in them.

1.5.3. Neon, krypton and xenon

The neon content of some igneous rocks is given in Table 1.11. The neon content and isotope ratios from radioactive minerals is given in Table 1.12. Wetherill [61] attributed the excess ^{21}Ne found in some radioactive minerals to a natural nuclear reaction occurring on ^{18}O:-

$$^{18}O\ (\alpha,n)\ ^{21}Ne$$

and concluded that a large fraction of the ^{21}Ne content of the atmosphere may have been formed in this way.

The ratio of Ne/Ar in the atmosphere is 1.9×10^{-3}. However, the cosmic abundance of neon is greater than that of argon. To explain the difference between the cosmic and terrestrial abundances of these gases, Russell and Menzel [62] assume that the earth lost practically all of its initial neon into interplanetary space, like most of its hydrogen and the bulk of its helium.

Table 1.11 Neon contents of some igneous rocks [60]

Rock	Ne content, 10^{-8} cm^3 g^{-1}
Eclogite	6.6
Dunite (average)	8.6
Granite (average)	6.9
Obsidian	8.6

Table 1.12 Isotope ratios and amounts of neon from some radioactive minerals.[61]

Sample	$^{21}Ne/^{20}Ne$	Excess ^{21}Ne, $cm^3\ g^{-1}$	Ne, $10^{-8}\ cm^3\ g^{-1}$
Atmospheric	0.00283		
Pitchblende	0.00519	1.36×10^{-7}	6380
Monazite	0.402	8.7×10^{-9}	3.3
Euxenite	1.05	8.0×10^{-9}	5.2

Comparison of the cosmic abundance of neon and xenon with the contents in the earth and its atmosphere show that the relative abundance of xenon (the ratio of the number of xenon atoms to the number of silicon atoms) is about 10^7 times smaller on the earth than it is in the universe, whereas for neon, this figure exceeds 10^{11}. A separation of Ne from Xe shifting the ratio of concentrations by a factor of more than 10^4 has obviously taken place during the evolution of the earth's atmosphere. This cannot be explained by chemical absorption or solution processes, but can be understood by assuming selective diffusion from the earth's gravitational field during a limited epoch of evolution.[63]

Suess[63] found that the ratios of terrestrial and cosmic abundances of Ne, $^{36}Ar + {}^{38}Ar$, Kr and Xe plotted against atomic weight, lie close to a curve, which is given by the following equation:

$$-\log_{10} \frac{N_{ter}}{N_{sol}} = 10 \times e^{-0.045M/m} + 7.1$$

where N_{ter} = number of atoms of rare gas present in the earth's atmosphere per 100 atoms of silicon present in the earth

N_{sol} = number of atoms of rare gas present in the universe per 100 atoms of silicon

M = atomic weight of rare gas

m = atomic mass unit.

This form of function is that expected from selective diffusion. The small value of the exponent makes it impossible to explain selective escape from the earth's gravitational field by thermal diffusion alone.[63] The equation indicates that approximately 10^7 parts to 1 of the rare gases originally present may have escaped from terrestrial matter without undergoing separation, leaving only the small residual fraction to be involved in the separation process.

Krypton and Xenon are found naturally in mineral waters, some volcanic gas and as constituents of the atmosphere. Isotopes of both gases are produced by spontaneous fission and neutron fission in nature, and uranium minerals have been found to contain ^{129}Xe (from $^{129}I(\beta^-)\ ^{129}Xe$), ^{131}Xe, ^{132}Xe and ^{134}Xe; and ^{83}Kr, ^{84}Kr and ^{86}Kr. The isotope abundance ratios for the fissiogenic gases differ greatly from the atmospheric abundance ratios, thus the bulk of the atmospheric heavy inert gases are not derived from the natural fission of any known heavy element.

1.6. THE NATURE OF GROUNDWATER

Rocks which contain significant quantities of chemically unbound water are known as aquifers, although nearly all rocks contain some water. The surface layers of the earth's crust act as a vast natural reservoir in the hydrological cycle, absorbing rainfall which would otherwise rapidly run-off to streams and rivers and maintaining stream flow during dry periods.

1.6.1. The occurrence of groundwater

Virtually all groundwater comprises precipitated atmospheric moisture which has percolated down into the soil and subsoil layers. Meteoric water may reach the zone of saturation directly, whereby rain infiltrates the soil layers or water vapour condenses in the interstices; or indirectly, by influent seepage from lakes, rivers, man-made channels and oceans. Other sources of groundwater are connate water, trapped in some sedimentary and volcanic rocks at the time of their origin and a quantity of juvenile water from deep within the earth's crust (although much of the present hydrosphere may be of juvenile origin).

Only a small proportion of the zone of saturation will be comprised of aquifer rocks which store and transmit a significant quantity of water. There will also be impermeable beds, or aquifuges', which contain no interconnected openings or interstices and, therefore, neither absorb nor transmit water, and semi-permeable beds or aquicludes, which, although porous and capable of absorbing water slowly, will not transmit it in a significant quantity to a well or spring, but may be important in regional groundwater movement.

1.6.2. Porosity

The degree to which a rock contains interstices is known as its porosity. Intergranular spaces vary widely in size from minute voids in clays, shales and slates, to large spaces between the pebbles of the well sorted, unconsolidated gravel. Massive spaces such as fractures, joints and bedding planes, which may be enlarged by solution, occur between large blocks of rock. Meinzer [64] used the relation of rock texture to porosity to classify types of rock interstices. (Figure 1.2).

1.6.3. Groundwater boundaries.

By definition, only in the zone of saturation are the interstices completely filled with water. Further downward movement of groundwater is made virtually impossible by a lower zone in which the interstices are small and scarce. This boundary is frequently formed by a layer of very dense rock, such as clay, or slate, or granite, or by the upper surface of the original parent rock in the case where the aquifer is a surface deposit of weathered material. Alternatively, the boundary may be formed by the gradual compression of strata with depth, as a result of the increasing weight of overlying rocks.

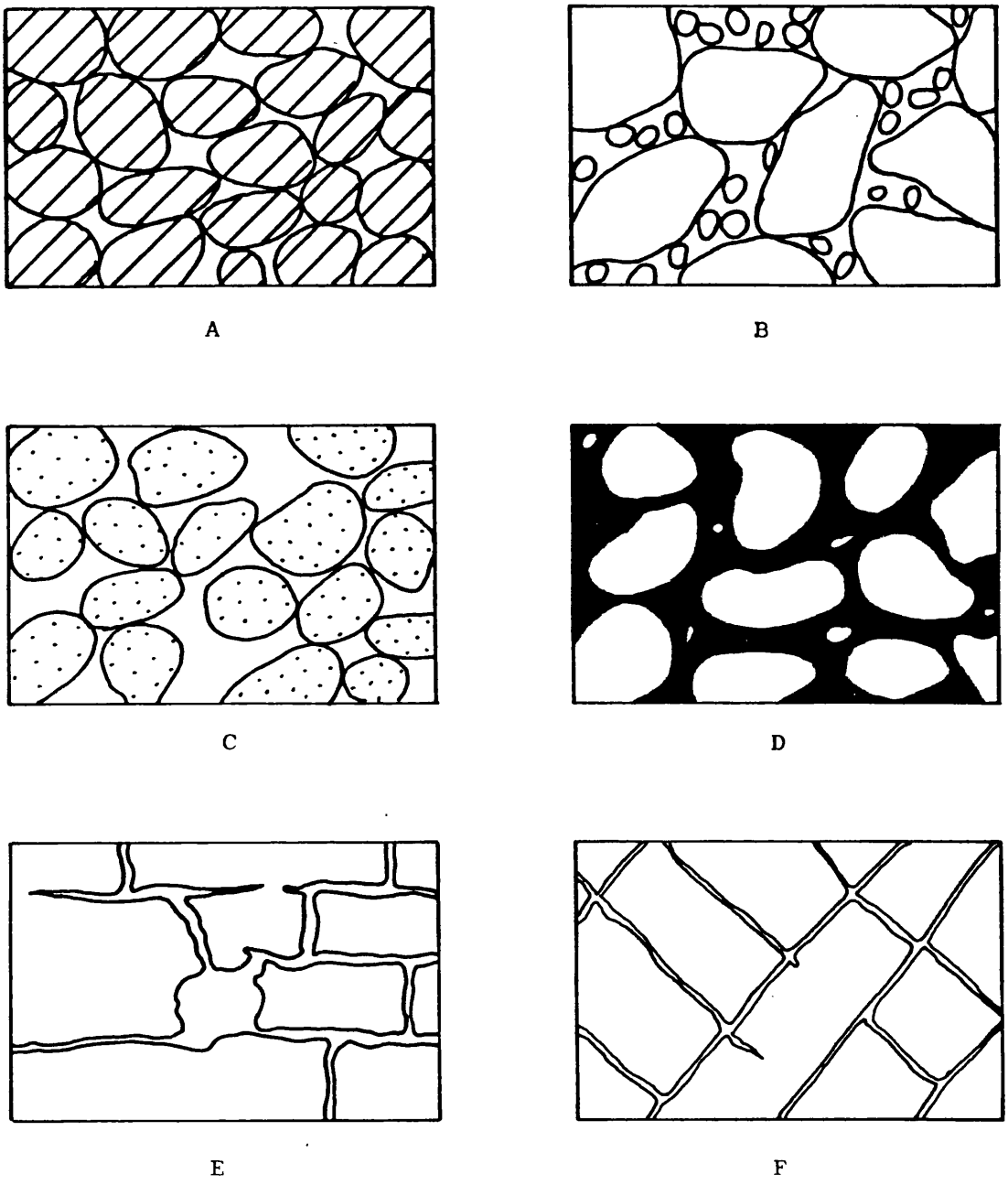

Fig. 1.2. Diagram showing several types of interstices (A) between relatively impermeable well-sorted particles, (B) between relatively impermeable unsorted particles, (C) between permeable particles, (D) between grains which have been partially cemented, (E) formed by solution along joints and bedding planes in carbonate rocks, and (F) formed by fractures in crystalline rocks.[64]

The upper boundary depends on whether the groundwater is confined or unconfined. In the case of an unconfined groundwater, this boundary is normally known as the water table, the contact plane of unconfined groundwater and the capillary fringe, [65] which approximates to the level where the porewater pressure is equal to atmospheric pressure. In the case of a confined groundwater, the upper boundary of the water is formed by an overlying impermeable bed, and for a semi-confined aquifer, by an overlying semi-permeable bed. All confined aquifers have an unconfined zone through which recharge occurs by means of infiltration and percolation. The confining impermeable bed rarely forms an absolute barrier to groundwater movement, so that there is normally some interchange, and therefore a degree of hydraulic continuity.

The pressure of groundwater in the confined zone is given by the difference in hydrostatic level between the water table and the confined level. The water level in a well sunk into a confined aquifer will rise to the height of the hydrostatic head. The level to which the water rises is known as the piezometric surface.

1.6.4. Groundwater storage and movement

Groundwater may reside in an aquifer with small interstices for thousands of years as its movement will be slow. Groundwater movement in large interstices is very much faster and its residence time in such an aquifer may range from a few hours (e.g. in Mendip conduit flow [66]) to a few years, (e.g. in Bunter Sandstone, England [67]).

The amount of groundwater stored in a saturated material depends on its porosity. The porosity is determined by the shape, arrangement and degree of sorting of the constituent materials and the extent to which modifications arising from solution, cementation, compacting and faulting have occurred. The combined effect of these factors is shown in Figure 1.3. Materials with a high porosity do not necessarily form good aquifers, as not all the water will be mobile. The mobility will depend on the way in which the interstices are interconnected and on the size of the interstices.

Aquifer recharge by atmospheric precipitation occurs by

(a) infiltration at the ground surface,

(b) seepage through the banks and bed of surface water bodies such as ditches, rivers, lakes and oceans;

(c) leakage and inflow from adjacent aquicludes and aquifers; and

(d) artificial recharge from irrigation, spreading operations and injection wells.[69]

The main components of groundwater discharge are (a) evapotranspiration, in unconfined aquifers particularly in low-lying areas where the water table is close to the ground surface; (b) natural discharge by springs and seepage into surface water bodies, (c) leakage and outflow through aquicludes and into adjacent aquifers; and (d) artificial abstraction.[69]

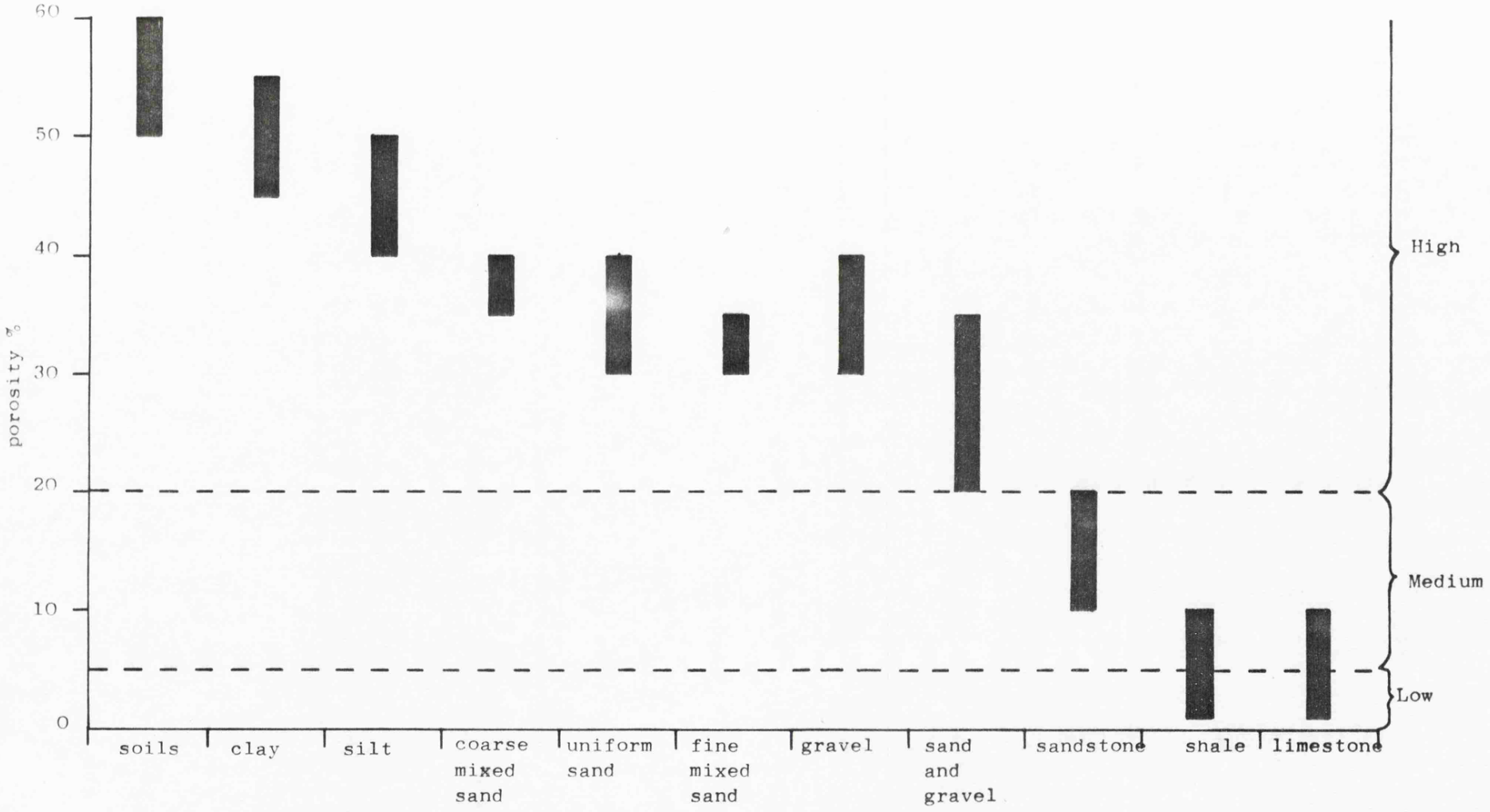

Fig. 1.3. Porosity ranges for various natural deposits (Based on data by Todd [68])

The driving force of groundwater movement is the hydraulic gradient. The rate and direction of groundwater flow are very variable and are described quantitatively by Darcy's Law:

$$Q = K_p A \frac{\emptyset_1 - \emptyset_2}{\Delta S}$$

where Q = volume flow velocity, $m^3 s^{-1}$

K_p = coefficient of permeability (or saturated hydraulic conductivity)

A = cross sectional area of the aquifer, m^2

$\emptyset$ = total potential, m

ΔS = length of flow, m

Dimensional analysis of the Darcy equation leads to dimensions of length/time for K_p, or $m\ s^{-1}$ in the S.I. system of units. The total discharge, Q, is proportional to the cross sectional area, A, and inversely proportional to the length of flow, ΔS. K_p can therefore be expected to be a constant for a particular material, independent of the size of the sample. The variables used in the expression of Darcy's Law are shown in Figure 1.4. The height to which the water rises in wells 1 and 2 has been denoted by $\emptyset_1$ and $\emptyset_2$ respectively. The resistance to flow in the aquifer is very large compared with the resistance offered in the standpipes and the velocity of the water is small due to this resistance, therefore the pressure at the bottom of each standpipe may be considered to be hydrostatic pressure only:

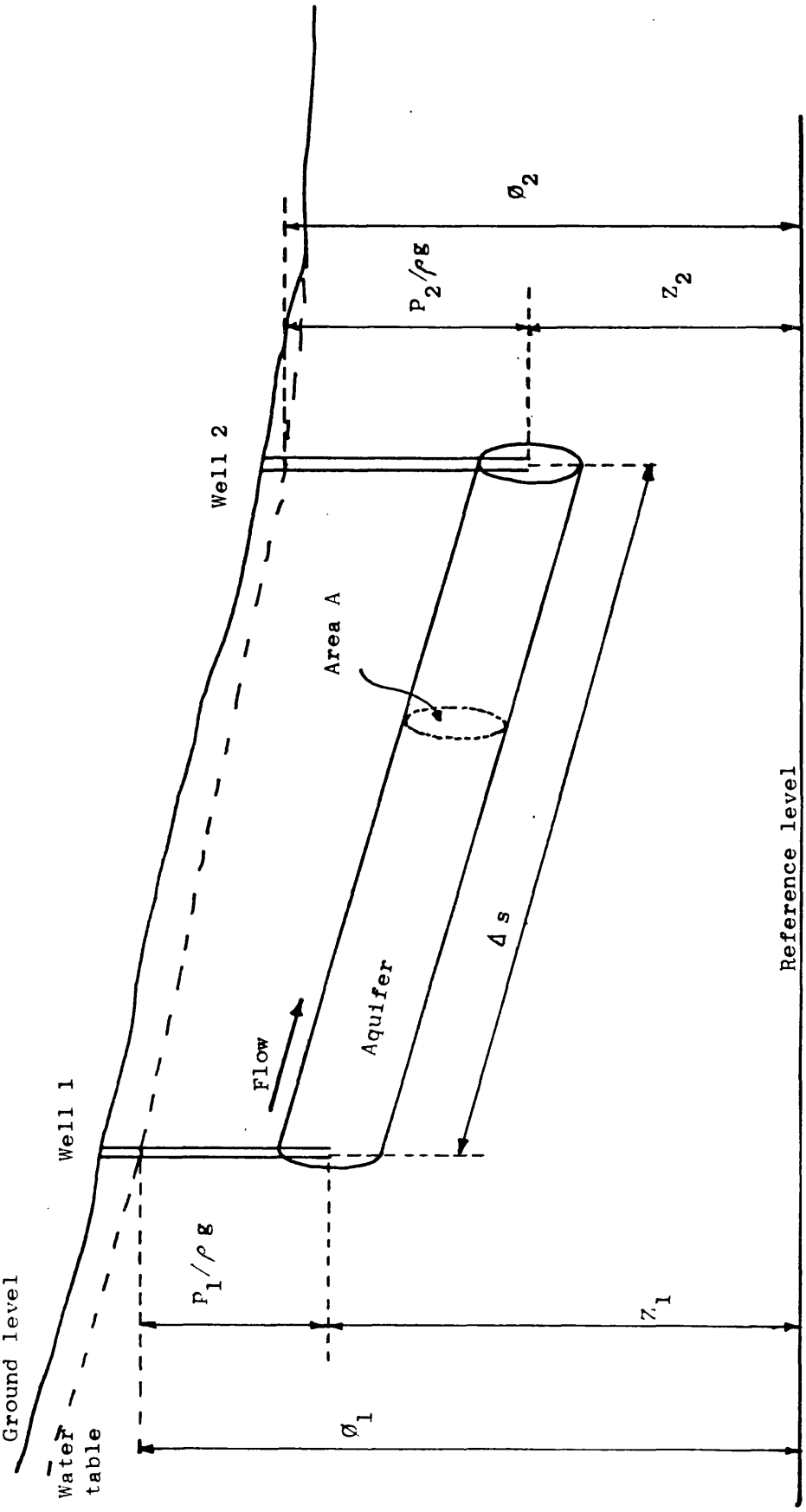

Fig. 1.4. Diagram showing the elevation head, pressure head and total potential (head) for a point in a flow field.

Therefore $p_1 = (\phi_1 - Z_1)\rho g$

and $p_2 = (\phi_2 - Z_2)\rho g$

where p_1 and p_2 are the pressures at the bottom of standpipes 1 and 2 respectively

ρ is the density of water ($\doteq$ 1000kg m^{-3})

g is the acceleration due to gravity ($\doteq$ 9.81 m s^{-2})

It follows that $\phi_1 = Z_1 + p_1/\rho g$

$\phi_2 = Z_2 + p_2/\rho g$

Therefore it is not merely the pressure that makes the water flow through an aquifer, but rather the combination of pressure and the height above a certain horizontal level. This combination is called the groundwater head, and Z and $p/\rho g$ are termed the elevation head and pressure head respectively.

The quantity Q/A, the total discharge per unit of cross-sectional area, is called the specific discharge, v. Letting $\phi_2 - \phi_1 = \Delta\phi$, the Darcy equation becomes:

$$v = -K_p \frac{\Delta \phi}{\Delta S}$$

The specific discharge has been defined as the total discharge per unit area of the aquifer, and not as the total discharge per unit area of the pore space. Therefore the specific discharge, which has dimensions of length/time, is not the actual velocity of the water particles. If the porosity is denoted by n, then the area through which the water can flow

is nA. Therefore, the average actual velocity of the water, V_w, is given by:

$$V_w = Q/nA = v/n$$

Since $n < 1$, the actual velocity of the water is always greater than the specific discharge.

The coefficient of permeability, K_p, is a material constant. However, its value depends not only upon the properties of the aquifer material but also upon the properties of the fluid percolating through it. The relationship between K_p and the material and fluid properties is given by:

$$K_p = k \frac{w}{\mu}$$

where w is the specific weight of the fluid

μ is the absolute viscosity of the fluid.

The constant k is called the intrinsic permeability and is a property of the aquifer material only, k may be expressed as:

$$k = C d^2$$

where C is a dimensionless constant involving the shape, packing, porosity and other characteristics of the aquifer material and d is the average pore size of the medium. Therefore the dimensions of k are area.

Substitution of $K_p = k w/\mu$ into the Darcy equation gives the alternative form:

$$V = - \frac{kw}{\mu} \frac{\Delta \phi}{\Delta S}$$

k is usually expressed in units of darcy s, where a darcy is defined as follows: a porous medium is said to have an intrinsic permeability of one darcy if a single-phase fluid of one centipoise viscosity that completely fills the pore space of the medium will flow through it at a rate of $1 cm^3 s^{-1}$ per cm^2 of cross-sectional area under a pressure gradient of 1 atm. cm^{-1} .[70] The magnitude of one darcy is therefore equivalent to $0.987 \times 10^{-12} m^2$.

Inserting the values of w and μ for water at $20^{\circ}C$, gives the relationship

$$1 \text{ darcy} \simeq 10^{-5} K_p$$

where K_p is in $m\ s^{-1}$

The approximate order of magnitude of k and K_p for natural soils is given in Table 1.13.

The Darcy equation yields only a macroscopic velocity value through a cross-sectional area of solid matrix and interstices. However, because of the variable shape and size of the interstices, the actual velocity is very variable. Flow velocities through the interstices alone will also be higher than the macroscopic value because the actual flow-path of a water particle exceeds the apparent flow-path as the average water particle has to travel around and between the grains of a porous medium. Another factor complicating the field application of the Darcy equation is that hydraulic conductivity is often markedly anisotropic, particularly in fractured and jointed rock.

Table 1.13. The order of magnitude of the permeability of natural soils.

Aquifer Classification	Soil Type	K_p (m s^{-1})	k (darcys)
Impervious	Clays	$< 10^{-9}$	$< 10^{-4}$
Poor aquifers	Sandy clays	$10^{-9} - 10^{-8}$	$10^{-4} - 10^{-3}$
	Peat	$10^{-9} - 10^{-7}$	$10^{-4} - 10^{-2}$
	Silt	$10^{-8} - 10^{-7}$	$10^{-3} - 10^{-2}$
	Very fine sands	$10^{-6} - 10^{-5}$	$10^{-1} - 1$
Good aquifers	Fine sands	$10^{-5} - 10^{-4}$	$1 - 10$
	Coarse sands	$10^{-4} - 10^{-3}$	$10 - 10^{2}$
	Sand with gravel	$10^{-3} - 10^{-2}$	$10^{2} - 10^{3}$
	Gravels	$> 10^{-2}$	$> 10^{3}$

Extreme flow velocities may result in deviations from Darcy's Law. The occurrence of turbulent eddies dissipates kinetic energy and means that the hydraulic gradient becomes less effective in inducing flow. At the other extreme, clay soils, with small pores and low hydraulic gradients, tend to adsorb water strongly, and the very low flow rates are less than proportional to the hydraulic gradient.

Despite minor deviations, Darcy's law can be successfully applied to virtually all normal cases of groundwater flow and is equally applicable to both confined and unconfined conditions. However, an understanding of most groundwater problems requires information not only on the velocity of groundwater flow, but also on the velocity of head transmission. The velocity of head transmission is proportional to the square root of the hydraulic diffusivity, a, which is given by

$$a = \frac{K_p m}{S}$$

where K_p is the hydraulic conductivity; m is the saturated thickness of the aquifer; and S is the storage coefficient, which is defined as the volume of water which an aquifer releases from, or takes into storage per unit surface area of aquifer per unit decline or rise of head. The coefficient of storage is therefore a ratio of a volume of water to a volume of aquifer. This is illustrated in Figure 1.5 in which the volume of water released from storage in the aquifer prism divided by the product of the prisms cross sectional area and the decline

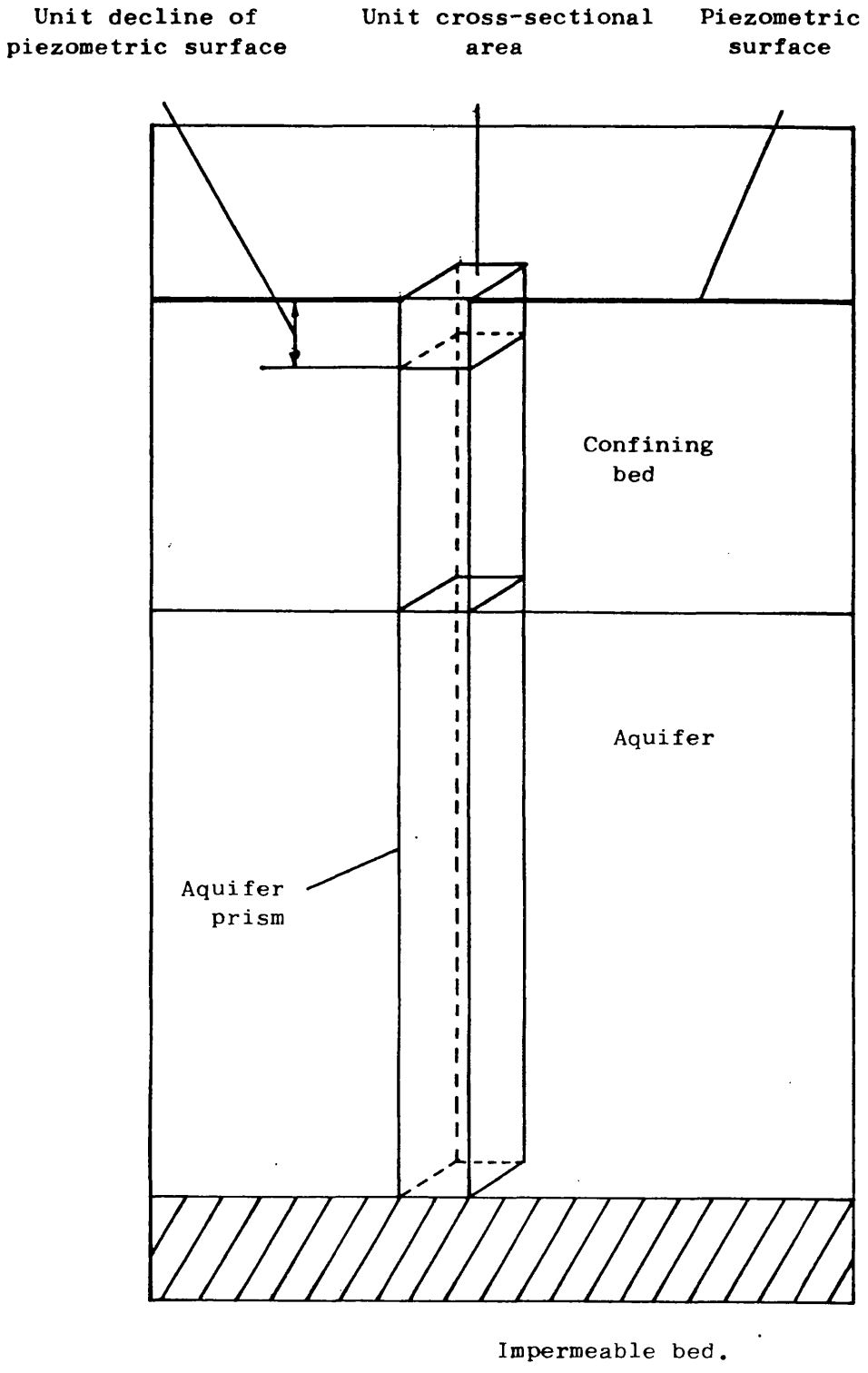

Fig. 1.5. Diagram to illustrate the storage coefficient of a confined aquifer (from an original diagram by Todd.[68])

in head results in a dimensionless number. The storage coefficients of confined aquifers may range from about 0.00001 to 0.001 [71]. For confined aquifers, therefore, the hydraulic diffusitivity depends not only on the conductivity of the aquifer material but also on its elastic properties.

By itself, Darcy's Law suffices to describe only steady flow conditions so that for most field applications the law must be combined with the mass-conservation law to obtain the general flow equation, or for saturated conditions, the Laplace equation. A direct solution of the latter equation for most groundwater flow conditions is generally not possible, so that it is necessary to resort to various approximate or indirect methods of analysis.

1.6.5. Groundwater quality.

Groundwater quality may be considered in terms of bacteriological content, physical characteristics such as temperature, turbidity, colour, taste and odour, and chemical content [69]. The chemical content of groundwater is highly variable, because of the variety of chemical changes which may occur when groundwaters interact with minerals. The chemical composition may be effectively represented on the trilinear diagram developed by Piper [72]. (Figure 1.6). In this, groundwater is treated as though it contained three cation species (Na^+, Mg^{2+} and Ca^{2+}) and three anion species (HCO_3^-, SO_4^{2-} and Cl^-). Silica, the other major constituent

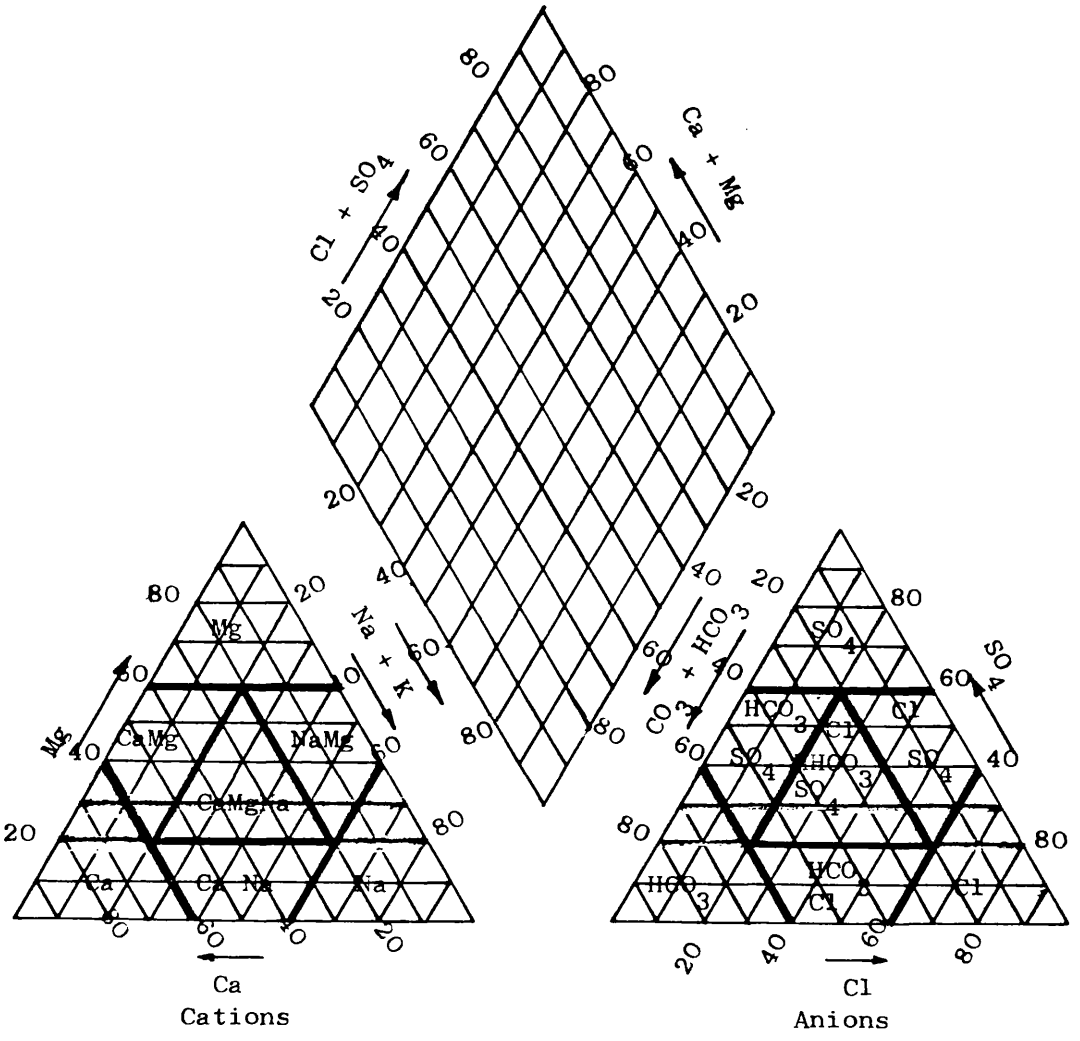

Fig. 1.6. Piper trilinear diagram used to represent the chemical composition of groundwater. [34]

is omitted and the less abundant cations and anions are summed with the major components to which they are related (Ba^{2+} + Ca^{2+}, K^{+} + Na^{+}; CO_3^{2-} + HCO_3^{-}; etc.). Toth [73] lists the factors which affect the chemical composition of groundwater:

(a) types of soluble minerals.

(b) amounts of soluble minerals

(c) solubility of minerals

(d) temperature of rock

(e) area of contact between rock and water, which is a function of porosity

(f) antecedent composition of the water

(g) antecedent temperature of the water

(h) fluid pressure

(i) flow velocity and direction, both of which are a function of groundwater potential.

The most important physical property is groundwater temperature. It is essentially constant, showing only a small seasonal and diurnal change in the case of shallow groundwater, and virtual constancy in the case of deeper water below about 30m . At depths of 10 - 20 m the temperature of groundwater will normally exceed the mean annual air temperature by 1 - 2°C. [68] Therefore groundwater temperatures tend to be lower than air temperatures during the summer and higher than air temperatures during the winter. At greater depths, groundwaters may be heated by the geothermal gradient in the crust (3°C/100 M on average, [74]).

Factors which result in extremes of temperature are important. Freezing, for example, removes groundwater from the hydrological cycle. High temperatures associated with thermal springs are also important as is the nature of the source heating the water. It is believed that most thermal springs are derived from the underground heating of meteoric water, although some may contain a component of juvenile or not connate water. The sources of heat may be the geothermal gradient, an underlying body of hot or molten rock, faulting, chemical heating or radioactive decay.

1.7. ISOTOPE TECHNIQUES IN HYDROLOGY

Groundwater dating is an important consideration in developing a water supply. In such development, it is important to determine the time, place and amount of recharge and to distinguish lateral and vertical differences in groundwater movement from points of recharge to points of discharge. It is important to obtain a reliable mean age of the groundwater especially in fissured rocks. For example, an apparent age of several thousand years for an outcrop water or near outcrop water does not necessarily indicate that it contains no recent components. Similarly a mixed water cannot be reliably dated because varying proportions of different components could give rise to the same apparent age.[75]

Groundwater dating may also be important when considering an aquifer rock as a resource. For example, the dating of groundwaters associated with geothermal reservoirs is a necessary aspect of the study of geothermal resources. Recently, the dating of groundwaters associated with crystalline metamorphic rocks, argillaceous sediments and salt deposits has become important because of the possibility of using such structures for the underground storage of radioactive waste. Thus groundwater dating is not only important when considering the properties of groundwater itself, but is also important when considering the physical and chemical properties of the aquifer in which the groundwater resides.

The operation of a groundwater system can be defined as:

$$I - O = \Delta S$$

where I = input, O = output and ΔS = change in storage.

The basic principle underlying the application of isotopes to the problem of groundwater tracing is the use of the variation of the isotope input to determine the time and place of recharge, and the use of radioactive decay to determine residence time. The most common isotopes employed are the stable isotopes ^{2}H and ^{18}O and the radioisotopes ^{3}H and ^{14}C. Significant exchange of deuterium and tritium during transit of groundwater has not been observed, although ^{18}O exchange can provide valuable information on the thermal history of a water. However, ^{14}C

which occurs in the dissolved carbonate compounds, is subject to dilution by non radioactive carbon dissolved from rock minerals. Its half-life of 5685 years [75] makes it valuable for dating slow moving groundwaters, if correction of the diluting effect of mineral carbonates is possible.

The tritium, ^{14}C and stable isotope concentrations in groundwaters are affected by the same natural mixing processes, but the inputs have been controlled by different processes. ^{3}H and ^{14}C are produced both naturally and artificially and shallow groundwaters tend to show a distinct layering of ^{3}H and ^{14}C with radioactivity decreasing with depth.

1.8. STABLE ISOTOPE TRACING

The principal heavy stable isotopic components of water are $HD^{16}O$ and $H_2{}^{18}O$ which occur in natural waters in concentrations of about 320 ppm (parts per million) and 2000 ppm respectively. The isotopic composition of a water sample is expressed in terms of the per mil deviation of the isotope ratio from that of a standard, rather than in terms of absolute ratios, and is expressed as delta (δ) units which are defined by:-

$$\delta = \frac{R_S - R_{SMOW}}{R_{SMOW}} \times 10^3 \quad {}^{o}/_{oo}$$

where R_s is the isotope ratio ($^{D}/_{H}$ or $^{18}O/^{16}O$) in the sample, R_{SMOW} is the isotope ratio in the standard and $^{o}/_{oo}$ denotes parts per mil (parts per thousand). The standard SMOW (Standard Mean Ocean Water) is defined by Craig [77] based on a set of ocean water samples related to a National Bureau of Standards isotopic reference water sample. Stable isotope fractionation occurs whenever water changes state through condensation or evaporation, mainly becuase the heavy isotopic components have lower vapour pressures than $H_2{}^{16}O$. Thus water evaporated from an open water body, such as the sea or a lake is depleted in deuterium and ^{18}O with respect to the surface water. The amount of depletion depends on the ratio of vapour pressures, the rate of evaporation, the water vapour exchange, and the isotopic composition of the water vapour already present in the air.[78] When the moist air masses formed by this process cool, the initial composition of the condensation is relatively close to that of the surface water from which it was derived. The precipitation at later stages becomes increasingly depleted in the heavy isotopes with respect to SMOW. This depletion is usually greater the more continental the location.

Fractionation is affected by the temperature at the time of condensation: the lower the temperature, the greater the depletion in heavy isotope content. This temperature effect causes variation of the stable isotope content of precipitation with lattitude because of the relationship of mean annual temperature

with lattitude. Similarly, variations in altitude result in variations in composition, and in areas of orographic rainfall there is often a close correlation between isotopic composition and land-surface altitude. Thus precipitation at high altitudes is characterised by depletion in the heavy stable isotopes relative to precipitation in nearby lower lands.

Waters which have not been subjected to evaporation have stable isotope compositions which are related by the equation

$$\delta D = 8 \delta^{18}O + \text{constant}$$

The constant represents the excess of deuterium and commonly takes the value +10. Waters which have been subjected to evaporation tend to fall off the general line.

Stable isotopes are important in the investigation of the origin and distribution of groundwater. Stable isotopes concentrations have been used to identify seasonal variation in rainfall and in some instances even specific storm events.[79] Reservoirs replenished during the pluvial episodes of pleistocene glaciations are characterised by their depleted stable isotope contents relative to present recharge. Lake waters may be identified by the non-reversible effect that open water evaporation produces on the D - ^{18}O relation, and

if these waters subsequently recharge groundwaters, they can be readily recognised. Similarly, waters that have been subjected to high temperatures underground, such as those of thermal springs, can be recognised by their D - ^{18}O content, as ^{18}O will exchange with oxygen compounds in the rock and ^{2}H is not affected. ^{80} Finally, the stable isotope composition of precipitation depends on lattitude. Groundwaters replenished by rivers spanning significant lattitude zones may be distinguished from local recharge on this basis alone. Similarly, waters recharged at high altitudes can be distinguished from those recharged at low altitudes.

1.9. TRITIUM

Tritium is produced in small amounts by cosmic ray interactions in the upper atmosphere and in very much larger amounts by thermonuclear explosions. Tritium has a half-life of 12.3 years and its greatest use is in the tracing of atmospheric waters, surface waters and certain groundwaters. It decays by β-emission to an isotope of helium, ^{3}He

For example

$$\left.\begin{array}{ll} ^{14}N\ (n,\ ^{12}C) & ^{3}H \\ ^{14}N\ (n,\ 3\alpha) & ^{3}H \end{array}\right\}\ 38$$

$$^{2}H\ (n, \gamma) \quad ^{3}H \quad 40$$

Then $^{3}_{1}H\ (\beta) \quad ^{3}_{2}He$

The occurrence of tritium results in an overall labelling of water in the hydrological cycle depending on the concentration of tritium in the atmosphere. Present concentrations of tritium in the atmosphere vary with season, exhibiting a maximum in late spring and summer. This phenomenon is observed in both the northern and southern hemisphere, although the concentrations are much lower in the southern hemisphere. Tritium also varies with lattitude, so that concentrations at any given time increase towards the poles over both the continents and the oceans. The concentration gradient with lattitude is usually greater over the continents and is greater in the northern hemisphere. To date, maximum tritium concentrations in the northern hemisphere were observed in 1963, while in the southern hemisphere the maximum occurred in 1964 and 1965, but was much lower. The causes of these variations are variations in the temperature and direction of air streams which mobilise tritium.

Because of the complex variations in the tritium content of the atmosphere, it is difficult to derive absolute ages from tritium contents. For water dating, tritium has the advantage that it is part of the water molecule, so it will be conserved to the same extent as the water.

Tritium is particularly useful in detecting recent recharge because of its short half-life and its high concentrations in the atmosphere since the beginning of atmospheric testing of thermonuclear devices in 1952. Before 1952, precipitation contained a level of tritium of about 5 - 10 T.U. throughout most of the world, where

1 T.U. = 1 tritium unit

= 1 atom of ^{3}H per 10^{18} atoms of ^{1}H

= 7.2 d.p.m. l^{-1} H_2O (3.2 pCi l^{-1} H_2O)

Within 50 years (four half-lives) natural tritium would have decayed to around 0.5 T.U., below which tritium is not easily detectable. Therefore, a groundwater containing a significant amount of tritium must contain at least some component of modern recharge.

There is a pronounced annual cycle of tritium in precipitation as the bulk of tritium injected into the upper atmosphere rains out during the following spring and summer. Each succeeding peak since 1963 has been lower than that of the previous year. Consequently recharge since 1954 and especially since 1963 can be readily identified, but because of the seasonal variations (Figure 1.7) the exact age cannot be determined.

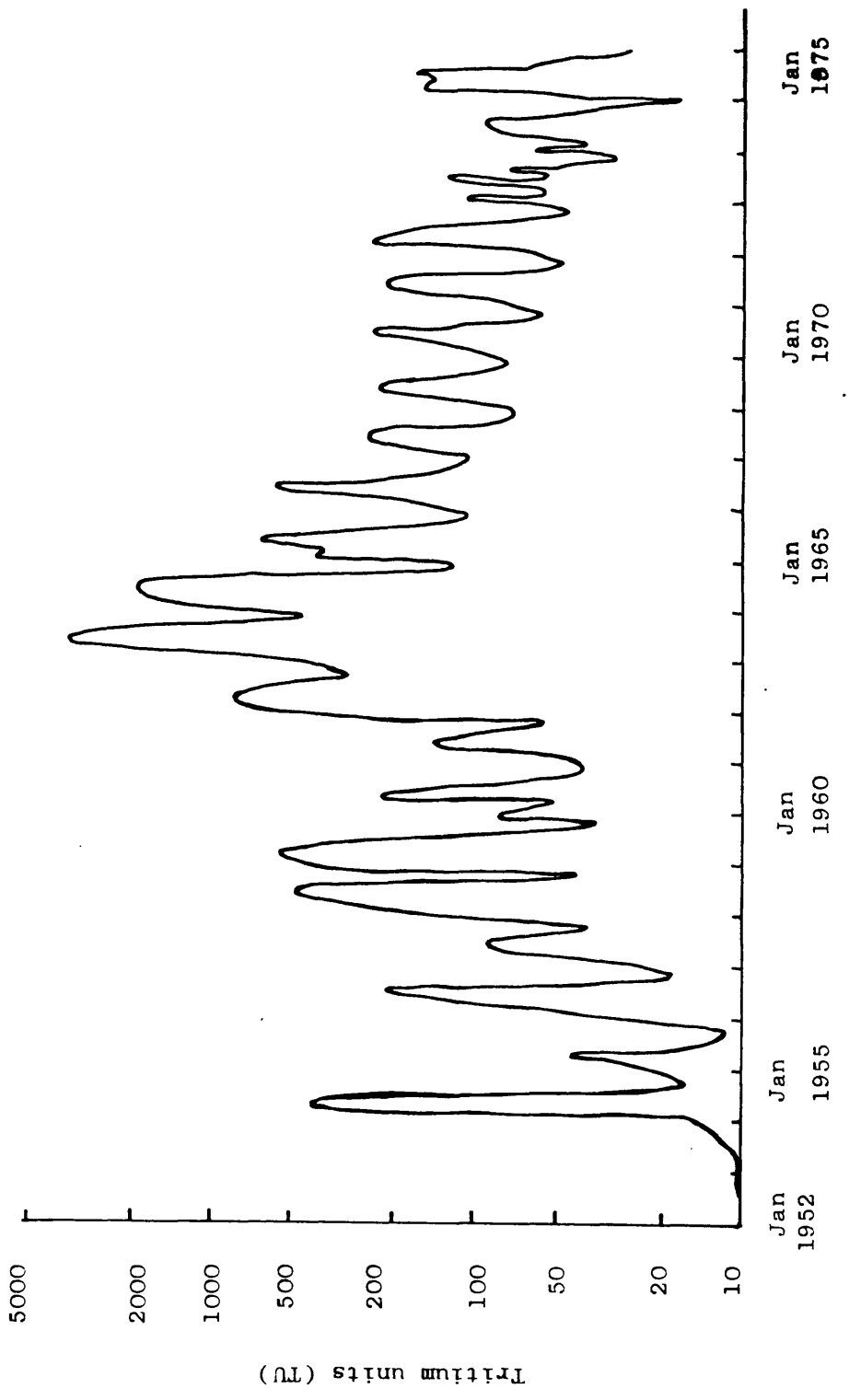

Fig. 1.7. Tritium concentration of rainfall over the United Kingdom. Observed or computed values for 1952-1974 (not corrected for radioactive decay) 80

Ideally it should be possible to trace the movement of a groundwater which has been recharged at a single point and has not been subjected to mixing. This situation is rare in nature, but, within its limitations it has been used to trace rapid flow in glacio-fluvial aquifers. These aquifers have restricted recharge areas and distinct boundaries, and the model is analogous to a gravel filled pipe. Tritium has also been used to trace mixing due to new inputs and tritium decay in aquifers of high permeability, such as Karstic limestones and basaltic flow rocks.

1.10 CARBON-14

^{14}C is produced by the interaction of ^{14}N with a neutron:

$$^{14}N\ (n,\ p)\ ^{14}C$$

The nuclear cross section for neutron absorption to occur, $\emptyset$, is $1.7 \times 10^{-24} cm^2$ (1.7 barns). ^{14}C is produced in the atmosphere by the interaction of cosmic rays with atmospheric ^{14}N at an essentially constant rate, as the cosmic ray flux is essentially constant for periods of the order necessary for age determination. The ^{14}C produced in the upper atmosphere is rapidly oxidised to $^{14}CO_2$ and once in this form, it is able to enter the carbon cycle and exchange with the reservoir carbon, comprising carbon dioxide, carbonate, organic carbon in the oceans, the air and the biosphere (Table 1.14).

Table 1.14. Carbon content of the carbon reservoir [82]

Material	g cm^{-2} earth surface
Ocean carbonate and bicarbonate	7.25
Dissolved organic matter	0.59
Biosphere	0.33
Atmosphere	0.12
Total	8.3

The natural secular equilibrium content of ^{14}C in the reservoir prior to thermonuclear weapon testing was about 1.2×10^{-12} g g^{-1}; which gave a ^{14}C activity of 16 disintegrations per minute per g of carbon. This abundance was affected by the addition of fossil carbon (dead carbon, containing no ^{14}C) from the combustion of coal and petroleum and the proportion of ^{14}C was reduced to 98% of the pre-Industrial Revolution equilibrium value. Subsequently, thermonuclear explosions which produce ^{14}C both directly and by the reaction of their neutron flash with the nitrogen of the atmosphere have added to the ^{14}C content of the reservoir. As a result, the ^{14}C activity in the atmosphere is now about 28 disintegrations per minute per g of carbon.

^{14}C decays by β-emission with a half-life of 5683 $\pm$ 35 years.[76] With current high sensitivity counting techniques, the maximum age range of the method is around 50,000 years at which age the statistical counting error becomes large. The method may be used to determine age provided no carbon is added to or lost from the system, no isotopic fractionation occurs and the fossil is rapidly removed from its equilibrium with the ^{14}C reservoir. Comparison of materials with different chemical properties from the same site, should lead to an absolute age, but the method is subject to a number of possible errors:-

(1) In old samples with a low ^{14}C activity , the statistical counting error may be high.

(2) There is evidence that the isotopes of carbon are fractionated in nature. Craig [83] showed that the $^{13}C/^{12}C$ ratio of carbonate exceeds that of organic matter by 2.6%

(3) Chemical exchange of ^{14}C with dead carbon occurs

(4) The exchange reservoir may be incompletely mixed. Nydal [84] found that the average residence times for the mixing of ^{14}C with various reservoirs ranged from two months to five years depending on the reservoir (stratosphere, troposphere or ocean mixed layer plus biosphere). For mixing of the troposphere with the ocean, the average life time was 4.5 ± 1.0 years.

(5) For very old samples, some of the ^{14}C content may have been produced by nuclear reactions in the earth.

(6) There is some evidence for the variation in the production rate of ^{14}C with sunspot activity [85]. This has been supported by evidence for fluctuations of the ^{14}C content of the atmosphere by determination of the ^{14}C content tree rings of a bristlecone pine [86]. As a result, it has been necessary to calibrate the radiocarbon time scale for the conversion of radiocarbon dates into true ages, given by the tree ring sequence.

The ^{14}C dating technique is particularly important in groundwater tracing. It is similar in principle and is used as a complement to the tritium method. The half-life of 5685 years makes it possible to date groundwaters as old as 40 - 50,000 years, compared with 50 years with tritium, but the method has

the disadvantage that the ^{14}C is present in dissolved compounds in the groundwater, not as part of the water molecule. Therefore, the carbonate content of the groundwater is an important consideration in interpretation. The method has been used for identifying ancient recharge, calculating groundwater flow rates and calculating mixing components.

The analytical result of a ^{14}C determination is commonly expressed as the percentage of ^{14}C present relative to a modern, pre-thermonuclear standard (% mod). The apparent age of a groundwater is given by the equation:

$$t = 8267 \ln {}^{A_o}/_{A_t} \qquad (1.6)$$

where t = time in years

8267 = mean life of ^{14}C, years

A_t = ^{14}C activity of sample (counts min^{-1} g^{-1} C)

A_o = ^{14}C activity of standard (counts min^{-1} g^{-1} C)

If all the carbon dissolved in a groundwater is in the form of carbon dioxide and is of biogenic origin, and no dilution with dead carbon has occurred, t represents the time since recharge occurred. Such a situation is extremely rare in nature. Normally, the situation is complicated by processes occurring within the aquifer, such as the dilution by non-radiogenic carbon and the mixing of waters of different ages.

Various procedures have been reported for correction for the dilution by non-radiogenic carbon.[87] One widely used technique is based on assessment of the simple dilution of biogenic carbon by rock carbon from the measured $^{13}C/^{12}C$ ratio of the total dissolved carbonates in the groundwaters.[88]

Evans et al[75] identified two distinct stages of ^{14}C dilution. Firstly, congruent solution, which involves the simple dissolution of bedrock carbonate by the dissolved biogenic carbon dioxide principally by:

$$CaCO_3 + CO_2 + H_2O \rightleftharpoons Ca^{2+} + 2HCO_3^-$$

Secondly, incongruent solution, involving continuous solution and reprecipitation of carbonate minerals, for example:

$$CaCO_3(s) + H_2O \rightleftharpoons CaCO_3(aq)$$

where (s) represents solid and (aq) represents aqueous solution.

The problem with incongruent solution is that not only is ^{14}C lost by precipitation, but it is also fractionated from ^{13}C and ^{12}C by precipitation and dissolution.

A correction which allows for both ^{13}C and ^{14}C fractionation has been developed[75] which results in the relationship

$$t = 8267 \ln \frac{50}{{}^{14}C_s} \left[\frac{K - \delta^{13}C_s}{K - \delta^{13}C_i} \right] \left(1 + \frac{\epsilon_{13}}{1000} \right)$$

where t is the groundwater age, years

K is $\delta^{13}C_r - \epsilon_{13}$

ϵ_{13} is the fractionation factor for ^{13}C (i.e. $\delta^{13}C_p - \delta^{13}C_s$)

subscript s refers to the sample, r to the rock

p to precipitate and i to the initial state of the incongruent dissolution

$$\delta^{13}C = \left[\frac{{}^{13}C/{}^{12}C_{\ s} - {}^{13}C/{}^{12}C_{\ std}}{{}^{13}C/{}^{12}C_{\ std}} \right] \times 10^3$$

where subscript std refers to a standard which is defined as marine carbonate.

An alternative correction is given by Wigley [89] who firstly considers the effect of incongruent solution on the fractionation of ^{13}C, then combines this with the radioactive decay expression for ^{14}C:

$$\delta^{13}C_o - \delta^{13}C_r \approx X(\delta^{13}C_i - \delta^{13}C_r) + F(X - 1)/\alpha$$

where subscripts r, p and i are as above and o represents conditions initially which are closed to carbon dioxide.

$F = \delta^{13}C_p - \delta^{13}C_o$

$= \frac{d(mD)}{d(mP)}$, that is, the relative dissolution to precipitation contribution to mC, the total dissolved inorganic carbon molality.

mD = contribution to changes in mC by dissolution

mP = contribution to changes in mC by precipitation

and $X = \left\{ \frac{mC}{mC_i} \right\}^{\alpha/1-\alpha}$ for $\alpha \neq 1$

or $X = e^{-mP/mC_i}$, $\alpha = 1$

For ^{14}C, the corresponding relationship is

$$A \approx A_i X$$

where A is the activity (in % modern).

A third method of correction is given by Reardon and Fritz.[90] ^{14}C ages are corrected by computer modelling involving the groundwater ^{13}C and ^{14}C isotope compositions with a FORTRAN IV computer subroutine (ISOTOP) incorporated with WATEQF, a water analysis treatment program[91]. Other open- and closed-system carbonate dissolution models to adjust ^{14}C ages of groundwaters for dead carbon contributions have been developed by Mook[92] and Fontes and Garnier[93].

The effects of mixing can be significantly greater than effects of different geochemical models of the area and it is important to understand that the use of highly sophisticated mathematical procedures does not in itself imply accuracy of interpretation.

Finally, there is a statistical limitation on the maximum age that may be determined by ^{14}C dating. Since, for very old samples, the source counting rate is generally not much greater than background, both the source and background are usually counted for the same length of time, usually about 48 hours, which gives $D = S - B$

where D = background corrected counting rate for source

S = counting rate for counter filled with source

B = counter background counting rate

For a counting time t, the standard deviation error, σ, on D will be given by

$$\left\{\frac{S + B}{t}\right\}^{\frac{1}{2}}$$

If D_{min} is the minimum corrected counting rate which can be determined, then its standard deviation, $\sigma_{D_{min}}$, is

$$\sigma_{D_{min}} = \left\{\frac{S + B}{t}\right\}^{\frac{1}{2}} = \left\{\frac{D_{min} + 2B}{t}\right\}^{\frac{1}{2}}$$

$$= \frac{2B}{t}^{\frac{1}{2}}$$

since $D_{min} \ll 2B$

However, D_{min} must be (95% probable) equal to twice the standard deviation for D_{min}, i.e. $(^{8B}/_{t})^{\frac{1}{2}}$

From the radioactive decay law,

$$D_T = D_0 e^{-\lambda T}$$

where D_T = background corrected counting rate for carbon of age T.

D_O = background corrected counting rate for modern carbon. (T = O)

λ = decay constant for ^{14}C

and, therefore, T is given by

$$T = \frac{1}{\lambda} \ln {}^{D_O}/_{D_T}$$

For $D_T = D_{min}$, the age T, is the maximum age determinable, T_{max}, and is given by:

$$T_{max} = 8267 \ln \left\{ \frac{D_O}{B} \left(\frac{t}{8}\right)^{\frac{1}{2}} \right\}$$

where T_{max} and ${}^{1}/_{\lambda}$ are in years.

The value of ${}^{D_O}/_{\sqrt{B}}$ depends upon the amount of carbon source present and on the counting system, and may be used to compare counters. The best counters can determine ages as great as 40 - 50,000 years.

The problem of arriving at an absolute age is complex, but uncorrected ages may be useful for identifying ancient waters. Differences in apparent ages can be used to calculate minimum rates of groundwater movement even though the absolute ages may not be known precisely[94]. Overall, it is essential that other hydrological information supports ^{14}C measurements for a correct interpretation to be made.

1.11. U-234/U-238 TRACING

In a closed system, given sufficient time, the members of a radioactive decay series will achieve secular equilibrium, wherein the rate of production of a nuclide is equal to its rate of removal by radioactive decay. If decay is in the same mode, the ratio of the activity of any two members in secular equilibrium will be unity. The use of variations in the $^{234}U/^{238}U$ activity ratio of dissolved uranium for groundwater dating [95,96] is complicated by the fact that uranium in solution does not form a closed system [97].

The properties of the $^{234}U/^{238}U$ disequilibrium which make it potentially useful are [98] :-

(a) The isotope variation is extreme, the activity ratio of ^{234}U to ^{238}U (A.R.) varies by a factor of more than 20.

(b) The determination of the abundance of the isotopes of uranium is made relatively straightforward due to their α-radioactivity.

(c) Uranium has two common valency states, +4 and +6, which makes its chemistry sensitive to electrochemical variations.

(d) The variable isotope, ^{234}U, is a daughter of ^{238}U, and both the rate of disequilibrium development and decay are governed by the half-life of ^{234}U, 250 000 years.

Secular equilibrium between ^{234}U and ^{238}U in a bulk rock matrix will be established according to the radioactive decay

law:-

$$^{234}A_t = {}^{238}\lambda \, {}^{238}N_0 \, (1 - e^{-{}^{234}\lambda t})$$

where $^{234}A_t$ = ^{234}U activity

$^{238}\lambda$, $^{234}\lambda$ = decay constants of ^{238}U and ^{234}U respectively

N_0 = number of ^{238}U atoms present initially

and t = time.

Growth to equilibrium will be complete in 1.25 million years (m.y.) during which time the decrease in $^{238}N_0$ will be insignificant, because of its relatively long half life (4.5×10^9 years).

The mechanism by which activity disequilibrium between ^{234}U and ^{238}U in solution is caused may be of two types. Firstly, ^{234}U atoms may be preferentially leached by groundwaters because they are in positions of lattice damage caused by the α-recoil process on their formation. ^{234}U atoms are in a higher oxidation state as a result of electron stripping on recoil and are able to form soluble uranyl complexes more easily than the ^{238}U atoms. Secondly, the recoil process itself may cause enhancement of ^{234}U in solution [99], whereby ^{234}Th, the immediate daughter of ^{238}U may be recoiled directly into solution. The dissolved ^{234}Th from α-recoil will reach a

maximum equilibrium activity after about 100 days of rock/water contact. The activity of ^{234}U will reach equilibrium with the ^{234}Th activity in solution after 1.25 m.y. provided the ^{234}Th activity remains constant, that is the α-recoil process continues at a constant rate. Only ^{234}Th atoms formed by ^{238}U decay within the ^{234}Th recoil range, R, of a mineral surface can escape that surface and enter solution as a result of α-recoil. It can be shown that this is only 23.5% of all recoil atoms generated within a surface layer of thickness, R [13].

Thus, the isotopic ratio for dissolved uranium will be given by:

$$^{234}U/^{238}U = \frac{^{234}U \text{ from recoil process} + ^{234}U \text{ from chemical etch}}{^{238}U \text{ from chemical etch}}$$

The possibility of calculating the $^{234}U/^{238}U$ activity ratio therefore exists if estimates of the ^{234}Th recoil range and chemical etch rates in aquifers can be made.

The relative contributions of α-recoil and chemical etch dictate the path along which the $^{234}U/^{238}U$ activity ratio and the uranium content of a groundwater will evolve. High chemical etch rates result in above average groundwater uranium contents and an enhanced ^{234}U content can only be generated in the initial stages of surface etch if ^{234}U is etched at a greater rate than ^{238}U. These conditions are generally found in surface

and shallow waters under oxidising conditions. Such waters generally have high uranium contents and moderate disequilibria, which are relatively insensitive to change. The uranium isotope ratio and abundance in these waters have been used to determine flow patterns and mixing proportions.[96]

As the etch rate decreases, the effect of preferential etch and α-recoil increases. In deep groundwaters the concentration of uranium is often found to be low because of the evolution to a reducing environment. The ages of deep groundwaters are higher than the ages of surface groundwaters and the uranium isotopic ratio is more susceptible to change. As a consequence of these trends, the activity ratio generally increases with decreasing uranium content.[97, 100]

1.12. RADON IN GROUNDWATERS

Radon is an inert gas with twelve isotopes of short half-lives. The most abundant isotope is ^{222}Rn with a half-life of 3.825 days. Most groundwaters contain ^{222}Rn produced by the radioactive decay of ^{226}Ra in rocks. The short half-life, together with the slow movement of most groundwaters allows the ^{222}Rn in solution to be in approximate equilibrium with the ^{226}Ra in the surface of the near-by rocks.

Generally, the rate of radon release from a rock particle into water is less than the rate at which radon is produced by the radioactive decay of ^{226}Ra. This indicates that some of the radon atoms are trapped in the rock particles and decay before they can escape into the water. Andrews and Wood [13] postulate four mechanisms which may lead to the release of radon atoms into the water phase:

(a) Recoil of radon atoms following radium decay at or near the surface of the rock particle, directly into the water phase.
(b) Diffusion of radon from within the crystal lattices of the mineral phases of the rock particle, into the water phase.
(c) Recoil of radon atoms within the particle into crystal imperfections, followed by comparatively rapid diffusion to the particle surface.
(d) Release of radon by any of the above mechanisms into relatively porous secondary phases in complex rock matrices - for example into the cementing material in sandstones, followed by its rapid diffusion to the surface, possibly from deep within the rock fragment. This process would be augmented by radon produced by decay of radium contained in the secondary phase itself, and may even be the dominant process.

The contribution which the direct recoil mechanism can make may be calculated from the recoil range of ^{222}Rn in the material and the particle size. The diameter of most rock particles is very much greater than the recoil range of ^{222}Rn

(0.036 μm in glass of composition $Na_2O.CaO.6SiO_2$ [101]) and the surface may be assumed to be flat. If it is assumed that the ^{226}Ra is uniformly distributed within the material, the calculated recoil escape percentage is given by 4.9/d, where d is the particle diameter (μm) [13]. Therefore, the calculated recoil escape percentage for even a very small particle size of 100 μm diameter is only 0.049%, so this mechanism contributes to a negligible extent to radon release in most minerals.

If the mechanism of radon release is diffusion through the crystal lattice to the particle-water or air interface, the rate of radon release is again found to be inversely proportional to the particle diameter. However, the percentage radon release was found to be inversely proportional to the square root of the diameter of the particles for the Carboniferous Limestone [13]. This indicates that the predominant mechanism of radon release in this aquifer is by primary recoil or diffusion into crystal imperfections, followed by rapid diffusion to the particle surface.

Radon released at the surface of rocks will be carried into the surrounding air or water by diffusion or solution transport. The concentration gradient normal to the rock surface caused by diffusion alone will be given by:

$$N_x = N_o e^{-x/\sqrt{1}}$$

where N_x = number of radon atoms at a distance x from the rock surface.

N_o = number of atoms at the surface

1 = diffusion length

$= D/\lambda$

where D = diffusion coefficient of ^{222}Rn

λ = decay constant for ^{222}Rn

The concentration gradient normal to the rock surface caused by solution transport is given by:

$$N_x = N_o e^{-\lambda x/v}$$

where, N_x, N_o, λ, and x are defined as for diffusion transport

v = velocity of movement of the water normal to the surface.

The relative contributions of diffusion and solution transport are compared in Figure 1.8, from which it is evident that solution transport is much more effective than diffusion in causing the migration of radon in an aqueous phase.

The close relationship of ^{222}Rn to ^{238}U, and the ease of detection of very small amounts with simple apparatus, make ^{222}Rn a good tool for prospecting for uranium [102].

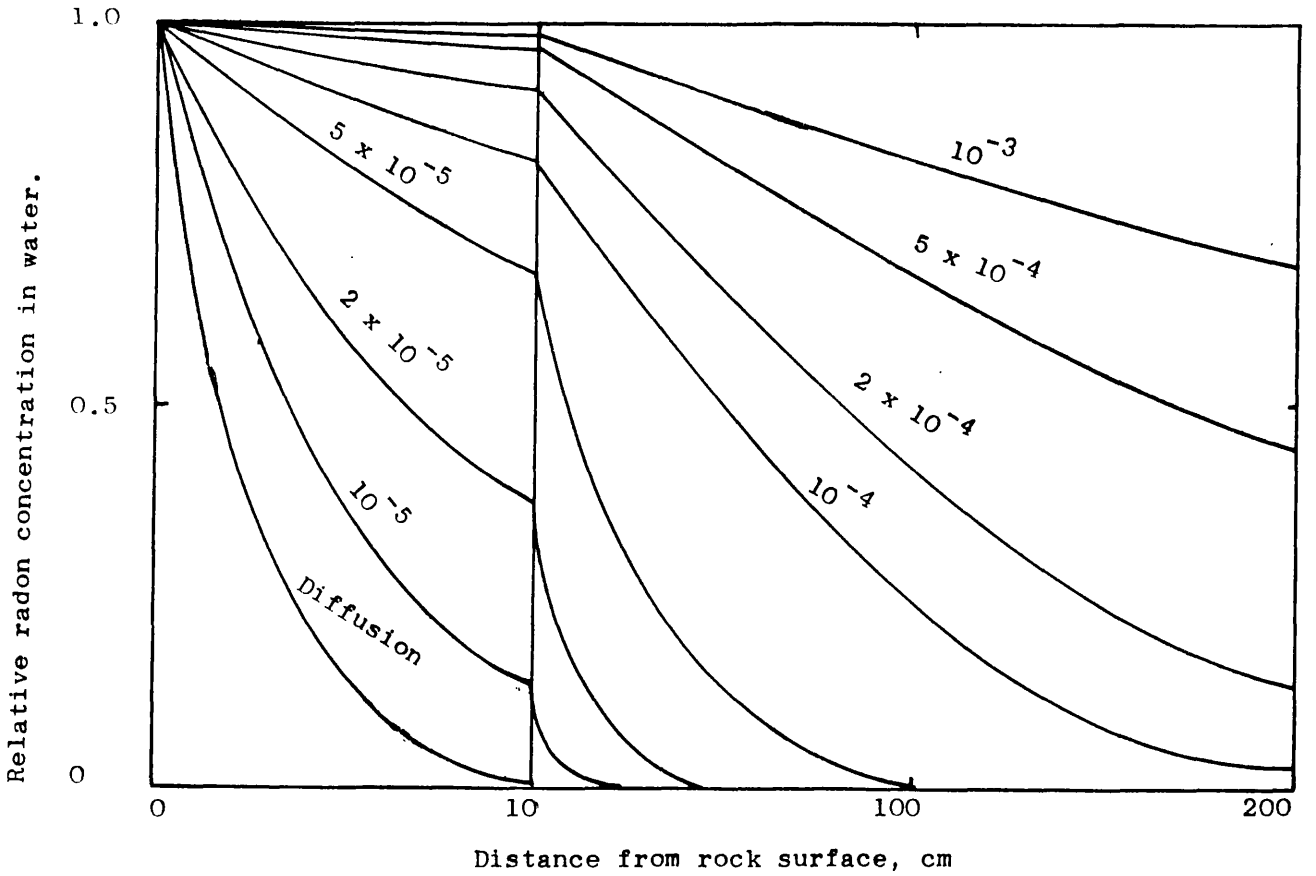

Fig. 1.8. Relative radon concentrations in water adjacent to rock surface due to radon movement by diffusion and by transport for various transport velocities (cm s^{-1}) [13]

^{222}Rn is also potentially useful for locating geothermal reservoirs because the amount of ^{222}Rn present in geofluids depends on the geological properties of the formation from which the radon is derived and the mechanism by which the fluid interacts with the geological formation [103]. High concentrations of ^{222}Rn have also been observed in groundwaters associated with underground reservoirs of oil, gas and brine [22] in thermal springs in the proximity of volcanic activity [104] and in the vicinity of faults [105]. In such situations, ^{222}Rn is a useful qualitative geochemical tool.

1.13. RADIUM IN GROUNDWATERS

Equilibrium between ^{238}U and ^{226}Ra in a uranium bearing mineral will be established according to the equation:-

$$A_t = A_e(1 - e^{-\lambda t}) \qquad (1.7)$$

where A_t = activity of ^{226}Ra at time t

A_e = equilibrium activity of ^{226}Ra

λ = ^{226}Ra decay constant.

Provided there is no geochemical separation of ^{238}U and ^{226}Ra, equilibrium will be established in about 8000 years. The time taken for equilibrium to be established is small compared with the timescale of geological and geochemical events and in most cases ^{226}Ra will be in radioactive equilibrium with ^{238}U in the bulk mineral.

Radium may be dissolved in a groundwater either by chemical etch effects or by an α-recoil effect. Chemical etch of mineral or rock surfaces will result in the solution of both ^{238}U and ^{226}Ra in radioactive equilibrium, provided there is no selectivity in the etch process. This situation is rare because the chemical conditions under which radium enters solution are very different to those under which uranium enters solution. Solution of radium, for example, is favoured in waters with a high chloride ion concentration and radium behaves chemically, similar to barium and calcium. Uranium, on the other hand, dissolves mainly in the form of the complex uranyl ion in oxidising conditions and is deposited in reducing conditions. Radium will be precipitated in carbonate waters as the highly insoluble carbonate and in sulphate waters as the sparingly soluble sulphate.

^{226}Ra may also enter solution by direct α-recoil. Following decay of the uranium daughter ^{230}Th, recoil ^{226}Ra atoms situated on or near the surface of a rock may be energetically ejected into the water phase. The ^{226}Ra activity due to recoil atoms entering solution will increase with time according to equation 1.7. and will reach a maximum after about 8000 years. The contribution of the α-recoil process for ^{226}Ra solution will therefore only be significant for old groundwaters.

Because of the different conditions under which ^{226}Ra and ^{238}U dissolve and the dissimilarity of their chemical behaviour in solution, ^{226}Ra is rarely found in radioactive equilibrium with ^{238}U in groundwaters.

1.14. INERT GASES IN GROUNDWATERS

1.14.1 Helium

Helium is being continuously produced in the earth's crust by the radioactive decay of the uranium and thorium series. The wide geochemical distribution of uranium and thorium in rocks gives rise to a wide dispersal of helium in the crust. Depending on the structure at its site of production, helium is either retained or diffuses away. The degree to which helium is retained at its site of production is important when considering both the determination of the geological age of rock samples by the helium method and the use of helium as a groundwater tracing technique. So a discussion of helium as a hydrological tracer would not be complete without discussing the helium age method.

The possibility that helium accumulation could be used for measuring geological time was suggested by Rutherford [106]. Strutt [107,108] studied the accumulation of helium in pitchblende and thorianite and found that a sample of thorianite contained 280 million times as much helium as was subsequently generated in the same mineral in a year. However, leakage of helium from these minerals indicated that only a minimum age could be determined.

Diffusion of helium from radioactive minerals is the most important limitation of the method, and because of this reason, work on the method for age determination diminished for a number of years. Interest was revived in the method by the work of Keevil [43], who found that some minerals retained a higher

proportion of the total helium generated in them than others. For example, ferromagnesian minerals generally retained more helium than feldspars and quartz, acid felsitic and glassy rocks were particularly low in helium content, and mafic rocks had generally higher helium retentivity which decreased with increasing age. Gerling [44] concluded that loose packed crystal structures, common in rock forming minerals, would be least likely to retain helium and that the presence of inclusions would also encourage helium loss.

Much work followed on the diffusion of helium from minerals [107-109]. Undisturbed crystals of zircon, magnetite and sphere were found to retain helium so that no measurable loss is observed in 10^9 years [41]. However, the diffusion constants in quartz and feldspar are much greater and ages determined from these minerals tend to be low compared with those determined from zircon, etc. The difference between the two sets of minerals lies in the fact that uranium and thorium substitute throughout the structure in zircon, magnetite and sphere, whereas in quartz and feldspar, the radioelements occur largely in small imperfections and inclusions and on the surfaces of fractures. So although the helium content of quartz and feldspar can be measured easily, a large proportion of it may be due to radioactive contamination.

Radiation damage caused by high concentrations of radioelements in localised centres that become intensely irradiated will also allow helium to escape, as will metamorphism and faulting.

Another problem is the difference in chemical mobility of uranium, thorium and helium; once helium is "locked into" the crystal structure of a mineral, the remaining uranium may be mobilised and the measured alpha-activity may be very different from the original alpha-activity.

Despite these problems, the helium dating method has found some applications. Schaeffer [110], applied the method to the dating of fossil carbonates. He found that while a calcite lattice does not appear to retain helium, an aragonite lattice does, at least for ages up to 20 million years. For corals, uranium is apparently distributed uniformly within the lattice as a trace element, and does not exchange or undergo concentration.

An investigation of zircons by Damon and Green [111] indicates that when uranium and thorium have a secure place in the crystal structure the helium dating method yields ages which compare favourably with the potassium/argon ages. However, metamict minerals are the exception to this generalisation because radiation damage produces a glass phase which is permeable to helium. The problems inherent to the helium method and the potassium/argon method are similar under these circumstances but the helium method is probably more sensitive to thermal events.

Once helium has diffused from within the crystal lattice it may then diffuse rapidly through the rock interstices and ultimately become dissipated into the atmosphere, trapped in underground reservoirs or dissolved in groundwaters.

Water virtually devoid of uranium and thorium decay products will enter the ground from the atmosphere and flow through the interstices of a porous rock. Some of the helium produced by the radioactive decay of uranium and thorium will remain in the rock, some will dissolve in the groundwater. If the helium generation rate is known and the uranium and thorium content of the rock is known, then the minimum residence time of the water in contact with this type of rock can be determined from the helium content of the water, assuming that the transfer rate of helium into the water from the rock is known. The method is limited by the fact that the uranium and thorium content of the rock for the whole path of the water must be known, or, at least, a good average must be available. Also, the transfer rate of helium from the rock to the water is not readily available, although it may be estimated from the diffusion coefficients of helium in different environments. The diffusion of helium into and away from the groundwater also imposes restrictions on the method. Helium may diffuse into the groundwater contained within an aquifer from confining rocks, from associated waters with higher helium contents, or from deep within the earth's crust. In this situation the calculated age would be high compared with the true age. The calculated age may also be low, if helium diffuses away from the groundwater or helium is not transferred as efficiently as predicted from its site of production.

The limitations have led to the helium contents of groundwaters being interpreted qualitatively rather than quantitatively. Clarke and Kugler [112] used the fact that minerals with a high uranium content tend to lose helium easily, because of lattice damage, to suggest that groundwaters in association with uranium occurrences would be high in helium. High helium contents in groundwaters have also been associated with faults that transport helium [113], petroleum hydrocarbon deposits [114] and for locating geothermal reservoirs [115].

1.14.2. Radiogenic argon

One of the assumptions necessary for the potassium/argon dating method for minerals and rocks to give correct ages is that no argon leakage occurs from the site of production. For some important minerals, this assumption holds, but, for many minerals there is a significant diffusion of ^{40}Ar out of the crystal lattice in which it was produced. Once free of the crystal lattice, the radiogenic argon will diffuse rapidly through the interstices of the rock in which it was formed and may dissolve in groundwaters. Because of the relatively large volume of ^{40}Ar which dissolves when a groundwater equilibrates with air in the soil zone, any slight enhancement by addition of radiogenic argon is difficult to detect.

The number of radioactive atoms which decay in a time interval, t, is governed by the radioactive decay law and is given by:-

$$N_o - N_t = N_o(1 - e^{-\lambda t})$$

where N_o = number of atoms present initially

N_t = number of atoms remaining at time, t

λ = radioactive decay constant.

Applying this to the case of ^{40}K decay, the number of atoms of ^{40}K which have decayed will be equal to the number of atoms of ^{40}Ar produced. Considering an average rock containing 6% potassium and with a density of 2.6 g cm^{-3}, the volume of radiogenic argon produced, V^*_{Ar}, will be given by:-

$$V^*_{Ar} = 1.16 \times 10^{-3}(1 - e^{-\lambda t}) \text{ cm}^3 \text{ STP cm}^{-3} \text{ rock}$$

Considering an average rock porosity of 15% and assuming that all the ^{40}Ar generated in a time, t, is dissolved in the interstitial fluid, the volume of radiogenic ^{40}Ar dissolved in the fluid in a time t will be:

$$7.73 \times 10^{-3}(1 - e^{-\lambda t}) \text{ cm}^3 \text{ STP cm}^{-3} \ H_2O$$

The volume of argon dissolved by a groundwater when it equilibrates with soil air at a temperature of 10^oC and a pressure of 1 atmosphere is 4.0×10^{-4} cm^3 STP cm^{-3} H_2O. The ratio $^{40}Ar/^{36}Ar$ in the atmosphere is 295.5, so the volumes of each isotope present are:-

^{40}Ar: 3.986×10^{-4} cm^3

and ^{36}Ar: 1.349×10^{-6} cm^3

Therefore, the $^{40}Ar/^{36}Ar$ isotopic ratio of the total argon dissolved in a groundwater in the model aquifer is given by:-

$$^{40}Ar/^{36}Ar = \frac{3.986 \times 10^{-4} + 7.73 \times 10^{-3}(1 - e^{-\lambda t})}{1.349 \times 10^{-6}}$$

where t = residence time of the groundwater, years

λ = decay constant of ^{40}K (5.33×10^{-10} year^{-1})

Table 1.15 Calculated values of $^{40}Ar/^{36}Ar$ for model groundwater

Groundwater age, t, years	$^{40}Ar/^{36}Ar$
0	295.5
10^5	295.8
10^6	298.5
5×10^6	310.7
10^7	326.0

The calculated values of the $^{40}Ar/^{36}Ar$ ratio for model groundwaters of various ages are given in Table 1.15. The model assumes firstly that all the argon generated in a rock is dissolved in a groundwater. This is not necessarily true as some minerals retain argon quantitatively.

Minerals releasing only a fraction of the argon produced would result in the $^{40}Ar/^{36}Ar$ ratio being lower than predicted.

A second assumption is that the amount of argon dissolved depends on the residence time of the groundwater. However, the total amount of argon present in an aquifer will depend on the age of the aquifer, provided no argon has been removed by groundwater. If there is a residual argon excess, then the

observed $^{40}Ar/^{36}Ar$ ratio would be higher than the predicted ratio.

For the above reasons the residence time of a groundwater must be long for enhanced $^{40}Ar/^{36}Ar$ ratios to be detected. Once detected, these ratios can only be interpreted qualitatively. Enhanced $^{40}Ar/^{36}Ar$ ratios have been observed for some ancient groundwaters.[116,117]

1.14.3. Neon, argon, krypton and xenon

Not only the radiogenic inert gases have proved useful in hydrological tracing, but the non-radiogenic gases have also proved useful. Because the gases are chemically inert, they do not undergo chemical exchange once they have entered the hydrological cycle. In systems where no physical fractionation occurs, the inert gas content of the abstracted groundwater reflects the conditions which prevailed when the water was recharged. Therefore, the occurrence of neon, argon, krypton and xenon in a groundwater in proportion to their atmospheric abundances and solubilities, indicates that the water had a meteoric origin[117]. By applying the temperature-solubility curves (appendix 4) to the observed concentrations of non-radiogenic argon and krypton and xenon, the original surface temperature at the time at which the water was recharged may be determined.[118]

In systems where the gases are fractionated by various physical processes (distillation, reequilibration at elevated temperatures, spontaneous steam release, etc.) the inert gas content may prove useful in recognising these phenomena.

Mazor [116] discusses the potential of non-radiogenic and radiogenic inert gases as tracers in geothermal reconnaissance surveys, studies of steam separation mechanisms and follow up of geothermal field exploration.

CHAPTER 2

EXPERIMENTAL METHODS

2.1. GROUNDWATER ANALYSIS

2.1.1 ^{226}Ra and ^{222}Rn in groundwaters

2.1.1.1 Sample collection

The average concentrations of ^{226}Ra and ^{222}Rn in groundwaters are around 0.1 - 0.4 pCi Kg^{-1} and 50 - 700 pCi Kg^{-1} respectively. In order to achieve 2% counting statistics (2σ) on a 20 Kg water sample it is necessary to count for 10.4 hours for ^{226}Ra (0.2 pCi Kg^{-1}) and 37.5 seconds for ^{222}Rn (200pCi Kg^{-1}). Generally therefore, samples were collected in 5 or 20 l glass bottles, and used to determine both ^{226}Ra and ^{222}Rn. In groundwaters where the ^{222}Rn content was very much higher than average, glass bottles as small as 500cm^3 were used for sampling. Samples for ^{226}Ra determination were occasionally collected in 20 l polyethylene bottles when sampling was difficult because of the inaccessibility of the source (for example in Cornish tin mines). However, these samples could not be used for ^{222}Rn determination because of the diffusive loss of ^{222}Rn through polyethylene. Because ^{226}Ra was determined by the equilibrium ^{222}Rn content, samples collected in polyethylene bottles were transferred to glass bottles before outgassing and storing for radioactive equilibrium to be established.

Samples for ^{222}Rn determination were collected as quickly as possible with as little aeration as possible so that ^{222}Rn was not lost by equilibration with air. In order to achieve this, bottles were filled from the bottom (Figure 2.1), then flushed through with a further volume of water so that equilibration occurred only over a small surface area at the neck of the bottle. ^{222}Rn was determined as soon after

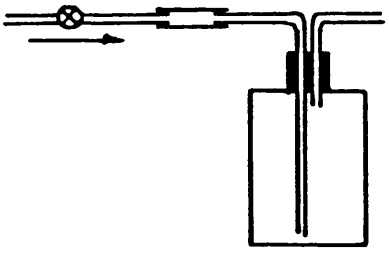

From pipe with tap

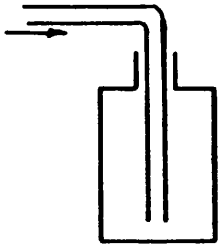

From fast flowing pipe

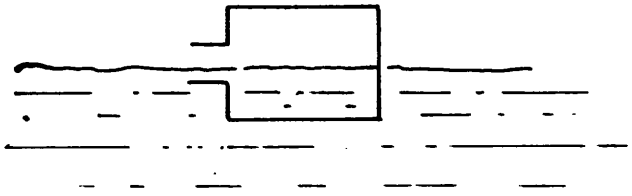

From a well

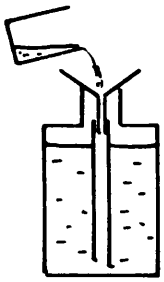

From a shallow well or stream

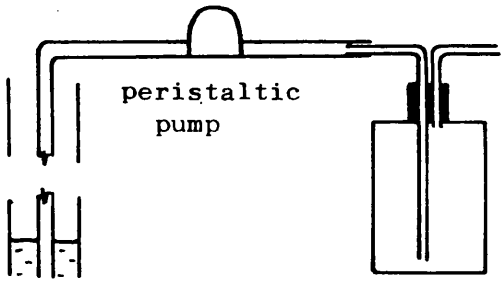

From a deep well

Fig. 2.1 ^{222}Rn sampling methods

collection as possible, because any excess ^{222}Rn present started to decay as soon as it was removed from equilibrium with the aquifer rock.

2.1.1.2. Determination of ^{222}Rn and ^{226}Ra by α-scintillation counting.

Radon-222

The ^{222}Rn content of samples in which the total radon activity was less than 10^5 pCi was determined by α-scintillation counting. ^{222}Rn in 500 cm^3 to 20 l glass bottles was outgassed with ten times the solution volume of ^{222}Rn free nitrogen bubbled through a number 1 porosity sintered glass disc at a flow rate of around 1.4 l min^{-1}. Andrews and Wood [13], found that 99% of the radon activity could be recovered by this procedure. The gas stream was dried by passing through a "U" tube held at 0^oC and $CaCl_2$ and $CaSO_4$ drying columns. ^{222}Rn in the gas stream was adsorbed on an activated charcoal trap held at -80^oC - solid CO_2/ethanol. (Figure 2.2).

The charcoal trap was subsequently removed from the drying system and connected to a vacuum line at one end and through a drying tube to an evacuated 50cm^3 conical flask coated internally with a ZnS(Ag) scintillator at the other end, maintaining it at solid CO_2 temperature. (Figure 2.3). The charcoal trap was then pumped down to a pressure of 0.1 mmHg to remove excess water vapour, N_2 and CO_2, then closed off. The trap was heated to 200^oC to desorb ^{222}Rn which was flushed into the evacuated scintillation flask by slowly admitting a stream of dry air through a needle valve. When the system pressure had reached

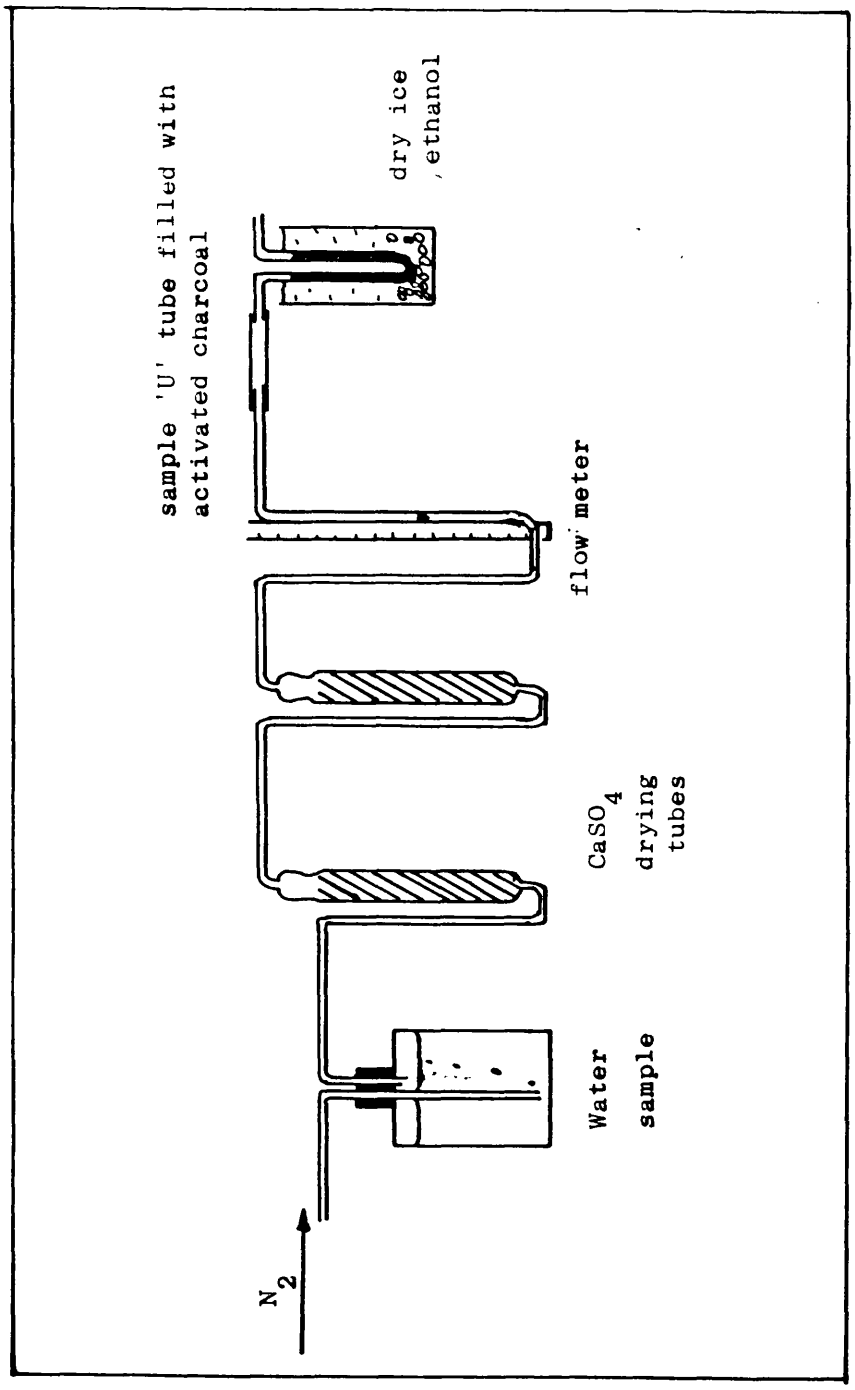

Fig. 2.2 ^{222}Rn outgassing and drying apparatus.

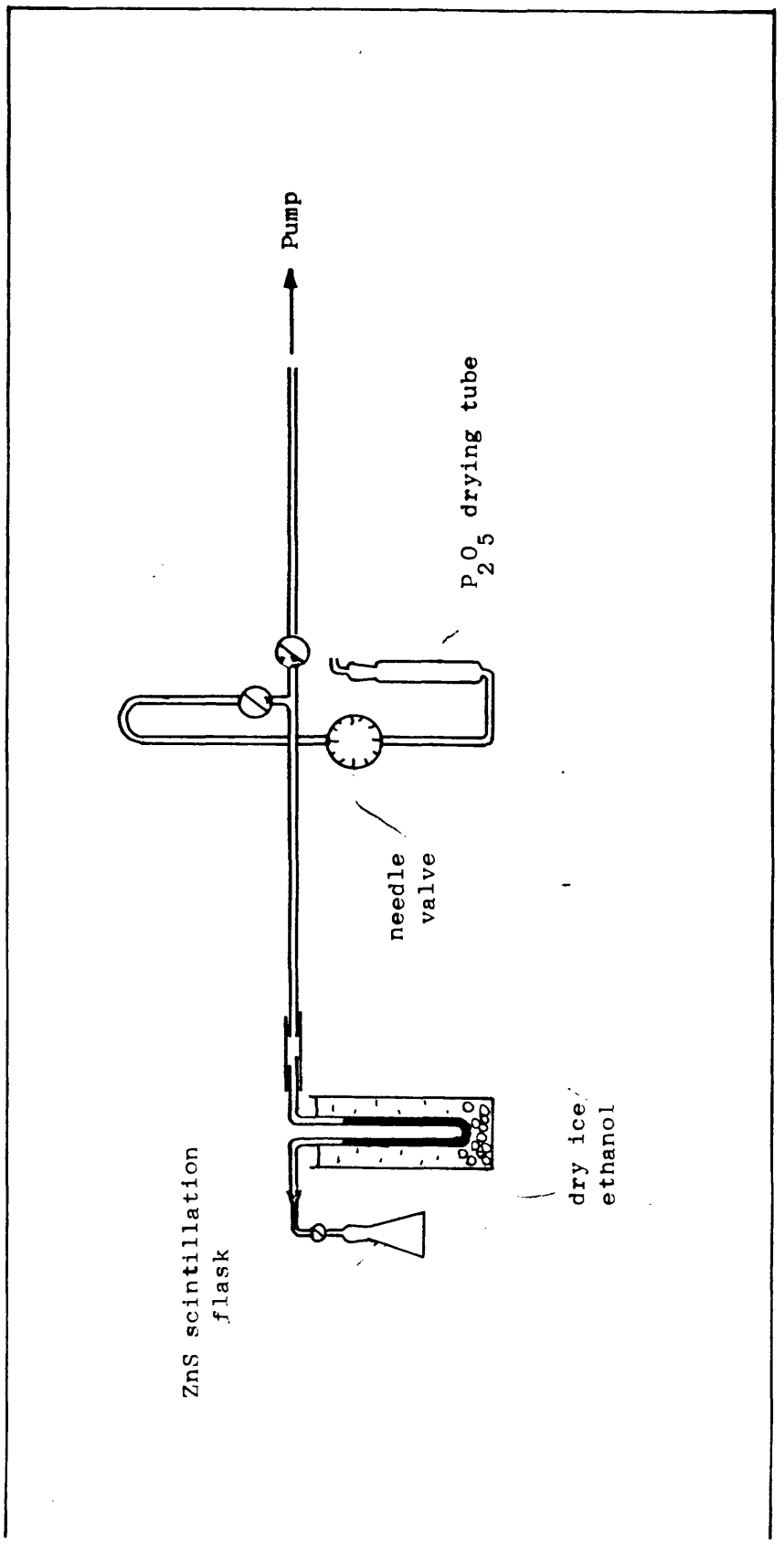

Fig. 2.3. ^{222}Rn vacuum extraction line.

atmospheric pressure, the stopcock on the conical flask was closed. The conical flask was then detached from the system and stored to allow equilibrium to be established among the short-lived daughters of ^{222}Rn:-

$$^{222}_{86}Rn \xrightarrow[3.825\ days]{\alpha} {}^{218}_{84}Po \xrightarrow[3.05min.]{\alpha} {}^{214}_{82}Pb \xrightarrow[26.8min.]{\beta} {}^{214}_{83}Bi \xrightarrow[19.9min.]{\beta} {}^{214}_{84}Po \xrightarrow[1.6 \times 10^{-4}\ sec.]{\alpha}$$

In-growth of the $^{214}_{84}Po$ activity was established in about $2\frac{1}{2}$ hours (>5 half-lives of $^{214}_{82}Pb$) after which time the flask was counted on the photocathode window of a 3" diameter photomultiplier (EMI type 9708 kA). (Appendix 2.2). The α-particle counting rate was corrected for flask background and ^{222}Rn decay during the time elapsed since the water sample was collected. The flask backgrounds, due to the build up of non-volatile ^{210}Pb which decays to an α-emitting daughter, ^{210}Po, were determined at regular intervals by counting the evacuated scintillation flasks alone.

The scintillation flasks and counting system were calibrated by loading the flasks with ^{222}Rn outgassed from equilibrated ^{226}Ra standard solutions. These solutions were prepared by dissolving a standardised radium salt (Radiochemical Centre, Amersham, Bucks) in 0.1 M HCl containing some $BaCl_2$ carrier.

The scintillation flasks were prepared by coating the walls of a $50cm^3$ conical flask with silicon grease, then shaking with ZnS(Ag) scintillator. This left the base of the flask as a window through which the scintillations could be counted. Little change in the detection efficiency was observed when the window of the flask as well as the walls were coated with ZnS(Ag), because, although more counts were produced, a lower percentage of the total counts reached the photomultiplier.

Lucas'[119] calculations showed that the walls of the flask were much more efficient for α-detection than the window. He achieved a counting efficiency of around 61% using helium as a carrier gas for ^{222}Rn. Flask calibrations for the present work using N_2 carrier gas are given in Table 2.1, together with typical flask backgrounds. The average flask calibration is 4.39 cpm pCi^{-1} (counts per minute per picocurie). This represents a counting efficiency of 66% which compares favourably with Lucas' value using helium as a carrier gas and for filling the flask, despite the fact that the range of α-particles in He is greater than the range of α-particles in air.

Table 2.1 Typical calibrations and backgrounds of α-scintillation flasks.

Flask Number	Calibration cpm pCi^{-1}	Background cpm
1	4.18	4.42
2	4.05	3.71
3	4.70	0.79
4	4.20	1.97
5	4.40	2.43
6	4.43	1.24
7	4.66	0.44
8	4.53	0.63

(cpm = counts per minute)

Radium -226

The ^{226}Ra contents of groundwaters were usually determined on the samples used for ^{222}Rn analysis. Following ^{222}Rn determination, the groundwater samples were acidified to pH 1 with distilled 6M HCl to ensure that ^{226}Ra remained in solution. They were then further outgassed with ^{222}Rn-free nitrogen to ensure that any remaining traces of excess ^{222}Rn were completely removed. Removal of excess ^{222}Rn must be at least 99.9% efficient to avoid errors in ^{226}Ra determination because the ^{222}Rn contents of environmental waters are frequently very much greater than the ^{226}Ra contents, typically 3 orders of magnitude greater. After outgassing, the samples were stored for a minimum of 20 days to permit equilibrium between ^{226}Ra and ^{222}Rn to be established. The equilibrium ^{222}Rn was then determined by the method described for ^{222}Rn determination. The counting rate obtained was similarly corrected for flask background and also corrected for decay during the time elapsed since outgassing, rather than the time elapsed since sample collection.

2.1.1.3. Determination of ^{222}Rn by γ-spectrometry

For samples in which the total ^{222}Rn activity was greater than 0.1 Ci, the technique adopted for analysis was γ-spectrometry. An alternative technique was found to be necessary because high levels of ^{222}Rn produced a high level of ^{210}Pb which rapidly contaminated the scintillation flasks. γ-spectrometry was chosen because a rapid, straightforward technique was required and although it is much less sensitive than α-scintillation counting, high ^{222}Rn activities give good counting statistics in short counting times.

For this method, the water sample was outgassed in the same way as described for the α-scintillation method and the ^{222}Rn was adsorbed onto an activated charcoal trap. The charcoal trap was then sealed at both ends, allowed to warm to room temperature and stored so that radioactive equilibrium could be established. The 0.609 Mev (27.6%) γ-ray of ^{214}Bi was then counted by laying the charcoal trap flat on a 4" x 6" diameter NaI(Tl) crystal of a γ-spectrometer. (appendix 2.1a). The method was calibrated by similarly outgassing ^{222}Rn from equilibrated standardised ^{226}Ra solutions as in the α-scintillation method, and counting.

The calibration was found to be 1.83×10^{-3} cpm pCi^{-1}. This represents a counting efficiency of 0.3%, which compares with 66% from the α-scintillation method. The counting efficiency is dependent on the geometry of the counting system and the crystal size, but for such a large crystal (4" x 6" diameter) the counting efficiency by this technique was found to be very low.

2.1.1.4. Errors in the determination of ^{222}Rn and ^{226}Ra

Sampling errors.

Once ^{222}Rn is separated from its parent ^{226}Ra, it decays with a half-life of 3.825 days. Significant decay may occur if a groundwater resides for a few days in the borehole away from the site of ^{222}Rn production. Sampling procedures must be designed to ensure that the sample is representative of the conditions prevailing in the aquifer. Equilibration with air may be a serious source of error, particularly in samples from shallow wells and streams. ^{222}Rn will be rapidly lost from sources

with a high surface area or from significantly aerated sources. The error introduced by ^{222}Rn decay and loss cannot be assessed quantitatively, but samples in which significant aeration on collection is thought to have occurred are indicated by an asterisk in the tables of results.

Decay and equilibration with air do not affect the concentration of ^{226}Ra in a groundwater. Only chemical fractionation may alter the ^{226}Ra concentration and it has been assumed that the ^{226}Ra concentrations determined, reflect closely the concentrations within the aquifer.

Experimental errors

Experimental errors were assessed by outgassing eight ^{226}Ra standards into a scintillation flask. The results are given in Table 2.2. The 2σ error on these results is 5% and this value has been used as a representative value of the analytical error in the ^{222}Rn determinations. This error is usually much greater than the counting error in both ^{222}Rn and ^{226}Ra determination provided that the counting time is sufficiently long. The errors in the ^{222}Rn and ^{226}Ra contents of groundwaters quoted in the following chapters are taken as the sum of the analytical errors and the statistical counting errors.

Statistical errors

The background of a freshly prepared flask is about 0.5 cpm, which is produced by the ^{238}U content of the glass walls of the conical flask. This increases with use to around 2.5 cpm, which,

Table 2.2. Results from repeat calibrations of an α-scintillation flask.

Run	Calibration	
	cpm	pCi^{-1}
1		4.30
2		4.05
3		4.26
4		4.27
5		4.09
6		4.02
7		4.21
8		4.24
Average		4.18

σ = 0.105 2σ = 5%

assuming a flask calibration of 4:39 cpm pCi^{-1}, is equivalent to 0.55 pCi. Generally, the total radon activity is very much greater than background and the 95% probable error (2σ) is given by:

$$2\sigma\% \text{ error} = \frac{\pm 2\sqrt{S + B}}{C} \times 100\%$$

$$= \pm 2\frac{\sqrt{S}}{C} \times 100\% \quad \text{as } S \quad B$$

$$= \pm 2\frac{\sqrt{C}}{C} \times 100\% \quad \text{as } C \quad S$$

where S = total count in t seconds

C = corrected count in t seconds

B = background count in t seconds

A typical 20 Kg sample for radon determination, 200 pCi Kg^{-1}, will accumulate 10,000 counts in 37.5 seconds, after which time, B = 1 - 2 counts, and the 2σ error is 2% (assuming a flask counting efficiency of 4 cpm pCi^{-1} and a background of 2.5 cpm).

A 20 Kg water sample containing 0.1 pCi Kg ^{226}Ra will yield 10,000 counts in 20.8 hours, under the same conditions, and the error introduced by background consequently becomes more important (B = 3120). In this case, C ≠ S, and the 2σ error is given by

$$2\sigma\% \text{ error} = \pm 2\frac{\sqrt{S + B}}{C} \times 100$$

$$= \pm 2.5\%$$

2.1.2. Inert gases in groundwaters.

2.1.2.1. Sample collection

Samples for inert gas determination were collected in 1 cm^3 glass sample tubes between vacuum stopcocks as shown in Figure 2.4. It is important that the sample represents the condition of the groundwater in the aquifer. To ensure that this was the case, water from pumped wells was allowed to flow so that any water that had been standing in a pipe was flushed through prior to collection. By this method, equilibration of the groundwater with air was avoided and any gases present in concentrations greater than their solubility and atmospheric partial pressure determined, were not lost to the air. For streams, flushing through occurred naturally, but significant loss of excess gas to the atmosphere was likely because of the high surface area exposed to the air and the aerated flow characteristics.

It was also important to avoid trapping air within the sample during collection. The seriousness of this problem is shown in Figure 2.5 which gives the ratios of inert gas concentrations in air to those dissolved in air equilibrated water. For example, the inclusion of 0.1% by volume of air contamination adds 3% to the dissolved argon, 1.5% to the krypton and 1% to the xenon (Table 2.3), generally within the range of analytical errors. Slightly higher air contaminations may cause serious problems. However, provided that the air contamination is not too large, it may be corrected for, by using the neon content as an indicator of contamination. This correction is discussed in section 2.1.2.3.

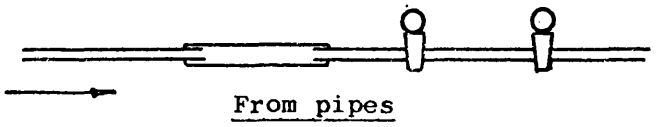

From pipes

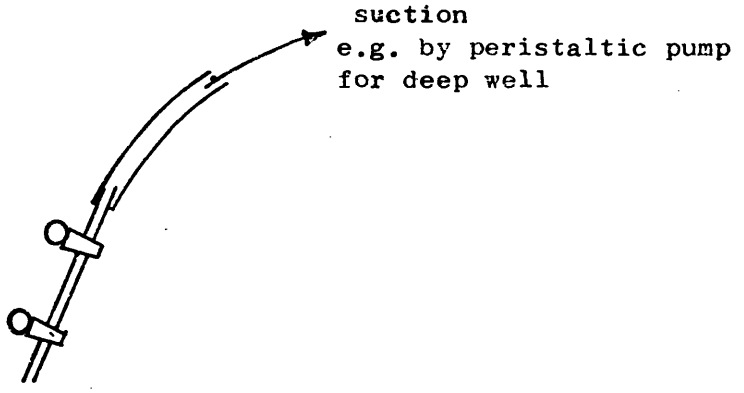

From wells or streams

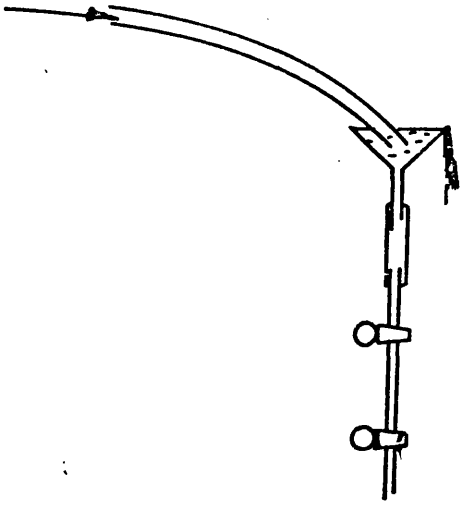

From fast flowing pipe

Fig. 2.4. Inert gas sampling methods.

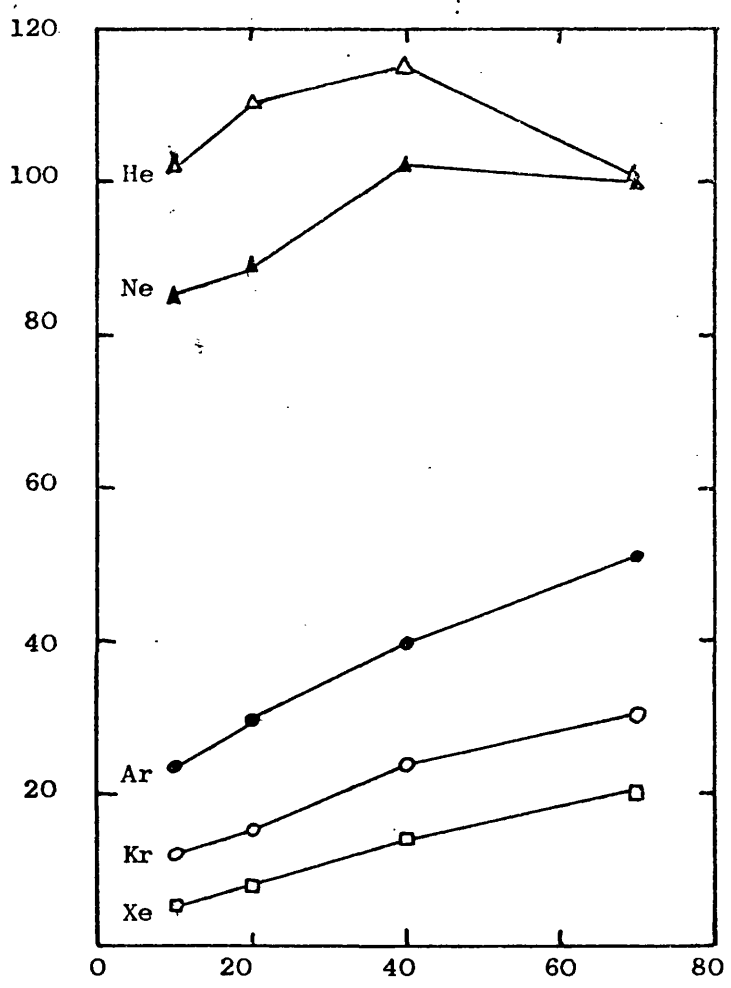

Fig. 2.5. Effect of air contamination deduced from the ratios of the amount of each inert gas in air to the amount dissolved in an equal volume of fresh water. If the collecting vessel is left half full of air this will introduce 100 times as much He as there is in the water. This value decreases to 10 for Xe. In fact, only 0.1% volume of air contamination is tolerable. (see text). [118]

Table 2.3. Effect of air contamination on inert gas contents of water.[119]

	He	Ne	Ar	Kr	Xe
a. Volume of gas in $1cm^3$ fresh water equilibrated with air at 15^oC (cm^3 STP)	4.6×10^{-8}	1.95×10^{-7}	3.5×10^{-4}	7.60×10^{-8}	10.5×10^{-9}
b. Volume of gas in $0.01cm^3$ air (cm^3 STP)	5.0×10^{-8}	1.82×10^{-7}	0.9×10^{-4}	1.14×10^{-8}	0.9×10^{-9}
c. Volume of gas in $0.001cm^3$ air (cm^3 STP)	0.5×10^{-8}	0.18×10^{-7}	0.1×10^{-4}	0.11×10^{-8}	0.1×10^{-9}
d. Volume of gas in a 1% volume air contamination i.e. a + b (cm^3 STP)	9.6×10^{-8}	3.77×10^{-7}	4.4×10^{-4}	8.74×10^{-8}	11.4×10^{-9}
e. Volume of gas in a 0.1% volume air contamination i.e. a + c (cm^3 STP)	5.1×10^{-8}	2.13×10^{-7}	3.6×10^{-4}	7.71×10^{-8}	10.6×10^{-9}
f. Volume % contamination of each gas in e	10%	9%	3%	1.5%	1%

2.1.2.2. Experimental technique

Sample tubes were sealed to the gas extraction line (Figure 2.6) with Apiezon wax and the system was evacuated to a pressure less than 10^{-5} torr with a mercury diffusion pump backed by a rotary pump. The gas separation line was then isolated from the pumping line and a metered volume of isotopically enriched tracers for the inert gases was admitted. Trap B was cooled to -80°C (solid CO_2/ethanol), trap A was heated to +80°C, and the water sample was admitted. Trap A was heated further to evaporate the water sample across to trap B, and in so doing release the dissolved gases from the water sample to mix with the tracer gases. Once the sample had been completely evaporated across to trap B, krypton and xenon were adsorbed on the charcoal trap cooled to solid CO_2 temperature. Traps A and B were cooled to liquid N_2 temperature to remove any residual water vapour and isolated from the system by closing tap 1.

Argon was adsorbed on the charcoal trap, together with krypton and xenon, by cooling to liquid N_2 temperature, and the charcoal trap was isolated. Oxygen and nitrogen were removed from the residual gas by adsorption on the titanium getter heated to 800 - 900°C by an induction coil. The remaining gases were admitted to a 2" radius, 180° magnetic deflection mass spectrometer, "Associated Electrical Industries MS10" (appendix 3.1) for isotopic ratio analysis. Isotopic ratios of helium were determined at a trap current of 50μA, a slit with of 0.01" and an electron voltage of 70V. Isotopic ratios of neon were determined at an electron voltage of 40V to eliminate interference

from $^{40}Ar^{2+}$. This ion has the same mass to charge ratio as the ion derived from the atmospherically most abundant neon isotope, $^{20}Ne^{+}$ and appears in an identical position on the MS10 mass spectrum. An electron voltage of 40V is not high enough for $^{40}Ar^{2+}$ to be formed (appendix 3.2) so interference can be avoided. After analysis, the residual helium and neon in the mass spectrometer and the vacuum line were pumped away.

Argon was released from the charcoal trap by exchanging the liquid nitrogen refrigerant for solid CO_2/ethanol. Oxygen and nitrogen were adsorbed on the titanium getter and an aliquot of the remaining gas was admitted to the mass spectrometer to determine the argon isotopic ratios, at an electron voltage of 70V. The residual argon in the system was pumped away and krypton and xenon were desorbed from the charcoal trap by heating to 200°C. The isotopic ratios of these gases were then similarly determined.

2.1.2.3. Calculation of the inert gas volumes

The volumes of inert gases released from water samples were calculated from the volume of tracer admitted and the change in isotopic ratios after mixing with the released gases. The following relationships for isotope dilution were used:

$$V_{at}(He) = V_t(He)\ \frac{^{3}x_t - {}^{4}x_t.R}{^{4}x_{at}.R - {}^{3}x_{at}} \qquad \text{where } R = {}^{3}He/{}^{4}He$$

$$V_{at}(Ne) = V_t(Ne)\ \frac{^{20}x_t - {}^{22}x_t.R}{^{22}x_{at}.R - {}^{20}x_{at}} \qquad \text{where } R = {}^{20}Ne/{}^{22}Ne$$

$$V_{at}(Ar) = V_t(Ar)\ \frac{^{38}x_t - {}^{40}x_t.R}{^{40}x_{at}.R - {}^{38}x_{at}} \qquad \text{where } R = {}^{38}Ar/{}^{40}Ar$$

$$V_{at}(Kr) = V_t(Kr)\ \frac{^{84}x_t - {}^{86}x_t.R}{^{86}x_{at}.R - {}^{84}x_{at}} \qquad \text{where } R = {}^{84}Kr/{}^{86}Kr$$

$$V_{at}(Xe) = V_t(Xe)\ \frac{^{124}x_t - {}^{132}x_t.R}{^{132}x_{at}.R - {}^{124}x_{at}} \qquad \text{where } R = {}^{124}Xe/{}^{132}Xe$$

where R = measured isotopic ratio

$V_{at}(\ )$ = volume of dissolved inert gas, cm^3 STP

$V_t(\ )$ = volume of inert gas in tracer, cm^3 STP

${}^{OO}x_t$ = mole fraction of inert gas isotope OO in the tracer

${}^{OO}x_{at}$ = mole fraction of inert gas isotope OO in the atmosphere.

These relationships assume that the isotopic composition of the dissolved inert gases is the same as that of the inert gases in the atmosphere. The volume derived from these relationships is the total volume of inert gas present in the sample. Results are expressed in cm^3 STP cm^{-3} water, by dividing this volume, $V_{at}(\ )$,

by the volume of water contained in the sample tube. The volume of the sample tubes had been previously determined by filling with mercury and weighing.

The volume of gas so derived will be seriously in error if a small air bubble became entrained in the sample during collection. The dissolved neon content served as a monitor for possible air contamination, and allowed a correction to be made.

The only source of neon in groundwaters is from the air (in contrast to helium, and possibly argon, which are often enriched by radiogenic additions). The neon sensitivity to air contamination is very much higher than that of argon, krypton and xenon (Figure 2.5), and its solubility varies least with temperature (appendix 4). At $0^{o}C$, the neon content of water equilibrated with air is 2.3×10^{-7} $cm^{3}STP\ cm^{-3}$ H_2O and this is the maximum amount of dissolved neon that a groundwater may contain, since $0^{o}C$ is the minimum possible recharge temperature. Samples which contain neon in excess of this value were considered to contain air trapped in the form of microscopic bubbles. In such cases, the inert gas contents were corrected by subtracting the neon, argon and krypton contents of small volumes of air until as close as possible agreement was obtained between the air equilibration temperatures (derived from the solubility/temperature curves) indicated by the corrected contents of these gases. Since the solubility temperature coefficients are different, this procedure leads to a unique solution for the dissolved inert gases in the sample. Once the volume of the air contamination had been established by this technique, the helium and xenon contents were similarly corrected.

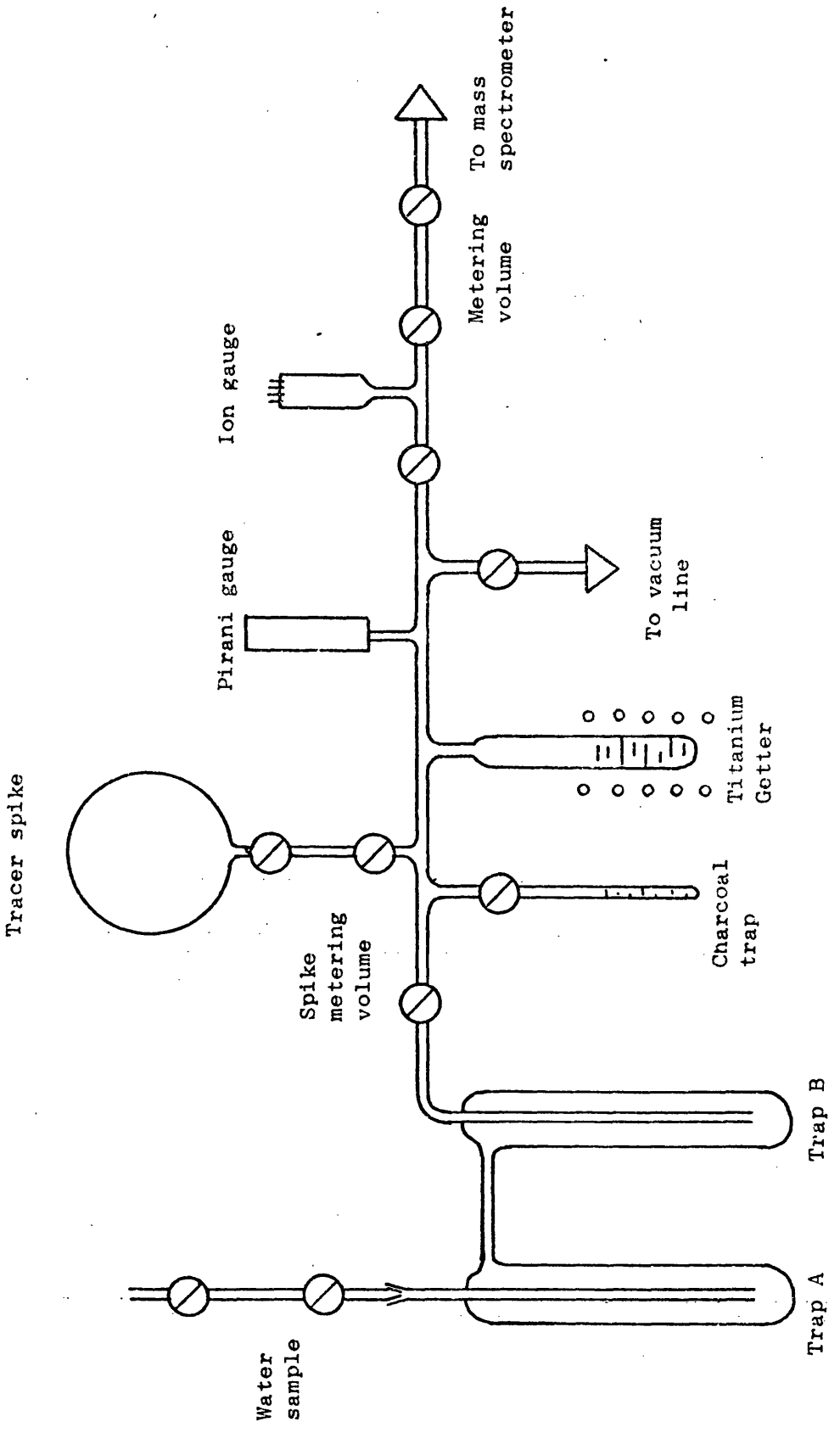

Fig. 2.6. Schematic diagram of inert gas extraction line.

2.1.2.4. Calibration of tracer ratios and volumes.

Tracer ratios

The isotopic ratios of the inert gases in the tracer were determined by admitting an aliquot of tracer into the gas extraction system, then analysing for the inert gases following the procedure used for a water sample. It was necessary to determine not only the ion currents due to the isotopes which were used in the isotope dilution calculations, but also those of the other inert gas isotopes present. This enabled the mole fraction of each isotope present to be calculated. For example for argon, not only were the ion currents for ^{38}Ar and ^{40}Ar determined, but also that for ^{36}Ar.

Initially, the values obtained for the mole fractions were within 1% of the suppliers quoted isotopic composition. However, it was found that the isotopic composition changed with time, so that it was necessary to calibrate the tracers ratios regularly (every fiftieth sample, approximately). The composition of the tracer gas changed because the inert gases diffused into and out of the tracer storage bulb. The magnitude of the change in concentration was greatest for helium because it diffuses much more readily through borosilicate glass than any of the other inert gases. The partial pressure of ^{3}He in the tracer storage bulb was greater than the partial pressure of ^{3}He in the atmosphere, so ^{3}He diffused out of the bulb. Conversely, the partial pressure of ^{4}He in the storage bulb was very much less than that in the atmosphere, and ^{4}He diffused into the bulb. This led to a gradually decreasing $^{3}He/^{4}He$ ratio in the tracer bulb. Similarly , the ratio $^{20}Ne/^{22}Ne$ in the tracer increased, although the rate of change was not as

great as that of the $^{3}He/^{4}He$ ratio. A similar process caused the $^{38}Ar/^{40}Ar$ ratio to decrease. The isotopic ratios of krypton and xenon remained relatively constant because diffusion into and out of the storage bulb is not as important for the heavier gases.

Tracer volumes

Tracer volumes were calibrated by two independent methods. In the first method, the tracer was mixed with a known volume of air, and the change in the isotopic ratios measured. Secondly, the tracer was mixed with the gas released from a distilled water sample which had been equilibrated with air at a known temperature and pressure.

The first method, air calibration, was particularly useful for calibrating the neon content, and to a lesser extent the helium and argon contents. This is shown in Table 2.4, which compares the volumes of inert gases contained in the air calibration spike with a typical water calibration sample. To admit the volumes of gases given in Table 2.4, the air spike (Figure 2.7) was operated in the following way:

1. T1 closed, T2, T3, T4, T5 opened and system pumped to ultimate vacuum.
2. T2 closed, T1 opened then closed.
3. T3 closed, T2 opened then closed.
4. T5 closed, T3 opened then closed to load spike.
5. T5 opened to deliver spike to the system.

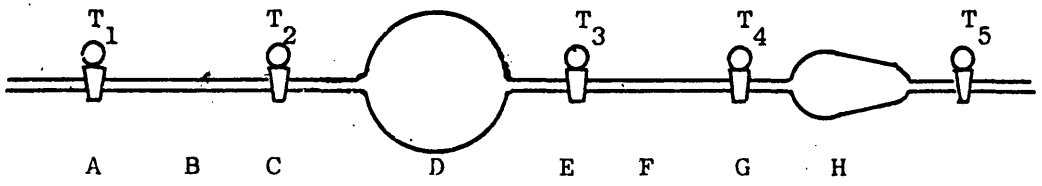

Fig. 2.7. The air spike system

Tube/key barrel	Volume (cm^3)
tube B	0.3481
key barrel C	0.0791
bulb D	61.4396
key barrel E	0.0643
tube F	0.3939
key barrel G bulb H	4.0312

Table 2.4. Typical inert gas contents of air spike and equilibrated air/water sample

	He	Ne	Ar	Kr	Xe
Partial pressure in the air (atmospheres)	5.2×10^{-6}	1.8×10^{-5}	9.56×10^{-3}	1.14×10^{-6}	8.06×10^{-8}
Volume in $1cm^3$ water at $10^{\circ}C$, atmospheric partial pressure (cm^3 STP)	4.71×10^{-8}	2.08×10^{-7}	4.02×10^{-4}	8.61×10^{-8}	1.20×10^{-8}
Volume in air spike at $20^{\circ}C$, 1 atmosphere air pressure (cm^3 STP)	12.0×10^{-8}	3.87×10^{-7}	2.05×10^{-4}	2.45×10^{-8}	0.17×10^{-8}

The gas from the air spike was mixed with an aliquot of tracer and the isotopic ratios of the inert gases were determined following the procedure used for a water sample. The volume of gas in the tracer was then calculated using rearranged forms of the isotope dilution equations. For example, for helium:-

$$V_t(He) = V_{at}(He) \frac{{}^4x_{at}.R - {}^3x_{at}}{{}^3x_t - {}^4x_t.R} \quad \text{where } R = {}^3He/{}^4He$$

As a cross check for the air calibration, a water calibration was also carried out. Several glass sample tubes were filled with distilled water which had been allowed to equilibrate with air at a measured temperature and pressure ensuring that no air bubbles were included. The tubes were then sealed to the gas extraction system and analysed by the method described for groundwaters. However, in this case, the volumes of gases in the water sample were known from the known solubility/temperature/pressure relationships, and the volumes in the tracer were calculated using the same isotope dilution equations as for air calibration. The neon content determined by air calibration was used as an indicator of air contamination. Only distilled water samples which gave a tracer neon content close to the air calibrated value were used for calibration of the tracer volumes, so that any correction for excess air present (indicated by a high Ne content) was small. Duplication of calibration was valuable as a cross check for $V_t(He)$, $V_t(Ne)$ and $V_t(Ar)$ and as an absolute calibration for $V_t(Kr)$ and $V_t(Xe)$. Calibration of $V_t(Kr)$ and $V_t(Xe)$ was more accurate by this method because of the higher abundance of these gases in an air equilibrated distilled water sample compared with the air spike (Table 2.4).

The tracer volumes as well as the tracer ratios were also subject to variation because of diffusion effects. It was therefore necessary to calibrate the tracer volumes at the same frequency as the tracer ratios, that is approximately every fifty samples.

Change in spike volumes

Sequential removal of an aliquot, volume v, from a spike system of total volume (V + v) leads to a gradual reduction of the volume of gas contained in the spike. If the initial volume of gas in the tracer storage bulb is x, the STP volumes of successive spike aliquots are given by:

1st aliquot, $V_{STP} = \left(\frac{v}{V + v}\right) x$

2nd aliquot, $V_{STP} = \left(\frac{v}{V + v}\right) \left(1-\left[\frac{v}{V + v}\right]\right)x$

$$= \frac{vV}{(V + v)^2} \; x$$

nth aliquot, $V_{STP} = \frac{vV^{n-1}}{(V + v)^n} .x$

$$\simeq \frac{v}{V} .x \qquad \text{for small v compared with V and n small}$$

Tracer spike volume

$v = 2cm^3$

$V \; 2100cm^3$

For n = 20, there is a 1.8% reduction in V_{STP}, and for n = 50, there is a 4.6% reduction in V_{STP}. This reduction is

similar to analytical error and the change in tracer volumes and ratios. The tracer volumes were therefore considered to be constant during the period covered by a tracer calibration.

Air spike volume

$v = 4.4251\ cm^3$

$V = 61.9311\ cm^3$

Clearly for the air spike, v is not small compared with V. Removal of ten aliquots results in a 46% reduction in the air spike volume and correction for reduction in successive spike volumes was necessary.

2.1.2.5. Errors in the determination of inert gases.

a) Sampling errors

Two opposite processes which occurred before or during sampling interferred with precise dissolved inert gas measurements, (a) air contamination led to an increase in the amounts of measured gases, and (b) exchange with the atmosphere before sampling caused gas losses in the case of air supersaturated thermal waters and waters containing excess helium. Air contamination was corrected for by the method outlined in section 2.1.2.3 using the neon content, but air equilibration could not be assessed. If several samples collected from the same site showed variation in their inert gas contents, the sample with the highest helium content probably most closely reflected conditions in the aquifer. In the case of air supersaturated waters, again the maximum values obtained were probably the correct ones, but if the contents of several samples from the same site were similar, the average content represented the best value that could be determined. These considerations were taken into account when choosing representative values for the inert gas contents of the groundwaters studied.

Once the sample had been collected, care was taken that the inert gas content of the groundwater remained constant during transportation and storage. For the heavy gases, this was not a problem. However, in samples with a significant amount of radiogenic helium, loss by diffusion occurred if the samples were stored for a long time. To minimise helium losses, samples were stored in a refrigerator at a temperature just greater than $0^{o}C$ during the time between collection and analysis and were analysed as soon as possible after collection. Nevertheless, correction for helium loss was found to be necessary. A calibration curve for helium loss was constructed by analysing several samples collected on the same day from a site with a significant amount of excess helium (Bath Thermal Spring) over a period of time (Figure 2.8). This method of correction for helium loss was used by Mazor [118] and his experimental values are also indicated in figure 2.10.

Groundwater samples in which a significant amount of helium is thought to have been lost by exchange with the air prior to collection are indicated in the tables of results by an asterisk.

b) Non systematic experimental errors.

The first stage of inert gas analysis involved sealing a $1cm^{3}$ sample tube to the extraction line and pumping to a pressure less than 10^{-5} torr. The light inert gases may, by this process, be pumped through a poorly greased stopcock and results from samples in which the grease on the stopcocks had streaked were discarded.

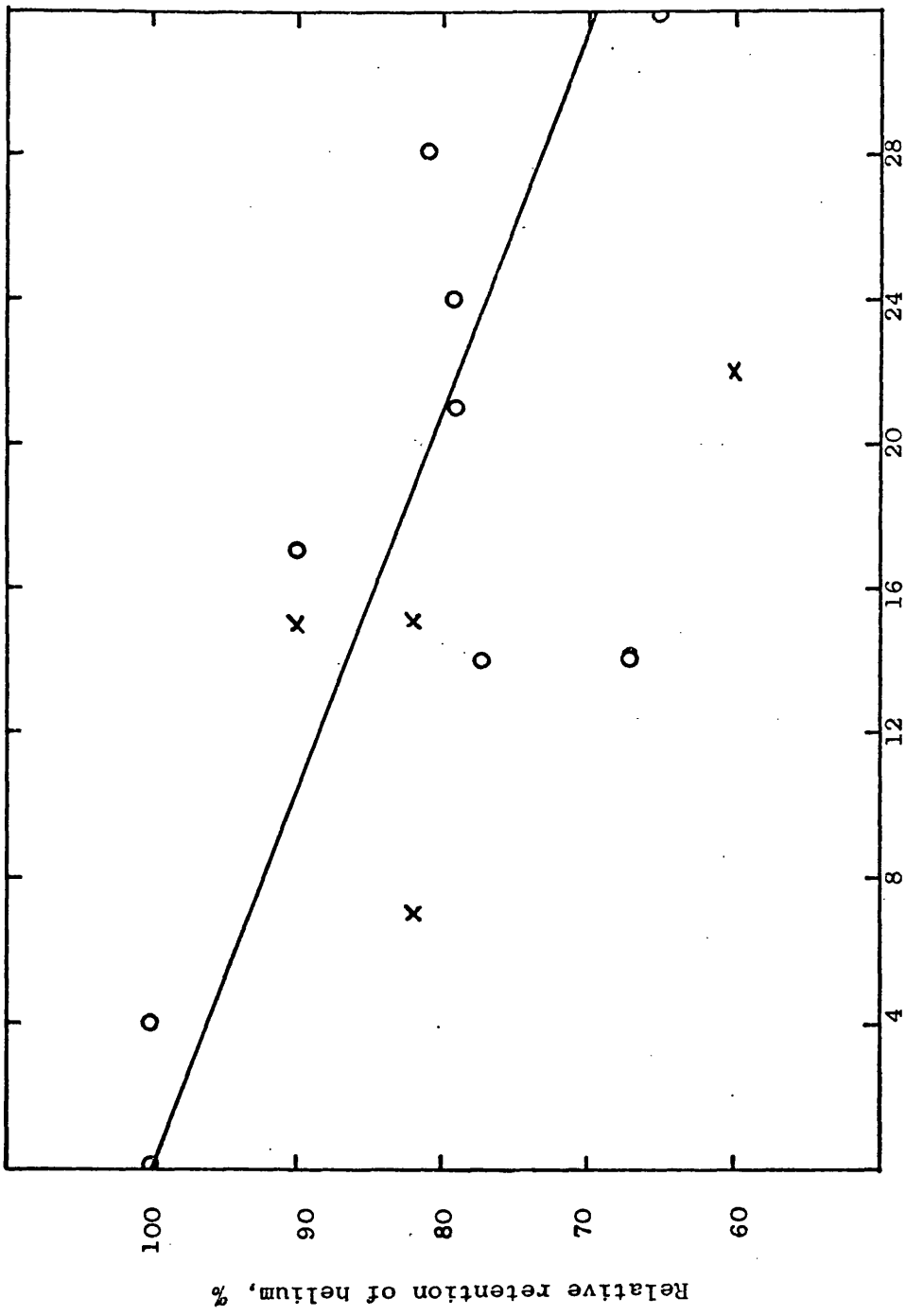

Fig. 2.8. Calibration curve for correction for ^{4}He losses during storage of samples.

o represent series of measurements on King's Spring, Bath

x represent values from Mazor et al. (1972)

Incomplete mixing of the gases released from the water sample with the tracer gases may also be a cause of errors. However, by analysing samples in which the evaporation was performed several times (trap A → trap B → trap A → trap B), the results were not found to differ significantly from samples from the same sites on which only one evaporation had been performed. Incomplete mixing therefore does not cause a significant error.

There is a possibility that helium may be lost from the gas extraction line by diffusion during sample preparation, and this error must also be considered. The overall experimental error for each inert gas was assessed by analysing a series of standard distilled water samples. The error was different for each gas because of the difference in physical properties (diffusion) and concentrations. Analytical errors were found to be $\pm$ 13.4% for helium, $\pm$ 4.6% for neon, $\pm$ 3.6% for argon, $\pm$ 2.2% for krypton and $\pm$ 5.0% for xenon. The tracer calibrations are subject to the same errors as the inert gas determinations. Calculation of the overall inert gas errors involves using the tracer calibration values. So errors in the tracer calibrations are accounted for in the overall inert gas errors given above.

c) Mass spectrometry errors

Errors may occur if the ion current due to the mass spectrometer background is the same order of magnitude as the ion current due to the mixture of sample plus tracer. For all the samples determined the background was found to be negligible as the operating pressure of the mass spectrometer was kept below 10^{-8} torr except during sample analysis.

The percentage error for measuring low ion currents is larger than the percentage error for high ion currents. Thus the smaller the abundance of the isotope, the less accurately it could be determined. The variation in the mass spectrometer error with abundance was, however, accounted for in the method used for determining the overall inert gas errors.

A mass spectrometer generally does not give precisely the true ratio of the isotopic masses present. This is due to the slight differences in the physical properties of the isotopes of different mass and also to the spectrometer itself, some spectrometers showing more bias than others. Such mass spectrometer bias can be corrected by periodically determining the mass spectrometer discrimination factor, F, which is defined as:

$$\left(^{40}Ar/^{36}Ar\right)_{atm.} = \left(^{40}Ar/^{36}Ar\right)_{meas.}\{1 + \Delta MF\} \quad -(2.1)$$

where $\left(^{40}Ar/^{36}Ar\right)_{atm.}$ = atmospheric ratio $^{40}Ar/^{36}Ar$.

= 295.5

$\left(^{40}Ar/^{36}Ar\right)_{meas.}$ = measured ratio $^{40}Ar/^{36}Ar$

F = mass discrimination factor.

ΔM = mass difference between ^{40}Ar and ^{36}Ar

= 4

F was determined by measuring the isotopic ratio $^{40}Ar/^{36}Ar$ in the air spike, without the addition of tracer in the same way that the $^{38}Ar/^{40}Ar$ ratio was measured for a water sample, and substituting in equation 2.1. The factor (1 + ΔMF) was then used to correct the measured isotopic ratios of the inert gases to true isotopic ratios.

2.1.2.6. Determination of $^{40}Ar/^{36}Ar$ in groundwaters

Samples for $^{40}Ar/^{36}Ar$ determination were collected in exactly the same way as samples for inert gas analysis. The sample tubes were sealed to the extraction line and the system was evacuated. The ratio $^{40}Ar/^{36}Ar$ was then measured on the air spike by the method described to determine the mass spectrometer discrimination factor F. This was done to ensure that no residual ^{36}Ar from the tracer was present in the system and to calibrate for mass spectrometer discrimination immediately prior to measuring the $^{40}Ar/^{36}Ar$ ratio in the sample. The residual gases were pumped away then the dissolved gases were released by the method described for inert gas analysis (paragraph 2.1.2.2.). No tracer for the inert gases was added. The ratio $^{40}Ar/^{36}Ar$ was then determined following the procedure for measuring $^{38}Ar/^{40}Ar$ in a water sample. The ratio was corrected using the air calibration in the following way:

$$(^{40}Ar/^{36}Ar)_{corr.} = (^{40}Ar/^{36}Ar)_{sample} \frac{(^{40}Ar/^{36}Ar)_{atm}}{(^{40}Ar/^{36}Ar)_{calib.}}$$

where $(^{40}Ar/^{36}Ar)_{corr}$ = corrected ratio

$(^{40}Ar/^{36}Ar)_{sample}$ = measured ratio from sample

$(^{40}Ar/^{36}Ar)_{atm.}$ = atmospheric ratio, 295.5

$(^{40}Ar/^{36}Ar)_{calib.}$ = measured ratio from air spike

The values obtained were subject to the same errors as the determination of the volume of argon in a water sample and can be measured to an accuracy of 1.8%.

2.2. ROCK ANALYSIS

2.2.1. Uranium content of rock samples

The uranium content of rock samples was determined by the delayed neutron activation method [120] at the Atomic Weapons Research Establishment, Aldermaston, under contract. The technique was chosen because it is non-destructive, rapid, inexpensive, sensitive and accurate. Approximately 1.5g of each sample was weighed accurately into a cylindrical polyethylene snap-top ampoule having a wall thickness of approximately 1.5mm and of internal dimensions 27mm high, 13mm diameter. Linearity of the method was confirmed by including with each sample set a batch of standards prepared by making known additions of natural uranium solutions to known weights of a chosen sample.

Each ampoule was heat sealed then irradiated. Uranium was determined by measuring the delayed neutron activity of the slow neutron fissioned ^{235}U using $^{10}BF_3$ counters at Aldermaston. The concentration of natural uranium was calculated by assuming a natural abundance ratio of $^{235}U/^{238}U$ (0.0073:paragraph 1.2) in the rock samples.

The method was subject to sampling errors because a weight of rock of 1.5g was taken to represent a large rock sample. Samples were taken by coning and quartering a crushed rock sample in an attempt to avoid such errors. The other significant error is the statistical counting error. The 95% probable (2σ) error is given by $C \pm 2\sqrt{c}$

where c = total count.

The 2σ errors are included in the tables of results for the U contents of rock samples.

2.2.2. Thorium content of rock samples

The thorium content of rock samples was determined by thermal neutron activation analysis.

0.25g samples of rock crushed to $<200\mu m$ were sealed in quartz ampoules then irradiated in the "DIDO" reactor at A.E.R.E., Harwell, in a neutron flux of approximately 6×10^{12} neutrons $cm^{-2} s^{-1}$ for 48 hours. Simultaneously, thorium standards, prepared by evaporating known amounts of thorium solution of known concentration in quartz ampoules, were sealed and irradiated. The short-lived radioactive isotopes produced by neutron activation of impurities were allowed to decay for 2-3 weeks then the 0.31 MeV ^{233}Pa γ-ray was counted using both NaI(Tl) and Ge(Li) detectors (appendix 2.1). The isotope ^{233}Pa is formed on decay of ^{233}Th which is produced when ^{232}Th absorbs a thermal neutron:

$$^{232}_{90}Th\ (n,\gamma)\ ^{233}_{90}Th \xrightarrow[22\ min]{\beta^-} {}^{233}_{91}Pa \xrightarrow[27.0\ day]{\beta} {}^{233}_{92}U - - - - -$$

β^- :	1.23 MeV 100%	β :	0.15 - 0.57 MeV
γ :	0.087 MeV 2.7%	γ :	0.313 MeV 42%
		I.C.	38%
		U x-rays	0.098 MeV

where $\xrightarrow[t]{\beta^-}$ represents the mode of decay and half-life

I.C. = internal conversion

The rate of production of activated nuclei $\frac{dNr}{dt}$ by neutron absorption is given by:

$$\frac{dNr}{dt} = \sigma N_{tg} \phi (1 - e^{-\lambda_r t})$$

where σ = neutron absorption cross section ($7.4 \times 10^{-24} cm^2$)

N_{tg} = number of atoms of ^{232}Th

ϕ = neutron flux, n $cm^{-2} s^{-1}$

t = irradiation time

and λ_r = decay constant of $^{233}_{91}Pa$

High energy γ-radiation, from the activation of iron, sodium potassium and cadmium particularly, interferred with the ^{233}Pa peak at 0.313 MeV. The γ-rays produced by isotopes of these metals have short half-lives and counting after 2-3 weeks eliminated most of the interference.

The sensitivity and resolution of the NaI(Tl) detector are very different to the sensitivity and resolution of the Ge(Li) detector. The NaI(Tl) detector has a low resolution (ca 4.15 KeV/channel) and a high sensitivity. Good statistical counting accuracy was achieved in short counting times but interference from γ-rays of similar energy occurred in some samples. Conversely, the Ge(Li) detector has a high resolution (ca. 1.55 KeV/channel) and there is little interference around the ^{233}Pa peak. The sensitivity, however, is very much lower and the counting times required were subsequently longer for good counting statistics.

The main source of analytical error was the accuracy with which the ^{232}Th standard samples could be prepared. Because of the small volume of sample that could be contained in the ampoules, it was necessary to use a micro-syringe for pipetting the thorium standards into the ampoules. The percentage error for pipetting volumes in the order of a few microlitres is very much higher than that involved with pipetting larger volumes.

The analytical error, nevertheless, was small compared with the error caused by interference and the statistical counting error. Typical 95% probable errors were in the range 4 - 7% for samples with average thorium concentrations (10ppm Th) on the NaI(Tl) detector and 15 - 30% on the Ge(Li) detector.

2.2.3. ^{222}Rn release from rocks

2.2.3.1. Sample collection

Rock samples were collected from some areas in which the ^{222}Rn content of the groundwaters had been determined. Samples of about 2 - 4Kg of rock were crushed in a hydraulic crusher to approximately 2" cubes in size. The fragments from the hydraulic crusher were then further crushed in a jaw crusher to give particle sizes ranging from a few μm to several mm in diameter. A representative sample from the jaw crushed fraction, taken by quartering and coning, was ground to a small (few tens of μm) particle size in a tema mill. The fractions were dried at 80°C for 24 hours and sieved to known particle sizes using a set of standard sieves. Two samples from each sieve size were retained: firstly, about 2g was used for uranium determination by delayed

neutron activation analysis, and secondly, the remainder was used for measuring ^{222}Rn release.

2.2.3.2 Experimental

Samples for ^{222}Rn determination were weighed into a 250cm^3 glass bottle, covered with distilled water, stoppered and stored for greater than twenty days so that equilibrium could be established between ^{226}Ra in the rock phase and ^{222}Rn in solution. The samples were analysed for ^{222}Rn by the α-scintillation method used for the determination of ^{222}Rn in groundwaters (paragraph 2.1.1.2). Samples for uranium analysis were weighed into snap-top polyethylene bottles and analysed by the method described for the determination of the uranium content of rocks (paragraph 2.2.1).

The ^{226}Ra content of the rock was determined from the ^{238}U content, using the assumption that the ^{226}Ra is in radioactive equilibrium with ^{238}U in the bulk rock i.e. activity of ^{238}U = activity of ^{226}Ra. This is a reasonable assumption for the granites, sandstones and limestone investigated as they are older than the time taken for equilibrium to be established between ^{238}U and ^{226}Ra (8000 years) and it was assumed that there had been no chemical fractionation of ^{226}Ra from ^{238}U in the rock phase in that time. From the total amount of ^{222}Rn released, the percentage release was determined as follows:

$$\% \text{ radon released} = \frac{[^{222}Rn]}{[^{226}Ra]} \times 100$$

where $[^{222}Rn]$ is the concentration of ^{222}Rn released from the rock in $pCiKg^{-1}$ rock and $[^{226}Ra]$ is the equilibrium concentration of ^{226}Ra in the rock, $pCiKg^{-1}$ of rock.

2.2.3.3. Errors

The percentage ^{222}Rn release is expressed as a function of the rock particle size, which is the average of the two sieve sizes used to separate the sample. In most cases, this average will be a reasonable value for the particle size, but errors could occur if the majority of the particles are of a single size or if a large amount of particles much smaller than the minimum sieve size (fines) have been included in the large particle sizes. The error caused by these effects could not be assessed, but it was not thought to be significant.

The analytical error and counting error, however, can be assessed, the analytical error by analysing a chosen sample several times and the counting error based on the 95% probable error. The cumulative effect of these errors resulted in an analytical precision of approximately 12 - 20%

2.2.4. Helium content of rock samples

2.2.4.1. Experimental

Samples for helium analysis were taken from cores which had been removed from recent boreholes drilled in the United Kingdom for geothermal energy research and hydrocarbon prospecting. The core section to be analysed was coated immediately after recovery from the core barrel with paraffin wax on site and then transported to the University of Bath for analysis. The wax was removed from the core and samples were broken from the centre of the core, weighed, and coated in paraffin wax. The samples

were placed in the apparatus shown in Figure 2.9 which was then sealed to the inert gas extraction line (Figure 2.6) in place of the dual trap system.

The sample was pumped down rapidly, initially through tap A, then through the gas extraction line, with trap B cooled to liquid nitrogen temperature. Once the pressure inside the gas extraction system had reached 10^{-3} - 10^{-4} torr, the pumping line was isolated. An aliquot of tracer was admitted and the rock sample was heated to 200 - 300°C, using a small furnace. The sample was held at this temperature for 2 hours so that the inert gases were released quantitatively. The isotopic ratios of helium and neon were then determined using the technique described for the determination of inert gases in groundwaters (paragraph 2.1.2).

2.2.4.2. Calculation

The volumes of helium and neon released from the water sample were calculated using the isotope dilution equations given in paragraph 2.1.2.3. The volume of neon in the sample, $V_{at}(Ne)$, was assumed to be totally due to air trapped in the sample when it was covered with wax. This was used as a correction for the volume of helium, $V_{at}(He)$, as follows:-

The volume of air (V_{at}) in which the volume of neon is $V_{at}(Ne)$ is given by

$$V_{at} = \frac{V_{at}(Ne)}{f_{at}(Ne)}$$

where $f_{at}(Ne)$ is the volume fraction of neon in air.
The volume of helium in this volume of air, V(He), is therefore, given by:

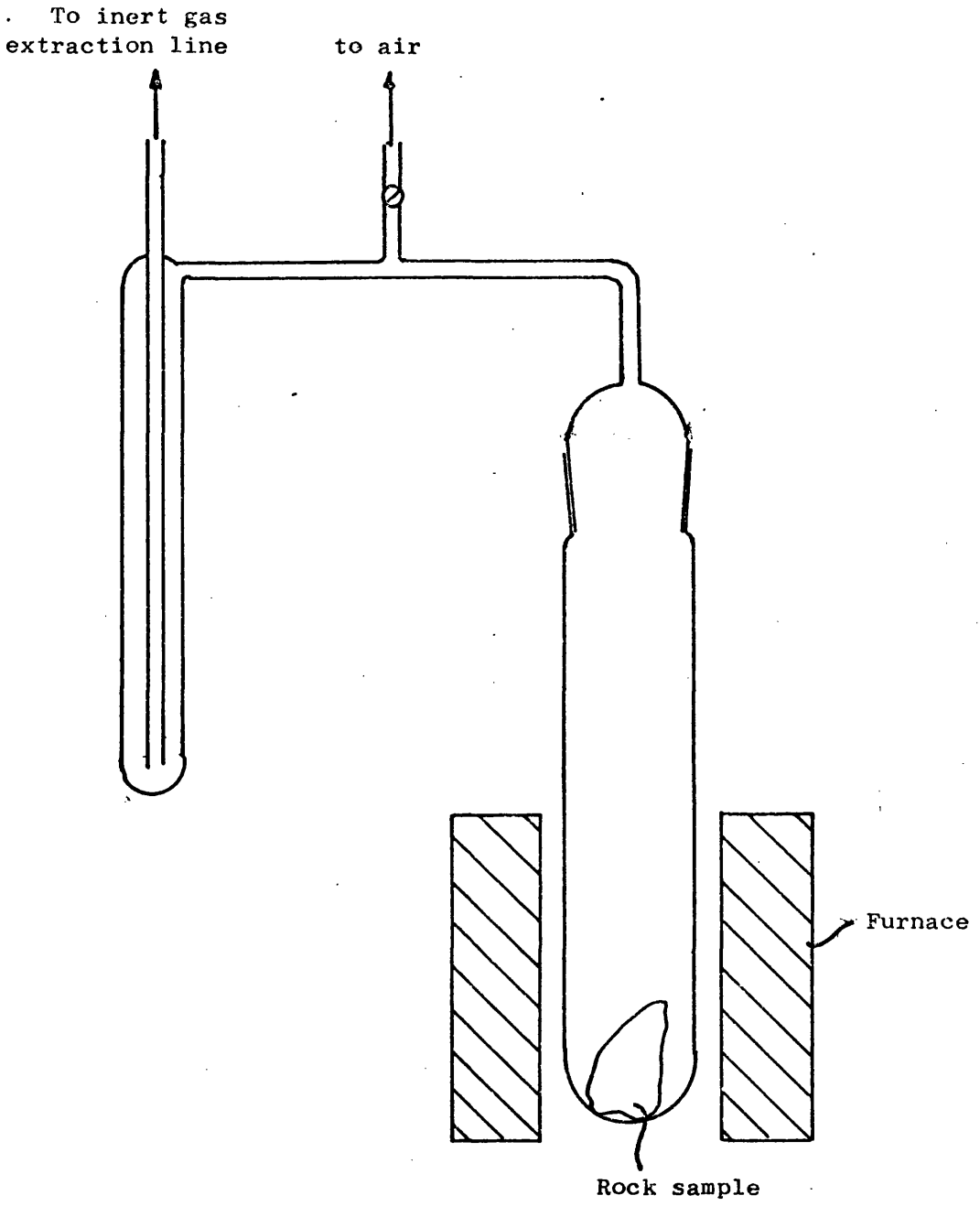

Figure 2.9. Apparatus for determining ^{4}He in cores.

$$V(He) = \frac{V_{at}(Ne)}{f_{at}(Ne)} \cdot f_{at}(He)$$

where $f_{at}(He)$ is the volume fraction of helium in air.

So the corrected helium content of the rock sample, $V_{corr}(He)$, is given by:

$$V_{corr}(He) = V_{at}(He) - \frac{V_{at}(Ne) \cdot f_{at}(He)}{f_{at}(Ne)}$$

This value is the total volume of helium in the rock sample.

In order to compare one rock sample with another, the results are expressed in terms of volume of helium per g of rock or volume of helium per g of interstitial water.

Let x = mass of rock sample, g

Then, volume of helium per g of rock is simply

$$\frac{V_{corr}(He)}{x} \text{ cm}^3 \text{ STP g}^{-1} \text{ rock}$$

The volume of helium per g of interstitial water is derived as follows:

$$\text{Ratio of } \frac{\text{water}}{\text{water saturated rock}} = \frac{S_1 - w}{S_1 - w + \rho_f w}$$

where S_1 = weight in air of rock saturated with isopropyl alcohol (Pr^iOH), g

S_2 = weight in Pr^iOH of rock saturated with Pr^iOH, g

w = dry weight in air of rock, g

and ρ_f = density of Pr^iOH, g cm^{-3}

Isopropyl alcohol was used to saturate the rock as it does not cause expansion of the clay matrices when it is absorbed into the rock structure.

The volume of pore water, V_p is given by:

$$V_p = \frac{(S_1 - w)\, x}{(S_1 - w + \rho_f\, w)} \quad cm^3$$

where x is the mass of the rock sample used for ^4He analysis. Therefore, the volume of ^4He per g of interstitial water is given by $\frac{V_{corr}^{(He)}}{V_p}$, assuming that the density of water is 1g cm^{-3}.

2.1.4.3. Errors

Loss of helium by diffusion is likely to be the most important error. This is partly overcome by sealing the sample on collection with paraffin wax and by using a sample from the centre of the core for analysis. However, helium does escape through paraffin wax and the helium content determined is a minimum content. Helium may also be pumped away during the initial stages of analysis. In order to reduce helium loss by this mechanism, the sample was pumped down as rapidly as possible. For this reason, the helium content measured is a minimum content. Finally air may be trapped between the wax and the sample in the outer pore spaces of the sample. It is possible to correct for this excess helium as explained earlier, but this correction is an over simplification of the physical situation because of the probability that helium due to air contamination will be pumped through the wax much more easily than neon.

The method is subject to the analytical errors discussed in the determination of inert gases in groundwaters (paragraph 2.1.2). The result of all errors is that the helium content of the rock sample is a minimum content, therefore for duplicate samples, the sample with the highest helium content was taken to reflect the actual helium content.

Experiments on the effectiveness of the technique to release all the helium present in the sample were not conclusive. In the presentation and interpretation of results, it has been assumed that all the helium has been released, but this is not necessarily the case.

CHAPTER 3

RADON, RADIUM AND DISSOLVED INERT GASES IN GROUNDWATERS FROM THE BUNTER SANDSTONE, NOTTINGHAMSHIRE.

3.1. INTRODUCTION

The significant geochemical processes - solution-mineral equilibria, redox and exchange reactions - occurring in the Bunter (Triassic) Sandstone aquifer of Nottinghamshire have been studied to interpret the distribution and mobility of minor and trace elements [121]. The outline hydrogeology of the area has been described by Land [122]. The Bunter Sandstone has a poorly cemented quartzose lithology and is generally red-brown or yellow in colour. The formation thickness varies from around 120m in the south to 300m in the north. The formation crops out in the west and is overlain towards the east of the region by younger sediments (Figure 3.1). The aquifer dips gently eastwards at a gradient of about 1 in 50 and is confined effectively in the east by thick overlying marls (Keuper) and underlying mudstones and marls (Permian).

Boreholes in both the outcrop and confined parts of the aquifer are used to provide public water supply in the region. Although there is evidence of a high degree of pollution in some of the outcrop areas, most of the area represents an uncontaminated body of groundwater where natural processes predominate. The ^{14}C activity of dissolved bicarbonate in the groundwaters decreases downgradient in the confined aquifer and indicates ages upward of 3×10^4 years for water about 30Km from the recharge zone [123].

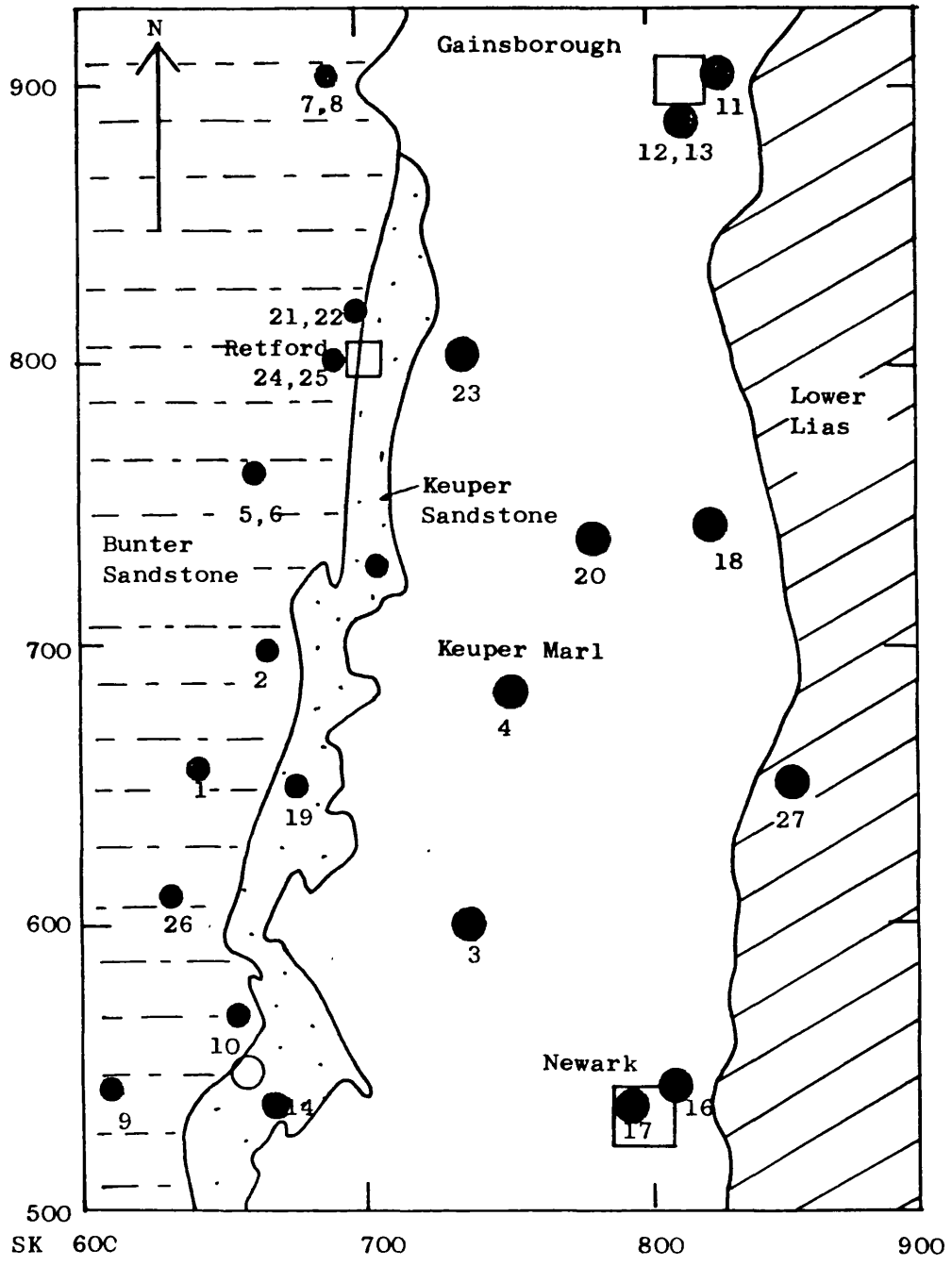

Fig. 3.1. Location map for sampling sites in Bunter Sandstone showing outcrop geology. (Sites are numbered as in tables 3.2 - 3.4. Sites indicated by the larger circles are in the confined part of the aquifer. The open circle is the site of Newhall borehole).

In the recharge zone, groundwaters equilibrate with soil, air and dissolve the stable inert gases in amounts proportional to their solubilities and atmospheric partial pressures. The amounts of these atmosphere derived inert gases are supplemented by radiogenic ^{4}He, ^{222}Rn and in some cases ^{40}Ar. The radon, radium and inert gas contents of the Bunter Sandstone groundwaters have been determined and their significance is discussed below. The uranium and thorium contents of a core sample of aquifer rock have also been determined. Variations in the ^{4}He contents of the groundwaters are related to the radioelement content of the rock, and the west to east groundwater movement and age trend. Recharge temperatures derived from the stable inert gas contents have been related to changes in the palaeo-environment deduced from the changes in δD and $\delta^{18}O$ with ^{14}C activity.

3.2. RESULTS AND DISCUSSION

3.2.1. Uranium and thorium contents of the Bunter Sandstone

The uranium and thorium contents of core from various depths in the Newhall borehole are given in Table 3.1. The average contents are 1.87 and 8.72 g g^{-1} for uranium and thorium respectively, yielding an average Th/U ratio of 4.7, which is somewhat higher than the average Th/U ratio of 3.5 for various sandstone types [124]. There is considerable variation in the distribution of uranium and thorium at various levels in the borehole, however, the average U and Th contents of the Newhall borehole core are the best available estimate for the natural radioelement contents of the Bunter Sandstone aquifer.

Table 3.1. Uranium and thorium contents of core samples from the Newhall borehole (SK 662 546)

Depth m	U content g g^{-1}	Th content g g^{-1}	Th/U ratio
6.70	2.12	10.8	5.1
6.95	1.79	11.1	6.2
10.30	2.11	9.0	4.3
39.10	3.47	14.6	4.2
48.40	2.52	9.6	3.8
64.60	1.00	7.7	7.7
65.50A	0.98	4.3	4.4
65.50B	2.23	7.6	3.4
78.50	1.85	11.4	6.2
135.50	0.93	4.3	4.6
159.40	0.99	4.0	4.0
175.50	1.25	5.5	4.4
186.05	3.04	13.2	4.3
197.00	1.92	9.2	4.8
average	1.87	8.7	4.7

3.2.2. ^{226}Ra and ^{222}Rn contents

The ^{226}Ra and ^{222}Rn contents of groundwaters from the Bunter Sandstone are reported in Table 3.2. The average ^{226}Ra and ^{222}Rn contents are 0.4 and 1 80 pCi Kg^{-1}, respectively. Histograms of the ^{226}Ra and ^{222}Rn contents and probability plots (Figures 3.2 and 3.3) indicate that both the ^{226}Ra and ^{222}Rn contents of the groundwaters are distributed normally about the mean values. In other words, both the ^{226}Ra and ^{222}Rn contents of the groundwaters form a set of data which may be described statistically as being normally distributed.

The ^{222}Rn contents are considerably in excess of the ^{226}Ra contents, as is invariably observed for groundwaters, and they are related to the U content of the host rock by the equation:

$$[Rn] = 0.33 \frac{A\rho[U]}{\phi} [1 - e^{-\lambda t}] \qquad 3.1$$

where $[Rn]$ = ^{222}Rn content of the water, pCi cm^{-3}

$[U]$ = U content of the host rock, g g^{-1}

ρ = bulk density of the rock, g cm^{-3}

ϕ = fractional porosity

A = fractional efficiency of ^{222}Rn release

λ = decay constant for ^{222}Rn

t = residence time of the interstitial water

Provided that the residence time of the pore water is greater than 25 days, and this is certainly the case for the Bunter Sandstone groundwaters, the exponential term, $1 - e^{-\lambda t}$, approaches unity. The half-life of 3.825 days means that the ^{222}Rn content of the groundwater is effectively determined by the part of the aquifer through which it moved during the 25 days prior to extraction.

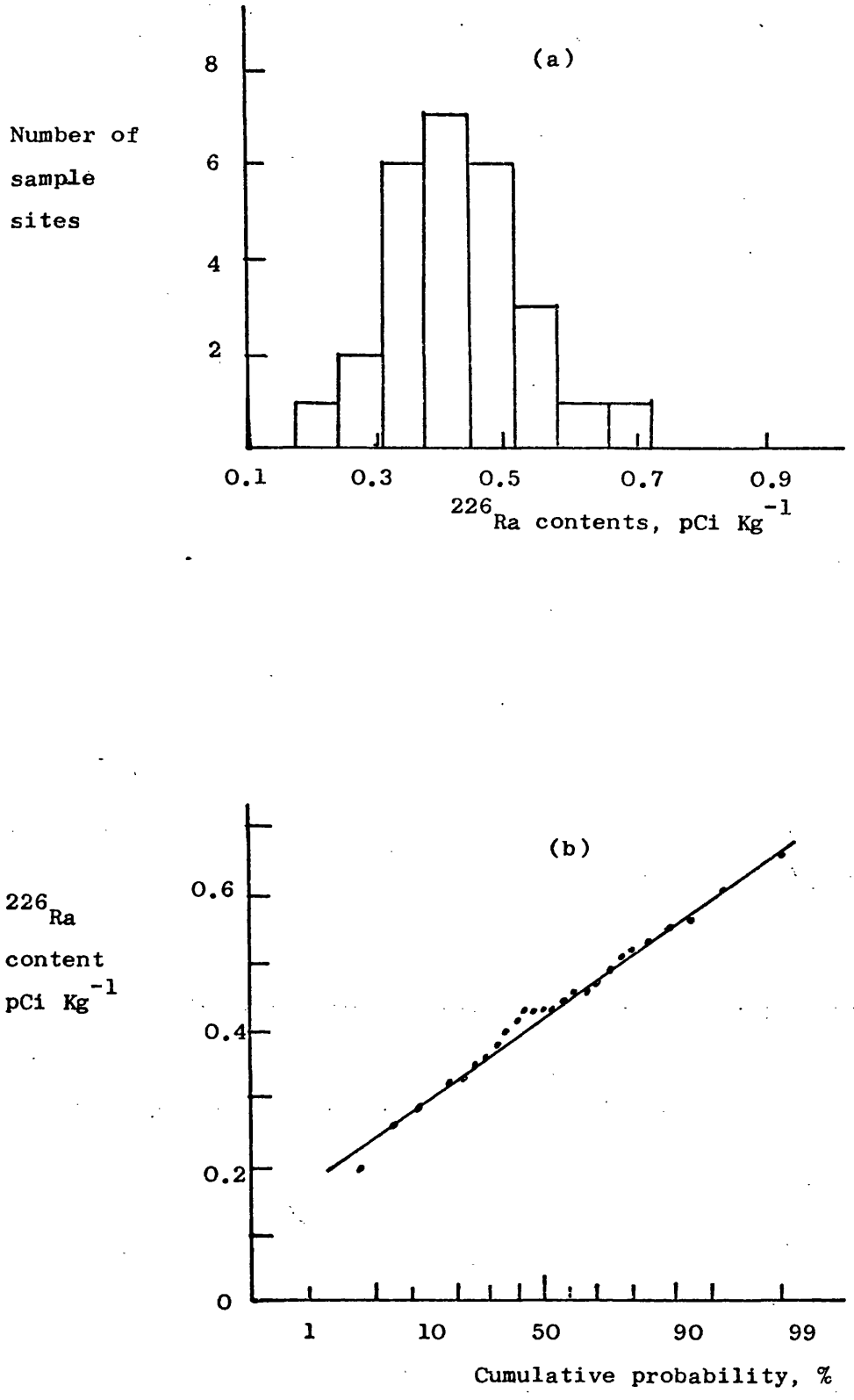

Figure 3.2. ^{226}Ra content of groundwaters from Bunter Sandstone, Nottinghamshire. (a) Histogram and (b) Normal probability plot of ^{226}Ra contents.

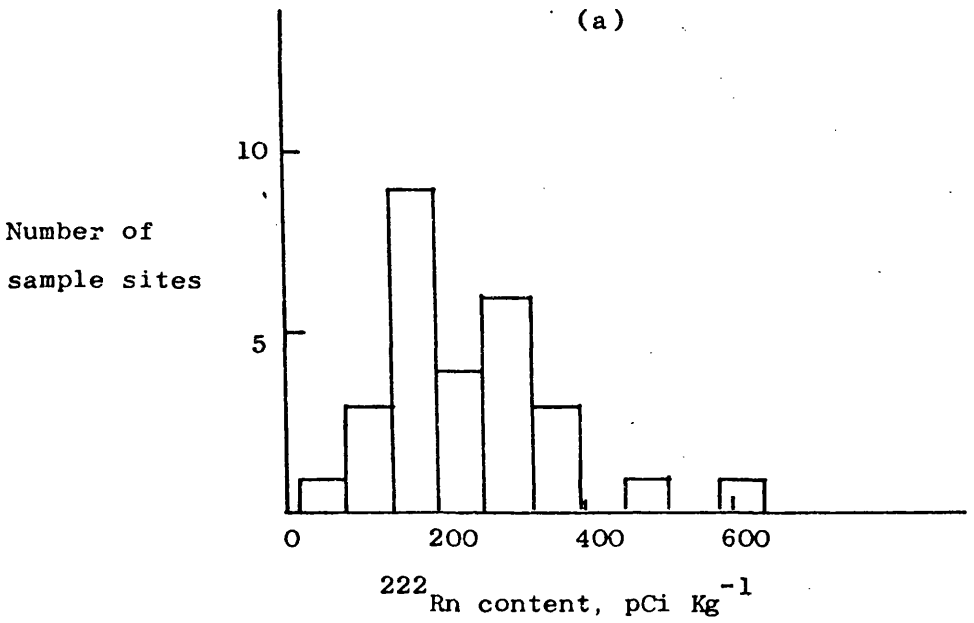

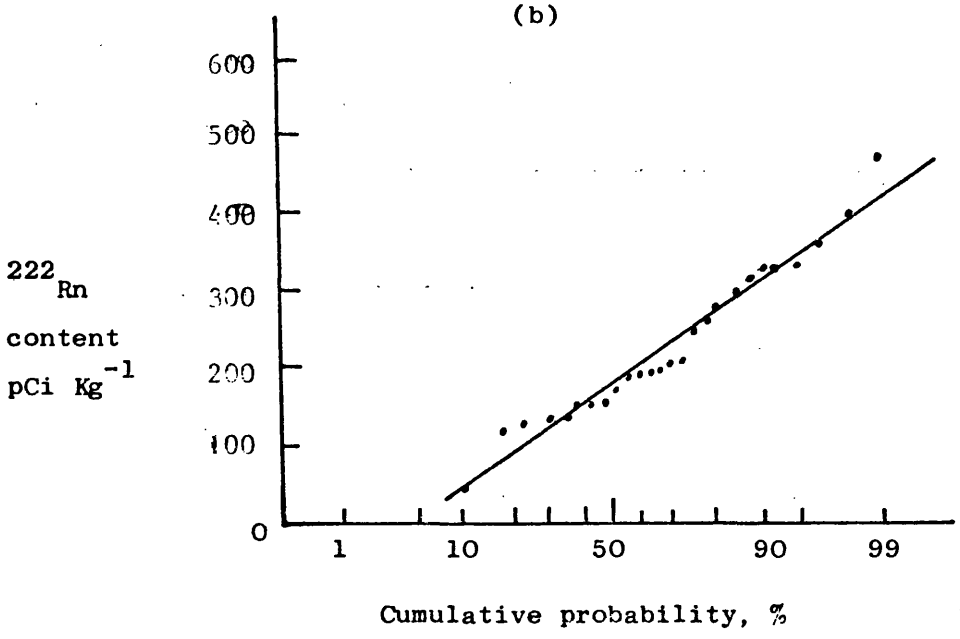

Fig. 3.3 ^{222}Rn content of groundwaters from Bunter sandstone, Nottinghamshire.
(a) Histogram and (b) probability plot of ^{222}Rn contents.

Table 3.2. ^{222}Rn and ^{226}Ra contents of groundwaters from the Bunter Sandstone, Nottinghamshire.

Site No.	Location	National Grid. Ref.	^{222}Rn pCi Kg^{-1}	^{226}Ra pCi Kg^{-1}
1	Amen Corner, No. 1	SK 642 655	329±21	0.36±0.02
2	Boughton, No. 2	SK 669 697	282±18	0.32±0.02
3	Caunton	SK 739 600	46±4	0.44±0.03
4	Egmanton, B.P.	SK 754 682	247±16	0 20±0.02
5	Elkesley, No. 5	SK 664 760	133±8	0.26±0.02
6	Elkesley, No. 6	SK 664 760	121±8	0.33±0.02
7	Everton, No.1	SK 692 902	148±10	0.52±0.04
8	Everton, No. 3	SK 694 901	195±13	0.60±0.04
9	Far Baulker, No. 3	SK 612 543	192±14	0.38±0.02
10	Farnsfield	SK 656 568	266±21	0.32±0.02
11	Gainsborough, B.P.	SK 832 902	330±21	0.43±0.03
12	Gainsborough, Humble Carr	SK 818 883	155±13	0.43±0.04
13	" Lea Rd. No. 3	SK 816 889	187±11	0.42±0.03
14	Halam, No. 1	SK 670 537	354±22	0.66±0.05
15	Markham Clinton, No. 1	SK 711 727	300±21	0.35±0.02
16	Newark, British Gypsum	SK 812 542	130±10	0.47±0.03
17	Newark, Castle Brewery	SK 798 536	280±17	0.46±0.03
18	Newton, No. 2	SK 826 742	153±9	0.42±0.03
19	Ompton, No. 2	SK 678 648	477±29	0.53±0.04
20	Rampton	SK 776 776	206±13	0.29±0.03
21	Retford, Clark's No. 1	SK 703 819	320±20	0.46±0.03
22	Retford, Clark's No. 2	SK 703 819	608±36	0.56±0.04
23	Retford, Grove No. 2	SK 740 803	211±13	0.51±0.04
24	Retford, Ordsall No.1	SK 695 801	141±9	0.55±0.03
25	Retford, Whisker Hill	SK 692 800	332±21	0.49±0.03
26	Rufford, No. 3	SK 632 610	392±25	0.43±0.03
27	South Scarle	SK 856 650	191±12	0.24±0.02

The efficiency of ^{222}Rn release, A is probably controlled by the size of particles in the cementing phase, as discussed in Chapter 9. The value of A of 0.04 compares with a value of 0.03 for the Old Red (Devonian) Sandstone groundwaters from Somerset, England [13]. Higher values of A are found for small grained, uncemented sands such as the Midford Sands (Liassic) for which A = 0.17 [13]

Variation of the ^{222}Rn contents of the Bunter Sandstone groundwaters may be attributed to aquifer variability around the extraction points, because the ^{222}Rn content is determined by the rock-water interaction during the 25 days before the groundwater is extracted. On the assumption that the entire yield is due to intergranular flow, a typical well into the Bunter Sandstone (Depth 100m into the Sandstone, flow $10^4 m^3 day^{-1}$) can derive all its water (and therefore all the ^{222}Rn) from within a radius of about 50m from the bore. ^{222}Rn may be transported from greater distances by fissure flow, but not in large concentrations, because the low ratio of rock surface to water in the fissures limits the ^{222}Rn content to a low value which may decay to an even lower value during transport in the fissure system. Therefore, the ^{222}Rn content of groundwaters is a useful indicator of the variation of porosity, grain size distribution of the rock, its radioelement content and the relative importance of intergranular and fissure flow in the aquifer.

3.2.3. Radiogenic ^4He contents

The presence of primordial helium in deep crustal rocks and the retention of radiogenic helium in minerals for long periods of time has been discussed in Chapter 1. Helium loss by diffusion is therefore slow compared with the circulation time of shallow groundwaters which may accumulate radiogenic helium as they percolate through an aquifer. Assuming that U and Th are in equilibrium with their decay products in the Bunter Sandstone and that all the ^4He generated by radioactive decay dissolves in the interstitial water, the rate at which the ^4He content of the water increases is given by:

$$^4He \text{ solution rate} = \rho/\phi \left\{1.19 \times 10^{-13}[U] + 2.88 \times 10^{-14}[Th]\right\} \quad 3.2$$

$$(cm^3 \text{ STP } cm^{-3} \ H_2O \ yr^{-1})$$

where Th is the Th content of the rock in $g\ g^{-1}$ and the other symbols have the same meaning as for equation 3.1. The assumption that all the He generated dissolves in the water is likely to be an over-simplification, as evidence from the helium content of pore water and core from the Bunter Sandstone at Winterbourne Kingston indicates that the helium is uniformly distributed between the water and rock phases. However, at Winterbourne Kingston, the interstitial water is not flowing and it is more likely that the He will distribute uniformly. In the Bunter Sandstone, Nottinghamshire, equilibrium (uniform distribution) is disturbed by ^4He being removed from the water phase with groundwater flow. Substituting the values for rock density, porosity and radioelement concentrations, the following relationship between residence time of the groundwater, t, and ^4He content is obtained:

$$t = 2.95 \times 10^{11} \ [He] \ yr \quad 3.3$$

where [He] is the radiogenic ^4He content of the groundwater in excess of that derived from atmospheric equilibration during recharge, expressed as cm^3 STP cm^{-3} H_2O. Any contribution to the ^4He content due to decay of dissolved U has been neglected, because even for high dissolved U contents, the ^4He generation rate is small compared with that generated by the rock radioelement contents. The dissolved inert gas contents of the Bunter Sandstone groundwaters are reported in Table 3.3. Groundwaters with high ^4He contents do not correlate with those with high ^{222}Rn contents (Figure 3.4). So the excess helium is not due to high radioelement concentrations or porosity variations in the locality of the extraction boreholes. It arises from a gradual solution of radiogenic ^4He as the water moves through an extensive part of the aquifer. This is shown in Figure 3.5 in which ^4He content is plotted against distance from outcrop. The high ^4He contents occur in the confined part of the aquifer.

The excess radiogenic ^4He contents were calculated by subtracting the amounts of ^4He dissolved from the atmosphere at the recharge temperature (see below) from the total ^4He contents of the groundwaters. These excess ^4He contents are plotted against the corrected ^{14}C ages [123] of the groundwaters in Figure 3.6. The excess ^4He content increases linearly with increasing groundwater age. Excess ^4He ages calculated from equation 3.2 are compared with the corrected ^{14}C age ranges in Table 3.4. ^4He ages are generally about double the corrected ^{14}C ages, although the linear correlation is good. The ^4He ages calculated from

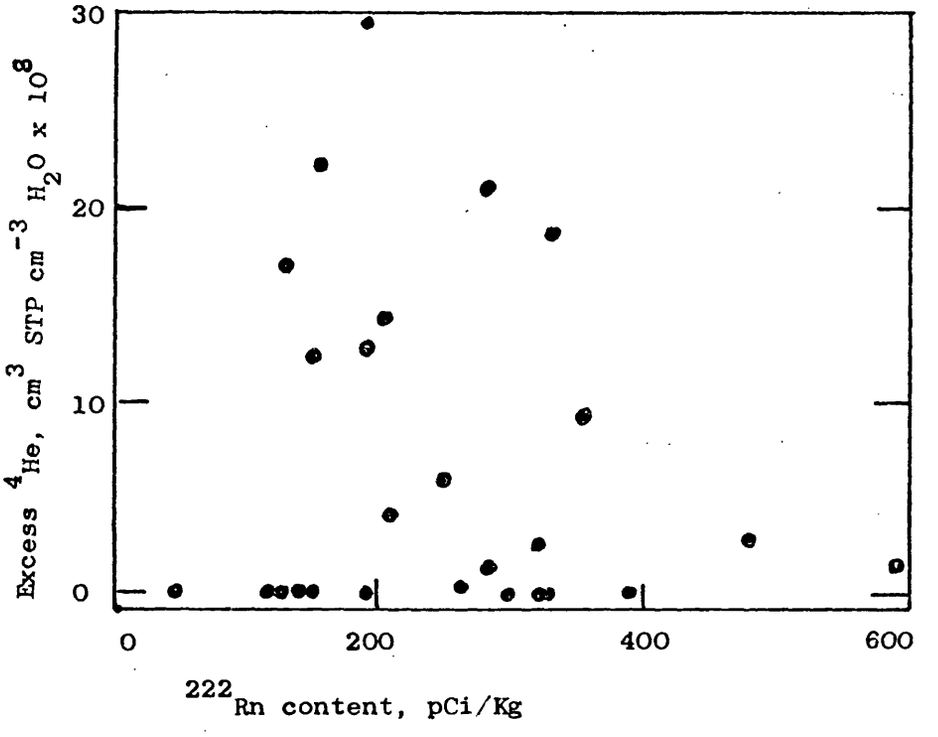

Fig. 3.4. Excess ^{4}He contents plotted against ^{222}Rn contents for the Bunter Sandstone groundwaters.

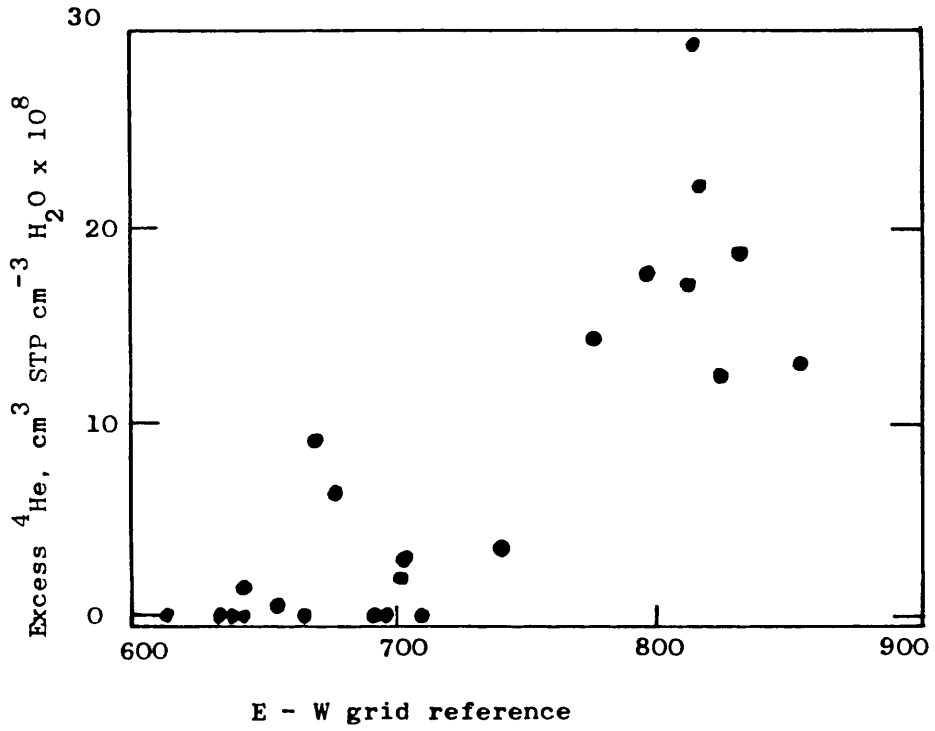

Fig. 3.5. Excess ^{4}He contents plotted against the E - W grid reference of the sample location for Bunter Sandstone groundwaters.

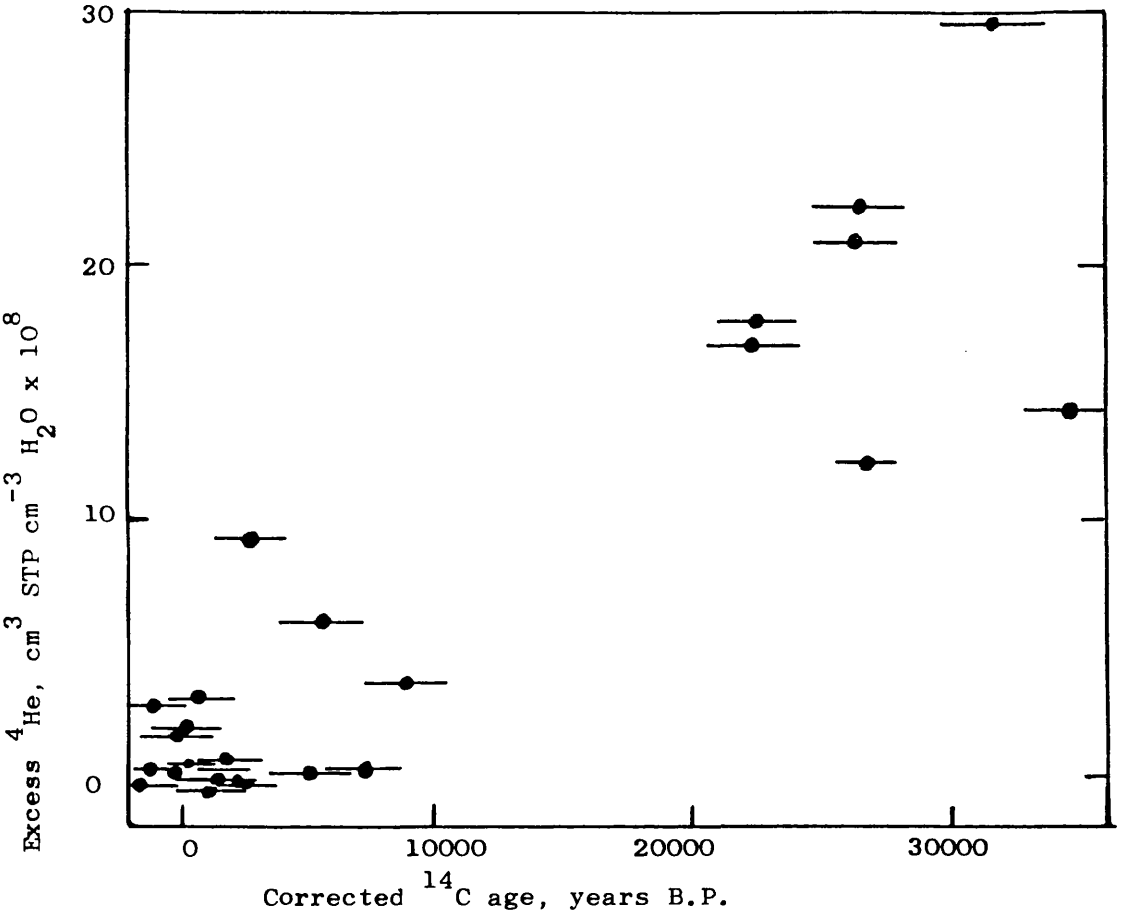

Figure 3.6. Excess ^{4}He content of the Bunter Sandstone groundwaters plotted against corrected ^{14}C age ranges.

Site No.	Location	National Grid. Ref.	Inert gas content, cm^3 STP/cm^3 H_2O					Recharge temp. °C		Collection temperature °C
			He x 10^8	Ne X 10^7	Ar x 10^4	Kr x 10^7	Xe x 10^8	from Ar	from Kr	
1	Amen Corner, No. 1	SK 642 655	4.2±0.6	2.09±0.10	3.83±0.14	0.91±0.02	1.21±0.06	11.9±1.4	8.3±0.8	9.2
2	Boughton, No. 2	SK 669 697	6.2±0.8	2.01±0.10	4.07±0.15	0.87±0.02	1.16±0.06	9.1±1.4	9.6±1.0	14.3
3	Caunton	SK 739 600	3.6±0.5	1.84±0.09	3.65±0.13	0.79±0.02	1.00±0.05	14.0±1.5	13.5±1.1	10.8
4	Egmanton, B.P.	SK 754 682	10.8±1.4	2.11±0.10	4.07±0.15	0.91±0.02	1.22±0.06	9.1±1.4	7.9±0.8	13.3
5	Elkesley, No. 5	SK 664 760	4.3±0.6	2.09±0.10	4.02±0.14	0.87±0.02	1.14±0.06	9.6±1.4	9.7±1.0	10.0
6	Elkesley, No. 6	SK 664 760	4.0±0.5	2.09±0.10	4.02±0.14	0.87±0.02	1.19±0.06	9.6±1.4	9.9±1.0	10.0
7	Everton, No. 1	SK 692 902	4.3±0.6	2.07±0.10	3.76±0.14	0.88±0.02	1.18±0.06	12.7±1.4	9.0±1.0	10.3
8	Everton No. 3	SK 694 901	4.2±0.6	2.05±0.10	4.28±0.15	0.91±0.02	1.18±0.06	7.2±1.4	7.9±0.8	10.4
9	Far Baulker, No. 3	SK 612 543	4.3±0.6	2.09±0.10	4.05±0.15	0.83±0.02	1.15±0.06	9.3±1.4	9.3±0.8	9.4
10	Farnsfield	SK 656 568	5.1±0.7	2.09±0.10	4.09±0.15	0.87±0.02	1.06±0.06	8.9±1.4	9.6±1.0	9.6
11	Gainsborough, B.P.	SK 832 902	23.7±3.2	2.20±0.11	4.58±0.16	0.99±0.02	1.22±0.06	4.3±1.5	4.8±0.8	15.8
12	Gainsborough, Humble Carr	SK 818 883	27.2±3.6	2.18±0.10	4.49±0.16	1.0±0.02	1.23±0.06	5.1±1.5	4.0±0.7	17.2
13	Gainsborough, Lea Rd No.3	SK 816 889	34.3±4.6	2.20±0.11	4.52±0.16	1.03±0.02	1.40±0.07	4.8±1.5	3.4±0.7	14.7
14	Halam No. 1	SK 670 537	14.1±1.9	2.23±0.11	4.15±0.15	0.88±0.02	1.15±0.06	8.4±1.4	9.1±0.8	10.8
15	Markham Clinton, No. 1	SK 711 727	4.3±0.6	2.09±0.10	3.99±0.14	0.86±0.02	1.24±0.06	9.9±1.4	9.9±1.0	12.7
16	Newark, British Gypsum	SK 812 542	21.9±2.9	2.29±0.11	4.8 ±0.17	1.06±0.02	1.27±0.07	1.7±1.6	2.2±0.7	16.5
17	Newark, Castle Brewery	SK 798 536	25.9±3.5	2.27±0.11	4.78±0.17	1.05±0.02	1.34±0.07	2.4±1.6	2.7±0.7	16.0
18	Newton, No. 2	SK 826 742	17.3±2.3	2.27±0.11	4.72±0.17	1.05±0.02	1.25±0.07	3.0±1.6	2.5±0.7	16.0
19	Ompton, No. 2	SK 678 648	7.8±1.0	2.12±0.10	4.16±0.15	0.90±0.02	1.23±0.06	8.3±1.4	7.9±0.8	10.4
20	Rampton	SK 776 776	19.3±2.6	2.27±0.11	4.68±0.17	1.05±0.02	1.38±0.07	3.4±1.6	2.7±0.7	14.0
21	Retford, Clark's No. 1	SK 703 819	7.4±1.0	2.09±0.10	3.87±0.14	0.37±0.02	1.19±0.06	11.4±1.4	9.7±1.0	10.5
22	Retford, Clark's No. 2	SK 703 819	6.5±0.9	2.07±0.10	3.94±0.14	0.91±0.02	1.23±0.06	10.5±1.4	7.8±0.8	10.7
23	Retford, Grove No. 2	SK 740 803	8.4±1.1	2.14±0.10	4.19±0.15	0.91±0.02	1.29±0.07	8.0±1.4	7.9±0.8	12.7
24	Retford, Ordsall No. 1	SK 695 801	3.5±0.5	2.09±0.10	4.04±0.15	0.80±0.02	1.20±0.06	9.4±1.4	9.9±1.0	11.5
25	Retford, Whisker Hill	SK 692 800	4.6±0.6	2.08±0.10	3.89±0.14	0.88±0.02	1.17±0.06	11.1±1.4	9.2±1.0	10.5
26	Rufford, No. 3	SK 632 610	4.9±0.7	2.02±0.10	3.89±0.14	0.87±0.02	1.16±0.06	11.1±1.4	9.5±1.0	10.3
27	South Scarle	SK 856 650	17.6±2.4	2.20±0.10	4.51±0.16	1.00±0.02	1.34±0.07	4.9±1.5	4.5±0.7	18.8

Table 3.4. Comparison of ^{4}He ages with corrected ^{14}C age ranges.

Site No.	Location	Excess ^{4}He cm^{3} STP cm^{-3} $H_2O \times 10^{8}$	^{4}He age	Corrected ^{14}C age range		
				min.	mean	max.
			y	y	y	y
1.	Amen Corner, No. 1	0.0	-	-1800	-100	1600
2.	Boughton, No. 2	1.5	4400	-1600	-100	1400.
3.	Caunton	0.0	-	5800	7350	8900
4.	Egmanton, B.P.	6.0	17700	4000	5650	7300
5.	Elkesley, No. 5	0.0	-	-	-	-
6.	Elkesley, No. 6	0.0	-	-3700	-2300	-1000
7.	Everton, No. 1	0.0	-	-200	1250	2700
8.	Everton, No. 3	0.0	-	800	2450	4100
9.	Far Baulker, No. 3	0.0	-	-2600	-1250	100
10.	Farnsfield	0.4	1200	-600	750	2100
11.	Gainsborough, B.P.	18.8	55450	21100	22600	24100
12.	Gainsborough, Humble Carr	22.3	54800	24900	26550	28200
13.	Gainsborough, Lea Rd. No.3	29.4	86700	29800	31750	33700
14.	Halam, No. 1	9.3	27400	1500	2900	4300
15.	Markham Clinton, No. 1	0.0	-	3500	5150	6800
16.	Newark, British Gypsum	16.9	49850	20600	22400	24200
17.	Newark, Castle Brewery	20.9	61650	24900	26400	27900
18.	Newton, No. 2	12.3	36300	25700	26850	28000
19.	Ompton, No. 2	3.0	8850	-500	850	2200
20.	Rampton	14.3	42200	33000	34550	36100
21.	Retford, Clark's No. 1	2.7	8000	-2900	-1300	300
22.	Retford, Clark's No. 2	1.8	5300	-1100	300	1700
23.	Retford, Grove No. 2	3.6	10600	7300	8950	10600
24.	Retford, Ordsall No. 1	0.0	-	40	1500	3000
25.	Retford, Whisker Hill	0.0	-	500	1900	3300
26.	Rufford, No. 3	0.2	600	200	1550	2900
27.	South Scarle	12.7	37500	-	-	-

equation 3.2. are however very dependent upon the aquifer parameters [U], [Th], ρ and Ø. [U] and [Th] were determined on core from a single borehole in the southern part of the aquifer and considerable lateral variation was found. Clearly, confidence in the numerical constant in equation 3.2 can only be improved by the acquisition of more extensive radioelement analyses for the Bunter Sandstone.

Part of the calculated ^4He age discrepancy may also arise by ^4He diffusion into the aquifer from the upper and lower confining marls. The diffusion coefficient of ^4He in water is large (10^{-5} $cm^2 s^{-1}$ [125]) compared with that in vitreous silica (10^{-8} cm^2 s^{-1} [126]) so ^4He movement by diffusion will be much aided by the presence of water in the pore spaces since the diffusion coefficient in rock-forming silicates is of the same order of magnitude as that in silica. The low-permeability confining marls will therefore act as ^4He diffusion barriers as well as aquifer confining strata and a proportion of the ^4He generated in the marls may diffuse into the aquifer rather than through the marls. The influence of He diffusion on the rate of increase of He content in a confined aquifer is discussed more thoroughly in chapter 10.

The ^4He content of the groundwaters increases downdip in the aquifer. This results in a concentration gradient which would cause diffusion of ^4He updip. The rate of ^4He movement updip is given by Fick's first law of diffusion:

$$F = -D \frac{dC}{dx}$$

where F is the rate of He movement in the x- direction, D is the diffusion coefficient of He in water and $\frac{dC}{dx}$ is the He concentration gradient in the x-direction. The He concentration gradient in the downdip direction may be calculated from Figure 3.5. The value is 2×10^{-13} (cm^3 He/cm^3 H_2O)cm^{-1} which yields an updip He diffusion rate of 2×10^{-18} cm^3 He cm^{-2} s^{-1}. The rate of water movement downdip, estimated using the ^{14}C ages, is about 40 cm yr^{-1}. He is transported downdip by the water at a rate of about 7×10^{-14} cm^3 He cm^{-2} s^{-1} in the recharge zone and at a greater rate in the confined zone where the He concentration is greater. This rate is much greater than the updip diffusion rate so all the He that is released into the water phase will be transported downdip. Any ^4He entering the aquifer from the confining marls will be similarly transported downdip and will contribute to enhanced ^4He ages.

Similarly, the rate of upwards diffusion of He may be shown to be small compared with its rate of transport downdip. In the extreme east of the confined aquifer, the base of the Bunter is about 500m deep and the average vertical He concentration gradient is about 6×10^{-12} (cm^3 He/cm^3 H_2O)cm^{-1}. From this, the upwards diffusion rate is 6×10^{-17} cm^3 He cm^{-2} s^{-1} for diffusion through water or 6×10^{-20} cm^3 He cm^{-2} s^{-1} for diffusion through silicates. Because of the high interconnected porosity in the Bunter Sandstone, the rate of diffusion will be approximately equal to that in water whereas the low permeability of the confining marls will give them a lower rate of diffusion. The rate of downdip transport is therefore at least 1000 times greater than the upwards diffusion rate.

In conclusion, the ^{4}He concentration increases in the confined part of the aquifer with increasing groundwater age. The calculation of groundwater age from excess ^{4}He contents is very dependent upon the aquifer radioelement contents and porosity. Since it is not possible to select single values of these parameters which adequately describe the aquifer and because there is insufficient radioelement concentration data to evaluate the contribution of the confining marls to the ^{4}He content, the use of the ^{4}He contents to estimate groundwater age in the Bunter Sandstone must be calibrated against the corrected ^{14}C ages.

3.2.4. Palaeotemperatures of recharge derived from inert gas contents.

Recharge temperatures for some thermal waters have been estimated from their inert gas contents [118]. In the Bunter Sandstone groundwaters the recharge temperatures were derived from the argon and krypton contents and the solubility/temperature relationships as described in Chapter 2. Inert gas solubilities decrease with increasing temperature in the temperature range of interest. Any small increase in groundwater temperature as the water moves from the soil zone to greater depths in the aquifer will not result in inert gas exsolution since the increase in hydrostatic pressure maintains the groundwater undersaturated with respect to the gases. It is therefore valid to derive recharge temperatures from inert gas contents in the Bunter Sandstone because the increase in groundwater temperature is small - the maximum groundwater temperature is $18.8^{\circ}C$. Derived recharge temperatures for the Bunter Sandstone groundwaters are included in Table 3.3, and are plotted against corrected ^{14}C ages in Figure 3.7.

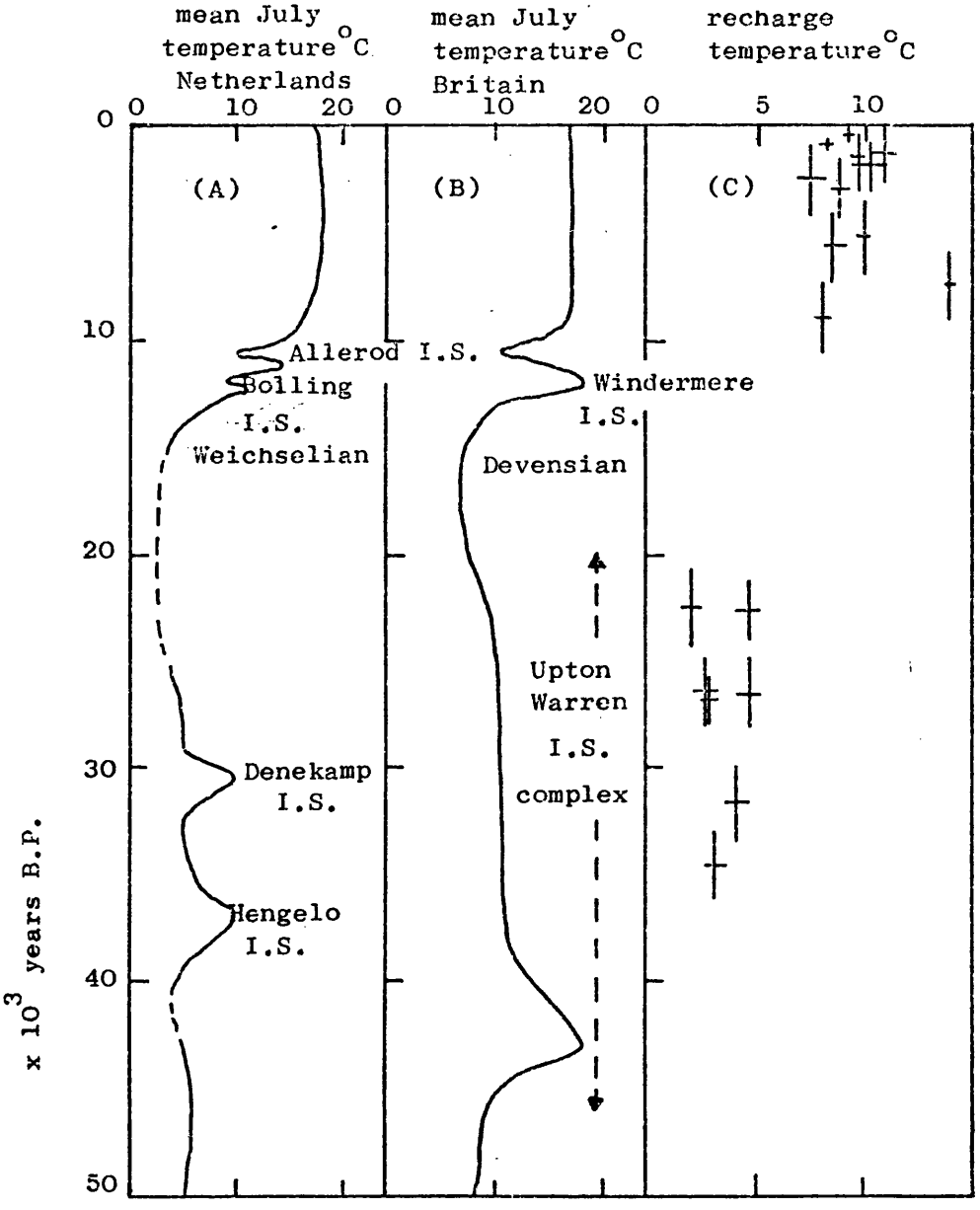

Fig. 3.7. Palaeoclimatic curves.

(A) Palaeoclimatic curve for The Netherlands (van der Hammen et al., 1967).

(B) Palaeoclimatic curve for Britain (Coope 1977).

(C) Recharge temperatures for the Bunter Sandstone groundwaters plotted against corrected ^{14}C age ranges.

The interruption to recharge indicated by the gap in groundwater ages between 10000 and 20000 years before present (yr. B.P.) may be attributed to absence of recharge during the last (Devensian) glaciation. Recharge prior to 20000 yr B.P. would have occurred during the climatic improvement in the mid-Pleniglacial interstadials. Palaeotemperature curves for the Pleniglacial are compared with the recharge temperatures derived from the inert gas contents in figure 3.7. Both palaeotemperatures are based on ^{14}C dating of glacial soil horizons and the temperatures are derived from pollen counts in the case of the Netherlands [127] and from Coleopteran assemblages in the case of Britain [128]. There is broad agreement in the main features of these palaeoclimatic curves, as would be expected as glaciation of the northern hemisphere had global effects [129]. The climatic improvements following the Devensian glaciation in Britain and the Weichselian glaciation of N.W. Europe are synchronous and occurred about 14000yr. B.P. Climatic deterioration in Britain and the Netherlands following the mid-Pleinglacial interstadials began about 24000 yr. B.P. In England, "climate deteriorated very rapidly after the Upton Warren interstadial to become Arctic and eventually to pass to polar desert before the advent of the late Devensian glaciers" [130]. This glaciation did not cover southern and central parts of England [131] but at its maximum advance the climate of central England would have produced a permafrost seal to aquifer recharge. Full polar desert conditions probably existed with mean annual air temperatures at least as low as $-16^{o}C$ [132].

Evidence from polar desert/tundra areas in N.W. America indicate that July air temperatures are about 16 - 21°C higher than mean annual air temperatures [132]. If the palaeotemperature curve minimum for the Devensian glaciation (figure 3.7) is reduced by this amount the mean annual air temperature derived is about -12°C and corresponds to permafrost conditions. Under present climatic conditions, the mean annual temperatures for the English Midlands are about 7°C lower than the mean July temperatures [133]. The average annual temperature for the Holocene may therefore be obtained by reducing the July temperatures in figure 3.7B by 7°C. This gives an estimated annual average temperature of about 9°C in good agreement with the estimated recharge temperatures in this period. Assuming that the July temperatures for the Upton Warren Interstadial may be similarly reduced by 7°C, the average annual temperature would have been about 3°C. This is also in good agreement with the recharge temperatures estimated from the inert gas contents of the Bunter Sandstone groundwaters.

It may be concluded that the derived recharge temperatures most closely reflect the mean annual temperatures. These palaeotemperatures represent the temperature at which the groundwater equilibrated with soil air in the unsaturated zone, rather than the temperature at which the rainwater equilibrated with the air, since re-equilibration in the soil zone must occur. The temperature difference of 5 - 7°C between the two recharge periods is in good agreement with the temperature changes indicated by the climatic record.

Bath et al [123] found a depletion of the ^{18}O content of groundwater recharged during the Upton Warren Interstadial compared with the Holocene. This decrease corresponds to an air temperature difference of 1 - 2°C using Dansgaard's [134] relationship between ^{18}O and temperature. Evans et al [75] derived a more recent relationship between $\delta^{18}O$ and temperature for Western Europe. Using this relationship, the observed $\delta^{18}O$ decrease corresponds to a temperature difference between the two recharge periods of 5 - 6°C which is in good agreement with that derived on the basis of inert gas contents.

3.3. CONCLUSIONS

The ^{222}Rn content of a groundwater is independent of the residence time provided that this is longer than 25 days and is dependent on aquifer characteristics in the locality of the extraction points, even for wells with high extraction rates. The parameters which determine the ^{222}Rn content are the U content of the rock, its porosity and pore size distribution and variability in the ^{222}Rn content is an indication of variability in these parameters.

The ^{4}He content of groundwater in the confined Bunter Sandstone aquifer increases with groundwater age. In principle, the groundwater residence time in the aquifer may be calculated from the ^{4}He content, the radioelement content of the rock and its porosity. For this purpose, it is necessary to select values of these parameters which adequately represent the aquifer values. However, this requires more extensive data on the aquifer than is at present available.

^{4}He generation in the confining strata contributing to the ^{4}He content in the groundwater is also a possible source of enhanced ^{4}He contents and data on these strata are necessary to establish the importance of this contribution. In the absence of sufficient data to enable ^{4}He ages to be calculated accurately, the increase in ^{4}He content must be correlated with another age dependent parameter. In the case of the Bunter Sandstone, the ^{14}C age was used. The ages of groundwaters which are older than the range of the ^{14}C dating method may then be determined by extrapolation of the ^{14}C age - ^{4}He content relationship.

The atmospheric inert gas contents of groundwaters from a confined aquifer may be used to determine the ground temperature during recharge. In the case of the Bunter Sandstone groundwaters, these temperatures have been interpreted in terms of palaeoclimatic changes over the past 50000 years.

CHAPTER 4

RADON, RADIUM AND DISSOLVED INERT GASES IN GROUNDWATERS FROM THE SEDIMENTARY BASINS AROUND AVON, SOUTH WALES AND THE DERBYSHIRE DOME.

4.1. INTRODUCTION

Semi-thermal waters in the United Kingdom occur in the region of the Derbyshire Dome (Carboniferous Limestone) and in the sedimentary basins of Avon and South Wales.[135] The most significant discharges occur in the Bath-Bristol sedimentary basin where thermal water rises through the Carboniferous Limestone at Hotwells, Bristol and through the Lias at Bath. Taff's well is the only source in South Wales and it emerges through the Lower Coal Measures close to the boundary with the Pennant Series. In the Derbyshire Dome, thermal sources occur at Buxton and Matlock and emerge through the Carboniferous Limestone.

Dissolved inert gases, ^{222}Rn and ^{226}Ra contents of these thermal waters and of groundwaters from the different geological horizons important in these sedimentary basins, have been determined with the aim of establishing the thermal water age and source rock, particularly of the Bath thermal spring. The locations of the sites investigated are shown in Figures 4.1-4.2. The constraints which analyses place upon the contribution of various aquifers to the thermal sources are discussed in the light of the inert gas contents, the ^{222}Rn and ^{226}Ra contents and other important physical and chemical factors. Some of the sources have been analysed repeatedly over a period of about 15 months to determine if any temporal variations occur and if these can be related to seasonal recharge.

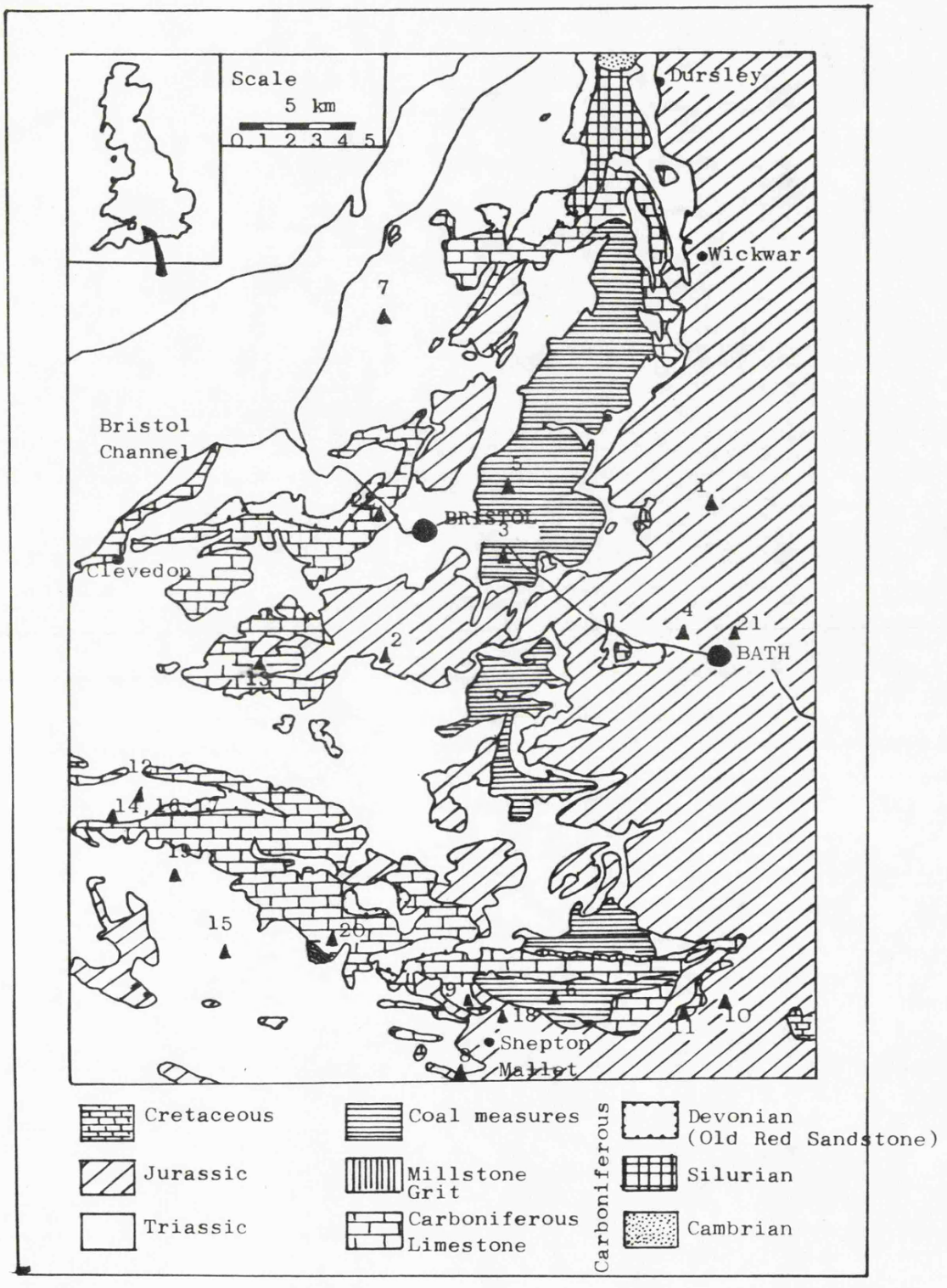

Fig. 4.1. Sketch map showing location of sampling sites and solid geology in the Bath/Bristol area. (Sites numbered as on tables 4.1 and 4.4).

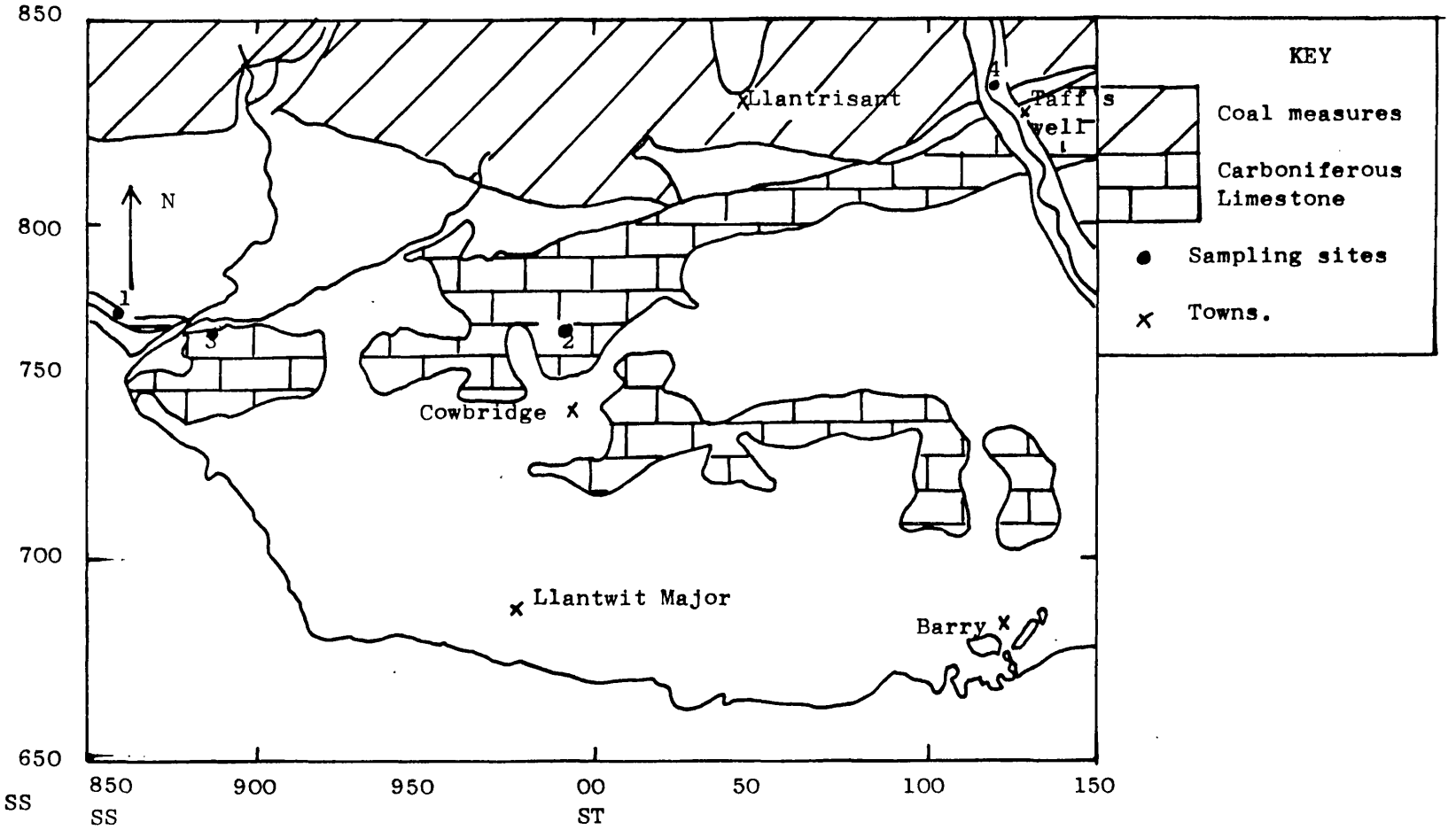

Fig. 4.2. Sketch map showing outline geology and location of sampling points in South Wales (sites numbered as in Table 4.2).

4.2. RESULTS AND DISCUSSION

4.2.1. ^{222}Rn and ^{226}Ra

The ^{222}Rn and ^{226}Ra contents of the groundwaters investigated are reported in Tables 4.1-4.3. The highest ^{222}Rn contents were observed for the thermal sources with the exception of Taff's Well, for which some ^{222}Rn loss may have occurred at the sampling site prior to collection. There is considerable variability in the ^{222}Rn content of the groundwaters studied, even in the same aquifer. This may be attributed to variations in the uranium content of the aquifer rock, its porosity and particle size distribution.

In the Avon sedimentary basin, the ^{222}Rn contents of groundwaters from the Carboniferous Limestone are generally less than those from the Sandstones and Marls in the area. This is expected as the most efficient ^{222}Rn release occurs from uncemented sands and Sandstones and the Carboniferous Limestone is ineffecient in this process [13]. Two exceptions to this generalisation are the groundwaters from B.A.C. Filton and Winford which have relatively high ^{222}Rn contents. This must be attributed to mineralisation in the limestone (e.g. haematite veins occur widely in some parts of the Mendips) or to mixing from other aquifers such as the Keuper Marls and Sandstones or the Old Red Sandstone. Mixing from the overlying Keuper Marl is likely at B.A.C. Filton.

The highest ^{222}Rn contents observed, apart from the thermal sources were for Burrington Adit C (Old Red Sandstone), A.B.M. Bath (Keuper Marl) and Norton Malreward (Lias). The Old Red Sandstone sample was taken from 500 m along a drainage adit.

Table 4.1 ^{222}Rn and ^{226}Ra contents of groundwaters from the Bath/Bristol area

Site number	Formation and location	National Grid Reference	^{222}Rn pCi kg^{-1}	^{226}Ra pCi kg^{-1}
	JURASSIC Midford Sand/Inf. Oolite			
1	Monkswood *	ST 755 710	469 ± 26	0.10 ± 0.01
	Lias			
2	Norton Malreward *	ST 598 650	1332 ± 73	0.54 ± 0.03
	TRIASSIC Keuper Marl			
3	Fry's, Keynsham	ST 655 695	588 ± 34	0.40 ± 0.02
4	A.B.M., Bath	ST 726 651	1597 ± 88	0.21 ± 0.01
	CARBONIFEROUS Pennant Sandstone			
5	Hanham	ST 650 716	437 ± 24	0.31 ± 0.02
	Coal Measures			
6	Edford	ST 671 489	65 ± 4	0.15 ± 0.01
	Carboniferous Limestone			
7	B.A.C., Filton	ST 600 795	386 ± 24	0.48 ± 0.03

Table 4.1 (contd)

Site number	Formation and location	National Grid Reference	^{222}Rn pCi kg^{-1}	^{226}Ra pCi kg^{-1}
8	Frampton's *	ST 629 432	61 ± 4	0.39 ± 0.03
9	Gurney Slade *	ST 631 494	156 ± 9	0.20 ± 0.02
10	Hapsford *	ST 760 492	162 ± 9	0.42 ± 0.04
11	Mells river sink *	ST 738 488	34 ± 2	0.82 ± 0.06
13	Winford	ST 541 650	733 ± 42	0.59 ± 0.03
	Carboniferous Limestone/ Lower Limestone Shales			
14	Burrington Adit A *	ST 476 582	662 ± 43	5.93 ± 0.39
	DEVONIAN Old Red Sandstone			
16	Burrington Adit B *	ST 476 582	105 ± 6	0.59 ± 0.04
17	Burrington Adit C *	ST 476 582	1811 ± 107	0.69 ± 0.08
18	Three Ashes	ST 653 464	744 ± 40	0.33 ± 0.03
20	Waldegrave	ST 574 523	347 ± 20	0.13 ± 0.01
	THERMAL SPRINGS			
21	Bath, King's Spring	ST 750 650	2321 ± 128	10.3 ± 0.6
22	Bristol, Hotwells	ST 566 726	1172 ± 66	0.99 ± 0.06

* Sites at which ^{222}Rn loss could occur before sampling.

Table 4.2. ^{222}Rn and ^{226}Ra contents of groundwaters from South Wales

Site No.	Formation and location	National Grid Ref.	^{222}Rn pCi Kg^{-1}	^{226}Ra pCi Kg^{-1}
	CARBONIFEROUS			
	Carboniferous Limestone			
1	Merthyr Mawr Warren*	SS 857 773	471 ± 26	1.05 ± 0.08
2	Penllyn Pumping Station	SS 992 766	283 ± 16	0.36 ± 0.03
3	Schwyll Pumping Station*	SS 887 770	144 ± 9	1.24 ± 0.08
	THERMAL SPRING			
	Lower Coal Measures			
4	Taff's Well *	ST 119 838	118 ± 7	3.7 ± 0.2

* sites at which ^{222}Rn losses could occur before sampling.

Table 4.3. ^{222}Rn and ^{226}Ra contents of groundwaters from the Derbyshire Dome

Site No.	Formation and location	Grid Ref.	^{222}Rn $pCiKg^{-1}$	^{226}Ra $pCiKg^{-1}$
	CARBONIFEROUS			
	Carboniferous Limestone			
1	Chelmorton Spring	SK 115 703	508±30	0.52±0.05
2	Hillcart Wood, Stanton	SK 259 637	305±19	0.54±0.05
3	Magpie Sough	SK 180 696	298±18	1.41±0.09
4	Stoke Hall Sough/Bath House	SK 240 764	152±9	2.49±0.16
	THERMAL SPRINGS			
	Carboniferous Limestone			
5	Buxton	SK 057 735	2093±139	0.93±0.07
6	Matlock Aquarium	SK 294 584	627±45	2.55±0.16
7	Matlock, New Bath Hotel	SK 293 579	2403±139	2.10±0.14

* sites at which ^{222}Rn losses could occur before sampling.

This corresponds to the sample depth as the strata were folded so that they appeared vertically. So the Burrington Adit C sample is a deep seated sample and high ^{222}Rn contents are often observed in samples from depth. For example, groundwater from the Bunter Sandstone horizon of the Winterbourne Kingston borehole had a ^{222}Rn content of 1290 pCi Kg^{-1} H_2O, compared with an average of 180 pCi Kg^{-1} for the near surface groundwaters from the Bunter Sandstone in Nottinghamshire. A possible explanation is that at depth, the water to volume ratio in an aquifer is reduced so for a constant U content and fractional radon release, a higher ^{222}Rn concentration in the groundwater is obtained.

The A.B.M. Bath source is drawn from a borehole into the Keuper Marl. The temperature of the water (13.2°C) is slightly above normal groundwater temperatures and there are chemical and radiochemical similarities with the thermal water of the King's Spring Bath. This suggests that A.B.M. Bath has a component of thermal water present and that the high ^{222}Rn content has possibly been derived from this source. It has therefore been included with the thermal waters in Table 4.7. so that a comparison can be made with the thermal sources more easily.

The groundwater from the Lias at Norton Malreward has an enhanced ^{4}He content as well as a high ^{222}Rn content. There is also a component of modern water indicated by the tritium content of 53 T.U.[136]. This would indicate that the high ^{222}Rn content is due to either an enhanced U content in the Lias or to some mixing with the underlying Keuper Marls.

All the thermal sources with the exception of Taff's Well have ^{222}Rn contents in excess of 1000pCi Kg^{-1}. This is generally higher than for groundwaters from the sedimentary formations in the Bath/Bristol area. It is also higher than the ^{222}Rn content of non-thermal groundwaters in the same geological horizons as thermal groundwaters in the Derbyshire Dome and South Wales. This suggests that there is something about the thermal nature of these sources which causes their high ^{222}Rn contents. The probable cause is that the thermal groundwaters have percolated to great depths to be ted and to acquire their high ^{222}Rn contents.

^{226}Ra may be dissolved in a groundwater either by chemical etch ects or by recoil from the parent ^{230}Th atoms situated near the face of the aquifer rock particles (see paragraph 1.3). It is ely found in radioactive equilibrium with ^{238}U in natural waters. ^{238}U contents of groundwaters in the Bath/Bristol sedimentary in have been determined [137] and these have been used to calculate $^{226}Ra/^{238}U$ activity ratios for the non-thermal groundwaters, ratio ranges from 0.3 - 8.3 which is within an order of nitude of the equilibrium value. Considering the different chemical behaviour of ^{226}Ra and ^{238}U once in solution, this ge of values could easily be generated following etch solution of both species. An increase in the $^{226}Ra/^{238}U$ ratio would occur if the groundwater evolved towards lower redox potentials and uranium was deposited. This mechanism is partly responsible for the very high $^{226}Ra/^{238}U$ ratio for the King's Spring Bath (515).

The ^{238}U content of this groundwater is unusually low (0.06 $\mu g\ Kg^{-1}\ H_2O$ [137]) as ^{238}U is deposited because of the reducing character of the water. This combined with an unusually high ^{226}Ra content caused by ^{226}Ra being held in solution by the presence of an appreciable concentration of Ca^{2+} and Ba^{2+} ions, leads to a unique $^{226}Ra/^{238}U$ ratio.

4.2.2. Radiogenic ^4He contents

The ^4He content of water equilibrated with air at 1 atmosphere and 10^oC is $4.7 \times 10^{-8}\ cm^3\ STP\ cm^{-3}\ H_2O$ (appendix 4.1). The ^4He contents of the groundwaters studied in Avon, Derbyshire and South Wales is generally close to this value (Tables 4.4-4.6). However, significantly enhanced ^4He contents are observed for all the thermal groundwaters. Enhanced ^4He contents also occur at A.B.M., Bath; Fry's, Keynsham; B.A.C. Filton and Norton Malreward. The excess ^4He in the groundwater from A.B.M., Bath is so high that its origin must be closely related to that of King's Spring, Bath. The groundwaters at Fry's, Keynsham and B.A.C., Filton contain a significant proportion of recent water (^3H contents = 50.2 and 40.6 T.U. respectively [136]) and their excess ^4He must be generated by high radioelement contents, perhaps locally in the Trias, or by mixing with water with a high concentration of radiogenic ^4He. The Norton Malreward source also contains a significant amount of recent water (^3H = 45.1 T.U.). Its enhanced ^4He content is due to either an enhanced radioelement concentration in the Lias or to mixing from the underlying Keuper Marls which may be rich in ^4He.

Site No.	Formation and location	Grid Ref.	$^4He \times 10^8$	$Ne \times 10^7$	$Ar \times 10^4$	$Kr \times 10^7$	$Xe \times 10^8$	Recharge temperature, °C from Ar	Recharge temperature, °C from Kr	Collection temperature, °C
	JURASSIC									
	Lias									
2	Norton Malreward‡	ST 598 650	61.8±8.3	2.10±0.10	4.82±0.17	-	-	2.0±1.5	-	
	TRIASSIC									
	Keuper Marl									
3	Fry's, Keynsham	ST 655 695	28.7±3.8	2.13±0.10	4.23±0.15	0.91±0.02	1.20±0.06	7.6±1.4	7.8±0.8	11.4
4	A.B.M., Bath	ST 726 651	1430. ±190	2.15±0.10	4.45±0.16	0.94±0.02	1.03±0.06	5.5±1.5	6.9±0.8	13.2
	CARBONIFEROUS									
	Pennant Sandstone									
5	Hanham	ST 650 716	6.0±0.8	1.76±0.08	3.71±0.13	0.82±0.02	1.10±0.06	13.3±1.5	12.1±1.1	12.5
	Coal Measures									
6	Edford	ST 671 489	8.3±1.1	2.12±0.10	4.14±0.15	0.91±0.02	1.02±0.05	8.5±1.4	8.3±0.8	10.2
	Carboniferous L.S.									
7	B.A.C., Filton	ST 600 795	188. ±25	2.10±0.10	4.12±0.15	0.88±0.02	1.10±0.06	8.7±1.4	9.3±0.8	14.7
9	Gurney Slade *	ST 631 494	4.1±0.5	2.09±0.10	4.04±0.15	0.86±0.02	1.08±0.06	9.4±1.4	10.2±1.0	10.5
10	Hapsford *	ST 760 492	4.0±0.5	2.08±0.10	3.93±0.14	0.86±0.02	1.23±0.96	10.6±1.4	10.2±1.0	10.4
11	Mells river sink *	ST 738 488	3.9±0.5	2.10±0.10	4.09±0.15	0.90±0.02	1.26±0.07	8.9±1.4	8.5±0.8	11.5
12	Rickford rising *	ST 487 592	5.8±0.8	2.03±0.10	3.96±0.14	0.87±0.02	1.12±0.06	10.2±1.4	9.8±1.0	10.3
13	Winford	ST 541 650	7.6±1.0	2.12±0.10	4.14±0.15	0.89±0.02	1.12±0.06	8.5±1.4	8.9±0.8	10.5
	Lower Limestone Shales									
15	Priddy	ST 531 516	5.0±0.7	2.13±0.10	4.24±0.15	0.90±0.02	1.13±0.06	7.5±1.4	8.5±0.8	10.2
	DEVONIAN									
	Old Red Sandstone									
18	Three Ashes	ST 653 464	5.7±0.8	2.12±0.10	4.20±0.15	0.90±0.02	1.15±0.06	7.9±1.4	8.5±0.8	11.0
19	Upper Chartorhouse	ST 505 555	4.6±0.6	2.10±0.10	4.08±0.15	0.86±0.02	1.08±0.06	9.0±1.4	10.0±1.0	10.4
20	Waldegrave	ST 574 523	6.1±0.8	2.14±0.10	4.21±0.15	0.93±0.02	1.17±0.06	7.9±1.4	7.3±0.8	10.0
	THERMAL SPRINGS									
21	Bath, King's Spring	ST 750 650	1080. ±140	2.10±0.10	4.04±0.15	0.91±0.02	1.19±0.06	9.4±1.4	8.0±0.8	45.5
22	Bristol, Hotwells	ST 566 726	412. ±55	2.08±0.10	4.05±0.15	0.86±0.02	1.16±0.06	9.3±1.4	10.0±1.0	24.1

‡ much sample variability found; ^4He ranged from air saturation to maximum value quoted.

* sites at which some air equilibration could occur before sampling.

Site No.	Formation and location	National Grid. Ref.	Inert gas content, cm³ STP cm⁻³ H_2O					Recharge temp °C		Collection temperature
			$^4He \times 10^8$	$Ne \times 10^7$	$Ar \times 10^4$	$Kr \times 10^7$	$Xe \times 10^8$	from Ar	from Kr	
	CARBONIFEROUS									
	Carboniferous Limestone									
1.	Merthyr Mawr Warren*	SS 857 773	3.7±0.5	2.07±0.10	3.77±0.14	0.87±0.02	1.23±0.06	12.6±1.4	9.6±1.0	10.8
2.	Penllyn Pumping Station	SS 992 766	4.7±0.6	2.17±0.10	4.36±0.16	0.97±0.02	1.34±0.07	6.4±1.5	5.6±0.8	11.1
3.	Schwyll Pumping Station*	SS 887 770	15.0±2.0	2.14±0.10	4.20±0.15	0.92±0.02	1.30±0.07	7.9±1.4	7.5±0.8	11.0
	THERMAL SPRING									
	Lower Coal Measures									
4	Taff's Well*	ST 119 838	544±73	2.17±0.10	4.38±0.16	0.97±0.02	1.39±0.07	6.2±1.5	5.4±0.8	19.0

* sites at which some air equilibration could occur before sampling.

Table 4.6. Inert gas contents, derived recharge temperatures and collection temperatures of groundwaters from the Derbyshire Dome.

Site No.	Formation and location	National Grid No.	Inert gas content, cm^3 STP cm^{-3} H_2O					Recharge temp. °C		Collection temp. °C
			^4He x 10^8	Ne x 10^7	Ar x 10^4	Kr x 10^7	Xe x 10^8	from Ar	from Kr	
	CARBONIFEROUS									
	Carboniferous Limestone									
2	Hillcarr Wood, Stanton	SK 259 637	4.1±0.6	2.17±0.10	4.35±0.16	0.98±0.02	1.35±0.07	6.5±1.5	4.9±0.8	8.9
3	Magpie Sough	SK 180 696	11.5±1.5	2.14±0.10	4.29±0.15	0.94±0.02	1.30±0.07	7.1±1.4	7.1±0.8	9.9
	THERMAL SPRINGS									
	Carboniferous Limestone									
5	Buxton	SK 057 735	50.0±6.7	2.09±0.10	3.98±0.14	0.88±0.02	1.18±0.06	10.0±1.4	9.4±0.8	27.5
6	Matlock Aquarium	SK 294 584	75 ± 10	2.18±0.10	4.43±0.16	0.96±0.02	1.32±0.07	5.7±1.5	5.9±0.8	20.0
7	Matlock, New Bath Hotel	SK 293 579	84 ± 11	2.21±0.10	4.56±0.16	1.00±0.02	1.40±0.07	4.5±1.5	4.6±0.8	19.9

Table 4.7. Comparison of selected parameters in some thermal springs

Name and Grid Ref.	Discharge temperature ^{o}C	Estimated recharge temp ^{o}C	^{4}He content $cm^{3}STPcm^{-3}$ H_2Ox10^{8}	^{222}Rn content $pCiKg^{-1}$	^{226}Ra content $pCiKg^{-1}$	$^{222}Ra/^{238}U$ activity ratio	$^{40}Ar/^{36}Ar$ ratio (air=295.5)
Bath, ABM** (ST 726 651)	13.2	6.2	1430	1600	0.21	0.37	293.7
Bath, King's Spring (ST 750 650)	45.5	8.7	1080	2320	10.3	515	295.4
Bristol, Hotwells (ST 566 726)	24.1	9.7	410	1172	0.99	3.0	-
Buxton (SK 057 735)	27.5	9.7	50	2090	0.93	1.0	307.9
Matlock (SK 293 579)	20.0	5.4	80	2400	2.10	3.2	-
Taff's Well (ST 119 838)	19.0	5.8	540	120	3.7	16	300.9

** included for comparison with King's Spring.

Anomalously high ^4He contents, apart from those associated with thermal springs, therefore generally occur where there is the possibility of a contribution from the Triassic sediments. Uraniferous nodules have been found in these sediments [138]. Alternatively, the high ^4He contents in these young groundwaters may be due to the diffusion of radiogenic ^4He from depth along structural faults in the vicinity of the extraction boreholes. Such an origin would be similar to that of the ^4He in thermal waters which must be generated at depth over a long period of time. However, in the case of the thermal waters, the ^4He is transported to the surface in solution rather than by gaseous diffusion along structural faults.

Groundwaters which have passed through the Carboniferous Limestone under the South Wales Coalfield syncline (Penllyn pumping station and Schwyll pumping station) show little enhancement of the ^4He content. This is a little surprising as the depth to the Carboniferous Limestone in the centre of the basin is about 2000m. Evidence from the recharge temperatures derived from the argon and krypton contents of the groundwaters (Table 4.5) supports the suggestion that these groundwaters were recharged on the North Crop, passed under the coalfield and re-emerged on the South Crop of the Carboniferous Limestone [139]. The absence of radiogenic ^4He from these waters suggests that their passage under the coalfield has been relatively rapid, taking a few thousand years only. ^3H analyses on these samples indicate that they contain a significant component of recent water [136]. The high ^4He content and the thermal nature of

Taff's Well indicate that its source is very different from the other Carboniferous Limestone groundwaters from South Wales. It is probably derived from much deeper in the Carboniferous Limestone where it acquires its high ^{4}He content after a long residence time. Such residence at depth would also lead to an enhanced temperature.

Thermal springs occur in Derbyshire at Buxton and Matlock. The three thermal sources analysed have ^{4}He contents greater than the non-thermal sources in the area. However, the ^{4}He contents are very much less than is found for the thermal sources in Avon and South Wales. The relevance of the ^{4}He content to the origin of the thermal springs in the Derbyshire Dome is discussed below (paragraph 4.4)

4.2.3. Radiogenic ^{40}Ar contents.

The isotopic ratio $^{40}Ar/^{36}Ar$ for atmospheric argon is 295.5. A deeply circulating groundwater may accumulate ^{40}Ar due to leakage from mineral phases of the host rock after ^{40}K has decayed. The rate of generation and loss of ^{40}Ar by this method is very slow compared with the circulation time of most groundwaters and very long residence times are required for a detectable change in the $^{40}Ar/^{36}Ar$ ratio to occur (paragraph 1.4.2). Nevertheless, slightly enhanced $^{40}Ar/^{36}Ar$ ratios have been observed in some thermal spring systems [140]. Of the thermal springs investigated in the United Kingdom, only Buxton and Taff's Well show slight enhancement of the $^{40}Ar/^{36}Ar$ ratio (Table 4.7.). The excess radiogenic ^{40}Ar may have been produced

by decay of potassium atoms close to the water/rock interface or it may have leaked from the deep aquifer rock at elevated temperatures. As there is no enhancement of the $^{40}Ar/^{36}Ar$ ratio at the King's Spring, Bath, the thermal component at Bath must either be younger than that at Buxton or Taff's Well or have been equilibrated with rock at a lower temperature which would imply a shallower origin. Alternatively, ^{40}Ar may diffuse more easily from minerals in the vicinity of Buxton and Taff's Well and the ^{40}K content may be greater. However, this would seem unlikely, because of the similar nature of the formations in which the thermal springs occur.

4.2.4. Recharge temperatures estimated from inert gas contents

The recharge temperatures derived from the argon and krypton contents of the groundwaters investigated are reported in Tables 4.4 - 4.6. In most cases, the recharge temperature is in the range 8.5 - 10.5°C, even for the thermal sources. This is close to the average autumn/winter regional temperatures. Higher estimated recharge temperatures are probably due to partial or complete re-equilibration of the groundwater with air at the collection site.

The groundwaters from Penllyn pumping station, Schwyll pumping station and Taff's Well have estimated recharge temperatures below the average rechargeseason ground temperatures. This could be due to recharge under cooler climatic conditions if the groundwaters are sufficiently old.

The minimum age for which there would be a sufficient decrease in average annual temperatures is about 12000 years, the end of the Devensian glaciation in Britain. However, ^{14}C ages and radiogenic ^{4}He contents indicate that they are probably not as old as this. It has been suggested that some of the groundwaters discharging on the South Crop of the Carboniferous Limestone in South Wales, are recharged on the North Crop and pass under the Coal Measures in the centre of the basin [139]. The altitude of the North Crop is about 500m above that of the South Crop. This corresponds to a reduction of about $5^{o}C$ in the average autumn/winter temperatures. The estimated recharge temperatures of Penllyn pumping station, Schwyll pumping station and Taff's Well are consistent with recent recharge on the North Crop. The passage under the coalfields must be sufficiently rapid for little excess radiogenic ^{4}He to be accumulated, requiring at most a few thousand years. Data from stable isotope determinations from these groundwaters would be of value to confirm this interpretation.

The recharge temperatures of the Derbyshire Dome waters are also lower than the average autumn/winter ground temperature. This may be explained by the fact that they too are recharged at higher altitude. Again, stable isotope data would be useful to confirm this interpretation.

4.3. TEMPORAL MONITORING OF ^{222}Rn, ^{226}Ra AND ^{4}He CONTENTS IN SOME GROUNDWATERS IN AVON

Periodic measurement of ^{222}Rn, ^{226}Ra and ^{4}He in some groundwaters in Avon was carried out in order to establish the response of the thermal water to the seasonal recharge pattern. The results of this temporal monitoring are reported in Tables 4.8 - 4.11. Figure 4.4 shows graphically the variation of ^{226}Ra, ^{222}Rn and ^{4}He contents of King's Spring, Bath and compares these with the regional and local rainfall records for 1977/78. There is no marked variation in the seasonal rainfall record over this period, though groundwater recharge will have been reduced in the summer months due to the greater importance of evapotranspiration. In contrast, in 1976, there was a marked summer drought, such as occurs with a frequency of about once in a hundred years. The effect of the drought appears to be reflected in the ^{226}Ra, ^{222}Rn and ^{4}He contents of King's Spring. The ^{226}Ra content of King's Spring has been constant since August 1977, but was considerably less when measurements were commenced in April 1977. The ^{222}Rn and ^{4}He contents show a similar marked increase over the period April to July 1977 and subsequently show only a slight tendency to increase towards the period of maximum groundwater recharge in winter. There is a similarity in the seasonal response of ^{4}He and ^{222}Rn as would be expected from their similar geochemical behaviour.

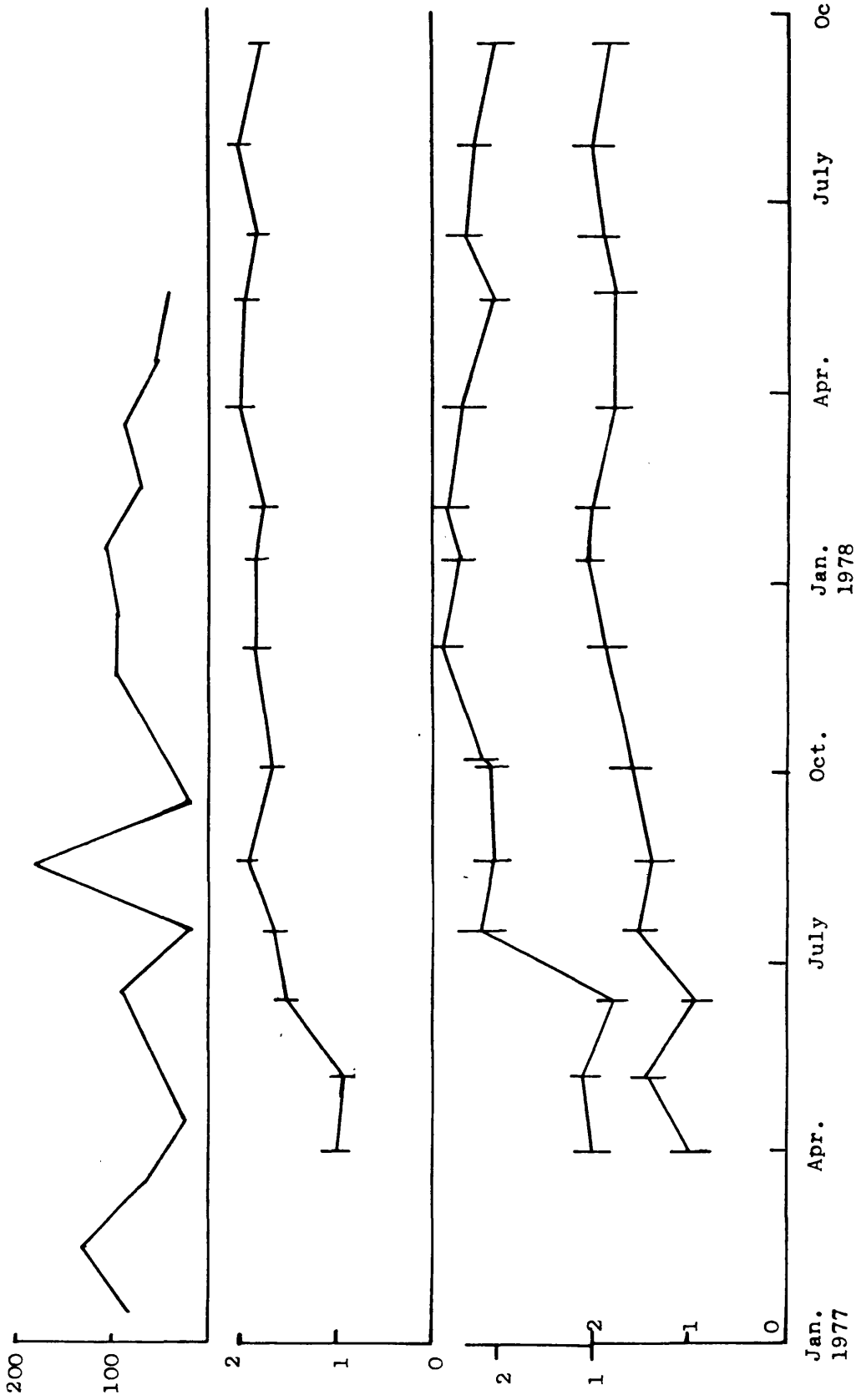

Fig. 4.3. Temporal monitoring of ^{226}Ra, ^{222}Rn and ^{4}He contents of King's Spring, Bath

Table 4.8. Temporal monitoring of ^{222}Rn, ^{226}Ra and ^{4}He contents of King's Spring, Bath (Thermal Spring)

Collection date	^{222}Rn pCi Kg^{-1}	^{226}Ra pCi Kg^{-1}	^{4}He cm^3 STP cm^{-3} H_2O x 10^8
29.3.77	1030 ± 60	5.9 ± 0.3	627 ± 84
6.5.77	1130 ± 60	5.5 ± 0.3	897 ± 120
13.6.77	777 ± 43	8.9 ± 0.5	564 ± 76
15.7.77	2240 ± 120	9.6 ± 0.5	946 ± 126
19.8.77	2110 ± 120	11.2 ± 0.6	853 ± 114
3.10.77	2120 ± 120	9.8 ± 0.5	1000 ± 130
6.10.77	2240 ± 120	-	-
1.12.77	2650 ± 150	10.9 ± 0.6	1170 ± 160
12.1.78	2450 ± 140	10.6 ± 0.6	1270 ± 170
7.2.78	2560 ± 140	10.3 ± 0.6	1240 ± 170
23.3.78	2429 ± 130	11.7 ± 0.6	1100 ± 150
19.5.78	2070 ± 110	11.3 ± 0.6	1090 ± 150
15.6.78	2390 ± 130	10.7 ± 0.6	1180 ± 160
18.7.78	2300 ± 130	11.8 ± 0.6	1240 ± 170
15.9.78	2050 ± 110	10.5 ± 0.6	1140 ± 150

Table. 4.9 Temporal monitoring of ^{222}Rn and ^{4}He contents of A.B.M., Bath (Keuper Marl)

Collection date	^{222}Rn pCi Kg^{-1}	$^{4}He_{-3}$ cm^3 STP cm^{-3} $H_2O \times 10^8$
11.7.77	1390 ± 80	-
11.1.78	1750 ± 100	1420 ± 190
27.1.78	1780 ± 100	1320 ± 180
7.2.78	1770 ± 100	1280 ± 170
21.3.78	1540 ± 90	1630 ± 220
9.5.78	1410 ± 80	1520 ± 200
26.7.78	1760 ± 100	1430 ± 190
15.9.78	1690 ± 90	1400 ± 190

Table 4.10 Temporal monitoring of ^{222}Rn and ^{4}He contents of Fry's Keynsham. (Keuper Marl)

Collection date	^{222}Rn pCi Kg^{-1}	^{4}He cm^3 STP cm^{-3} H_2O x 10^8
9.9.77	426 ± 25	33.7 ± 4.5
30.11.77	522 ± 30	35.7 ± 4.8
11.1.78	665 ± 39	16.5 ± 2.2
7.2.78	662 ± 38	-
21.3.78	584 ± 34	21.3 ± 2.9
17.5.78	599 ± 35	30.0 ± 4.0
12.7.78	710 ± 41	58.0 ± 7.8
14.9.78	423 ± 25	68.0 ± 9.1

Table 4.11 Temporal monitoring of ^{222}Rn content of Waldegrave borehole (Old Red Sandstone)

Collection date	^{222}Rn pCi Kg^{-1}
15.7.77	304 ± 17
28.11.77	391 ± 22
13.1.78	377 ± 21
29.3.78	381 ± 22
17.5.78	327 ± 19
12.7.78	419 ± 24
14.9.78	354 ± 20

The ^{226}Ra and ^{222}Rn contents subsequent to August 1977 are similar to those determined in 1969/70 by Andrews and Wood[25]. The low concentrations of these radioelements prior to August 1977 must be related to the 1976 drought and a reduction in flow rate of the spring is thought to have occurred during the drought. Since August 1977, no large reductions in the radioelement contents have occurred and therefore the groundwater systems involved must have returned to their normal peizometric levels. Only minor seasonal variations now take place.

The ^{222}Rn and ^{4}He contents tend to be higher in the winter. At this time, the peizometric levels in the superficial aquifers (Lias and Keuper Marl) are at their highest. This would have two effects. Firstly, diffusive losses of ^{222}Rn and ^{4}He through the Lias and Keuper Marl would be minimised because of their increased level of saturation. Secondly, the priming of the interstitial or percolation flow at depth may be increased and lead to more effective solution of ^{222}Rn and ^{4}He.

The variation of the ^{222}Rn contents of groundwaters from A.B.M. Bath; Fry's, Keynsham and Waldegrave are compared with the rainfall record in Figure 4.5. As with the thermal water, there is a tendency for the maximum ^{222}Rn contents to coincide with the periods of maximum aquifer recharge in the winter months. For these groundwaters, it is primarily the more efficient priming of the interstitial pore spaces at times of maximum recharge which results in the increased ^{222}Rn contents.

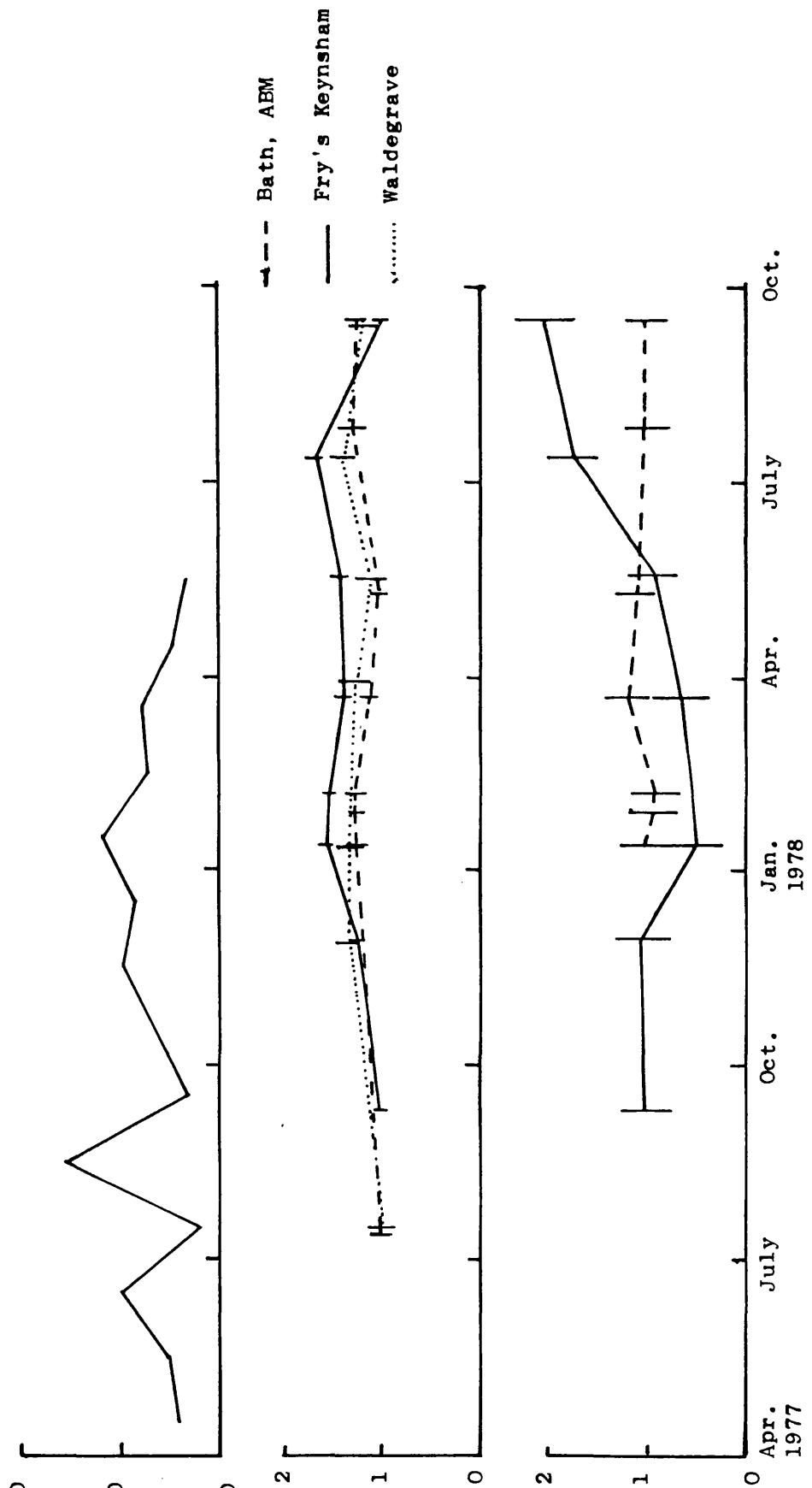

Fig. 4.4. Temporal monitoring of ^{222}Rn and ^{4}He contents of ABM, Fry's and Waldegrave boreholes.

The variation of the ^4He contents of the groundwaters from A.B.M. Bath and Fry's Keynsham are plotted in Figure 4.4. The ^4He content of A.B.M., Bath is essentially constant whereas the ^4He content of Fry's Keynsham is highly variable. There are also large variations in the U concentration at Fry's, which is generally rather high [137]. The variations in ^4He and U may be due to variations in the amount of recharge or large influxes of water diluting the U and ^4He concentration. This is consistent with the fact that the groundwater has been recently recharged. (^3H = 50.2 T.U., Eh = 319 mV, dissolved O_2 = 20% [136]). Nevertheless, the enhanced ^4He content at Fry's is remarkable for such a recent groundwater.

4.4. INTERPRETATION OF THE ORIGIN OF THE THERMAL SPRINGS IN THE UNITED KINGDOM.

The thermal springs at Buxton and Matlock arise in the Carboniferous Limestone of the Derbyshire Dome. They are high in sulphate compared with other local groundwaters [141]. The sulphate must be formed by sulphide oxidation or from gypsum deposits within the limestone. It is possible that some of the sulphate in the Avon and South Wales thermal sources might be derived by a similar mechanism at depth in the limestone. Buxton has a high ^{222}Rn content and an enhanced ^4He content (which may be artificially low because of difficult sampling conditions). The low ^4He content of Buxton compared with King's Spring and Taff's Well suggests a lower age or that the

proportion of thermal component is lower. Therefore, the ^{222}Rn at Buxton is probably derived nearer to the surface than the ^{4}He since the larger volume of recent water is likely to contribute more to the ^{222}Rn content than the smaller volume of thermal water. The presence of excess radiogenic ^{40}Ar at Buxton indicates a high age for the thermal component or that it has originated at a depth where the elevated temperatures have facilitated the release of radiogenic ^{40}Ar from the mineral phases. Evidence from the ^{4}He content and the ^{14}C activity (the ^{14}C age is 3300 years [75]) confirm that the proportion of recent water in the spring may be substantial.

Taff's Well thermal water has a higher ^{4}He content, a lower ^{222}Rn content and a less enhanced $^{40}Ar/^{36}Ar$ ratio than Buxton thermal water. The ^{4}He content and temperature suggest a higher proportion of thermal water than at Buxton but with more cooling as the water ascends than at Buxton. The slow ascent may account for the relatively low ^{222}Rn content at Taff's Well. It is possible that some ^{222}Rn (and ^{4}He) is lost by reequilibration with air at the sample site.

Both ^{222}Rn and ^{4}He are high at King's Spring, implying a greater proportion of thermal water than for either Buxton or Taff's Well. However, there is no detectable enhancement of the $^{40}Ar/^{36}Ar$ ratio, so there can have been little or no leakage of radiogenic ^{40}Ar at depth. This may indicate that the source

rock for King's Spring has a higher ^{40}Ar retention than the Carboniferous Limestone in which Buxton and Taff's Well originate. Alternatively, it may mean that the Bath thermal water originates at a lower temperature than the thermal component at Buxton and Taff's Well, but that its ascent is comparatively rapid with little cooling. The ^{226}Ra content of King's Spring is uniquely high amongst the thermal springs in the United Kingdom. It diminished coincidentally with the ^{222}Rn and ^{4}He contents during the 1976 drought conditions, a behaviour for which no explanation has yet been found.

Comparison of the chemistry of Hotwells and King's Spring with that of the Carboniferous Limestone groundwaters suggest that Hotwells could be a mixture of about two parts thermal water similar to that at Bath, with five parts Carboniferous Limestone water. ^{222}Rn contents and ^{4}He contents indicate that Hotwells contains about 40% thermal water. However, the relative ^{226}Ra contents suggest that the thermal component in Hotwells is less than 10%. The estimates assume that the composition of the thermal water remains constant for both locations. This need not necessarily be the case.

There is a close relationship between the King's Spring and Keuper Marl groundwater at A.B.M., Bath. There are remarkable similarities between the chemistry, radiochemistry and ^{14}C ages. The temperature at A.B.M., however, is only slightly elevated (13.2^{o}C) and the ^{226}Ra content is low compared with that at King's Spring. The ^{222}Rn and ^{4}He contents at A.B.M.

are very similar to the values at King's Spring. It is possible that ^{4}He and ^{222}Rn diffuse from the nearby thermal water. However, the chemical similarity between the Keuper groundwater at A.B.M. and the thermal water, suggests that the thermal water chemistry is strongly influenced by passage through the Keuper. If the residence time of the thermal water in the Keuper exceeded 20 days, its ^{222}Rn content would be entirely determined by the uranium content, porosity and fractional ^{222}Rn release in that aquifer. This seems unlikely, as other Keuper groundwaters in the area have ^{222}Rn contents which are very much less than those at A.B.M. and King's Spring. Data on U content and porosity of the Marls would clarify the interpretation.

The ^{4}He content at A.B.M., Batn is higher than that of the thermal water. A major source of ^{4}He is necessary to explain such a high ^{4}He content. The possibilities are that there could be U concentrations in the Keuper Marl close to A.B.M.; that the thermal water transports ^{4}He near to A.B.M. or that ^{4}He diffuses from depth, perhaps along the nearby Pennyquick fault. Since the ^{4}He content at A.B.M. is greater than at King's Spring, the A.B.M. borehole could be closer to the deep geothermal source than the thermal spring itself.

It is likely that the crustal geothermal gradient provides the heat source for the thermal water. Assuming a geothermal gradient of $25^{o}C\ km^{-1}$, a depth of about 1400m would be required

to heat a groundwater from 10°C to the 45°C measured at King's Spring. The temperature at which the King's Spring thermal water equilibrated with the geothermal heat source is likely to be higher than the collection temperature. The Na/K/Ca and SiO_2 geothermometers indicate a rock equilibration temperature of approximately 68°C. This represents a depth of 2300m at a geothermal gradient of 25°C Km^{-1}. This explanation could be applied to all the thermal sources in the United Kingdom, but the degree of cooling during ascent must also be taken into account. Data from the U geochemistry [137] suggest that Buxton, Matlock and Taff's Well have origins deep in the Carboniferous Limestone, whereas the U geochemistry of King's Spring is probably determined in the Trias.

4.5. CONCLUSIONS

The possible evolution of the thermal waters investigated is summarised in Table 4.12. It is apparent that determination of the stable inert gases, ^{222}Rn and ^{226}Ra can provide important information on the origin of such waters. The ^{222}Rn and ^{4}He contents of thermal waters is usually high. These gases may diffuse into the local groundwaters so that the occurrence of ^{222}Rn and ^{4}He anomalies could provide a useful tool for prospecting for geothermal groundwaters. High ^{226}Ra contents characterise some thermal waters. The ^{226}Ra content of these thermal waters may influence adjacent groundwaters only by direct mixing.

Table 4.12. Evolution of U.K. thermal waters

	Buxton	Taff's Well	King's Spring	A.B.M., Bath	Hotwells, Bristol
^{3}H content	1.8 T.U.	-	0.0 - 0.4 T.U.	6.1 T.U.	38.3 T.U.
^{14}C age	13,000 y uncorr. 3,300 y corr.	-	21 - 28,000 y uncorr.	19,600 uncorr.	3500 y uncorr.
^{4}He content	50×10^{-8}	544×10^{-8}	1078×10^{-8}	1432×10^{-8}	412×10^{-8} $cm^3/cm^3 H_2O$
^{222}Rn "	2093	118	2321	1597	1172 pCi/kg
temperature	27.5	19.0	45.5	13.2	24.1 °C
Eh	-	45.	31. - 46.		350. mV
mixing, ^{14}C indication	large fraction modern water	not known	<10% modern	<10% modern	about 65% modern
^{4}He indicates	small proportion deep thermal water	Intermediate fraction thermal water	large proportion thermal water	considerable ^{4}He diffusion from thermal water or fault aided diffusion	intermediate fraction thermal water
^{222}Rn indicates	largely derived from modern component	low radon suggests slow ascending thermal water, much cooling	partly derived in Keuper?	derived from Keuper?	derived from mixture Carboniferous L.S. and thermal groundwaters.
$^{234}U/^{238}U$ interpretation	Carboniferous L.S.	Carboniferous L.S.	close relationship between these sources Some recharge from west to King's Spring		Carboniferous L.S. source
Overall interpretation	small fraction of rapidly rising thermal water, large extent of mixing	Slowly ascending thermal water	Rapidly rising thermal water, perhaps shallower origin (Ar isotopes) than Buxton and Taff's Well	Some thermal contribution ^{4}He content indicates proximity thermal water or fault	Thermal water mixed with Carboniferous L.S. water of very recent origin.

^{226}Ra anomalies are useful as an index of mixing with certain thermal waters since ^{226}Ra is not readily removed from waters with appreciable Ca^{2+} and Ba^{2+} concentrations.

The $^{40}Ar/^{36}Ar$ ratio is also useful in providing data on the origin of thermal springs. An enhanced $^{40}Ar/^{36}Ar$ ratio may indicate that a groundwater has interacted with a potassium bearing mineral at a high temperature, facilitating release of ^{40}Ar produced by the radioactive decay of the ^{40}K isotope. Alternatively, variation in the $^{40}Ar/^{36}Ar$ ratio for old groundwaters indicates variation in the degree to which the minerals in the aquifer rock retain ^{40}Ar.

CHAPTER 5

RADON, RADIUM AND DISSOLVED INERT GASES IN GROUNDWATERS FROM THE LINCOLNSHIRE LIMESTONE

5.1. INTRODUCTION

The age of the Lincolnshire Limestone is Middle Jurassic. The Limestone outcrops along a north-south line, some 120 km long, between the Humber and Kettering in eastern England. It exhibits considerable lateral and vertical lithological variations, but two principle divisions can be made. In the outcrop area, the lower half is a cemented oolitic limestone with locally sandy facies near the base; the upper half is generally a more massive freestone facies which is extensively quarried. The limestone is over 30m thick at outcrop, thinning to less than 20m in the east, where it dips less than 1^{o} to the east. It is overlain by sands, clays, shales and limestones of the Upper Estuarine Series which vary in thickness from 4.5 to 14m. It is underlain by a sequence of sands with silts, clays and shales (Lower Estuarine Series). Slow leakage of groundwater from the Lincolnshire Limestone may occur through these locally semi-permeable strata.

The limestone has been extensively exploited for water supply for some 200 years particularly in the confined area in the south east of the region. Recharge to the limestone is by infiltration derived mainly from direct precipitation and to a lesser extent from influence streams. Movement of the groundwater is predominantly through fissures, although the rates of movement are locally variable and are related to the size and frequency of fissure development.

The hydrochemistry of the Lincolnshire Limestone has been described by Downing and Williams [142]. At outcrop, the groundwater is calcium bicarbonate in type. Some distance down gradient, the water becomes sodium-rich as the Ca^{2+} ion in solution exchanges for the Na^{+} ion in the aquifer rock. The chloride content increases simultaneously and further down gradient the groundwater becomes strongly sodium chloride in character. The oxidising capacity of the groundwater decreases down gradient. There is a sharp oxidation-reduction barrier some 10 - 12 km from outcrop [143]. The tritium content of the groundwater has been used to estimate the flow rate which is about 2 km/year [143]. However, the rate of eastwards movement of the E_H barrier and of other reaction fronts in the aquifer will be much less than the rate of groundwater movement. Evidence from the hydrochemistry of the Lincolnshire Limestone indicates the mixing of two fundamentally different water types. Supposed connate water mixes with recharge water along a narrow interface zone. [144]

The radiocarbon content of the groundwater generally decreases down gradient but not in a very regular manner and ^{14}C ages in excess of 25000 years are indicated in the east of the region [28]. The distribution of water of different ages in the aquifer is closely related to recent groundwater abstraction patterns. The temperature at recharge for water older than 9000 years has been calculated as $8^{o}C$ from the $\delta^{18}O$ and δD values. [145]

The inert gas, ^{222}Rn and ^{226}Ra contents of groundwaters from the recharge zone, the mixed zone and the fully confined zone of the Lincolnshire Limestone have been determined. The location of the sampling sites is shown in Figure 5.1. together with the outcrop geology of the Lincolnshire Limestone. The ^{4}He contents of groundwaters from artesian wells in the mixing zone have been used to estimate mixing proportions. These correlate well with the mixing pattern derived from chlorinity variations. The pore water is shown to have a minimum age of 4.7 million years (m.y.). The recharge temperatures derived from the argon and krypton contents of the groundwaters have also been interpreted in terms of a mixing model. ^{222}Rn and ^{226}Ra have been used to assess aquifer variability in the locality of the extraction boreholes.

5.2. RESULTS AND DISCUSSION

5.2.1. ^{222}Rn and ^{226}Ra contents

The ^{222}Rn and ^{226}Ra contents of groundwaters from the Lincolnshire Limestone are reported in Table 5.1. The average ^{222}Rn and ^{226}Ra contents are 127 and 0.99 pCi Kg^{-1}, respectively. Histograms of the ^{222}Rn and ^{226}Ra contents and probability plots (Figures 5.2 and 5.3) indicate that both the ^{222}Rn and ^{226}Ra contents of the groundwaters are distributed log-normally. Log-normal or skew distributions of ^{222}Rn and ^{226}Ra contents are commonly found in natural water systems.

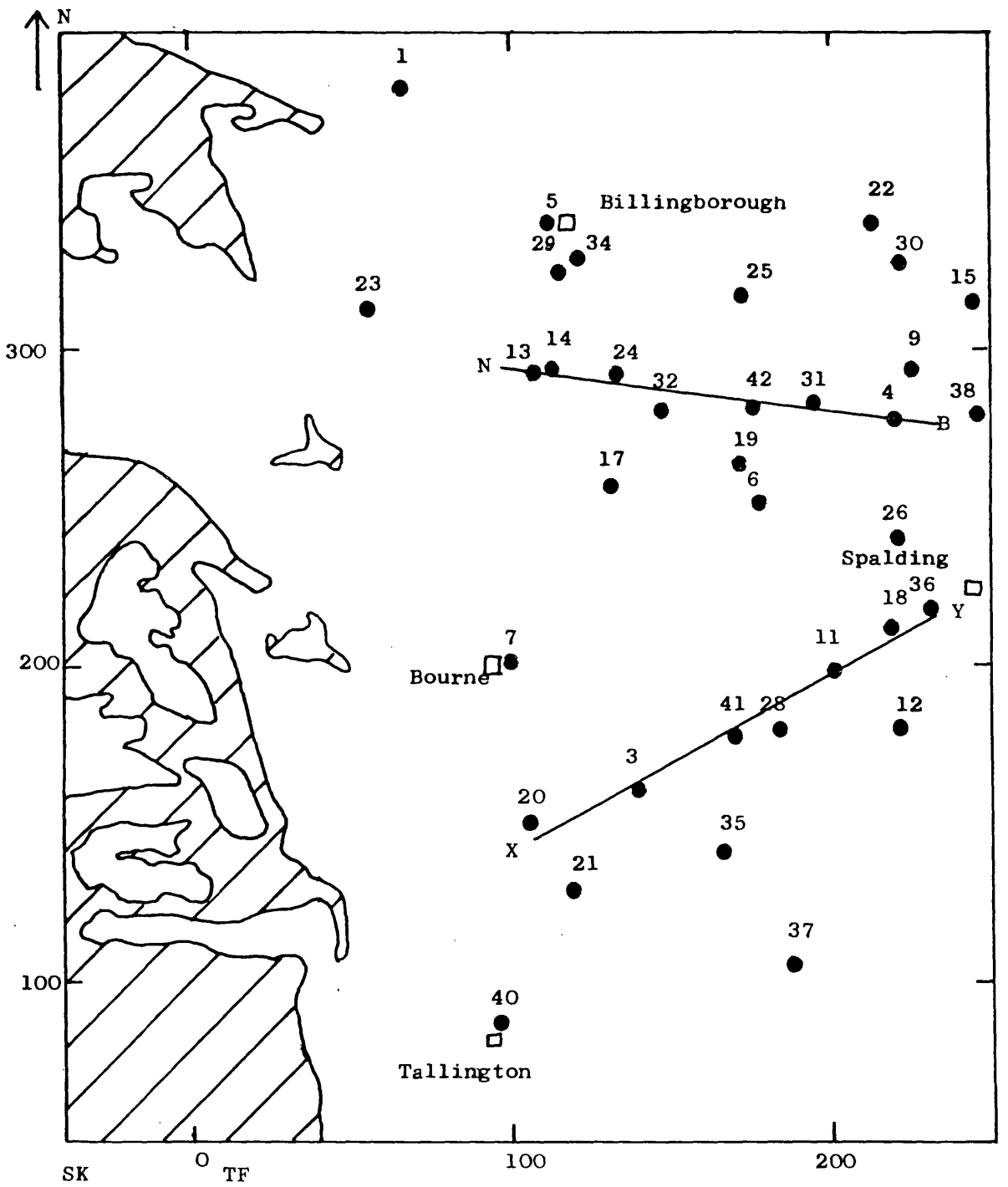

Figure 5.1. Location of sampling sites and outcrop geology of the Lincolnshire Limestone (shaded area)

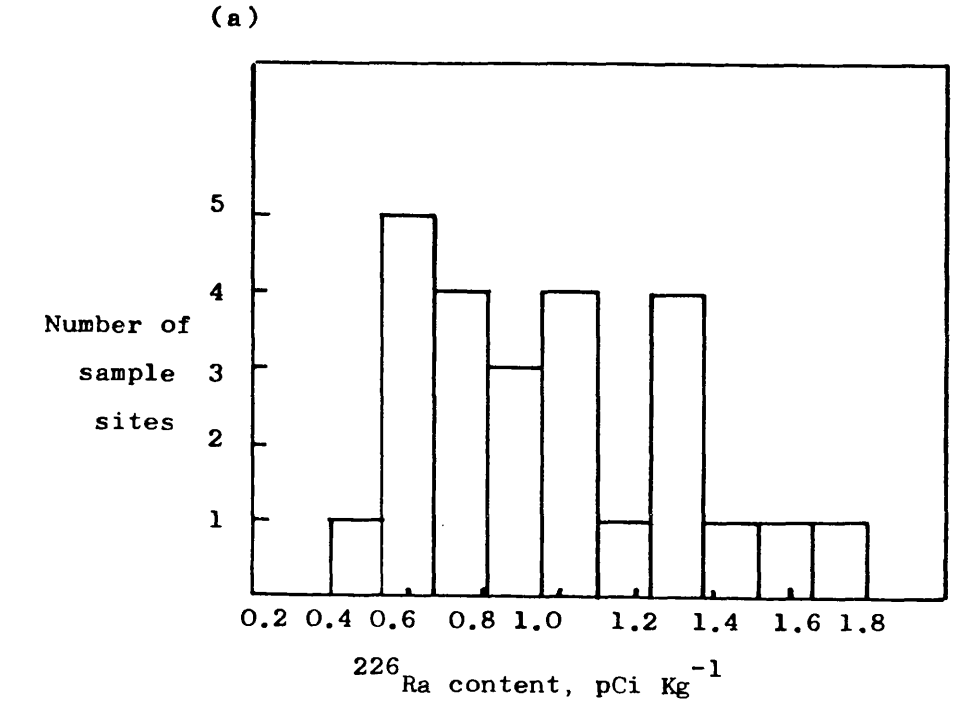

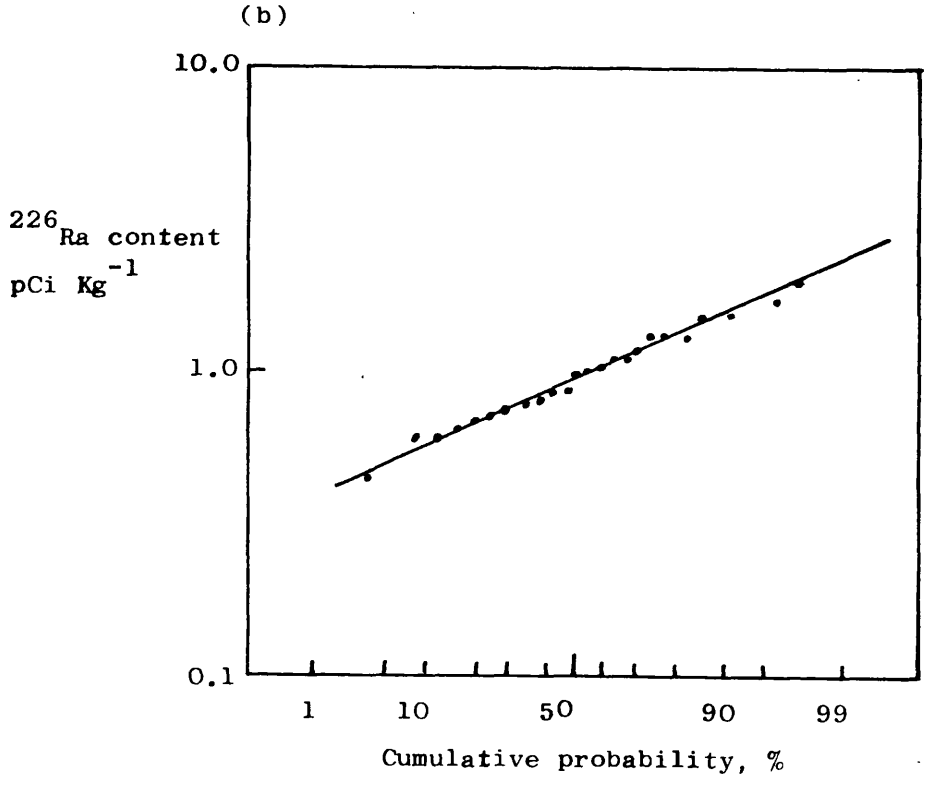

Fig. 5.2. ^{226}Ra contents of groundwaters from the Lincolnshire Limestone. (a) Histogram and (b) log normal probability plot of ^{226}Ra contents.

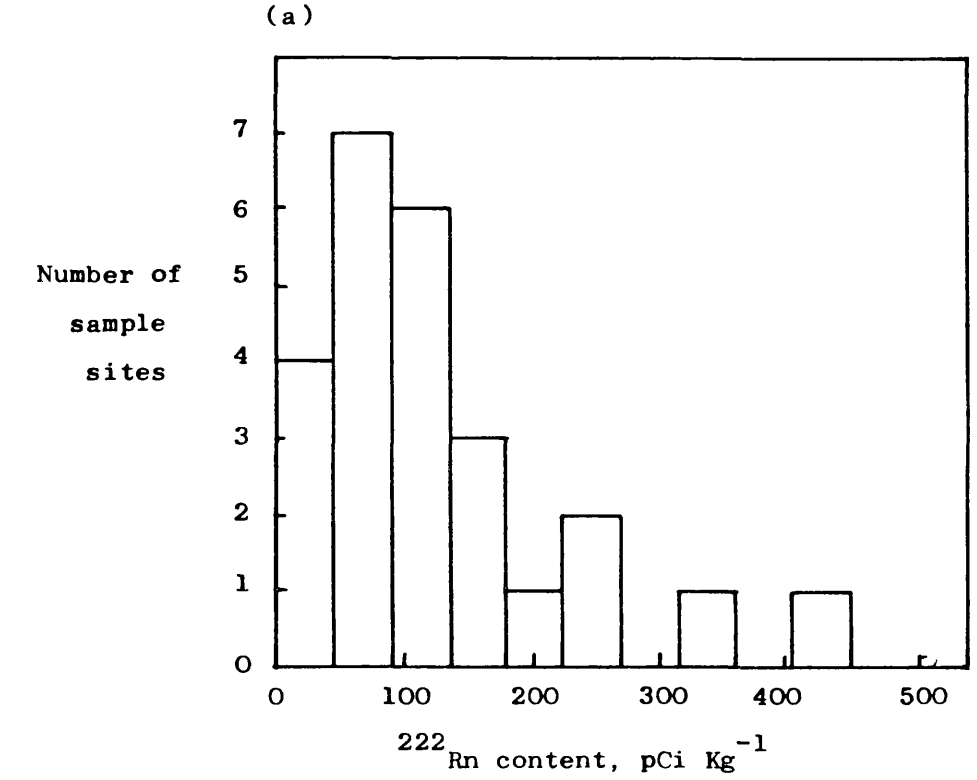

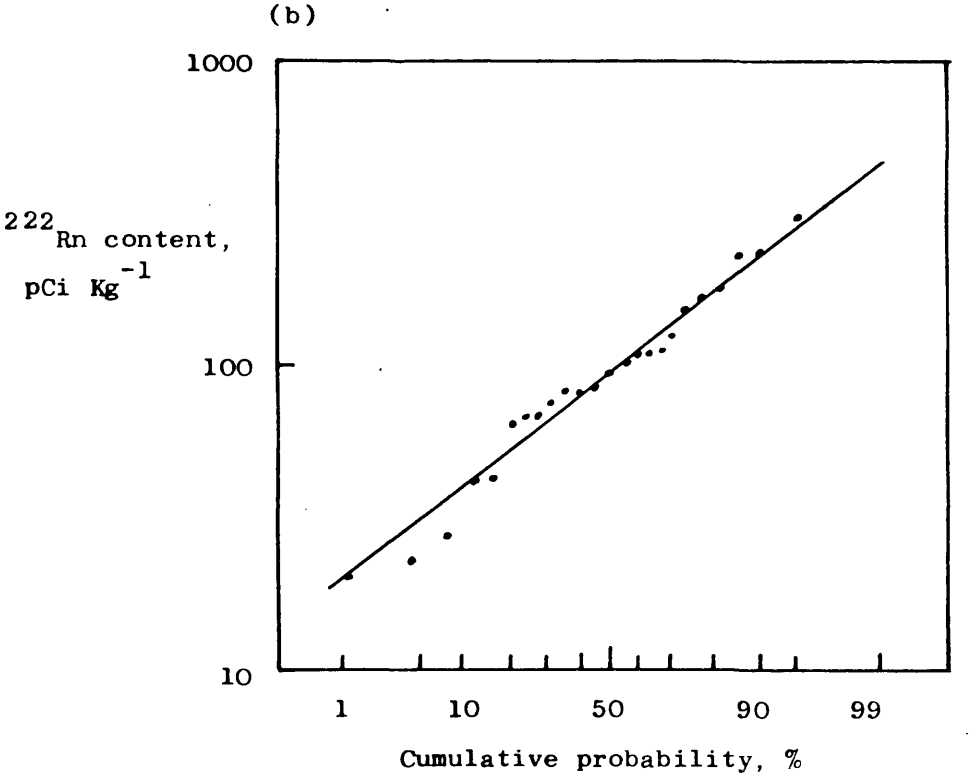

Fig. 5.3. ^{222}Rn contents of groundwaters from the Lincolnshire Limestone. (a) Histogram and (b) log normal probability plots of ^{222}Rn contents.

Table 5.1. ^{222}Rn and ^{226}Ra contents of groundwaters from the Lincolnshire Limestone.

Site No.	Location	National Grid. Ref.	^{222}Rn pCi kg^{-1}	^{226}Ra pCi kg^{-1}
1	Aswarby Pumping Station	TF 067 392	173±11	0.68±0.06
3	Baston Fen Farm	TF 140 160	84±5	0.64±0.05
4	Bertie Fen Farm	TF 221 278	76±5	0.79±0.06
5	Billingborough Pumping Stn.	TF 112 340	184±10	0.75±0.06
6	Black Hole Drove Farm	TF 178 252	146±9	1.38±0.09
7	Bourne Pumping Station	TF 100 202	332±20	1.07±0.07
11	Cuckoo Bridge observation borehole	TF 201 198	441±26	0.45±0.04
13	Dowsby, Burtt's Farm	TF 108 293	253±14	0.66±0.04
14	Dowsby, Spinney Farm	TF 114 294	69±4	1.52±0.10
17	Hacconby Fen Farm	TF 132 257	42±3	0.98±0.06
19	Jockey Pumping Station	TF 172 264	70±5	1.34±0.10
20	Kate's Bridge	TF 106 150	144±8	n.d.
21	Langtoft Farm	TF 119 129	17±1	0.61±0.05
22	Leggatt's Farm	TF 213 341	101±6	0.78±0.06
23	Lenton Pumping Station	TF 056 313	251±15	0.60±0.05
24	Middle Fen Farm	TF 134 292	67±4	1.32±0.08
26	Newlands Farm	TF 221 241	n.d.	0.84±0.06
29	Pointon	TF 116 324	114±7	1.31±0.09
31	Rigbolt House	TF 195 283	92±6	1.62±0.10
32	Rippingale Pumping Station	TF 147 281	42±8	0.85±0.07
34	Sempringham House Farm	TF 122 328	81±5	1.00±0.07
35	Sixscore Farm	TF 166 141	96±6	1.74±0.11
36	Spalding Bulb Company	TF 231 219	22±2	1.15±0.07
40	Tallington Pumping Station	TF 097 087	81±5	1.05±0.07
41	Tongue End Farm	TF 170 177	102±6	0.71±0.06
42	Vicarage Farm	TF 176 283	102±7	0.94±0.07
		Average	127	0.99

The ^{222}Rn contents are considerably in excess of the ^{226}Ra contents, in common with groundwaters from the Bunter Sandstone and the Avon sedimentary basin. The ^{222}Rn contents are plotted against the penetration of the extraction boreholes into the Limestone in Figure 5.4 and the depth to the limestone and penetration of the boreholes into the limestone are given in Table 5.2. There is little correlation between the ^{222}Rn contents and depths into the limestone, although the highest ^{222}Rn contents originate from the lower part of the aquifer, and the lower ^{222}Rn contents are derived from the top 10m of the aquifer. These observations may be explained by the fact that the lower limestone is more highly fractured with locally sandy facies near the base; whereas the upper limestone is generally a more massive freestone facies. Consequently in the lower limestone, a greater degree of water/rock interaction occurs compared with the upper limestone and ^{222}Rn may enter the groundwater more effectively from the more fractured part of the limestone.

The average ^{222}Rn content of groundwater from the lower part of the limestone is 258 pCi Kg^{-1} (mean of 3), whereas that for the upper part is 84 pCi Kg^{-1} (mean of 15). Although the deeper wells probably draw water (and consequently ^{222}Rn) from both facies, the ^{222}Rn content can be used as an indicator of the depth of origin of the groundwater. High ^{222}Rn contents indicate that the groundwater arises from a more highly fractured zone of the limestone. The ^{222}Rn contents are not definitive, however, because changes in U content, porosity and possibly residence time, will also cause changes in the ^{222}Rn contents of the groundwaters. The mechanism of ^{222}Rn release into groundwaters from a similar limestone (Inferior Oolite, Avon) is discussed more fully in paragraph 9.1.

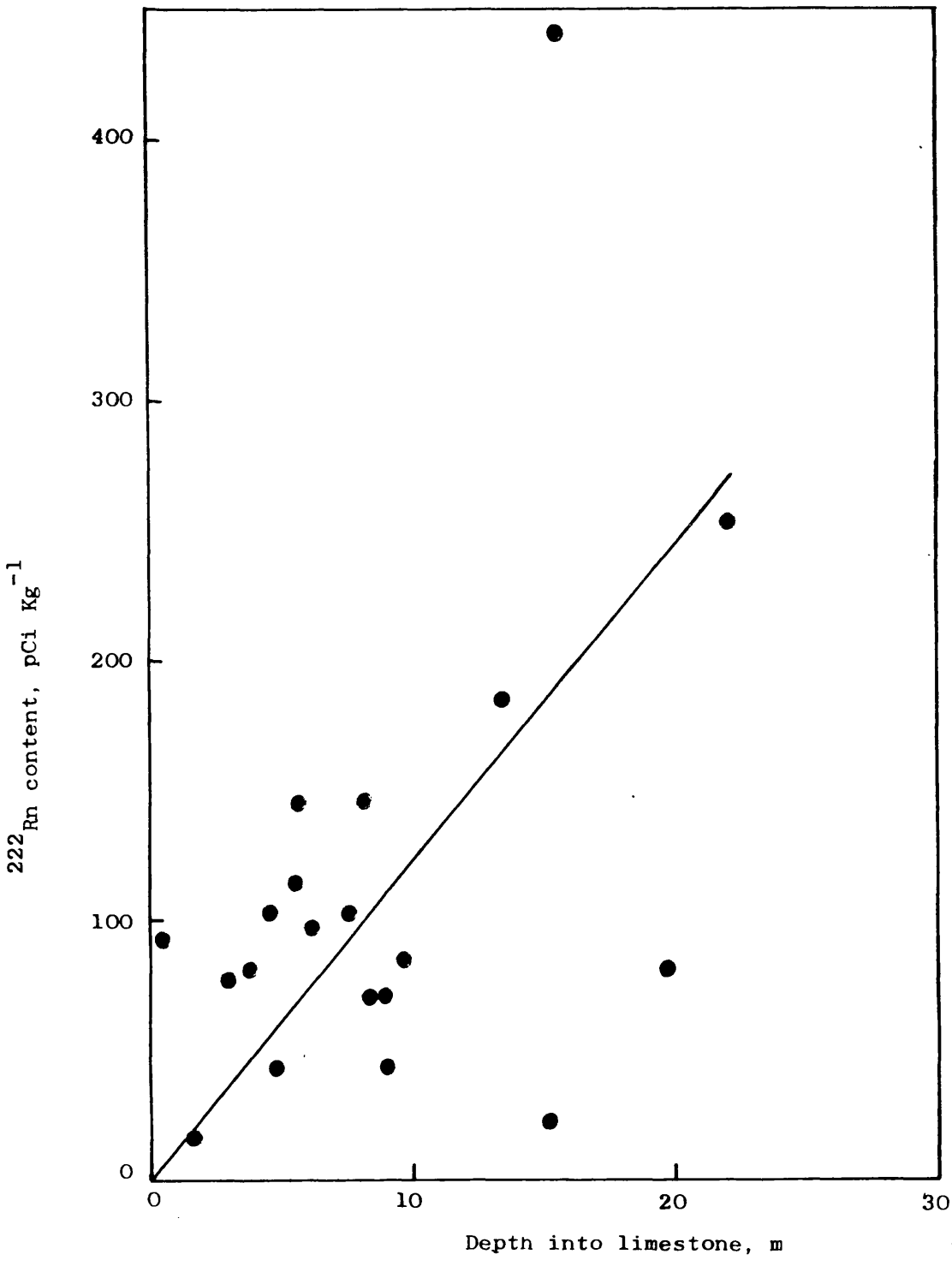

Fig. 5.4. Variation of ^{222}Rn content of groundwaters from the Lincolnshire Limestone with depth into the Limestone.

Table 5.2. Depths of Wells to the Lincolnshire Limestone and penetration of Wells into The Limestone

Site No.	Location	Depth to limestone, m	Penetration into limestone, m
3	Baston Fen Farm	44.5	9.7
5	Billingborough Pumping Station	25.6	13.4
6	Black Hold Drove Farm	55.5	8.2
11	Cuckoo Bridge Observation borehole	75.3	15.6
13	Dowsby, Burtt's Farm	24.0	22.0
14	Dowsby, Spinney Farm	22.4	8.4
17	Hacconby Fen Farm	31.2	4.8
19	Jockey Pumping Station	55.6	9.0
20	Kate's Bridge	20.2	5.7
21	Langtoft Farm	29.7	1.6
24	Middle Fen Farm	30.0	3.0
29	Pointon	25.0	5.5
31	Rigbolt	67.0	0.4
32	Rippingate Pumping Station	35.4	9.0
34	Sempringham House Farm	27.0	3.5
35	Sixscore Farm	59.6	6.2
36	Spalding Bulb Company	81.9	15.2
40	Tallington Pumping Station	37.4	19.7
41	Tongue End Farm	55.8	4.6
42	Vicarage Farm	57.0	7.6

The ^{226}Ra contents of groundwaters from the Lincolnshire Limestone do not exhibit any correlation with penetration of the extraction borehole into the limestone. The average ^{226}Ra content (0.99 pCi Kg) is a factor of 2.5 greater than the average ^{226}Ra content of the Bunter Sandstone, Nottinghamshire. The ^{226}Ra content of the groundwater is derived from the U content of the aquifer rock. For the Bunter Sandstone, this is 1.87 g g^{-1} (Table 3.1) and for the Lincolnshire Limestone the best available U content is 2.87 g g^{-1} (Table 9.12, for the Inferior Oolite, Avon). The ratio of ^{226}Ra in the groundwater to U in the aquifer rock for the Limestone to that of the Sandstone is therefore 1.6. This difference is probably caused by the higher concentrations of chloride and calcium ions in the limestone groundwater which will tend to stabilize the ^{226}Ra in solution. However, there is no direct correlation between ^{226}Ra concentration and the calcium and chloride ion concentrations in the Lincolnshire Limestone groundwaters.

5.2.2. Radiogenic ^{4}He contents

The ^{4}He contents of groundwaters from the Lincolnshire Limestone are reported in Table 5.3. together with the contents of the other stable dissolved inert gases. The ^{4}He contents are generally much greater than those of the Bunter Sandstone groundwaters, reaching a maximum of 1414 x 10^{-8} cm^{3} STP cm^{-3} H_2O. Two sections on which ^{4}He contents have been plotted show that in both the north and south of the region the ^{4}He contents of the groundwaters increase downdip (Figures 5.5 and 5.6) but that the rate of increase is greater in the south. ^{4}He isopleths for the aquifer are shown in Figure 5.7.

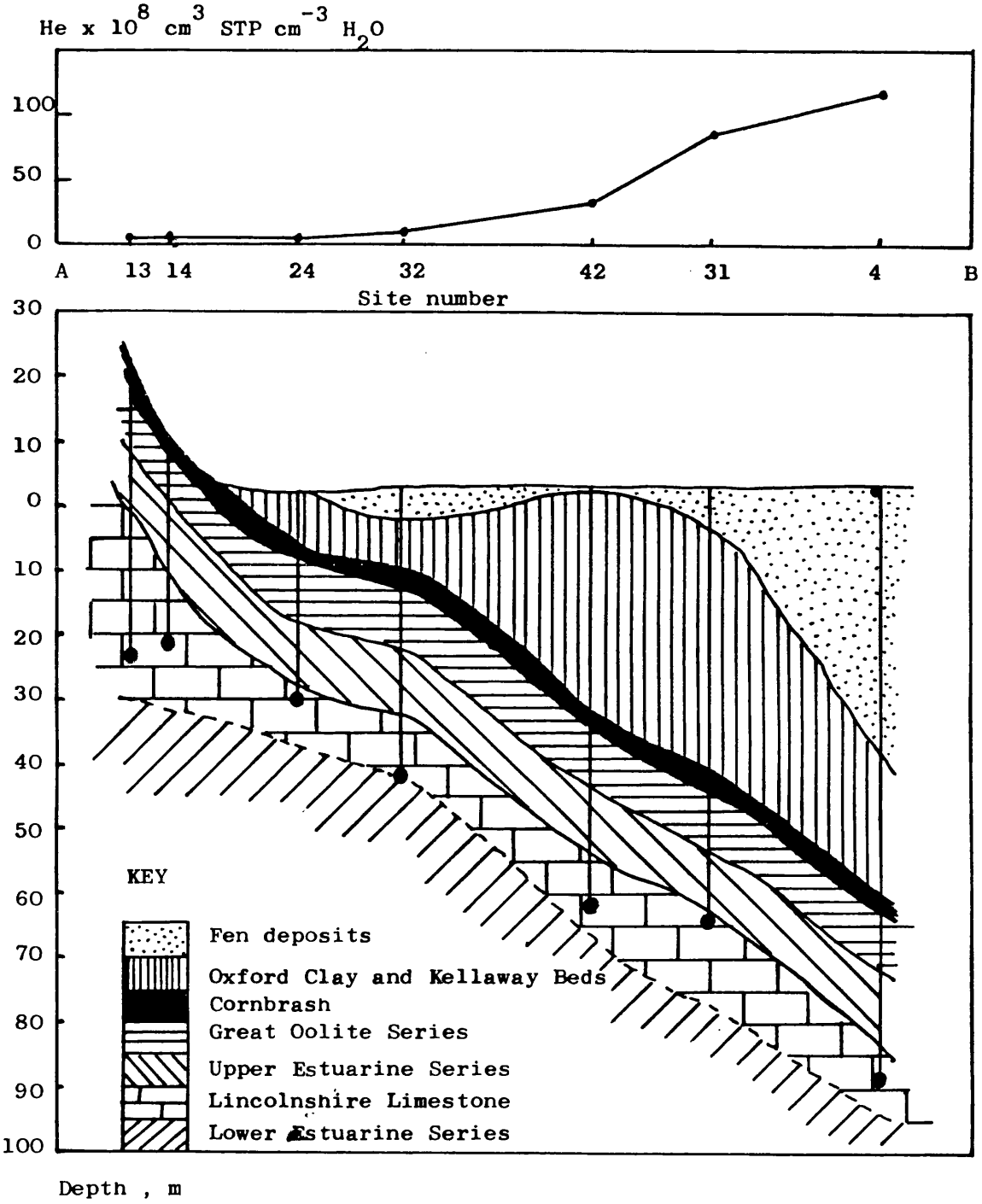

Fig. 5.5. Diagram showing variation of the ^4He content of groundwaters from the Lincolnshire Limestone with increasing confinement of the aquifer for the traverse A - B (West - East) in Fig. 5.1.

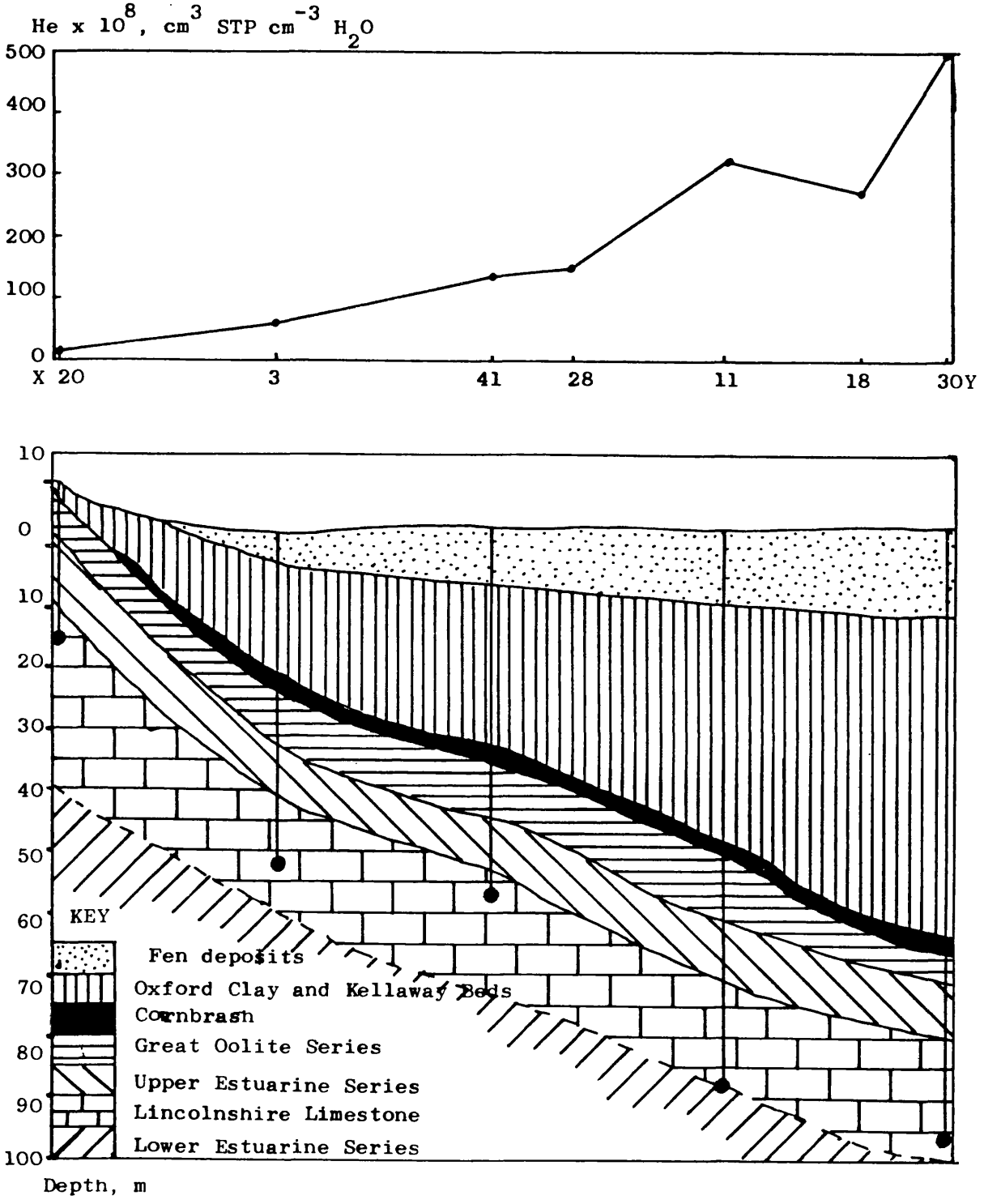

Figure 5.6. Diagram showing variation of the ^{4}He content of groundwaters from the Lincolnshire Limestone with increasing confinement of the aquifer for the traverse X - Y (SW - NE) in Figure 5.1.

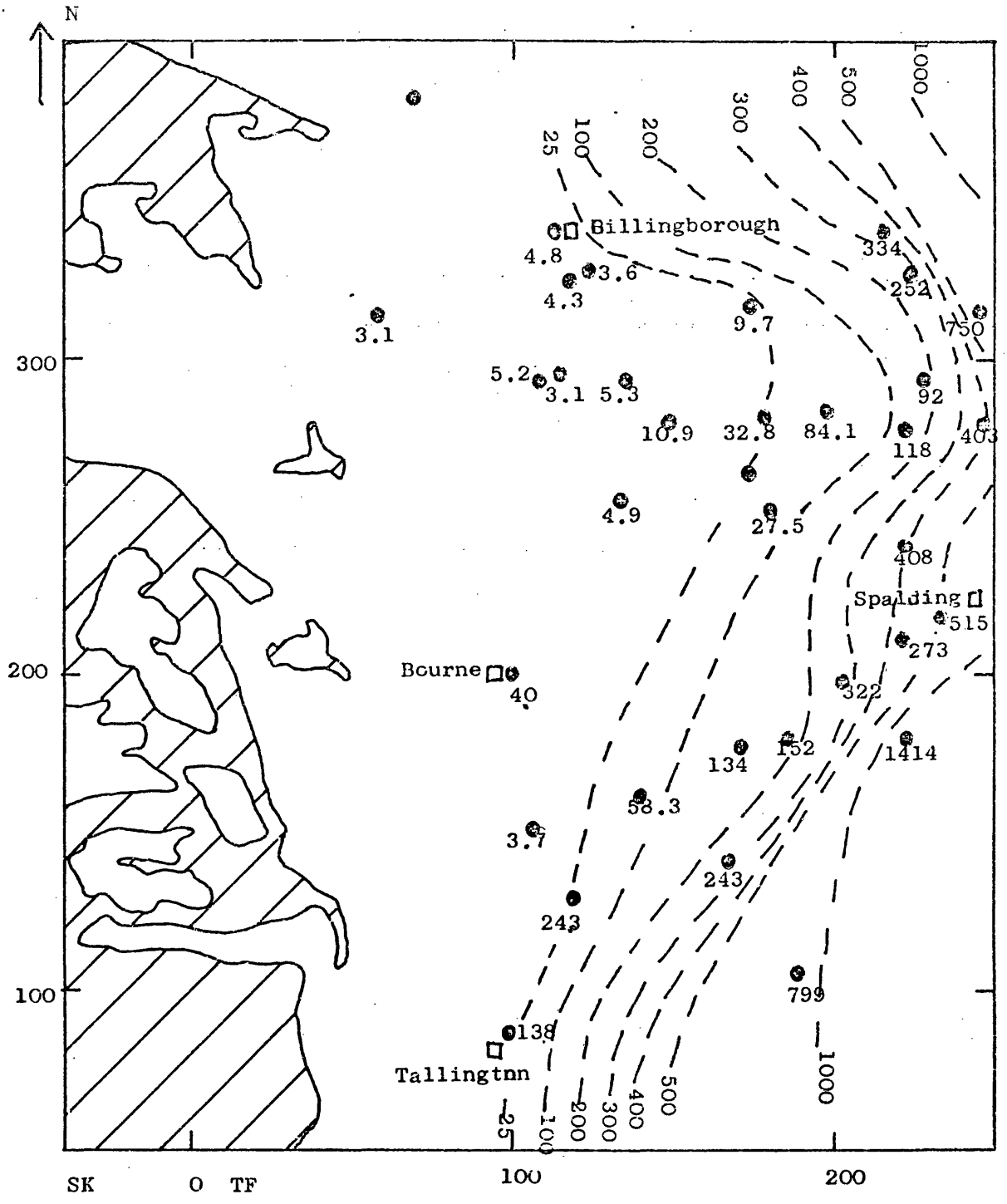

Fig. 5.7. Diagram showing ^{4}He contents and interpolated ^{4}He isopleths (cm^{3} STP cm^{-3} H_2O x 10^{8}) of groundwaters from the Lincolnshire Limestone.

Table 5.3. Inert gas contents, derived recharge temperatures and collection temperatures of groundwaters from the Lincolnshire Limestone

Site No.	Location	National Grid Ref.	Inert gas content, cm^3 STP cm^{-3} H_2O					Recharge temperature °C		Collection temperature °C
			He x 10^8	Ne x 10^7	Ar x 10^4	Kr x 10^7	Xe x 10^8	from Ar	from Kr	
3	Baston Fen Farm	TF 140 160	58.3±7.8	2.11±0.10	4.34±0.16	0.95±0.02	1.37±0.07	6.6±1.5	6.3±0.8	
4	Bertie Fen Farm	TF 221 278	118. ±16	2.14±0.10	4.28±0.15	0.94±0.02	1.40±0.07	7.2±1.4	6.6±0.8	9.5
5	Billingborough p.s.	TF 112 340	4.8±0.6	2.14±0.10	4.36±0.16	0.91±0.02	1.25±0.07	6.4±1.5	7.9±0.8	10.2
6	Black Hole Drove Farm	TF 178 252	27.5±3.7	2.11±0.10	4.16±0.15	0.91±0.02	1.35±0.07	8.3±1.4	8.0±0.8	8.5
7	Bourne p.s.	TF 100 202	4.0±0.5	2.13±0.10	4.24±0.15	0.93±0.02	1.42±0.07	7.5±1.4	7.3±0.8	10.8
9	Cheal Bridge o.b.	TF 226 294	92 ±12	2.18±0.10	4.47±0.16	0.97±0.02	1.40±0.07	5.3±1.5	5.5±0.8	12.1
11	Cuckoo Bridge o.b.	TF 201 198	332. ±43	2.18±0.10	4.46±0.16	0.97±0.02	1.32±0.07	5.4±1.5	5.7±0.8	12.5
12	Deeping R.A.C. o.b.	TF 222 180	1414. ±189	2.14±0.10	4.25±0.15	0.90±0.02	1.14±0.06	7.4±1.4	8.4±0.8	12.7
13	Dowsby, Burtt's Farm	TF 108 293	5.2±0.7	2.15±0.10	4.31±0.15	0.95±0.02	1.34±0.07	6.9±1.4	6.4±0.8	10.6
14	Dowsby, Spinney Farm	TF 114 294	3.1±0.4	2.16±0.10	4.24±0.15	0.95±0.02	1.44±0.07	7.5±1.4	6.5±0.8	9.9
15	Gosberton o.b.	TF 245 315	750. ±101	2.10±0.10	4.08±0.15	0.89±0.02	1.25±0.07	9.0±1.4	9.0±0.8	13.1
17	Hacconby Fen Farm	TF 132 257	4.9±0.7	2.14±0.10	4.30±0.15	0.93±0.02	1.30±0.07	7.0±1.4	7.2±0.8	10.4
18	Horseshoe Bridge	TF 219 212	273. ±37	2.12±0.10	4.13±0.15	0.95±0.02	1.35±0.07	8.6±1.4	6.5±0.8	12.6
19	Jockey p.s.	TF 172 264	17.3±2.3	2.14±0.10	4.28±0.15	0.93±0.02	1.39±0.07	7.2±1.4	7.1±0.8	11.6
20	Kate's Bridge	TF 106 150	3.7±0.5	2.11±0.10	4.13±0.15	0.91±0.02	1.31±0.07	8.6±1.4	7.9±0.8	10.1
21	Langtoft Farm	TF 119 129	24.3±3.2	2.17±0.10	4.42±0.16	0.97±0.02	1.36±0.07	5.8±1.5	5.4±0.8	8.8
22	Leggatt's Farm	TF 213 341	389. ±52	2.16±0.10	4.34±0.16	0.96±0.02	1.32±0.07	6.6±1.5	5.9±0.8	13.3
23	Lenton p.s.	TF 056 313	3.1±0.4	2.11±0.10	4.06±0.15	0.90±0.02	1.30±0.07	9.2±1.4	8.6±0.8	10.2
24	Middle Fen Farm	TF 134 292	5.3±0.7	2.16±0.10	4.32±0.16	0.95±0.02	1.40±0.07	6.8±1.5	6.2±0.8	10.9
25	Mornington House	TF 173 317	9.7±1.3	2.13±0.10	4.23±0.15	0.94±0.02	1.38±0.07	7.6±1.4	6.9±0.8	10.0
26	Newlands Farm	TF 221 241	408. ±55	2.15±0.10	4.30±0.15	0.94±0.02	1.35±0.07	7.0±1.4	6.8±0.8	3.0
28	Pepper Hill o.b.	TF 184 180	152. ±20	2.04±0.10	-	-	1.35±0.07	-	-	11.2
29	Pointon	TF 116 324	4.3±0.6	2.14±0.10	4.25±0.15	0.93±0.02	1.37±0.07	7.4±1.4	7.2±0.8	10.0
30	Quadring	TF 222 328	252. ±34	2.16±0.10	4.37±0.16	0.96±0.02	1.62±0.08	6.3±1.5	5.9±0.8	13.2
31	Rigbolt House	TF 195 283	84.1±11	2.13±0.10	4.17±0.15	0.93±0.02	1.37±0.07	8.2±1.4	7.2±0.8	12.1
32	Rippingale p.s.	TF 147 281	10.9±1.5	2.19±0.11	4.49±0.16	0.99±0.02	1.45±0.08	5.1±1.5	4.5±0.7	11.0
34	Sempringham House Farm	TF 122 328	3.6±0.5	2.13±0.10	4.23±0.15	0.92±0.02	1.36±0.07	7.6±1.4	7.7±0.8	10.5
35	Sixscore Farm	TF 166 141	243. ±33	2.18±0.10	4.47±0.16	0.98±0.02	1.35±0.07	5.3±1.5	5.2±0.8	11.7
36	Spalding Bulb Company	TF 231 219	515. ±69	2.15±0.10	4.36±0.16	0.94±0.02	1.15±0.06	6.4±1.5	6.8±0.8	10.3
37	Stowgate o.b.	TF 188 105	799. ±107	2.13±0.10	4.22±0.15	0.92±0.02	1.33±0.07	7.8±1.4	7.4±0.8	-
38	Surfleet o.b.	TF 248 280	403. ±54	2.30±0.10	-	-	-	-	-	13.2
40	Tallington p.s.	TF 097 087	13.8±1.8	2.11±0.10	4.10±0.15	0.91±0.02	1.36±0.07	8.8±1.4	8.2±0.8	10.7
41	Tongue End Farm	TF 170 177	134. ±18	2.15±0.10	4.39±0.16	0.94±0.02	1.33±0.07	6.1±1.5	6.6±0.8	11.9
42	Vicarage Farm	TF 176 283	32.8±4.4	2.13±0.10	4.00±0.14	0.95±0.02	1.33±0.07	9.8±1.4	6.2±0.8	11.5

NOTES: p.s. = pumping station

o.b. = observation borehole

These may be compared with the chlorinity isopleths and the discharge rates in Figure 5.8 and the chlorinity contents given in Table 5.4. The similarity of the ^{4}He distribution and the chloride ion concentration is striking.

The increase in chlorinity in an easterly direction has been attributed to mixing of recharge water with a high-salinity (NaCl dominated) water stored in the pores of the limestone. The rate of water movement in the fissure system has been estimated at 11 km a^{-1} [142] and 2 km a^{-1} [143]. Hence recharge water moves rapidly eastwards, drawn by the high abstraction rates in the east of the region. The presence of high levels of tritium in groundwaters from many of the sites in the artesian part of the aquifer confirms the rapid water movement. The decreasing tritium, increasing chlorinity and increasing ^{4}He content in an easterly direction is a consequence of the progressive exchange of fissure water with pore water. The extent of exchange depends on the rate of water transport, the total flow in the fissure system and the degree of interaction between the fissures and the pores. Freshwater penetration eastwards is greatest just north of Spalding and is probably a result of the high abstraction rates in this part of the aquifer drawing the fissure water through more rapidly. This eastwards penetration is less marked south of Spalding because the high abstraction wells between Bourne and Tallington intercept the eastwards flow and a relatively small volume of water is abstracted to the east of a line drawn between Bourne and Tallington.

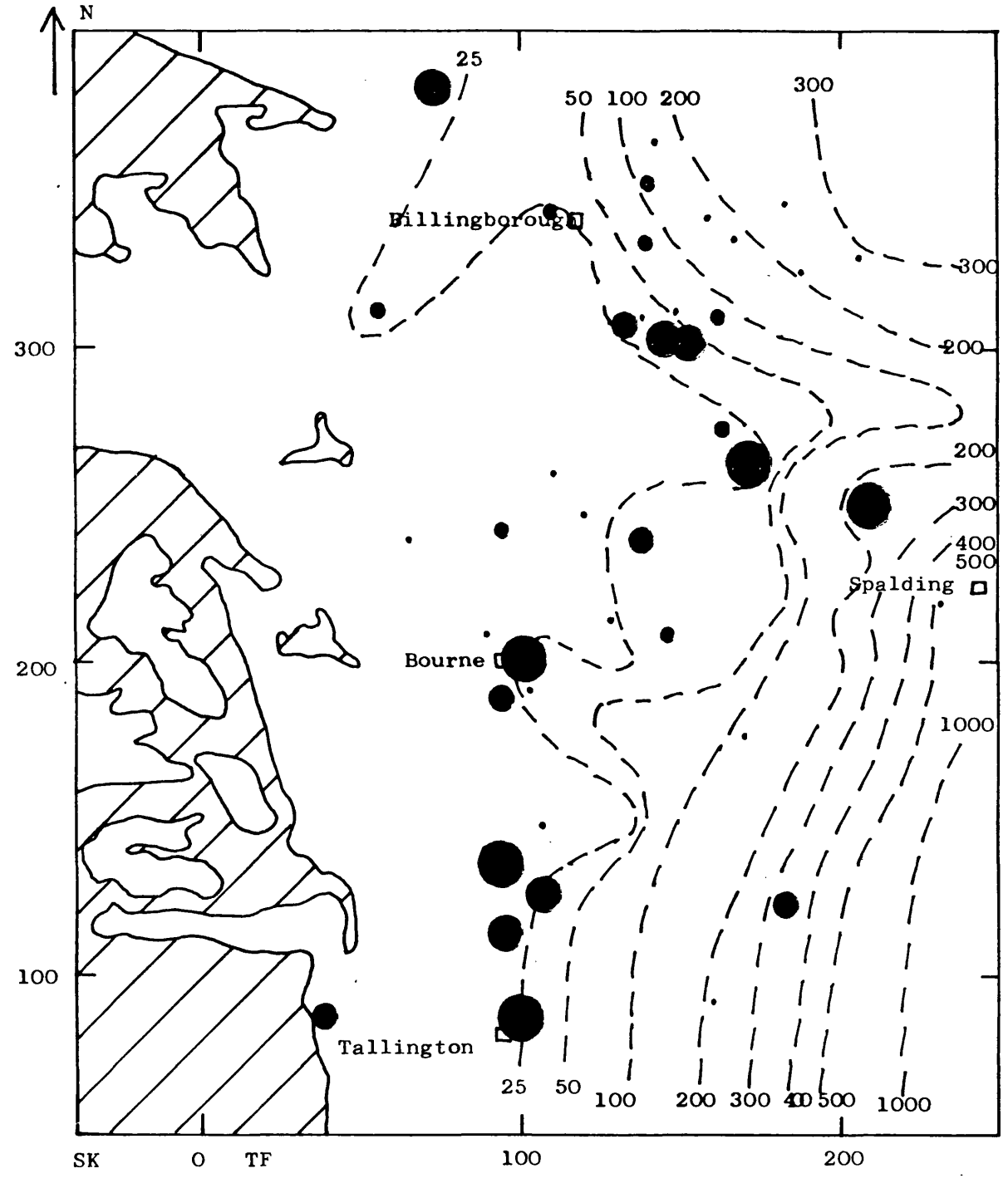

Fig. 5.8. Discharge and leakage rates and isochlorinity contours of groundwaters from the Lincolnshire Limestone [142-145, 148]
Discharge rates are in $m^3 d^{-1}$:-

• 50-500 ● 500-1500 ● 1500-2500 ● 2500-5000
● 5000-10,000

Table 5.4. Chloride contents of groundwaters from the Lincolnshire Limestone.

Site No.	Location	Chloride content, mg kg^{-1}				
		Ref [148]	Ref [143]	Ref [145]	Ref [144]	Average
3	Baston Fen Farm	59	-	52	58	56
4	Bertie Fen Farm	60	55	-	-	58
5	Billingborough P.S.	27	22	-	-	25
6	Black Hole Drove Farm	46	45	-	-	46
7	Bourne P.S.	27	-	24	28	26
9	Cheal Bridge	89	-	-	94	92
10	Clipsham O.B.	34	-	21	-	28
11	Cuckoo Bridge O.B.	189	-	-	181	185
12	Deeping R.A.C.	1118	-	-	-	1118
13	Dowsby, Burtt's Farm	-	25	-	-	25
14	Dowsby, Spinney Farm	-	28	-	-	28
15	Gosberton O.B.	864	-	-	779	822
17	Hacconby Fen Farm	24	-	-	-	24
18	Horseshoe Bridge	222	-	-	-	222
19	Jockey P.S.	28	21	-	26	25
20	Kate's Bridge O.B.	27	-	-	-	27
21	Langtoft Farm	27	-	-	29	28
22	Leggatt's Farm	360	-	-	-	360
23	Lenton P.S.	20	32	-	-	26
24	Middle Fen Farm	24	23	-	-	24
25	Mornington House	19	-	-	-	19
26	Newlands Farm	280	300	-	-	290
28	Pepper Hill	115	-	-	95	105
29	Pointon	25	26	-	-	26
30	Quadring	321	-	-	-	321
31	Rigbolt House	50	45	-	-	48
32	Rippingale P.S.	24*	17*	-	22*	21*
34	Sempringham House	-	21	-	-	21
35	Sixscore Farm	194	-	-	-	194
36	Spalding Bulb Co.	628	510	-	529	556
37	Stowgate O.B.	366	-	-	-	366
38	Surfleet O.B.	246	-	-	-	246
39	Swayfield O.B.	34	-	-	-	34
40	Tallington P.S.	27	-	-	-	27
41	Tongue End Farm	113	-	117	111	114
42	Vicarage Farm	26	-	-	-	26
43	Woodhall Spa	-	-	13591	-	13591

* Figures for Rippingale Fen Farm.

The ^4He contents of groundwaters from the Lincolnshire Limestone increase approximately linearly with increasing chlorinity (Fig. 5.9) according to the equation

$$[He] = 1.15 \times 10^{-8} [Cl] \qquad 5.1$$

where [He] is the ^4He content of the groundwater, cm^3 STP cm^{-3} H_2O and [Cl] is the chlorinity of the groundwater, mg Kg^{-1} (Table 5.4) This is a line calculated by linear regression with a data correlation coefficient of 0.93. Such a relationship between two very different chemical species is remarkable, considering that the mechanism by which the groundwaters achieve their ^4He and chloride contents is exchange of pore water with fissure water. A linear relationship between ^4He and chloride contents for groundwaters from Israel has been reported in the literature [146], but this was in a spring complex where direct mixing was responsible for the variation in ^4He contents and chlorinities. In this system, direct mixing was confirmed by the linear relationship of both temperature and ^{226}Ra contents with chlorinity.

Groundwaters with very high chlorinities have been determined in the extreme north-east of the aquifer. For example at Woodhall Spa (TF 190 630) the chlorinity is 13591 mg kg^{-1} [142]. This chlorinity is close to that of sea-water -18980 mg kg^{-1} [147]. It is possible, therefore, that the chlorinity of the original pore water is close to that of sea-water and this is reasonable if the pore water is connate water. If it is assumed that the linear relationship between ^4He content and chlorinity is valid for high chlorinities, the ^4He content of the original pore water may be calculated by extrapolation. Using equation 5.1 a value of 21850×10^{-8} cm^3 STP cm^{-3} H_2O is obtained for the ^4He content of the original pore-water.

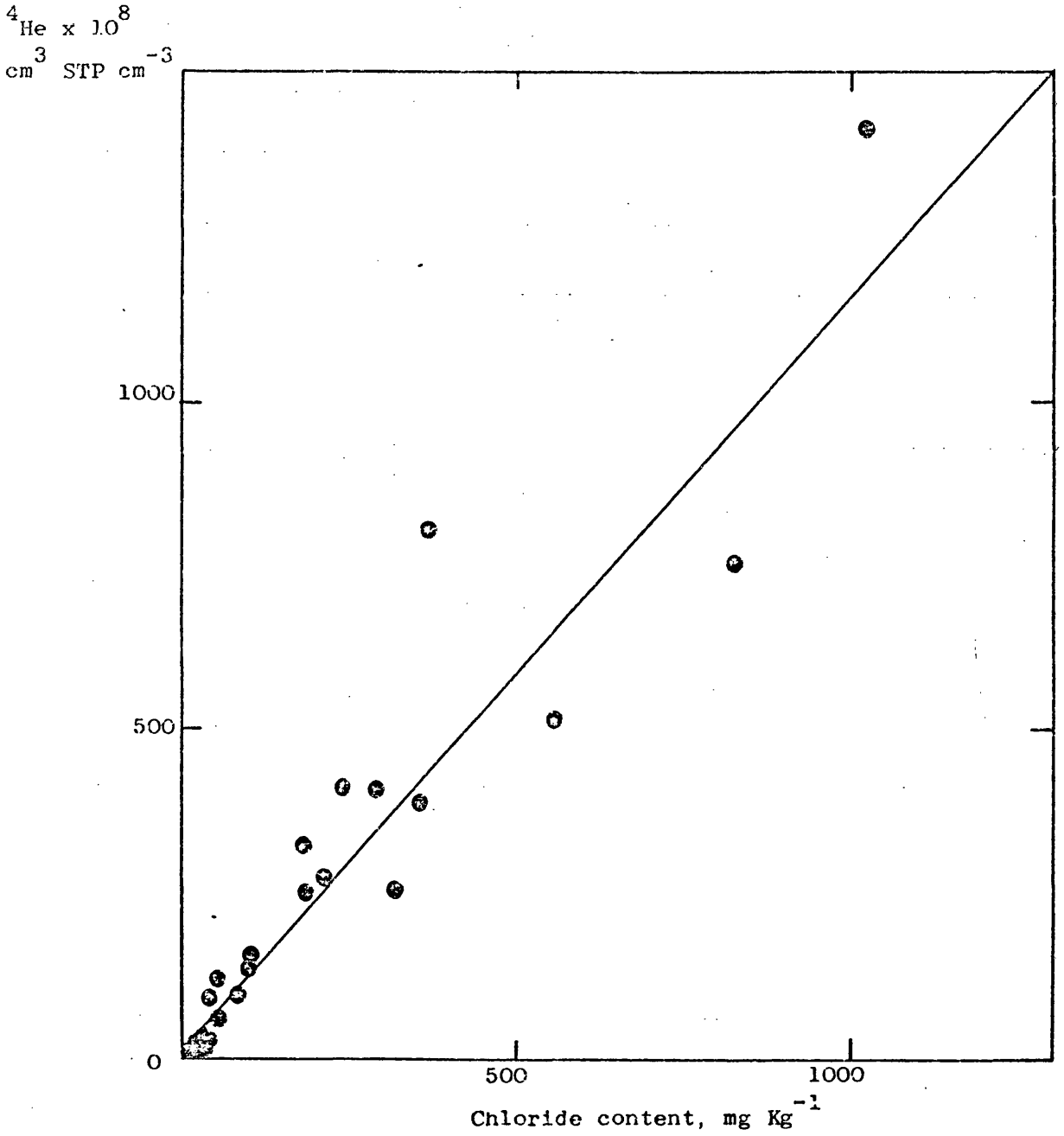

Fig. 5.9. Plot of ^4He contents against chloride contents of groundwaters from the Lincolnshire Limestone.

A minimum residence time for the pore-water to accumulate this ^4He content by radioactive decay may be calculated from the equation

$$He_t = \rho t \{1.19 \times 10^{-13} [U] + 2.88 \times 10^{-14} [Th]\} \qquad 5.2$$

where He_t is the amount of radiogenic ^4He (cm^3 STP cm^{-3} H_2O) produced in t years in 1g of rock of density ρ and U and Th contents of [U] and [Th] ppm respectively. This equation assumes that the ^4He generated is distributed uniformly between the solid and aqueous phases in the aquifer. The calculated age is a minimum age since it has been assumed that there is no diffusive loss of ^4He from the pore water. Using values of [U], [Th] and ρ for the Inferior Oolite, Avon, ([U] = 2.87 μg g^{-1}, [Th] = 10.0 ρ = 2.80), the calculated minimum age of the pore water with the ^4He content of 21850 x 10^{-8} cm^3 STP cm^{-3} H_2O is 124 million years. This value is remarkably similar to the age of the Limestone (135 - 190 million years).

Clearly this system requires a closer examination. Firstly, the He content of the groundwater increases linearly with the chloride content, within the range of He and chloride contents determined. The assumption has been made that this linear relationship may be extrapolated to much higher He and chloride contents. If diffusion of He has not made a significant contribution to the He contents of the Lincolnshire Limestone groundwaters analysed, then this extrapolation is valid, even if He diffusion becomes important at higher ^4He contents. It is likely that ^4He will have diffused from the ancient pore water. The theoretical ^4He content associated with a sea water chlorinity will therefore not necessarily be observed in nature, even if a groundwater of sea-water salinity is encountered.

The derived ^{4}He content of a groundwater of sea-water chlorinity has been calculated assuming that the ancient pore-water is connate in origin. The fact that the age of the pore-water calculated from this ^{4}He content is similar to the age of the aquifer is evidence in support of the view that the pore water is connate in origin. It is also evidence in support of the assumption that the ^{4}He generated in the Lincolnshire Limestone is partitioned equally, volume for volume, between the groundwater phase and the solid rock phases.

The ^{4}He and chloride contents of the groundwaters from the Lincolnshire Limestone indicate that a considerable exchange of fissure water for pore water has occurred throughout the area studied. The extent of mixing has been calculated on the basis that the artesian flow in the west of the confined aquifer is 100% modern water and that the pore water is connate in origin. However, even the groundwater with the highest ^{4}He content (Deeping R.A.C.) still contains 94% modern water. ^{14}C ages are available for several sites in the south east of the area. Mixing percentages calculated from the ^{14}C ages generally agree with mixing volumes calculated from the ^{4}He and chlorinity data in the west of this area (Table 5.5). However, in the east of the area, ^{14}C data indicates that the groundwaters comprise 100% ancient water, (older than 50,000 years). The ^{4}He and ^{14}C data are not necessarily conflicting. It is possible that in the east of the region, the recent water is older than 50,000 years, an age which is recent compared with the age of the formation. The effects of the possible ingress of pleistocene water on the mixing proportions are discussed in paragraph 5.2.3.

Table 5.5. Mixing proportions of groundwaters from the Lincolnshire Limestone.

Site No.	Location	Mixing proportion, % modern			
		From ^{4}He (sea-water end member)	From Cl	From recharge temp.	From ^{14}C
3	Baston Fen Farm	100	100	84	15
4	Bertie Fen Farm	99	100	91	
5	Billingborough P.S.	100	100	97	
6	Black Hole Drove Farm	100	100	100	
7	Bourne P.S.	100	100	100	
9	Cheal Bridge O.B.	100	100	66	
11	Cuckoo Bridge O.B.	99	99	69	31
12	Deeping R.A.C. O.B.	94	94	100	
13	Dowsby, Burtt's Farm	100	100	88	
14	Dowsby, Spinney Farm	100	100	93	
15	Gosberton O.B.	97	96	100	
17	Hacconby Fen Farm	100	100	95	
18	Horseshoe Bridge	99	99	100	
19	Jockey P.S.	100	100	97	
20	Kate's Bridge	100	100	100	100
21	Langtoft Farm	100	100	69	
22	Leggatt's Farm	98	98	81	
23	Lenton P.S.	100	100	100	
24	Middle Fen Farm	100	100	84	
25	Mornington House	100	100	98	
26	Newlands Farm	98	99	91	
28	Pepper Hill O.B.	99	100	-	18
29	Pointon	100	100	98	
30	Quadring	99	98	78	
31	Rigbolt House	100	100	100	
32	Rippingale P.S.	100	100	55	
34	Sempringham House Farm	100	100	100	
35	Sixscore Farm	99	99	64	21
36	Spalding Bulb Company	98	97	86	
37	Stowgate O.B.	96	98	100	
38	Surfleet O.B.	98	99	-	
40	Tallington P.S.	100	100	100	90
41	Tongue End Farm	99	100	83	13
42	Vicarage Farm	100	100	100	

5.2.3. Recharge temperatures

The recharge temperatures derived from the Ar and Kr contents of groundwaters from the Lincolnshire Limestone are reported in Table 5.2. The average recharge temperatures are plotted on a location map in Figure 5.10. Two zones are identified in Figure 5.10, separated by a 7°C recharge temperature isotherm. Groundwaters to the west of this isotherm are closest to outcrop. In general, the recharge temperatures are greater than 7°C, although there are some exceptions. The average recharge temperature in this zone is 7.6°C (variance 0.6°C). The anomalous temperature of 4.8°C derived for the groundwater from Rippingale pumping station has been omitted from this calculation. Immediately eastwards of the 7°C isotherm, the estimated recharge temperatures average 6.2°C (variance 0.6°C). The recharge temperatures of some groundwaters in the extreme east of the study area are greater than 7°C. These are denoted by brackets in Figure 5.10 and have been omitted for the purpose of the average calculation. The indication is that the present artesian flow in the zone east of the 7°C isotherm must have been at least partially recharged under climatic conditions which were colder than at present. The 7°C isotherm extends eastwards towards the north of Spalding confirming the eastwards incursion of recent water indicated by both the radiogenic ^{4}He and chlorinity isopleths.

The present average annual temperature in this part of England is 9.5°C (range 9.3-9.9°C). Over the period of aquifer recharge, September to April, the 30 year average temperature is 7.1°C

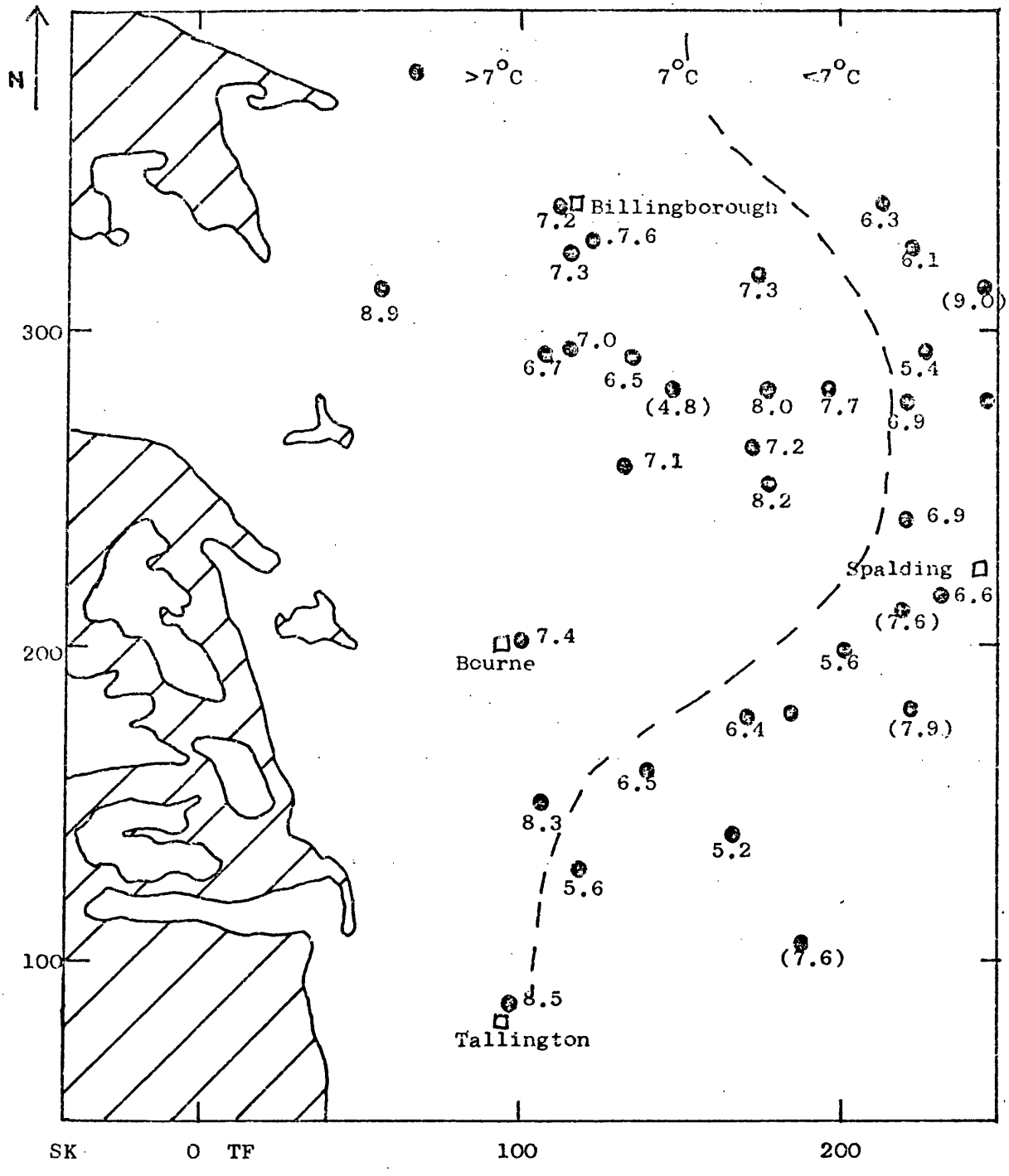

Fig. 5.10 Derived average recharge temperatures of groundwaters from the Lincolnshire Limestone.

(range 6.8-7.4°C) [148], in general agreement with the average estimated recharge temperature of groundwaters west of the 7°C isotherm. The $^{18}O/^{16}O$ isotopic ratio for rainfall at an average temperature of 7.6°C may be estimated both from Dansgaard's equation relating $\delta^{18}O$ to temperature for world-wide precipitation [134] and from Evans et al equation for precipitation in maritime Europe [75]. The $\delta^{18}O$ estimates are -8.4°/oo and -7.2°/oo respectively and compare with measured values of -7.7°/oo for groundwaters in the western part of the aquifer [145]. As the actual value of $\delta^{18}O$ for the recharge waters lies between the two estimated values, the oxygen isotope data are consistent with the recharge temperatures derived from the inert gas contents of these groundwaters.

Explanation of the lower recharge temperatures in the east is more complicated. The ^{14}C and ^{3}H contents [143] and some of the chloride and ^{4}He contents of the artesian water in this region indicate that the groundwaters are mixed, and contain a significant proportion of recent water. This water was recharged at 7.6°C and consequently temperatures east of the 7°C isotherm must result from mixing with water which equilibrated with air at a temperature lower than the estimated recharge temperature of the mixed water. This low temperature component must have been precipitated under climatic conditions significantly colder than at present. Aquifer recharge cannot have taken place during the most recent (Devensian) glaciation since permafrost prevailed in this part of England at that time [131]. Recharge could have occurred during the preceeding Upton Warren Interstadial when

temperatures generally were about 6°C lower than the post glacial temperatures [128]. Recharge of the Bunter Sandstone aquifer in Nottinghamshire took place during this interstadial at 5 - 7°C lower than modern recharge [149]. If the modern recharge temperature for the Lincolnshire Limestone is similarly reduced by 6°C, the low temperature end-member of the mixed groundwaters must have equilibrated with air at about 1.6°C. Mixing proportions have been calculated on the basis of these end-member temperatures, however, these are rather speculative (Table 5.5). These mixing volumes cannot be equated with mixing proportions derived from the chloride and ^{4}He contents of the groundwaters based on a sea-water end-member. They do, however, indicate the likely proportions of pleistocene water in the mixed groundwaters.

5.2.4. A model of the aquifer.

A simple model of the Lincolnshire Limestone can be proposed to account for the pattern of ^{222}Rn, chloride and ^{4}He contents of the groundwaters and their estimated recharge temperatures. The aquifer comprises a matrix of structural units of various sizes surrounded by fissures along which groundwater percolates. The size of these units depends on the extent of fracturing within the aquifer. If it is assumed that the aquifer is homogeneous in U content, then the extent of fracturing can be qualitatively assessed from the ^{222}Rn contents of the groundwaters. The greater the extent of fracturing, the greater the water/rock interaction and the higher the ^{222}Rn contents of the groundwaters. Low ^{222}Rn contents tend to be derived from the less fractured freestone facies.

The pores of the structural units were initially filled entirely with connate water. This connate water originated as sea-water and with a high chlorinity. Since deposition of the aquifer, the pore water has accumulated a significant quantity of ^{4}He. The linear relationship of chloride content with ^{4}He content indicates that little exchange has occurred with the connate water over millions of years, as such exchange would have rapidly reduced the ^{4}He content. However, recharge temperatures of groundwaters abstracted east of the $7^{o}C$ isotherm indicate that exchange between pleistocene water and the connate water has occurred. Subsequently, with the development of the aquifer for water supply, a significant proportion of recent water in the fissures has exchanged with the mixed pleistocene and connate water in the pores. The pores of the structural units now contain a mixture of these three types of groundwater (and probably other types of groundwater from leakage, infiltration, etc.). The composition of the pore water depends on the degree of exchange between the connate water and the pleistocene and recent groundwaters. A schematic diagram of the structural units showing the composition of the pore water is shown in Figure 5.11. The actual pore water probably consists of pure connate water at the centre of each structural unit followed by a graded mixture of connate, pleistocene and recent water away from the centre. The chemical composition of the pore water at any point in the structural unit will depend on the relative volumes of connate, pleistocene and recent water and the degree of exchange between them. The mechanism by which exchange occurs within the pores is complex, but is probably diffusion controlled. It is such that both

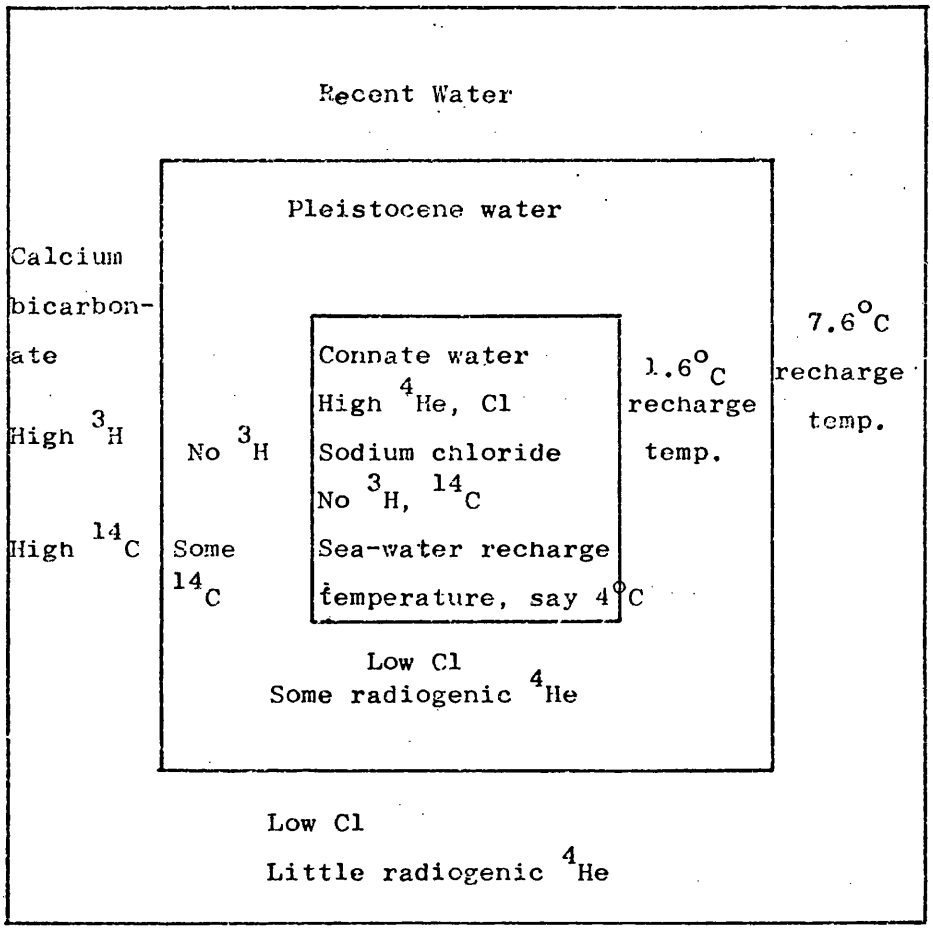

Fig. 5.11 Schematic diagram of a Lincolnshire Limestone "structural unit" showing the composition of the pore water.

the original chloride and accumulated ^{4}He are retained in the same proportions in the groundwaters studied.

5.3. CONCLUSIONS

The ^{222}Rn contents of groundwaters from the Lincolnshire Limestone have been used as an indicator of aquifer variability. The important variable which affects the ^{222}Rn contents is the part of the aquifer from which the ^{222}Rn is derived. High ^{222}Rn concentrations tend to be derived from the highly fractured sandy facies of the aquifer whereas low ^{222}Rn contents arise from the less fractured freestone facies.

The radiogenic ^{4}He contents have been correlated with the chlorinity and used to estimate mixing proportions. The relationship between the ^{4}He and chloride contents has been extrapolated to sea-water chlorinity and an age for the pore water has been calculated from the derived ^{4}He content. The estimated age of the pore water exceeds 100 million years suggesting that it is connate in origin.

Recharge temperatures derived from the Ar and Kr contents of the groundwaters have been interpreted in terms of mixing of recent water with pleistocene water, although this interpretation is speculative. A $7^{o}C$ isotherm has been identified and its shape is consistent with that of the chlorinity and ^{4}He isopleths.

The mixing of three types of water - recent, pleistocene and connate - has been discussed. A simple model of the structural units of the aquifer has been proposed to account for the observed ^{222}Rn, chloride, ^{4}He and recharge temperature data. The pore water is believed to comprise a gradation of mixed waters caused by exchange with fissure water over thousands of years.

CHAPTER 6

RADON, RADIUM AND DISSOLVED INERT GASES IN GROUNDWATERS FROM THE CORNUBIAN GRANITE.

6.1. INTRODUCTION

The geological structure of south-west England is dominated by an elongated granite batholith, at least 200km long forming a spine to the peninsula. The granite is of Hercynian age and is emplaced in intensely folded Ordovician to Carboniferous rocks. Granite is exposed at Dartmoor, Bodmin Moor, Hensbarrow, Carnmenellis and Lands End. Gravity surveys [150,151] have shown that the granite outcrops are linked as a single batholith with a well-defined roof and outwards sloping wall regions. Seismic studies [152,153] have revealed a remarkably uniform structure along the line of the batholith.

Measurements of heat flow in the region have identified a zone of unexpected high surface heat flow referred to as the south-west England thermal anomaly zone [154]. Such high heat flows are unexpected for a granite of Hercynian emplacement. Possible enhancement of the surface heat flow could occur through convective transfer arising from deep groundwater circulation within the fracture system of the mineralised belt. That such a mechanism exists, at least on a small scale, is clear from the warm spring activity in a number of the underground mines.

The redevelopment of Mount Wellington, Pendarves, South Crofty and Wheal Jane as tin producers has provided an opportunity to study these warm springs. The chemistry and origin of the thermal waters has been studied by Alderton and Sheppard [155].

The waters studied were near neutral Na - Ca - Cl brines with less than 15000 ppm of total dissolved solids. The hydrogen and oxygen isotopic compositions indicated that the waters were of meteoric origin. The radiogenic ^{4}He, dissolved inert gas, ^{222}Rn and ^{226}Ra contents have been determined for the thermal springs and for some shallow groundwaters from south-west England. The shallow groundwaters are non-thermal, acidic, mainly Na - Ca - Cl brines with less than 400 ppm of total dissolved solids [156]. A sketch map showing the location of the sampling sites in relation to the granite outcrops is shown in Figure 6.1

6.2. RESULTS AND DISCUSSION

6.2.1. ^{222}Rn and ^{226}Ra contents

The ^{222}Rn and ^{226}Ra contents of groundwaters from the shallow boreholes of south-west England are generally much higher than those of groundwaters from the sedimentary aquifers of England. The ^{222}Rn contents range from 3080 to 21110 pCi Kg^{-1} with an average value of 10350 pCi Kg^{-1} and the ^{226}Ra contents range from 0.6 to 17.0 pCi Kg^{-1} with an average of 3.7 pCi Kg^{-1} (Table 6.1). Both the ^{222}Rn and the ^{226}Ra contents of the shallow groundwaters are distributed statistically log-normally (Figures 6.2, 6.3).

The ^{222}Rn contents of the thermal groundwaters are generally much the same as those of the non-thermal groundwaters ranging from 1700 to 19800 pCi Kg^{-1} with a mean of 9100 pCi Kg^{-1} (Table 6.2). There are two exceptions which have been excluded for the purpose of calculation of the mean ^{222}Rn content. The sample from Pendarves 5B

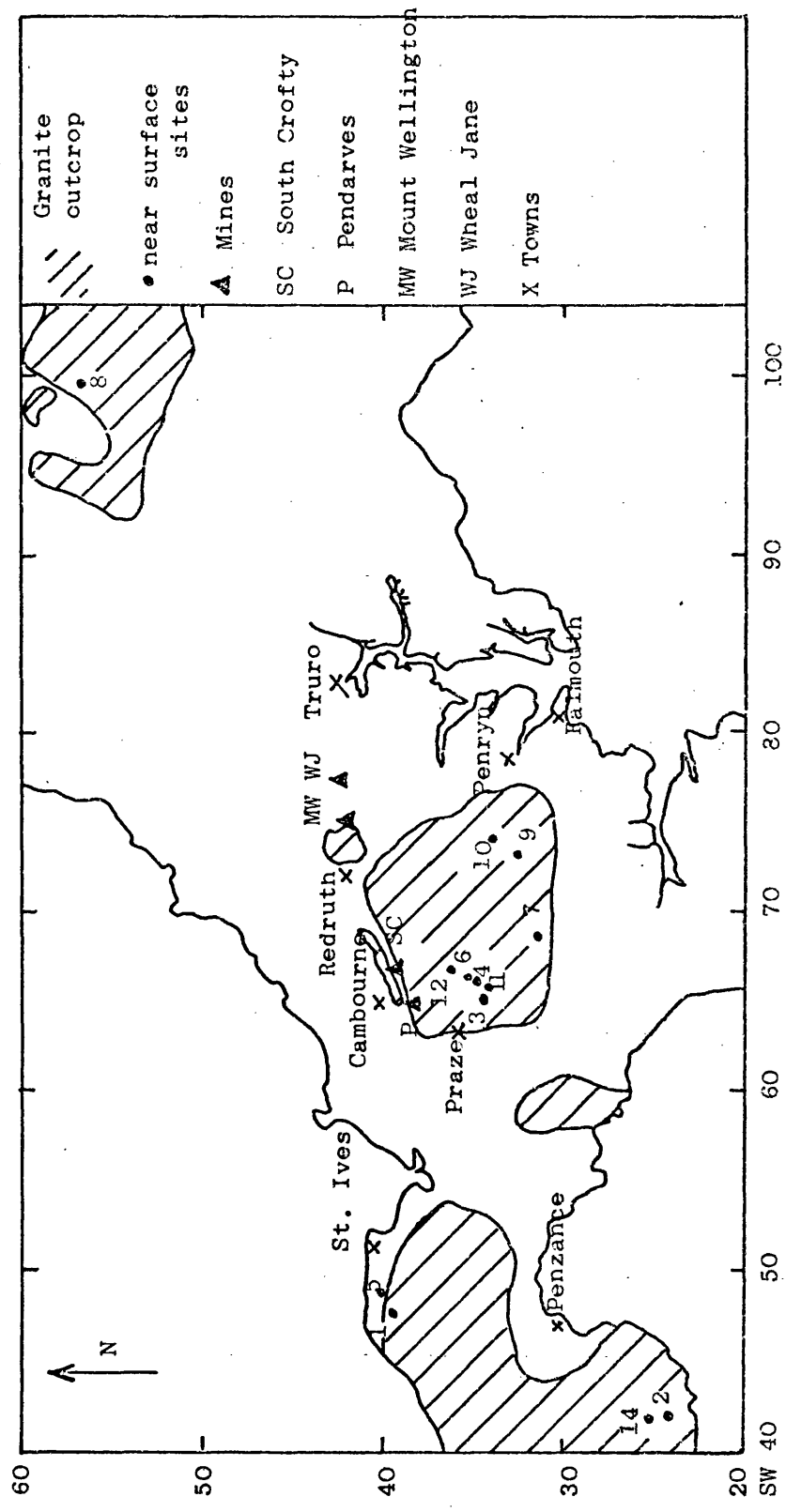

Fig. 6.1. Sketch map showing location of sample sites and granite outcrops in Cornwall
(Sites numbered as in table 6.1).

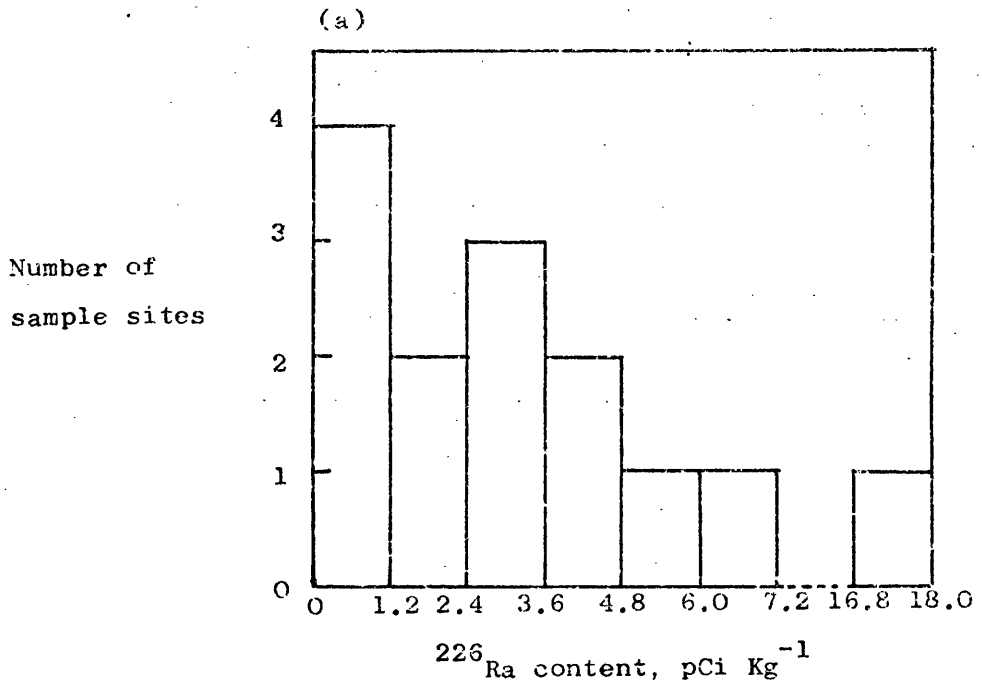

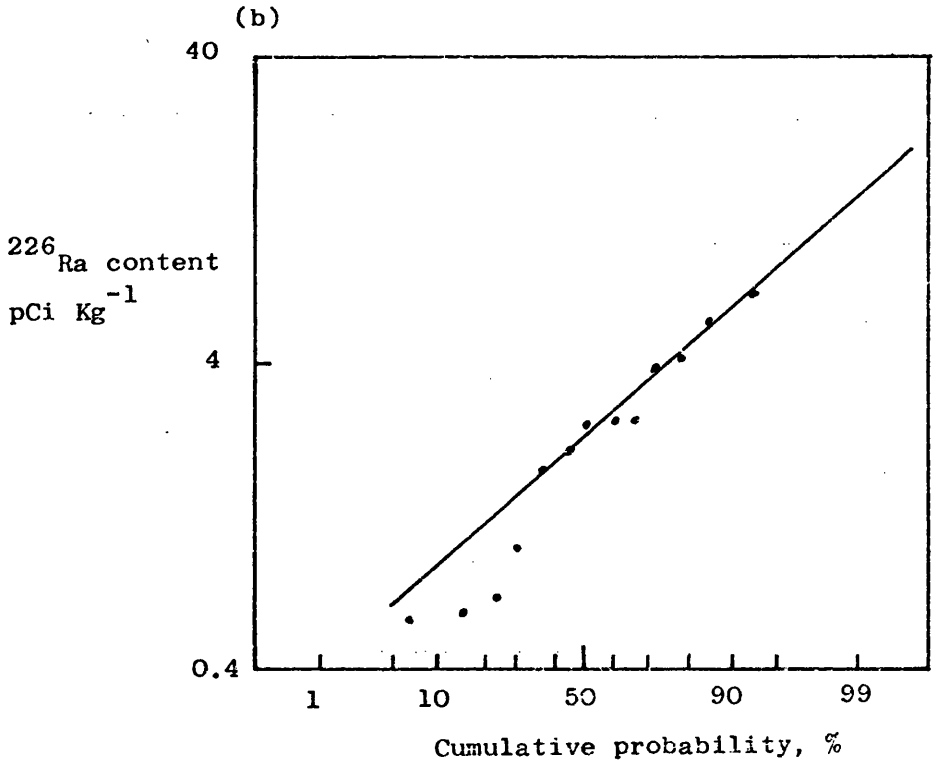

Fig. 6.2. ^{226}Ra contents of shallow groundwaters from the Cornubian granites (a) Histogram and (b) Log normal probability plot of ^{226}Ra contents.

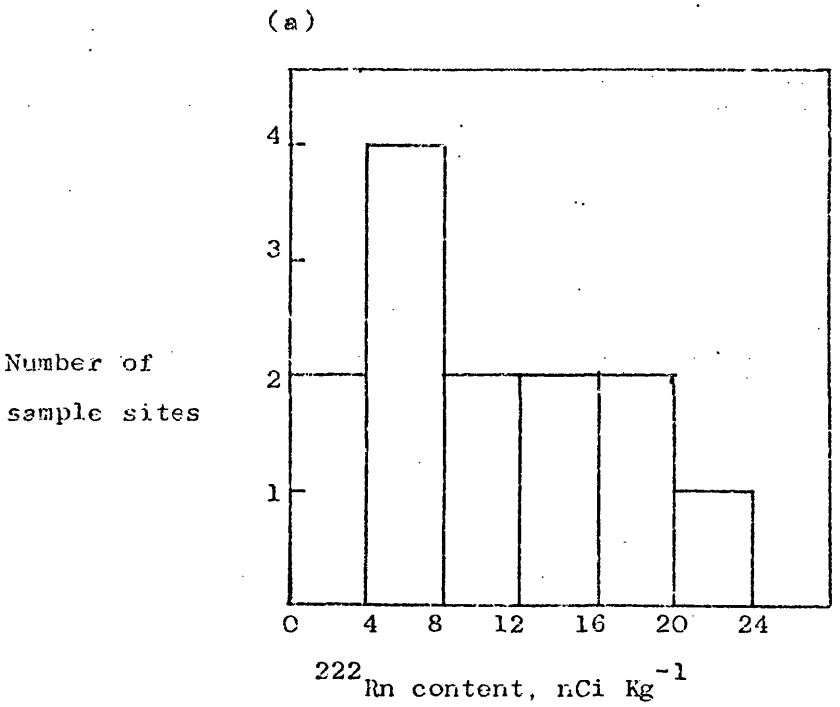

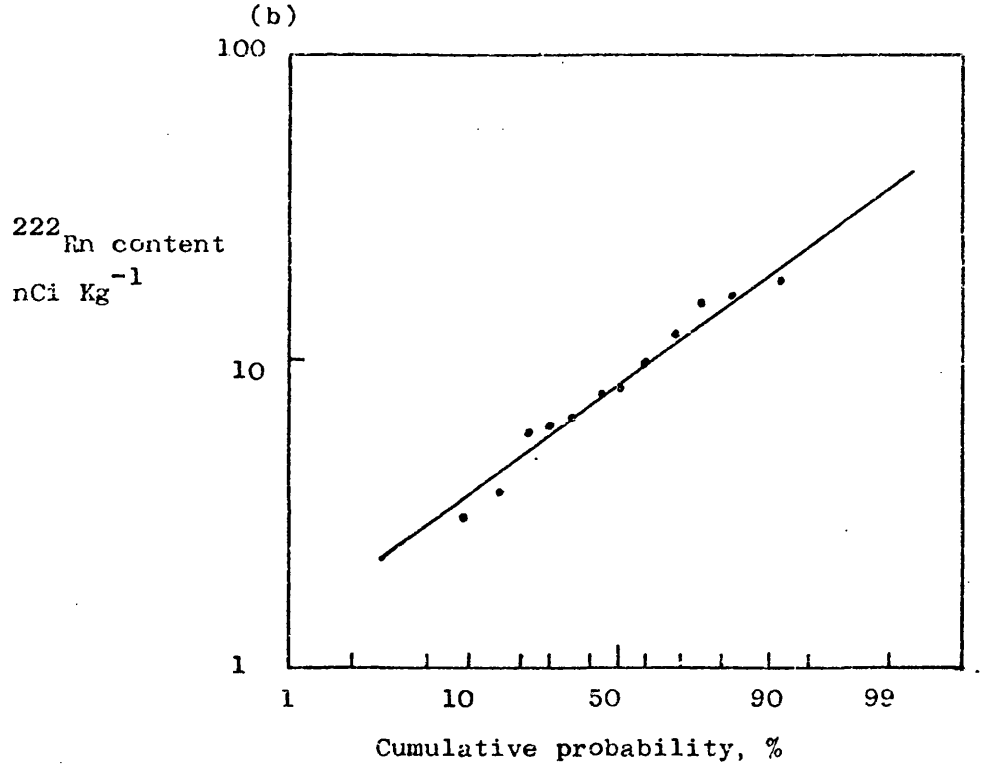

Fig. 6.3. ^{222}Rn contents of shallow groundwaters from the Cornubian granites. (a) Histogram and (b) Log normal probability plot of ^{222}Rn contents.

Table 6.1 ^{222}Rn and ^{226}Ra contents of shallow groundwaters from the granites of South West England.

Site No.	Location	National Grid Ref.		^{226}Ra pCi Kg^{-1}	^{222}Rn pCi Kg^{-1}
1	Ansell, Zennor	SW 475 394			
	a. upper spring		c	1.0±0.1	15270±860
	b. trough		c,e	1.0±0.1	240±14
	c. lower spring		c		12250±690
2	Care, St. Buryan	SW 419 244	b,	5.4±0.3	3710±200
3	Crowan Spring	SW 650 344	c	2.6±0.2	21110±1160
4	Harvey, Praze	SW 660 348	a,	17.0±1.0	n.d.
5	Hocking, St. Ives	SW 484 398	a,	6.7±0.4	16100±900
6	Jeffrey, Praze	SW 662 350	a,	2.5±0.1	18600±1000
7	Jenkin, F.K. Wendron	SW 687 313		2.6±0.1	7960±470
8	Kent, St. Austell	SW 995 566		0.60±0.04	7320±430
9	Michell, Penryn	SW 732 327	a,	2.0±0.1	8170±480
10	Ready Mixed Penryn	SW 741 338	a,	3.9±0.2	3080±170
11	Spence, Spring Farm	SW 658 345	a,	0.69±0.04	6730±410
12	Streatfield, Praze	SW 669 362	a,	1.8±0.1	9940±580
13	Taw Marsh**	SX 618 908	a,	0.58±0.04	6260±380
14	Warren, Bosliven	SW 418 252	b,	4.1±0.2	n.d.
			Mean	3.68±4.1	10350±5 700

NOTES:
a. pumped b/h with depth in m
b. b/h depth sampled
c. surface spring or well
d. surface stream
e. probable equilibration with air
** Dartmoor

Table 6.2. ^{222}Rn and ^{226}Ra contents of groundwaters from the Cornish tin mines

Site number	location	National Grid Ref.		Depth below surface, m	^{222}Rn pCi kg^{-1}	^{226}Ra pCi kg^{-1}
	South Crofty	SW 670 398				
SC A	78/407	380L, 4	Hot Dry	689	12700±800	677±40
SC B	78/408	380L, 4	Cross-cut	689	19800±1200	579±34
SC C	77/774	380L, 4	Hot Dry	689	5680±360	720±42
SC D	78/410	380L, 4E	Robinson's	689	17500±1200	416±25
	Pendarves	SW 647 382				
P 5A	78/421	5L	Harriet Drive East	230	13500±800	8.8±0.5
P 5B	-		working face	230	126000±7000	195±11
P 6	78/419	605	Harriet Drive East	260	4300±240	13.1±0.9
	Mount Wellington	SW 748 420				
MW 6B	78/411			210	4600±270	19.5±1.2
MW 7C	78/412			240	1700±110	7.3±0.4
MW 7D	78/413		Moor Cross-cut	240	2500±150	14.0±0.8
	Wheal Jane					
WJ 9L	78/415		working face	288	470±28	83±4

has a ^{222}Rn content of 126000 pCi Kg^{-1} which is more than one order of magnitude higher than the mean ^{222}Rn concentration. Conversely Wheal Jane 9L has a ^{222}Rn content of 470 pCi Kg^{-1}, which is much lower than expected. This is probably due to the method by which the sample was collected as significant aeration of the sample occurred during collection.

The ^{226}Ra contents of the thermal groundwaters (Table 6.2) range from 7.3 pCi Kg^{-1} to 677 pCi Kg^{-1}. These values are much higher than are found for the ^{226}Ra contents of the non-thermal, shallow groundwaters. The ^{226}Ra contents are also much higher than in any of the other thermal springs that have been studied in the U.K. The highest ^{226}Ra content previously determined was 10.3 pCi Kg^{-1} at King's Spring, Bath. A plot of log ^{226}Ra content against cumulative probability, % Figure 6.4 shows two statistical groupings of ^{226}Ra contents. The first group comprises groundwaters with ^{226}Ra contents less than 20 pCi Kg^{-1} and the second group is of groundwaters with ^{226}Ra contents less than 80 pCi Kg^{-1}.

The factors which control the concentration of ^{222}Rn in the groundwaters of south-west England have been discussed in Chapter 9. The representative ^{222}Rn content, [Rn], for the near surface and most of the mine groundwaters is about 10.5 pCi cm^{-3}. The efficiency of ^{222}Rn release, A, has been determined on sized rock particles and has been estimated as 0.33. Using typical values of the bulk density (2.62 g cm^{-3}) and U content (134 g g^{-1}) of the aquifer rock, given in Table 9.11, Ø,

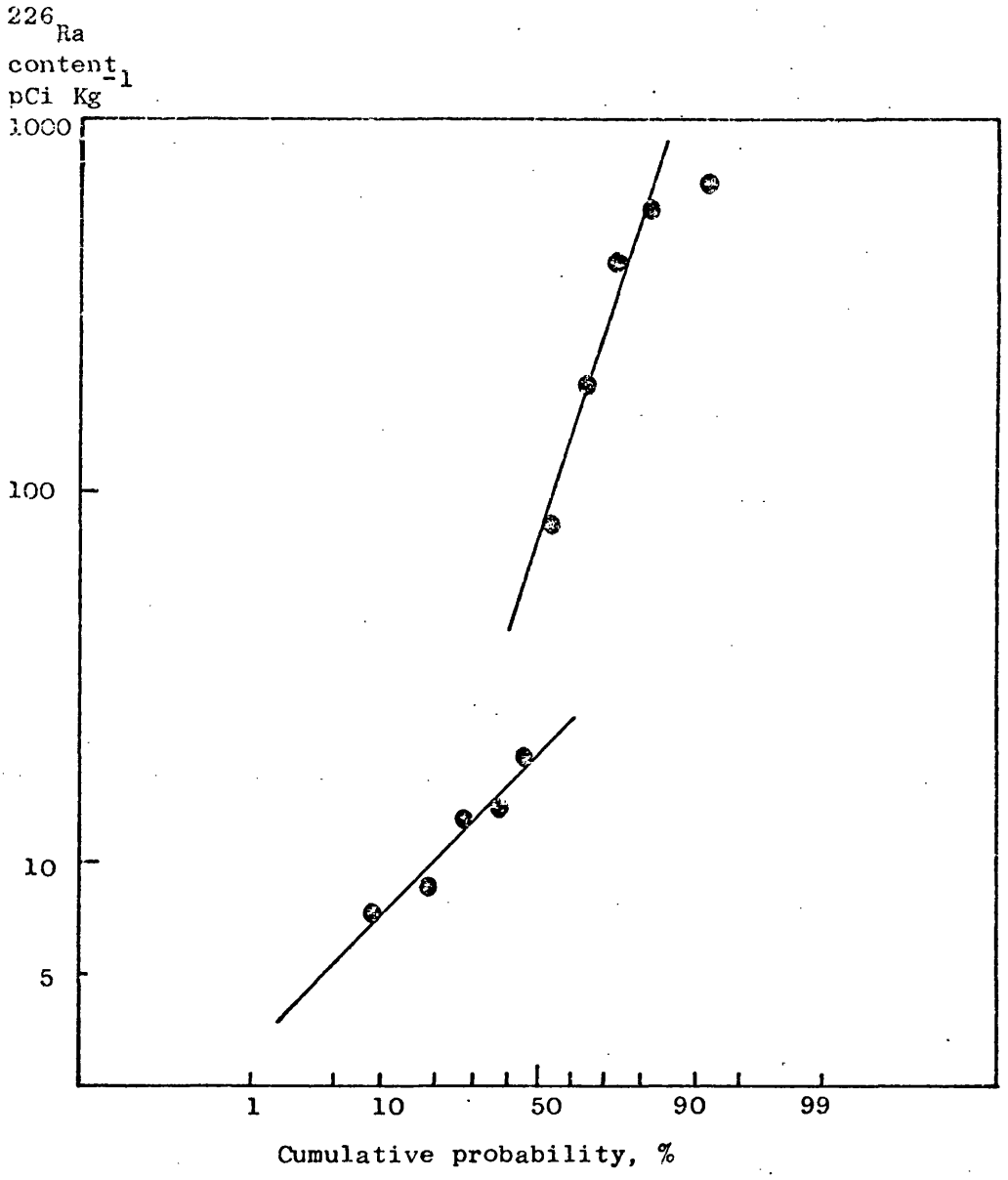

Fig. 6.4. ^{226}Ra contents of groundwaters from mines in the Cornubian granites and country rocks.

the volume of water to volume of rock ratio (porosity) can be calculated using equation 3.1 for residence times greater than 25 days:

$$[Rn] = 0.33\ A\ \frac{\rho}{\emptyset}\ [U]$$

This gives a relatively high porosity of 0.36. Such a porosity would tend to generate a low groundwater ^{222}Rn content as from equation 3.1, $[Rn] \propto \frac{1}{\emptyset}$. The high observed ^{222}Rn contents of the groundwaters from south-west England therefore result from a combination of high fractional ^{222}Rn release into the groundwater (A), and high U contents of the host rock.

The anomalously high ^{222}Rn content in the Pendarves 5B groundwater must result from a high A or [U] or a low $\emptyset$ in the locality of the borehole. It is unlikely that A can be much higher than 0.33. It is probable that the high ^{222}Rn content of Pendarves 5B groundwater is due to combination of an enhanced U content and a reduced porosity in the locality of the granite from which the water is derived.

6.2.2. Radiogenic ^{4}He contents

The ^{4}He contents of groundwaters from south-west England are reported in Tables 6.3 and 6.4. The shallow groundwaters contain little or no radiogenic (excess) ^{4}He, but the thermal mine waters contain a considerable amount of excess ^{4}He. The collection temperature is plotted against sampling depth in Figure 6.6. The relationship is essentially linear, however, collection

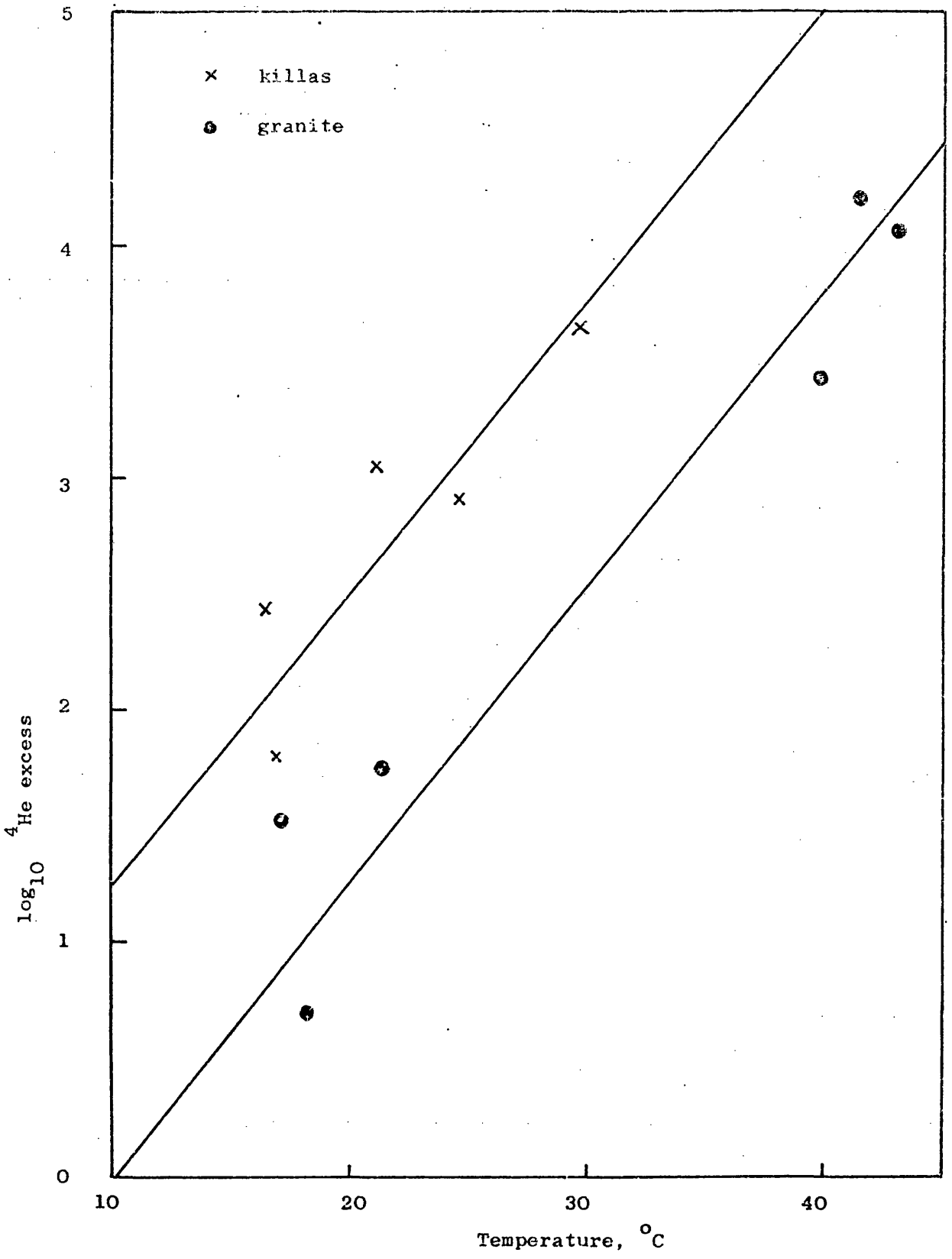

Fig. 6.5. Plot of ^{4}He against collection temperature of groundwaters from the Cornish mines.

Table 6.3. Inert gas contents, derived recharge temperatures and collection temperatures of shallow groundwaters from South West England.

Site No.	Location	National Grid Ref.	Inert gas content cm^3 STP cm^{-3} H_2O					Recharge temp. °C		Collection temp. °C
			He $\times 10^{8}$	Ne $\times 10^{7}$	Ar $\times 10^{4}$	Kr $\times 10^{7}$	Xe $\times 10^{8}$	from Ar	from Kr	
1	Ansell, Zennor	SW 475 394	5.3±0.7	2.08±0.10	3.95±0.14	0.85±0.02	1.17±0.06	10.4±1.4	10.8±1.0	11.5
3	Crowan Spring	SW 650 344	6.1±0.8	1.99±0.10	3.84±0.14	0.83±0.02	1.14±0.06	11.8±1.4	11.8±1.1	11.1
5	Hocking, St. Ives	SW 484 398	3.8±0.5	2.05±0.10	3.89±0.14	0.83±0.02	1.12±0.06	11.1±1.4	11.9±1.1	11.2
6	Jeffrey, Praze	SW 662 350	5.3±0.7	2.04±0.10	3.79±0.14	0.83±0.02	1.11±0.06	12.3±1.4	11.9±1.1	10.8
7	Jenkin, F.K., Wendron	SW 687 313	5.3±0.7	2.07±0.10	4.02±0.14	0.86±0.02	1.17±0.06	9.6±1.4	10.2±1.0	11.2
8	Kent, St. Austell	SW 995 566	4.4±0.6	2.09±0.10	4.01±0.14	0.87±0.02	1.20±0.06	9.7±1.4	9.4±0.8	7.4
10	Ready Mixed, Penryn	SW 741 338	4.6±0.6	2.04±0.10	3.79±0.14	0.80±0.02	1.12±0.06	12.3±1.4	12.9±1.1	-
11	Spence, Spring Farm	SW 658 345	4.9±0.7	2.02±0.10	4.11±0.15	0.88±0.02	1.17±0.06	8.8±1.4	9.2±0.8	12.4
12	Streatfield, Praze	SW 669 362	3.2±0.4	2.08±0.10	3.81±0.14	0.81±0.02	1.09±0.06	12.1±1.4	12.5±1.1	10.5

Table 6.4. Inert gas contents, derived recharge temperatures and collection temperatures of groundwaters from the Cornish tin mines.

Site No.	Location	National Grid reference		Inert gas contents, cm^3 STP cm^{-3} H_2O					Recharge temp. °C		Collection temperature °C
				^4He $\times10^8$	Ne $\times10^7$	Ar $\times10^4$	Kr $\times10^7$	Xe $\times10^8$	from Ar	from Kr	
	South Crofty	SW 670 398									
SC A	78/407	380L,4	Hot Dry	21100+2800	0.84+0.04	2.19+0.08	0.51+0.01	0.81+0.04	48 +2.0	35+1.0	41.5
SC B	78/408	380L,4	Cross-cut	3520±470	1.48±0.07	3.13±0.11	0.72±0.02	1.04±0.05	22.5±2.0	18±0.9	37.1
SC C	77/774	380L,4	Hot Dry	9080±1220	1.33±0.06	2.41±0.09	0.54±0.01	0.82±0.04	39.5±2.0	32±1.0	41.5
SC D	78/410	380L,4E	Robinson's	15500±2100	1.55±0.07	3.18±0.11	0.70±0.02	1.02±0.05	21.5±2.0	19±1.0	43.0
	Pendarves	SW 647 382									
P 5A	78/421	5L	Harriet Drive East	7.6±1.0	2.10±0.10	4.15±0.15	0.87±0.02	1.16±0.06	8.4±1.4	9.5±1.0	18.2
P 5B		5L	Working face	38.2±5.1	2.10±0.10	4.19±0.15	0.89±0.02	1.18±0.06	8.0±1.4	8.9±0.8	-
P 6	78/419	605	Harriet Drive East	56.8±7.6	2.08±0.10	3.97±0.14	0.83±0.02	1.11±0.06	10.1±1.4	11.7±1.1	21.4
	Mount Wellington	SW 748 420									
MW 6B	78/411			94±13	2.00±0.10	4.01±0.14	0.84±0.02	1.21±0.06	9.7±1.4	11.0±1.0	16.8
MW 7C	78/412			328±44	2.07±0.10	3.96±0.14	0.84±0.02	1.13±0.06	10.2±1.4	11.2±1.1	16.4
MW 7D	78/413		Moor Cross-cut	1360±180	2.10±0.10	4.26±0.15	0.88±0.02	1.18±0.06	7.4±1.4	9.3±0.8	21.4
	Wheal Jane										
WJ 9LA	78/415		working face	848±114	2.07±0.10	3.86±0.14	0.83±0.02	1.04±0.06	11.6±1.4	11.3±1.1	24.8
WJ 9LB	78/417		943	5440±730	1.83±0.09	3.89±0.14	0.85±0.02	1.20±0.06	11.1±1.4	10.6±1.0	29.5

temperature is probably a better indicator of the precise depth from which the thermal waters originated. In Figure 6.5, the excess ^4He content of the thermal groundwaters is plotted against collection temperature. The data is plotted so as to differentiate between groundwaters which arise from the granite and groundwaters which are found in the metamorphosed Devonian sediments (killas). The general trend is for the ^4He content to increase with collection temperature (and therefore depth). Groundwaters from the granite (South Crofty and Pendarves) generally have higher ^4He contents than groundwaters from the killas (Mount Wellington and Wheal Jane) for the same collection temperature. From Figure 6.6 the difference is about a factor of 10.

The ^4He content of the thermal waters is derived from radioactive decay of natural U and Th and their daughter isotopes present in the granite and metamorphosed Devonian sediments. If it is assumed that all the ^4He generated in the granite and killas dissolves in the proximate groundwater, then the ^4He content of the groundwater, $[^4He]$ in cm^3 STP cm^{-3} H_2O is given by:

$$[^4He] = \frac{\rho}{\phi} \{ p_U [U] + p_{Th} [Th] \} t . \qquad 6.1$$

where ρ is the bulk density of the rock, g cm^{-3}

ϕ is the fractional porosity of the rock

p_U, p_{Th} are the production rates of ^4He from U and Th decay respectively, cm^3 STP g^{-1} $year^{-1}$

$[U], [Th]$ are the respective U and Th contents of the rock, μg g^{-1}

and t is the residence time of the groundwater, $year^{-1}$

The increased ^{4}He content in the killas, relative to the granite, may now be considered in terms of the variables in equation 6.1 and other mechanisms by which ^{4}He may enter groundwaters . The bulk density of the granite and killas are essentially the same, around 2.6 g cm^{-3}. So if the ^{4}He content is entirely derived from the local rock, the killas must have a higher U and Th content or a lower porosity than the granite. Data from the ^{222}Rn contents of the groundwaters indicate that the porosity of the granite is very high (0.36) and that the porosity of the killas is similarly high. This would suggest that it is the high U and Th content of the killas that is responsible for the high excess ^{4}He for groundwaters of the same age, t. However, in general the average U and Th contents in Devonian sediments are less than in granites. One explanation is that U (and Th) may be deposited locally in the killas as a result of hydrothermal mineralisation. Alternatively, ^{4}He diffusion in the killas may be greater than in the granite and contribute to the higher ^{4}He contents in the killas groundwaters.

An alternative way of explaining the difference between the ^{4}He in the granite and killas groundwaters is that the thermal waters are derived from much deeper than their collection depths and have undergone different degrees of cooling. Such a mechanism is unlikely as it would tend to lead to a random distribution of collection temperature against sampling depth (Figure 6.6) and collection temperature against ^{4}He content (Figure 6.5), rather than the observed correlations.

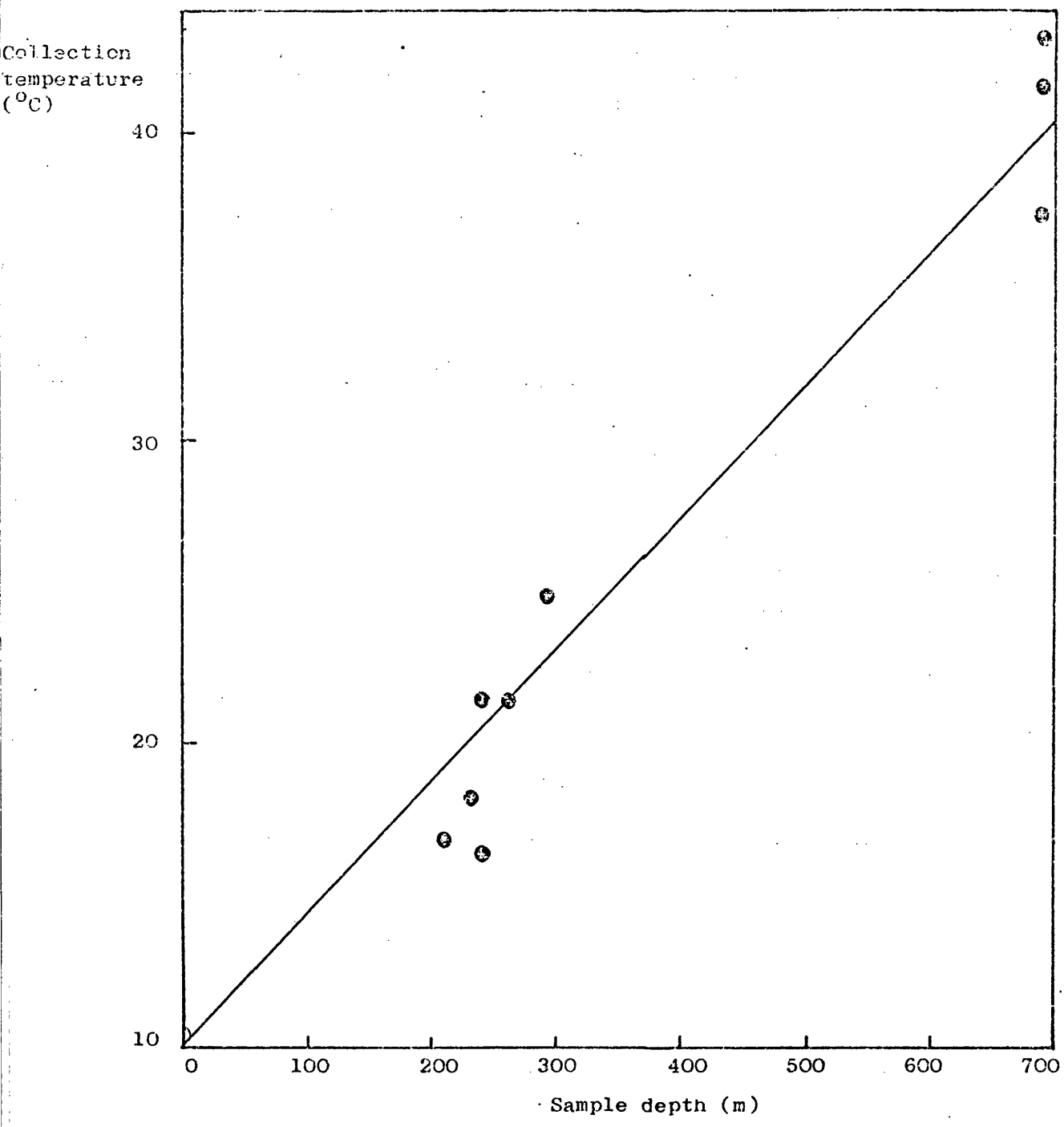

Fig. 6.6. Plot of collection temperature against sampling depth of groundwaters from the Cornish mines.

The use of ^{4}He as a tool for prospecting for geothermal energy has been suggested. The "hot rocks" of Cornwall may provide such an energy resource, but variability of ^{4}He with source may limit the usefulness of the ^{4}He technique for geothermal energy prospecting. Tritium measurements on some of the groundwaters from South Crofty and Wheal Jane indicate that even the groundwaters with very high ^{4}He contents contain some proportion of recent water [156]. The circulation patterns and mixing proportions are complex in these groundwaters and their ^{4}He contents can only yield qualitative information on relative ages, mixing volumes, source of ^{4}He, etc.

6.2.3. Radiogenic ^{40}Ar contents

The $^{40}Ar/^{36}Ar$ ratios of three groundwaters from south-west England are reported in Table 6.5. The limited data indicates that the shallow groundwaters, as expected, show no enhanced $^{40}Ar/^{36}Ar$ ratio. However, the groundwater with the highest ^{4}He content, from one of the hottest springs shows significant enhancement of the $^{40}Ar/^{36}Ar$ ratio. This reflects the probable high proportion of ancient water in the source and the high temperature at which the groundwater interacted with rock at depth. This enables ^{40}Ar from the radioactive decay of ^{40}K to migrate readily from its site of production into the groundwater.

6.2.4. Estimated recharge temperatures

The recharge temperatures estimated from the Ar and Kr contents of the groundwaters of south-west England range from 9.0 to 12.6°C.

Table 6.5. $^{40}Ar/^{36}Ar$ ratios of groundwaters from South-west England

	Site	$^{40}Ar/^{36}Ar$
SCD	South Crofty	311.9
7	Jenkins	295.6
5	Hocking	296.7
	Air	295.5

The recharge temperatures do not correlate with the collection temperature and represent the temperature at which the groundwaters equilibrated with soil air. There is no pattern in the geographical distribution of the recharge temperatures. The average recharge temperature is 11.0°C. This is somewhat higher than the average recharge temperatures of groundwaters from the Bunter Sandstone, Nottinghamshire (7.0°C); the Bath/Bristol area (9.0°C) and the Lincolnshire Limestone (7.0°C) and reflects the warmer climate of south-west England.

The estimated recharge temperatures of groundwaters from Pendarves, Mount Wellington and Wheal Jane are similar to those of the shallow groundwaters, reflecting temperature at which these waters equilibrated with soil air and confirming their meteoric origin. The recharge temperatures estimated for the South Crofty groundwaters are, however, very much higher than the average recharge temperature for the shallow groundwaters. This indicates that the groundwaters have reequilibrated with air at an elevated temperature at depth, since such temperatures could not have resulted from air equilibration at ground level. The estimated temperatures are generally lower than the collection temperatures for these groundwaters indicating that the groundwaters were equilibrated with air at a temperature lower than the collection temperature.

6.3. CONCLUSIONS

The ^{222}Rn and ^{226}Ra contents of groundwaters from the granite of south-west England are generally much higher than those from the sedimentary aquifers of England. The ^{222}Rn contents have been used to calculate the porosity, $\emptyset$, for the Cornish granite. The value of

Ø (0.36) is relatively high. But a high fractional release of ^{222}Rn from the granite and a high U content lead to high concentrations of ^{222}Rn found in the groundwaters.

The radiogenic ^{4}He content of the groundwaters from the Cornish mines has been discussed in terms of the relative U contents of the granite and killas. Evidence that the U content of the killas is enhanced by hydrothermal mineralisation or that ^{4}He diffusion in the killas is easier than in the granite is an important consideration when evaluating the potential of the area for producing geothermal energy. The distribution of ^{4}He in the groundwaters is further complicated by mixing with recent water, indicated by the high tritium contents.

The estimated recharge temperatures of the Cornish groundwaters have been used to differentiate between waters which equilibrated with soil air in the recharge zone and waters which have been reequilibrated at temperatures higher than the recharge temperature. The $^{40}Ar/^{36}Ar$ ratio can be used as an indicator of long residence times and high water/rock interaction temperatures.

CHAPTER 7

RADON, RADIUM AND DISSOLVED INERT GASES IN GROUNDWATERS FROM STRIPA MINE, SWEDEN.

7.1. INTRODUCTION

The most feasible option available for the long-term storage of radioactive waste is presently thought to be disposal to geological formations. The three most likely rock-types are argillaceous sediments, salt deposits and hard crystalline igneous or metamorphic rocks (granites, gabbro's, gneisses, granulites etc.). The need to predict the behaviour of these rocks under the conditions in which the waste will be stored has promoted research in many countries. In Sweden, an abandoned iron ore mine near Stripa has been chosen as a site for investigating the storage of radioactive waste in mined granite caverns.

Stripa mine is located approximately 200 km west of Stockholm and is constructed in a granitic intrusion. Iron ore beds within the associated metasedimentary rock sequence have been mined for about 400 years to depths of up to 410m below ground level. This mining activity will have had an important effect on the groundwater flow regime in the area. The geochemistry of uranium and its daughter products is likely to be influenced by these complicated flow patterns and by local enrichments of uranium minerals.

Heater experiments and fracture hydrologic studies have been supplimented by a detailed geochemical study on the complex hydrochemistry.

This has been carried out jointly by The University of Waterloo, Canada; The University of Bath, England; The University of Florida, U.S.A; the International Atomic Energy Agency, Vienna; and The University of California, U.S.A.[157] The geochemical study has included field

determinations of pH, alkalinity, EH and dissolved oxygen combined with major ion analyses. These describe the chemical characteristics of the groundwaters. Stable isotope analyses (^{18}O and ^{2}H) have been used to characterise different water masses and to obtain information on their origin. Groundwater ages have been estimated from the abundance of radioactive elements and/or their decay products: tritium has been used to identify groundwaters which contain a component of recent recharge whereas older waters have been identified by their ^{14}C activity, and uranium content and isotopic composition.

Information on groundwater ages has also been obtained from determination of the ^{4}He, ^{40}Ar and ^{222}Rn contents of the groundwaters. The other dissolved inert gas contents have been used to provide information on the environment of groundwater recharge.

The groundwater chemistry has been found to change significantly with sampling depth. The surface waters are low in total dissolved solids, t.d.s. (<30 mg/l) with pH's ranging from 6.5 to 6.8. In the shallow groundwaters, the t.d.s. content increases to 120 - 325 mg/l and the pH values are as high as 8. These waters are calcium bicarbonate in character. The deeper groundwaters (330m level) are sodium-chloride-bicarbonate waters with a t.d.s. content of 200-230 mg/l and pH values between 8.8 and 9.1. Groundwaters flowing into the 410m borehole to a depth of about 770m below ground level have a similar chemistry to the 330m level groundwaters but the deeper samples show an increase in salinity (810 mg/l at the deepest point), a chloride-sodium-calcium-sulphate character and a pH of 9.8, which is unusually high. It has been suggested that small amounts of fossil sea water mixed with fresh water may be partially responsible for values of

t.d.s. exceeding 800 mg/l.

The ^{18}O and ^{2}H contents of the groundwaters show that different types of groundwaters circulate at different levels. Modern surface waters do not penetrate to the mine levels. Between 330 and 770m below ground the isotopic compositions of the groundwaters are similar and the groundwaters probably have the same origin. The lowest ^{18}O and ^{2}H contents occur in the deepest groundwaters which were recharged under the coolest climatic conditions. The data indicates that groundwaters from different levels have different ages. The ^{13}C contents of the groundwaters indicate that recharge did not occur during periods of glaciation by subglacial recharge. ^{14}C age determinations are complicated by exchange reactions. Data from uranium determinations support the observations that these groundwaters are old. The dissolved inert gas, radon and radium contents have been determined for shallow and mine groundwaters. The results support the evidence obtained from the stable isotope, ^{14}C and U contents. They confirm that the mine groundwaters are old and that some of the groundwaters were recharged under cold climatic conditions.

7.2. RESULTS AND DISCUSSION

7.2.1. ^{222}Rn and ^{226}Ra contents.

The ^{222}Rn and ^{226}Ra contents of the Stripa groundwaters are given in Tables 7.1 and 7.2. The ^{222}Rn contents of the shallow groundwaters range from 3720 to 19300 pCiKg^{-1} water with an average content of 8940 pCi Kg^{-1}. These are very much lower than the ^{222}Rn contents of the Stripa mine samples which range from 0.36 to 2.01 μCi Kg^{-1}

Table 7.1. ^{222}Rn and ^{226}Ra contents of groundwaters from shallow boreholes near Stripa Mine, Sweden.

Sample Number	Location	^{222}Rn pCi Kg^{-1}	^{226}Ra pCi Kg^{-1}
Stripa 20	Private well No. 3	5140 ± 300	0.64 ± 0.06
Stripa 21	Private Well No. 5	3720 ± 230	0.41 ± 0.04
Stripa 71	Water table well No. 2	19300 ± 1100	0.72 ± 0.06
Stripa 80	Private well No. 4	10300 ± 640	0.83 ± 0.10
Stripa 83	Private well No. 1	6240 + 340	0.57 + 0.07

Table 7.2. ^{222}Rn and ^{226}Ra contents of groundwaters from Stripa Mine, Sweden

Sample location	Sample depth, m		^{222}Rn content $\mu Ci\ Kg^{-1}$	^{226}Ra content $pCi\ Kg^{-1}$
R1 borehole, ventilation drift	323 - 337		1.01 ± 0.06	6.7 ± 0.5
M3 borehole, 338 m level	338 - 352	(a)	1.30 ± 0.07	34. ± 2
		(b)	2.01 ± 0.11	4.6 ± 0.4
R9 borehole, ventilation drift	338 - 368		1.13 ± 0.06	4.9 ± 0.4
471 m borehole, 410m level	416 - 432.4		0.36 ± 0.02	
	786.5 - 881		0.56 ± 0.03	40 ± 2
	811 - 838.4		0.81 ± 0.05	56 ± 3

water. The average ^{222}Rn content is 1.03 μCi Kg^{-1} water - one hundred times greater than the shallow groundwater average. The factors which affect ^{222}Rn release from U bearing minerals have been discussed in paragraph 1.3. Experiments measuring the amount of ^{222}Rn released from sized rock fragments of Stripa granite (para. 9.2) indicate that the low concentrations of ^{222}Rn in the shallow groundwaters compared with the mine waters result primarily from a high ratio of the volume of water to the volume of rock near the surface. (Calculated porosity, $\emptyset_{calc.}$=0.87). This porosity is higher than the theoretical maximum porosity for close packed spheres in a cubic configuration (0.4764). Fracture porosity will increase the theoretical maximum and this is discussed in Chapter 9. The remarkably high ^{222}Rn concentrations in the mine groundwaters result from an extremely low volume of water per unit volume of rock at depth ($\emptyset_{calc}$=0.003 at 832m). There is no correlation of the ^{222}Rn contents with overall depth although in the 410m bore hole, the ^{222}Rn concentration increases with depth. The highest ^{222}Rn concentrations occur at an intermediate depth in a hole bored from the 338m level - the M.3 borehole.

The ^{226}Ra contents are several orders of magnitude less than the ^{222}Rn contents. The average ^{226}Ra concentration in the shallow groundwaters is 0.63 pCi Kg^{-1} water and ranges from 0.41-0.83 pCi Kg^{-1}. The range of the ^{226}Ra contents in the mine waters is, however, much greater - 4.59 to 56 pCi Kg^{-1} with an average value of 24 pCi Kg^{-1}. These values are similar to those found in waters from depths of about 200m in the Cornish tin mines but are much less than the ^{226}Ra contents from deeper in the Cornish mines. At Stripa, the lower

^{226}Ra contents generally occur at depths up to about 345m below ground level with higher ^{226}Ra concentrations occurring deeper than 345m. It is possible that the ^{226}Ra solution at depths exceeding 345m could be recoil controlled. This process would result in a constant ^{226}Ra content in solution for waters older than 8000 years on the assumption that the granite composition is uniform.

The ^{226}Ra contents of two samples from the M3 borehole (338 in level) are very different (Table 7.2). Sample (a) has a ^{226}Ra content of 34 pCi Kg^{-1} compared with 4.6 pCi Kg^{-1} for sample (b). The collection temperatures of the samples also differ - 11.0°C for sample (a) and 14.5°C for sample (b). (Table 7.4). Sample (a) was collected on 29 March 1978 and sample (b) on 16 May 1979. It must be concluded that a significant change has occurred in the nature of this groundwater between the two sampling dates. It is possible that the nearby "heater experiments" have raised the temperature of the local groundwater. This has had the effect of decreasing the ^{226}Ra content, possibly by precipitating the ^{226}Ra in solution or by lowering the rate at which ^{226}Ra enters solution. It is also possible that the high ^{226}Ra content was the equilibrium concentration with little or no flow occurring when the experimental programme was started. Subsequently groundwater has been continuously removed and ^{226}Ra equilibrium between the solid and aqueous phases is no longer established. This change in the character of the groundwater from the M3 borehole has important implications in regard to the storage of radioactive waste in mined granite caverns, particularly if it has been caused by the simulated radicactive waste heater experiments.

7.2.2. Radiogenic ^{4}He and ^{40}Ar contents

The ^{4}He content of groundwaters from shallow boreholes in the vicinity of Stripa are reported in Table 7.3. Three of the sites investigated show a possible small contribution to the ^{4}He contents from radiogenic ^{4}He, but the fourth site, Stripa 83, contains a high proportion of radiogenic ^{4}He. The value of 3540×10^{-8} cm^{3} STP cm^{-3} H_2O is remarkably high for a shallow groundwater with a likely low age. It is possible that the groundwater contains a component of ancient groundwater of the type found in the mine waters although this is unlikely because the ^{222}Rn and ^{226}Ra contents are low and the ^{18}O and ^{2}H data indicate that no mixing occurs between the shallow and deep groundwaters [157]. A second alternative is that the Stripa 83 borehole intersects a fault which transports ^{4}He from depth to the surface. However, this system would be likely to transport ^{222}Rn to the surface and this is not detected. ^{222}Rn transported along faults to the surface may not be detected because of radioactive decay during its ascent, so this model may not be entirely ruled out. A third possible mechanism by which the ^{4}He content of Stripa 83 may be enhanced is a local concentration of U. The concentration of U would have to be fairly high to produce the observed ^{4}He content in a short residence time (approximately 1% ^{238}U for a residence time of 1000 years, bulk density of 2.8g cm^{-3}, fractional porosity 0.1 and assuming all the ^{4}He generated dissolved in the groundwater - see equation 3.2).

Table 7.3. Inert gas contents, derived recharge temperatures and collection temperatures of groundwaters from shallow boreholes near Stripa Mine, Sweden.

Sample No.	Location	Inert gas content, cm^3 STP cm^{-3} H_2O					Recharge temperature, °C		Collection temperatures °C
		He x 10^8	Ne x 10^7	Ar x 10^4	Kr x10^7	Xe x10^8	from Ar	from Kr	
Stripa 21	Private well No. 5	8.1±1.1	2.22±0.11	4.58±0.16	1.06±0.02	1.64±0.09	4.3±1.5	2.5±0.7	5.8
Stripa 71	Water table well No. 2	7.7±1.0	2.30±0.11	4.90±0.18	1.15±0.02	2.02±0.11	1.2±1.6	-0.5±0.6	5.2
Stripa 80	Private well No. 4	9.3±1.2	2.30±0.11	5.00±0.18	1.11±0.02	1.56±0.08	0.3±1.6	0.7±0.7	10.7
Stripa 83	Private well No. 1	3540 ± 470	2.24±0.11	4.60±0.17	1.04±0.02	1.53±0.08	4.1±1.6	3.1±0.7	7.4

Table 7.4. Inert gas contents and collection temperatures of groundwaters from Stripa mine, Sweden.

Sample location	Sample depth, m	Inert gas content, cm^3 STP cm^{-3} H_2O					Collection temperature °C
		He x 10^8	Ne x 10^7	Ar x 10^4	Kr x 10^7	Xe x 10^8	
R1 borehole, ventilation drift	323-337	25500±3400	3.19±0.15	5.80±0.21	1.27±0.03	-	10.5
		30400±4100	3.63±0.17	6.13±0.22	1.31±0.03	-	
M3 borehole, 338m level	338-352	(a)35900±4800	3.61±0.17	6.26±0.23	1.21±0.03	1.56±0.08	11.0
		50500±6800	4.22±0.20	6.52±0.23	1.21±0.03	1.58±0.08	
		34900±4700	3.38±0.16	6.19±0.22	1.20±0.03	1.50±0.08	
		(b)59500±8000	-	-	-	-	14.5
		47700±6400	3.70±0.18	6.27±0.23	1.64±0.04	-	
R9 borehole, ventilation drift	338-368	28600±3800	1.92±0.09	-	-	-	8.0
471m borehole, 410m level	419-446	57900±7700	4.70±0.22	7.95±0.29	1.48±0.03	1.92±0.10	8.0
		75400±10100	4.13±0.20	7.21±0.26	1.37±0.03	1.77±0.09	
	742-769.4	100000±13400	6.26±0.30	8.16±0.29	1.46±0.03	1.78±0.09	5.5
		84500±11300	-	-	-	-	
	786.5-881	182000±24000	6.26±0.30	9.69±0.35	1.49±0.03	1.92±0.10	7.0
		162000±22000	6.13±0.29	9.62±0.35	1.48±0.03	1.77±0.09	
		98300±13200	4.31±0.21	9.12±0.33	1.50±0.03	1.78±0.09	
	811-838.4	95900±12900	2.70±0.13	7.01±0.25	1.22±0.03	1.93±0.10	8.0
		112000±15000	3.40±0.16	7.88±0.28	-	-	

The ^4He contents of the mine groundwaters are reported in Table 7.4. Without exception, the samples have a considerable component of radiogenic ^4He present. The amount of ^4He present increases with depth (Figure 7.1) to a value of 182000×10^{-8} cm^3 STP cm^{-3} H_2O at a depth of 786.5-881m below ground level. The ^4He contents can be related to the age of the groundwaters by equation 3.2:

$$[He] = \frac{\rho}{\phi} \left\{ 1.19 \times 10^{-13} [U] + 2.88 \times 10^{-14} [Th] \right\} t$$

if all of the ^4He generated is dissolved in the water phase. Data from Chapter 9 indicate that ρ, ϕ, [U] and [Th] are essentially constant within the mine system, so the ^4He content may be used as an indicator of relative ages of the groundwaters. Consequently the ^4He data indicate that the groundwater ages increase with depth.

Calculation of absolute age is only possible if the values of ρ, ϕ, U and Th and the partition of ^4He between the water and rock are known. The U contents and the bulk densities of the Stripa granites have been determined and are reported in Table 9.11. The value of ϕ has been calculated from these values, the value of fractional ^{222}Rn release and the ^{222}Rn contents of the Stripa mine groundwaters. The values of [Th] have also been determined and are reported in Table 7.5. Using these values, the age of the groundwaters from different levels in Stripa mine has been calculated (Table 7.6). The average ^4He contents of each level in the mine has been used as the representative ^4He concentration and firstly it has been assumed that all the ^4He dissolves in the water phase (equation 3.2).

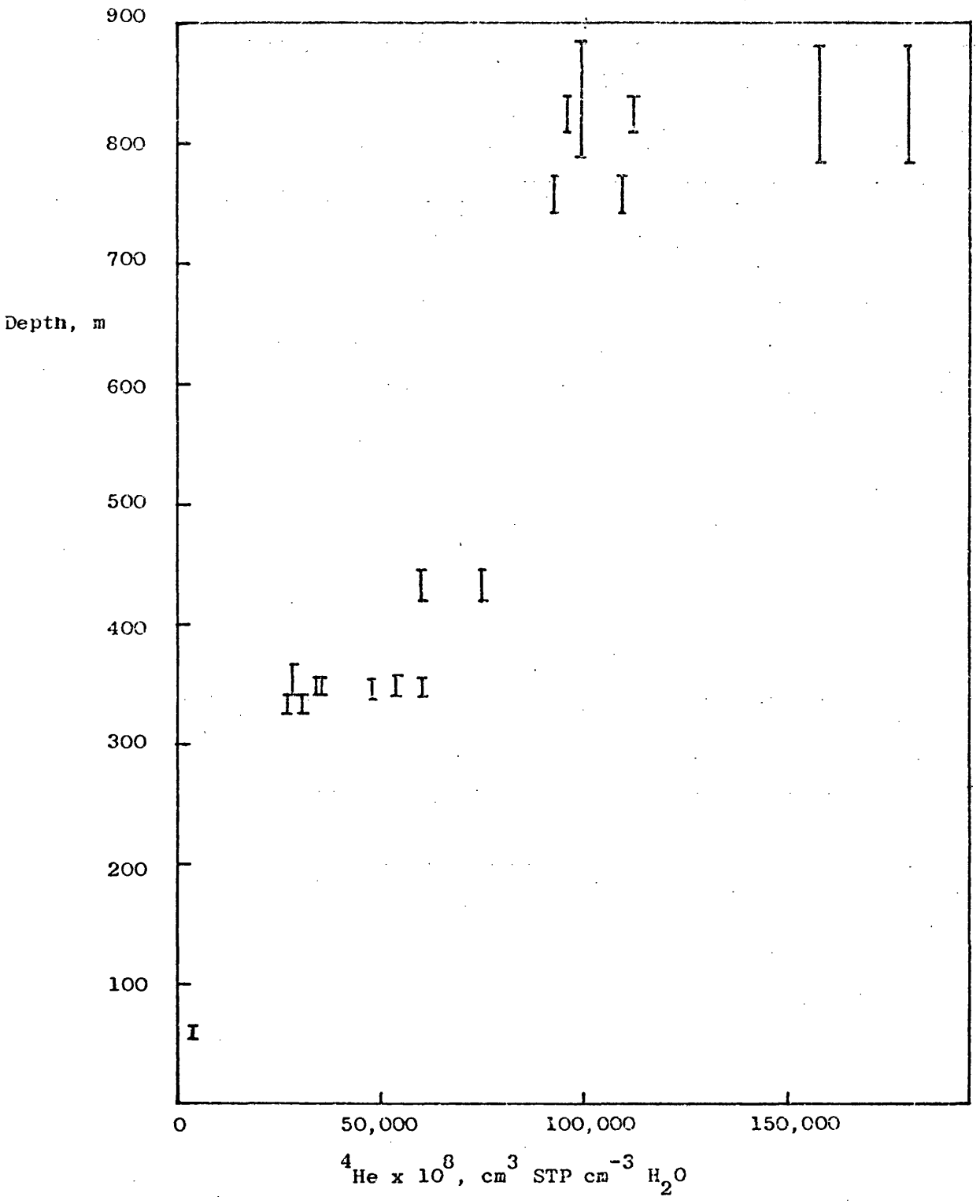

Fig. 7.1. Plot of ^4He contents against sample depth of groundwaters from Stripa mine.

Table 7.5. Th and U contents of granite samples from Stripa Mine, Sweden.

Sample depth, m	Th(Ge/Li) $\mu g\ g^{-1}$	Th(NaI) $\mu g\ g^{-1}$	Average Th $\mu g\ g^{-1}$	U $\mu g\ g^{-1}$	Th/U
338	59	32	46	37	1.24
350	62	32	47	39	1.21
410	56	35	46	40	1.15

Table 7.6. Ages calculated from ^4He contents of Stripa mine groundwaters

Approx. Sample depth, m	Average [^4He] $cm^3 STP cm^{-3} H_2O \times 10^8$	Density, ρ $g\ cm^{-3}$	Porosity, Ø	U content $\mu g\ g^{-1}$	Th content $\mu g\ g^{-1}$	Age, t years *	Age, t years ‡
350	39100(1)	2.61	0.006	39	47	1.5×10^5	2.5×10^7
410	66700(2)	2.61	0.011	40	46	4.6×10^5	4.2×10^7
750	92000(2)	2.61	0.030(4)	17(4)	20(5)	4.1×10^6	1.4×10^8
850	130000(3)	2.61	0.030(4)	17(4)	20(5)	5.7×10^6	1.9×10^8

NOTES:
(1) Average of 8 values
(2) Average of 2 values
(3) Average of 5 values
(4) Value for sample from 832m
(5) Calculated from average Th/U ratio of 1.2
* Assumes all ^4He dissolved in groundwater.
‡ Assumes ^4He partitioned equally, volume for volume, between groundwater and rock.

As the values of Ø are extremely small (Table 7.6) the assumption that all the ^{4}He generated dissolves in the water phase is an extremely important one, and ages calculated on the basis that the ^{4}He partitions itself equally between the water phase and the solid phase are up to two orders of magnitude higher, as shown in Table 7.6. It is not clear which is the correct assumption. Clearly the ages calculated by both ^{4}He methods differ greatly from the ^{14}C ages. ^{14}C data indicates that the maximum groundwater age (for M3 borehole, 338-352m) is around 25000 years. This compares with a maximum age of 5.7 million years if all the ^{4}He dissolves in the groundwater, and 190 million years if the ^{4}He is partitioned equally (volume for volume) between the water and granite (Table 7.6). ^{14}C dating of the deeper groundwaters has proved to be difficult and unreliable because of the much lower bicarbonate content at depth. These ^{14}C ages must be carefully interpreted and correlated with age determinations by other methods.

A closer examination of the partitioning of ^{4}He is necessary. ^{14}C data would suggest that the younger ^{4}He age is the most likely age. That is, that all the ^{4}He dissolves in the groundwater. Data from the Bunter Sandstone aquifer suggests that in a cemented sandstone, the ^{4}He does partition itself in the water phase. In the Lincolnshire Limestone, ^{4}He is probably divided equally (volume for volume) between the water and the rock phases. In the Bunter sandstone, U and Th are concentrated in the cementing phase whereas in the Inferior Oolite these radioelements tend to be more

widely dispersed. Moreover, ^{222}Rn is released much more readily into groundwaters from the Bunter Sandstone than from the Inferior Oolite.. The release of ^{222}Rn may be used as a qualitative indicator of ^{4}He partitioning. The value of the fractional ^{222}Rn release for the Stripa granite ranges from 0.120 - 0.370. This compares with 0.10 for the Bunter sandstone and 0.05 for the Inferior Oolite. Clearly, ^{222}Rn is released much more effectively in the granite. This would indicate that ^{222}Rn diffuses much more easily into the granite groundwaters. ^{4}He would also diffuse readily from its site of production into the groundwater and would be concentrated in the aqueous phase. Consequently, the ^{4}He age of the oldest groundwater is likely to be at most 5.7 million years. It is likely that ^{4}He diffusion has an important role to play in determing the ^{4}He content of the Stripa mine groundwaters. The flow rates of the Stripa groundwaters are very low. ^{4}He would be removed relatively slowly from a comparatively large volume of granite. This would lead to a build up in the concentration of ^{4}He in the granite since it became emplaced. Consequently the ^{4}He content of the groundwater would be greater than would have been produced by radioactive decay of U and Th during the residence time of the groundwater. This would lead to an over-estimate of the groundwater age by the ^{4}He method. It is unlikely that there would be any diffusion of ^{4}He from the groundwater and there is no possibility of contribution to the ^{4}He content by production in confining strata. It is likely that 5.7 million years is an upper limit to the groundwater age of the deepest source and that the ages at other depths are similarly upper limits. These ages are plotted against sample depth in Figure 7.2. It is difficult to reconcile these ages with the ^{14}C ages. Evidence from the uranium isotopic data indicates that the

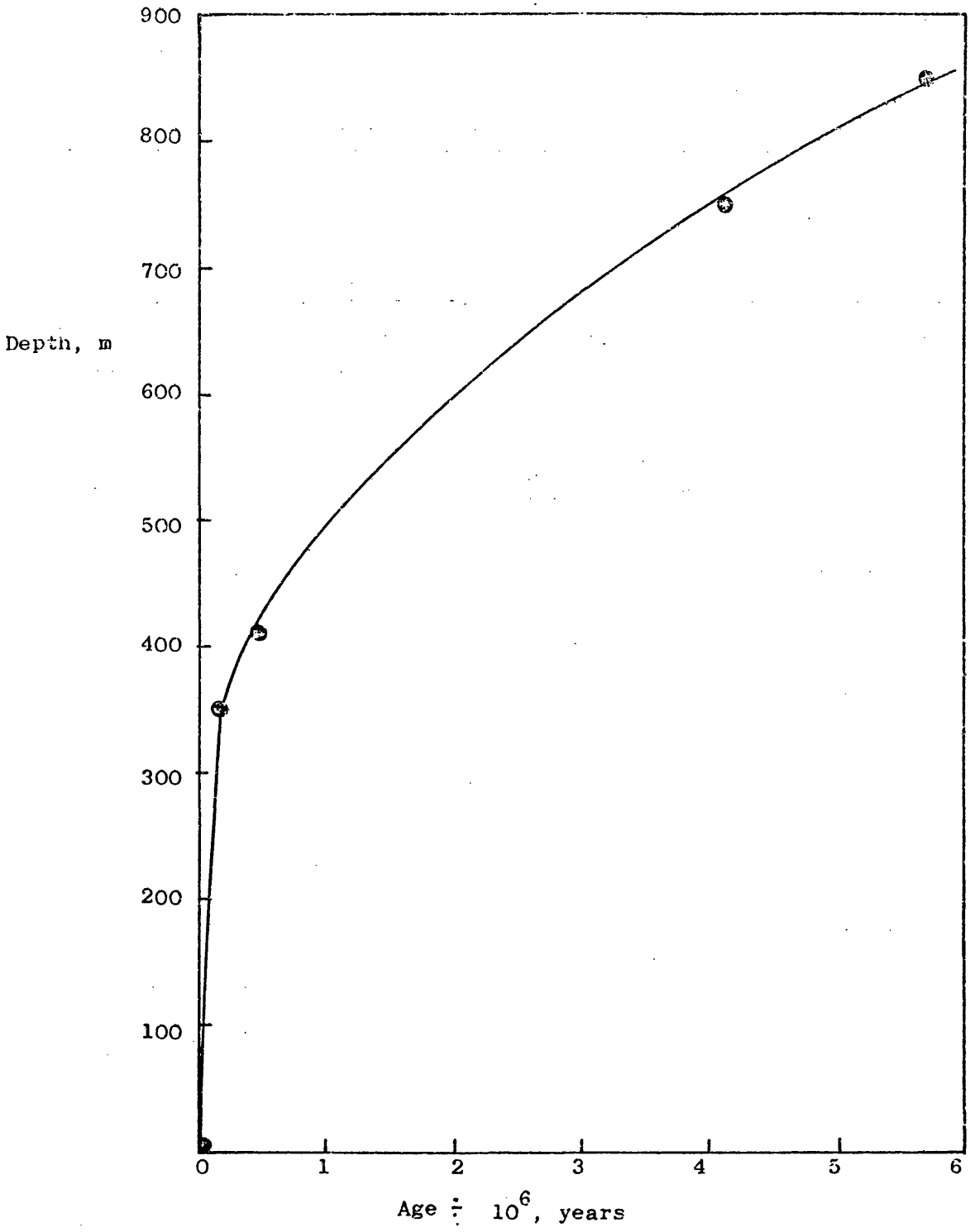

Fig. 7.2. Plot of ^{4}He age against sample depth of groundwaters from Stripa.

deepest groundwater from the 410m level borehole (786.5 - 881m below surface) is more than 4 x 10^5 years older than the groundwater from the 338m level (338 - 352m) if the closed system evolution model is used [157]. This is much less than the difference in age indicated by the ^{4}He contents (5.2 x 10^6 years), but much more than that indicated by the ^{14}C data.

Samples from the 410m level borehole and the 338m level have been analysed for radiogenic ^{40}Ar. At the 338 - 352m sampling interval, the ^{40}Ar/^{36}Ar ratio is 302.8 and at 786.5-881m, the ratio is 315.6. This compares with a value of 295.5 for air. Such enhanced ratios indicate very high ages for normal release rates of ^{40}Ar. It is not known whether the mining and drilling activities in the area as well as the release of hydrostatic pressure through the flowing wells could induce an enhanced release of such accumulated radiogenic ^{40}Ar (and ^{4}He). A long term monitoring program at the test site should provide an answer. However, the relative ^{40}Ar/^{36}Ar ratios indicate that the deep groundwater (786.5-881m) is very much older than the 338m level groundwater.

7.2.3. Dissolved inert gas contents and recharge temperatures

The dissolved inert gas contents and estimated recharge temperatures of the shallow groundwaters from Stripa are reported in Table 7.3. The Ar and Kr contents are consistent with groundwater recharge occurring between temperatures of 0.5 and 3.6°C. The average recharge temperature is 2.0°C. Such a temperature would result from recharge during the late Autumn, Winter and early Spring months. These are the most likely months for recharge by infiltration of Winter precipitation and Spring melt-waters.

The inert gas contents of the Stripa mine groundwaters are given in Table 7.4. Apart from the strikingly high ^{4}He contents, the Ar and Ne contents are also high and exceed the values resulting from water/air equilibration at temperatures around $0^{o}C$. High Ne contents usually suggest air contamination of the sample during collection. However, when the Ne contents are used to correct for entrained air, the resulting Ar contents still exceed the air equilibration value at $0^{o}C$, but the Kr and Xe contents generally no longer exceed the $0^{o}C$ air equilibration values. (Table 7.7). The Ar contents are not consistent with the Kr and Xe contents. When corrected for air contamination, the Kr and Xe contents indicate that the deep groundwaters recharged at temperatures between 0 and $2^{o}C$. The estimated recharge temperatures of the 338m level groundwaters are slightly higher ($3 - 5^{o}C$). Overall, the deepest groundwaters recharged at similar temperatures to the shallow groundwaters. Recharge at the 330m level occurred at temperatures a few degrees higher. Data from stable isotope determinations confirm that the deepest groundwaters recharged under the coldest climatic conditions. The probable cause is that the deep circulating groundwater recharged during a time of colder climate many thousands of years ago as indicated by the ^{14}C, $^{234}U/^{238}U$ and ^{4}He ages.

A possible explanation for the enhanced Ar contents and for the high uncorrected Ne, Kr and Xe contents is that entrained air dissolves in the groundwaters under increased hydrostatic pressure.

Table 7.7. Estimated recharge temperatures of groundwaters from Stripa mine.

Sample location	Sample depth, m	Estimated recharge temperature, °C		
		from Ar	from Kr	from Xe
R1 borehole, 338m level	323-337	-2.3	1.0	-
		-3.0	0.5	-
M3 borehole, 338m level	338-352 (a)	-3.9	3.5	4.6
		-3.5	4.6	4.9
		-4.2	3.5	5.6
	(b)	-	-	-
		-3.7	-9.4	-
R9 borehole, 338m level	338-368	-	-	-
471m borehole, 410m level	419-446	-10.0	-5.1	0.0
		-7.7	0.0	1.8
	742-769.4	-7.0	1.0	3.2
		-	-	-
	786.5-881	-14.0	0.2	1.0
		-13.9	0.2	3.2
		-15.6	-5.9	1.7
	811-838.4	-10.4	1.7	-1.0
		-12.7	-	-

NB. Recharge temperatures are corrected to a Ne temperature of 0°C - Ne = 2.30×10^{-7} cm^3 STP cm^{-3} H_2O

Both Ne and Ar increase with depth (Figure 7.3) and with He content (Figures 7.4 and 7.5). This supports the view that the enhancement of Ar and Ne is caused by increased hydrostatic pressure causing entrained air in the granite system to enter solution. However, the proportion of Ne and Ar in the trapped air should be the same as that found in the atmosphere and the Ne corrected Ar content should yield similar recharge temperatures to those from the Kr content. That the corrected Ar temperatures are less than $0^{o}C$ is at present not explained.

7.3. CONCLUSIONS

The high ^{222}Rn contents of groundwaters from Stripa have been explained in terms of the ratio of the volume of water in the granite system to the volume of rock, together with relatively high U concentrations and fractional release of ^{222}Rn generated. High ^{226}Ra contents could result from a recoil controlled mechanism leading to a constant ^{226}Ra concentration in groundwaters older than 8000 years for a uniform ^{238}U distribution. In the M3 borehole a change in the ^{226}Ra content and temperature of the groundwater has been attributed to a perturbation of the groundwater system at the 338m level.

Groundwater ages have been calculated from the radiogenic ^{4}He contents of the waters. The ages indicated are up to a few million years for the deepest source. This is generally much older than the maximum ^{14}C and U isotope ages but in broad agreement with a qualitative assessment of the radiogenic ^{40}Ar contents.

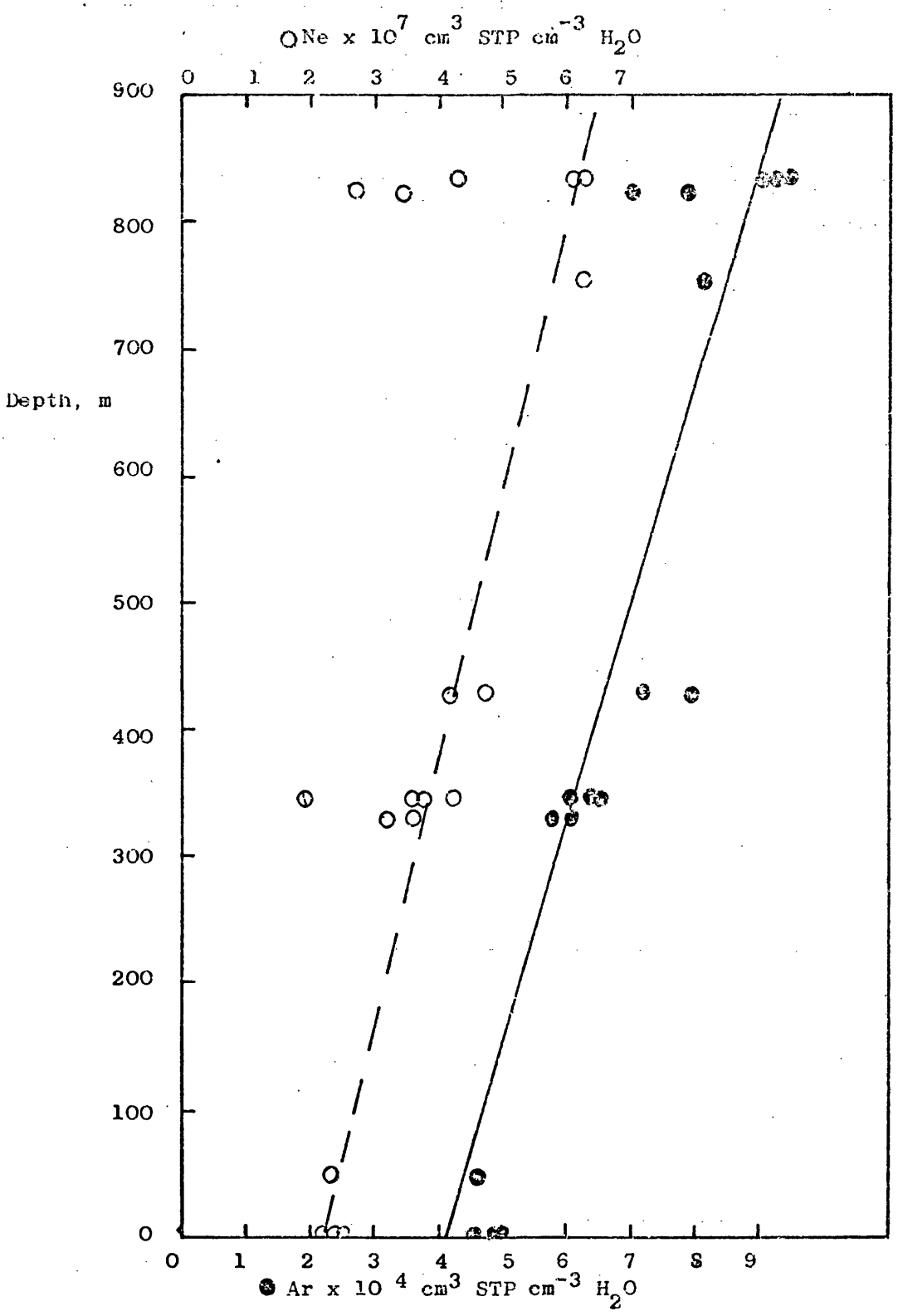

Fig. 7.3. Plot of Ne and Ar contents against sample depth for groundwaters from Stripa mine.

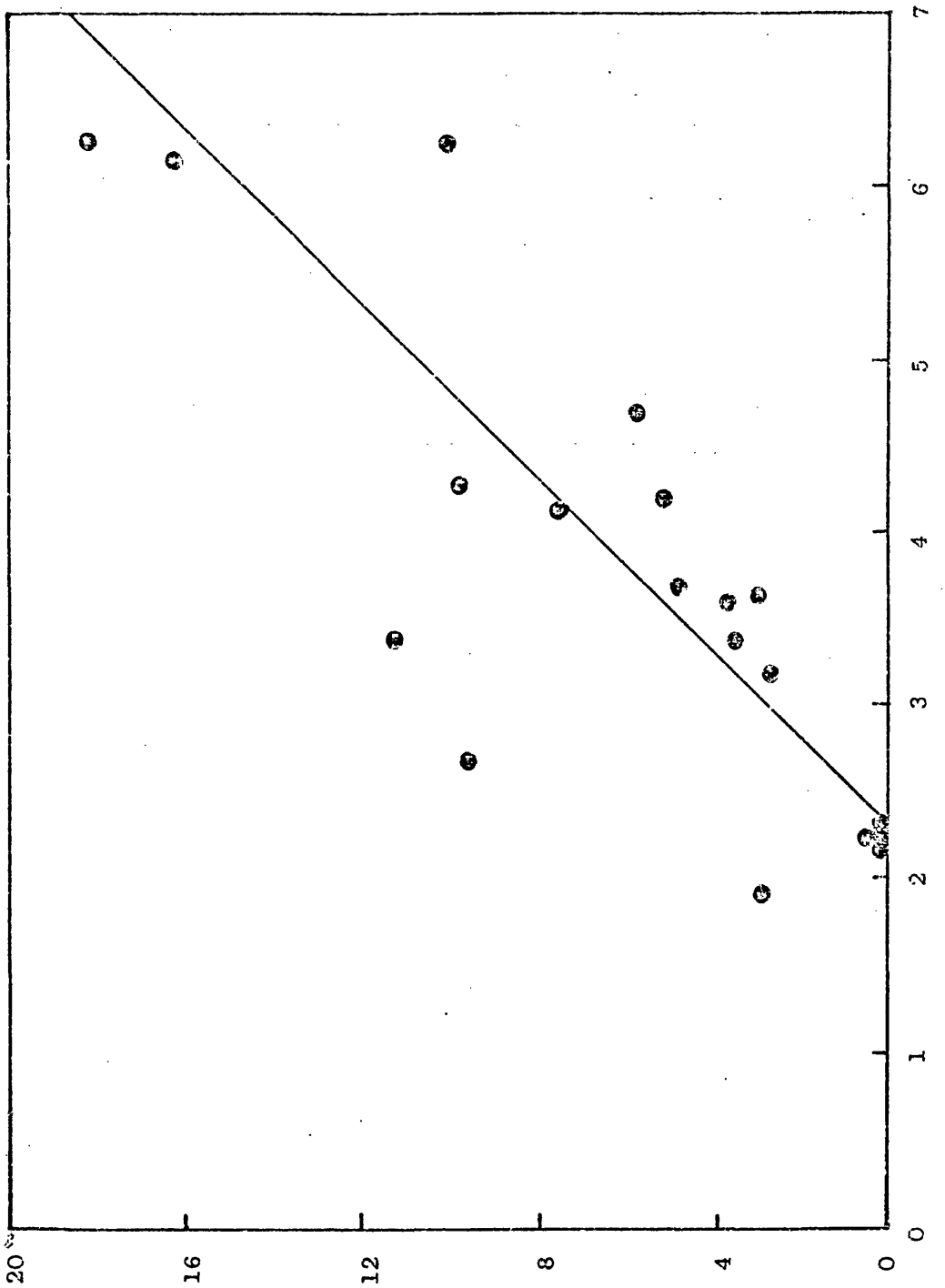

Fig. 7.4. Plot of ^{4}He against Ne contents of groundwaters from Stripa mine.

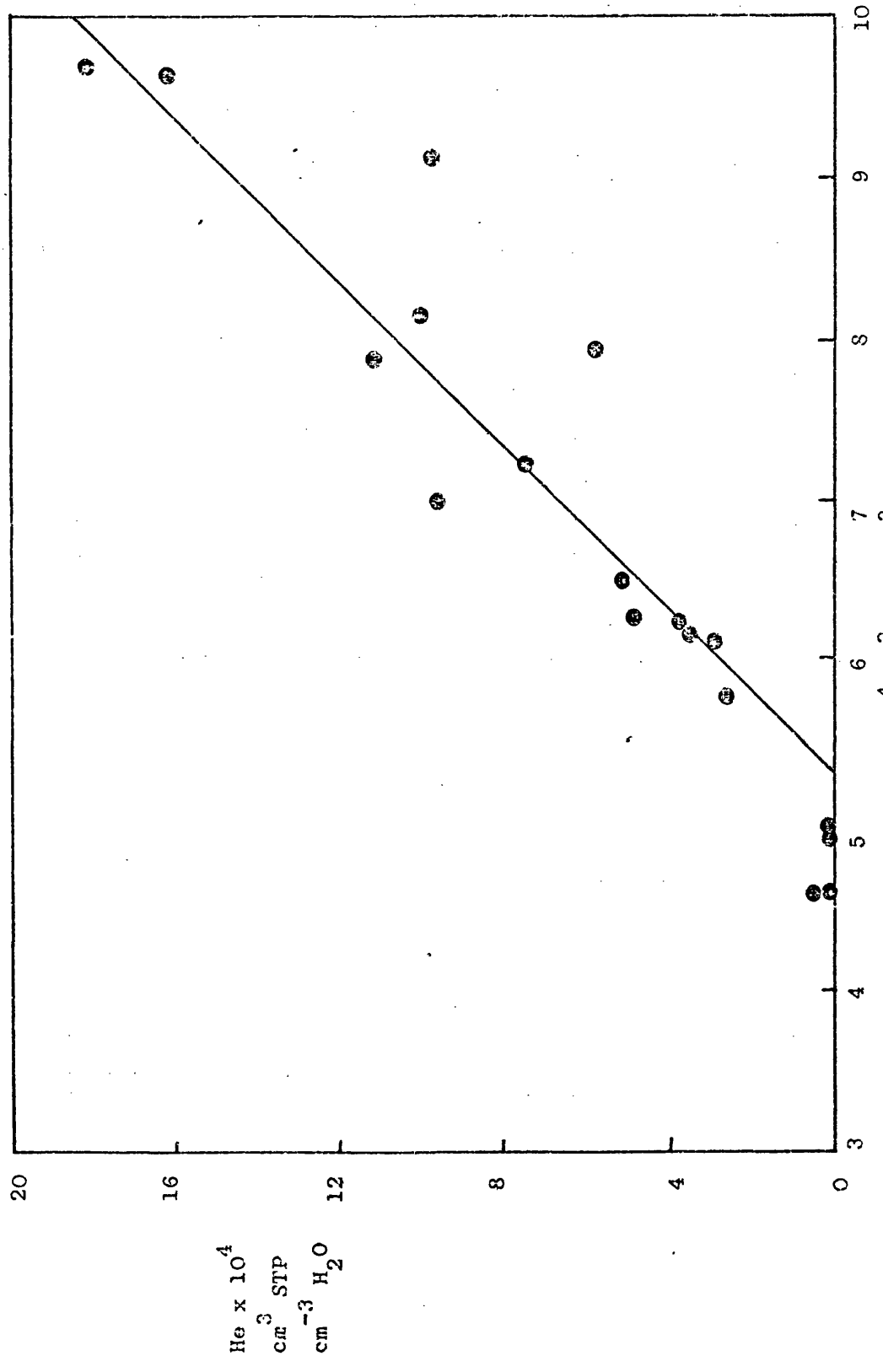

Fig. 7.5. Plot of ^4He against Ar contents of groundwaters from Stripa mine.

The non-radiogenic inert gas contents have been used to estimate the temperatures at which the various groundwaters were recharged. Ar and Kr contents indicate that the surface waters were recharged at 2°C whereas Ar contents of the deep groundwaters indicate negative recharge temperatures. In this case, Kr and Xe contents have been used to calculate recharge temperatures which are 3 - 5°C for the intermediate level groundwaters and 2°C for the deep waters. Recharge during different periods of climatic history has been proposed as the explanation for these values. No explanation has been found for the negative recharge temperatures indicated by the high Ar contents.

CHAPTER 8

DISSOLVED INERT GASES IN GROUNDWATER AND GAS SAMPLES FROM ICELAND.

8.1. INTRODUCTION

Iceland is almost exclusively built up of volcanic rocks, mainly floor basalts with subordinate andesitic and rhyolitic rocks and minor intrusions of gabbro and granophyre. The oldest rocks exposed are basaltic lava flows of Tertiary age. These tertiary rocks are confined to two areas: (a) W. Iceland, the N.W. Peninsula and the Middle N. Iceland and (b) E. and S.E. Iceland (Figure 8.1). The Tertiary rocks are separated by a zone of younger volcanics of Quarternary and Recent age, mainly basaltic tuffs, palagonite breccias, lava flows and pillow lavas.[158]

The thermal areas of Iceland have been identified as high temperature areas and low temperature areas although no well defined limits exist between the two areas. Bodvarsson[159] distinguished these areas by base temperatures. The concept of base temperature is derived from a hydrothermal model where all the thermal water is considered to be of meteoric origin and that it becomes heated by contact with hot rock. The highest temperature reached by the water during its deep circulation is defined as its base temperature. Present data suggest that subsurface temperatures exceed 200°C at depths of less than 1000m in high temperature areas but are generally less than 150°C at similar depths in low temperature areas.[158]

The high temperature areas are characterised by large regions of hot ground, fumaroles, mud-pools and sometimes solfataras. Near the surface the rocks are intensely altered. Water issued at the surface is in most cases negligible. The low temperature areas are characterised by hot water springs often with high flow rates and surface temperatures ranging from 15° - 100°C. Hydrothermal alteration around the springs is as a rule insignificant.

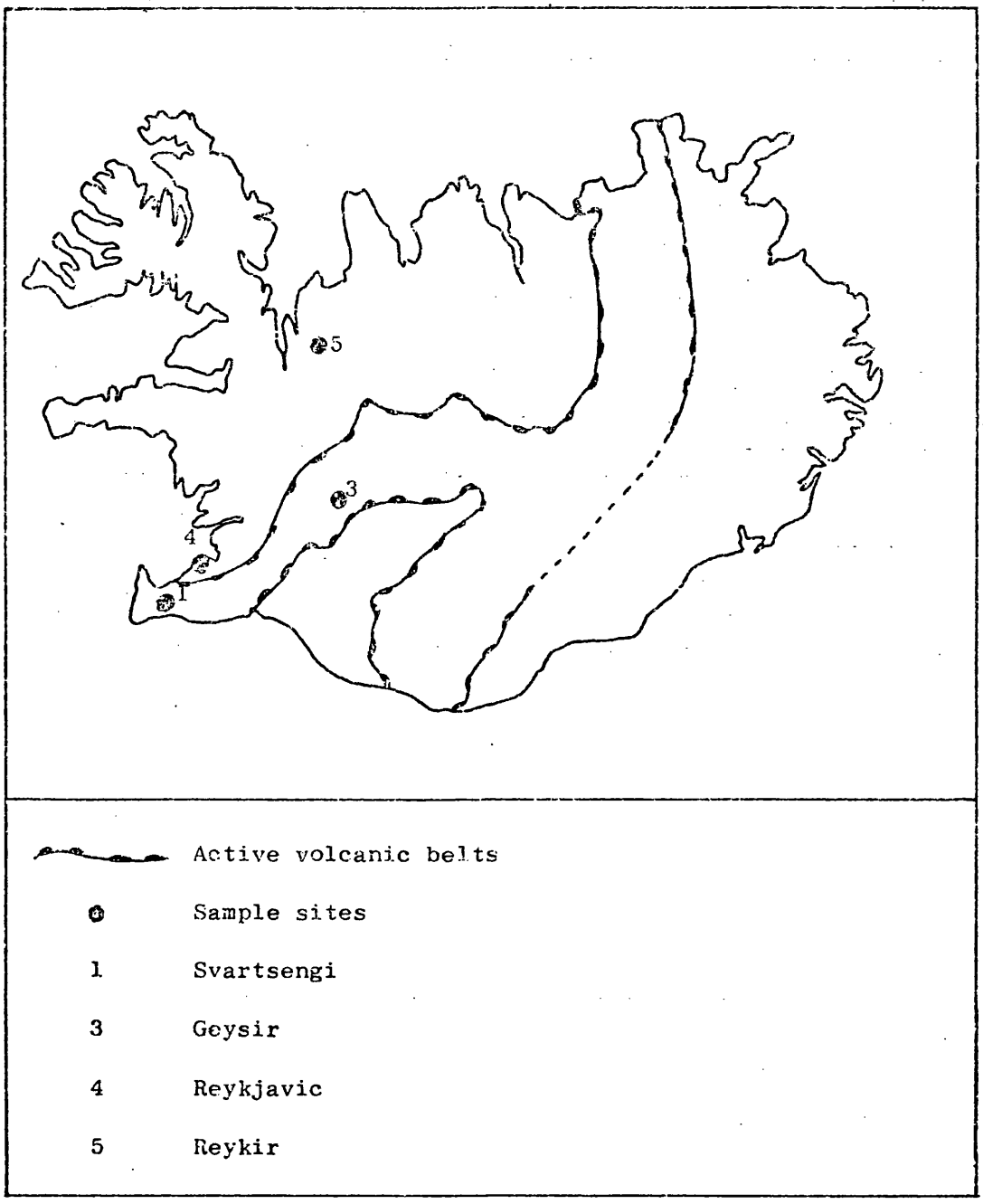

Fig. 8.1. Location of sampling sites and active volcanic belts, Iceland.

The chemical composition of the thermal waters in Iceland is characterised by the low total dissolved solids in comparison with thermal waters in other parts of the world. Waters from the low temperature areas are lower in total dissolved solids than those from the high temperature areas [158]. The hot spring water in the low temperature areas and the deep water tapped from drill holes in both low and high temperature areas are usually alkaline. Acid sulphate springs and occasional carbonate springs are more typical in the high temperature areas. Evidence from deuterium analysis suggests that the water in the sulphate and carbonate springs is of local meteoric origin.

Drilling in recent years for thermal water in low temperature areas and outside thermal areas has revealed hot water of the connate type scarcely known in surface springs. This water is higher in total dissolved solids, in particular Cl^- and Ca^{2+}. It is often connected with marine sediments. All the drill holes are situated close to present sea level so percolation of sea water into the hydrothermal system cannot be excluded. Gas analyses show that CO_2, H_2S and H_2 are the dominant gases in the high temperature areas. Whereas N_2 is dominant in the low temperature areas.

The hot springs have been used to provide geothermal energy, which is one of the most valuable natural resources in Iceland. Most of it is used for domestic heating purposes although it is also used for heating greenhouses and in industries which require low grade heat supplies.

The dissolved inert gas contents of some groundwaters and gases from Iceland have been determined. For groundwaters, these have been interpreted in terms of the meteoric origin of the water and the temperature at which the water/air equilibration took place. High ^{4}He contents have been explained by the presence of radiogenic ^{4}He and similarly, the presence of radiogenic ^{40}Ar causes the ratio $^{40}Ar/^{36}Ar$ to be enhanced in some of the samples.

8.2. RESULTS AND DISCUSSION

8.2.1. Radiogenic ^{4}He contents

The ^{4}He contents of two gas samples from Iceland are given in Table 8.1. Also shown are the volumes of the other inert gases and the inert gas volumes relative to the argon content. From the figures for the ^{4}He contents and the $^{4}He/Ar$ ratios , it is evident that a significant component of radiogenic ^{4}He is present in the gas samples from Svartsengi and Hveragerdi. This is particularly evident if the ^{4}He contents of the gas samples are compared with the ^{4}He contents of the same volume of air (Table 8.1). The Ne, Ar, Kr and Xe contents are generally less than in the equivalent volume of air but the ^{4}He contents are 5 to 10 times greater than in the same volume of air.

The ^{4}He contents of the water samples are given in Table 8.2. There is evidence for a slight enhancement of the ^{4}He contents relative to air equilibrated water, but this is not as marked as in the gases. The $^{4}He/Ar$ ratios are presented in Table 8.3., togetner with the ratios expected for air and air equilibrated water at $10^{o}C$. The $^{4}He/Ar$ ratios

Table 8.1. Inert gas contents of gas samples from the Icelandic Basalts.

Location	Inert gas content, cm^3 STP cm^{-3} gas				
	He x 10^8	Ne x 10^7	Ar x 10^4	Kr x 10^7	Xe x 10^8
ABSOLUTE VOLUMES					
Svartsengi	6050±810	4.54±0.22	4.12±0.15	0.71	0.88
Hveragerdi	2800±380	19.1±0.9	25.2±0.9	5.52	6.81
Air, 1 atm. total pressure	586	203	85.0	10.5	6.44
VOLUMES WITH RESPECT TO ARGON CONTENT					
	He/Ar	Ne/Ar	Ar/Ar	Kr/Ar	Xe/Ar
Svartsengi	1.47×10^{-2}	1.10×10^{-3}	1	1.72×10^{-4}	2.14×10^{-5}
Hveragerdi	1.11×10^{-2}	0.76×10^{-3}	1	2.19×10^{-4}	2.70×10^{-5}
Air	5.56×10^{-4}	1.95×10^{-3}	1	1.22×10^{-4}	9.21×10^{-6}
Air saturated water at 10°C	1.19×10^{-4}	5.23×10^{-4}	1	2.16×10^{-4}	3.02×10^{-5}

Table 8.2. Inert gas contents, derived recharge temperatures and collection temperatures of groundwaters from the Icelandic Basalts.

Location	Inert gas content, cm^3 STP cm^{-3} H_2O					Recharge temperature °C		Collection temp. °C
	He x 10^8	Ne x 10^7	Ar x 10^4	Kr x 10^7	Xe x 10^8	from Ar	from Kr	
Hveragerdi condensate	17.6±2.4	0.96±0.05	0.66±0.02	0.17±0.00	0.34±0.02	-	-	200
Geyser	5.3±0.7	0.78±0.04	0.71±0.03	0.15±0.00	0.07±0.00	-	-	100
Reykjavic No. 10	11.1±1.5	0.73±0.04	1.09±0.04	0.30±0.01	0.52±0.03	-	-	142
Reykjavic No. 17	6.2±0.8	1.19±0.06	0.77±0.03	0.17±0.00	0.29±0.02	-	-	135
Reykir No. 21	27.6±3.7	2.01±0.10	3.63±0.13	0.86±0.02	1.17±0.06	14.4±1.5	10.2±1.0	88.5
Reykir No. 17	15.5±2.1	1.85±0.09	3.71±0.13	0.88±0.02	1.21±0.06	13.3±1.5	9.2±0.8	75
Reykir No. 5	13.9±1.9	1.94±0.09	3.16±0.11	0.74±0.02	1.02±0.05	22.0±1.5	16.8±1.1	82

Table 8.3. Inert gas contents relative to Ar contents of groundwaters from the Icelandic Basalts.

Location	Inert gas contents relative to Ar			
	He/Ar	Ne/Ar	Kr/Ar	Xe/Ar
Hveragerdi condensate	2.68×10^{-3}	1.46×10^{-3}	2.65×10^{-4}	5.15×10^{-5}
Geyser	7.51×10^{-4}	1.11×10^{-3}	2.09×10^{-4}	1.07×10^{-5}
Reykjavic No. 10	1.02×10^{-3}	6.67×10^{-4}	2.72×10^{-4}	4.76×10^{-5}
Reykjavic No. 17	8.04×10^{-4}	1.55×10^{-3}	2.16×10^{-4}	3.79×10^{-5}
Reykir No. 21	7.60×10^{-4}	5.54×10^{-4}	2.36×10^{-4}	3.22×10^{-5}
Reykir No. 17	4.18×10^{-4}	4.99×10^{-4}	2.38×10^{-4}	3.26×10^{-5}
Reykir No. 5	4.53×10^{-4}	7.46×10^{-4}	2.22×10^{-4}	3.00×10^{-5}
Air	5.56×10^{-4}	1.95×10^{-3}	1.22×10^{-4}	9.21×10^{-6}
Air/water $10^{\circ}C$	1.19×10^{-4}	5.23×10^{-4}	2.16×10^{-4}	3.02×10^{-5}

of the water samples are generally much higher than the ratio for air saturated water at 10°C and in most cases higher than the ratio for air. These $^4He/Ar$ ratios are shown diagramatically in Figure 8.2. Two of the groundwaters have $^4He/Ar$ ratios which lie between the values for air and air saturated water at 10°C. Enhancement of the ratio for these waters compared with air equilibrated water may be due to the presence of radiogenic ^4He or may result from the presence of ^4He from an air phase mixed with a water phase. The ^4He content of the other groundwater samples cannot be explained by phase mixing alone, and must be due to the presence of significant amounts of radiogenic ^4He. The fact that mixing of an air phase with a water phase occurs in the Icelandic groundwaters is evident from the Ne/Ar ratio shown in Figure 8.2., and is discussed in paragraph 8.2.2.

8.2.2. Ne, Ar, Kr and Xe contents and some derived recharge temperatures

The inert gas contents of the gas samples from Iceland are reported in Table 8.1. together with the gas contents relative to Ar. As discussed in paragraph 8.2.1. the Ne, Ar, Kr and Xe contents (except for the Xe content of Hveragerdi) are less than would be found in the same volume of air whereas the ^4He contents are enhanced by the presence of radiogenic ^4He. The ratios of the inert gas contents relative to Ar are shown in Figure 8.2. These plot between values for air saturated water at 10°C and air and suggest that the Ne, Ar, Kr and Xe in the gas samples are derived from a mixture of those from air and air equilibrated water.

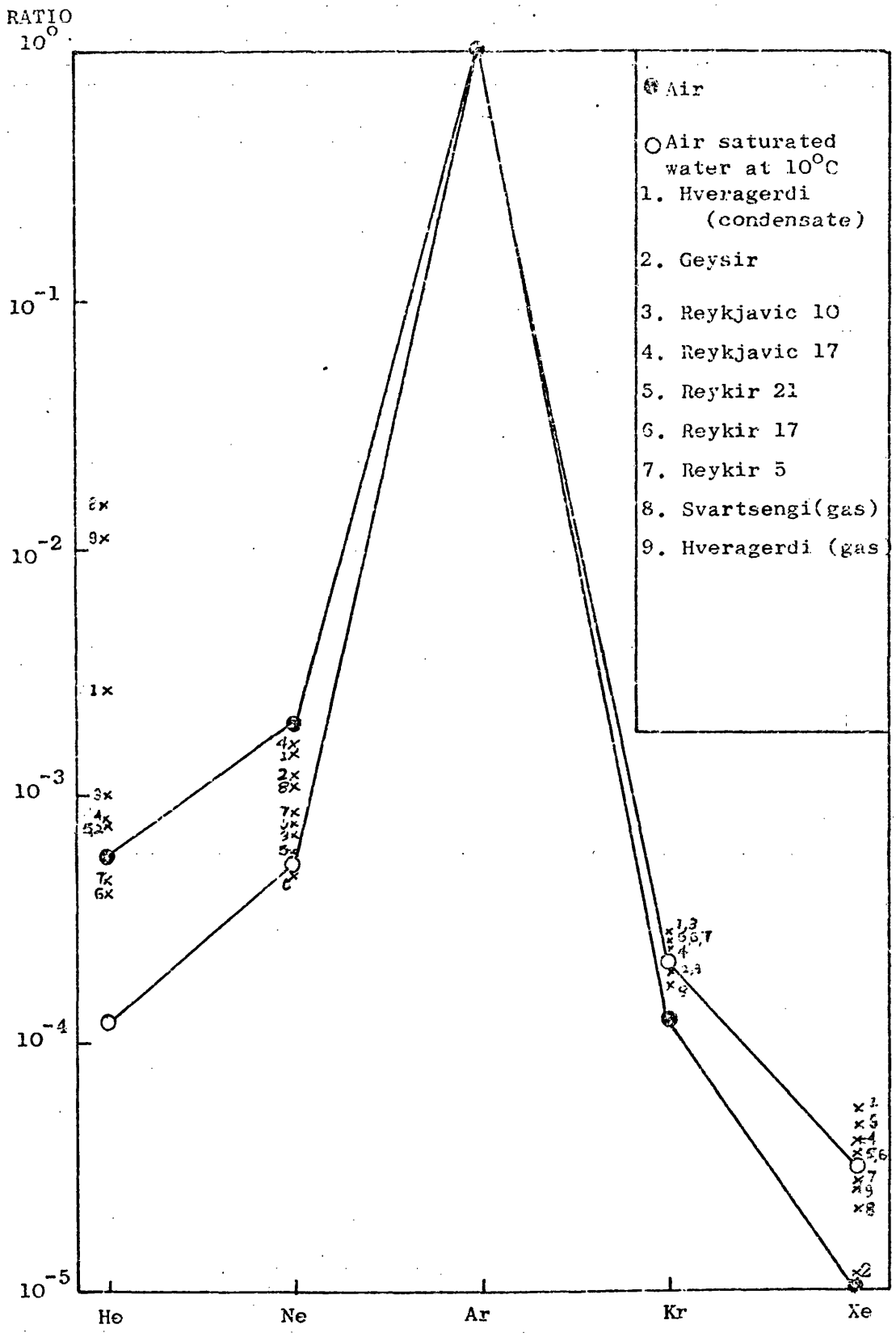

Fig. 8.2. Inert gas contents relative to Ar contents of gas and water samples from Iceland.

The inert gas contents of the water samples from Iceland are given in Table 8.2. together with some estimated recharge temperatures where applicable. Table 8.3. presents the values of the ratios of the inert gas contents to the Ar contents. These ratios are plotted in Figure 8.2., together with the ratios for air, air saturated water at 10°C and the gas samples. Generally, the Ne/Ar ratio lies between the ratio for air and air saturated water indicating that the inert gas contents are derived from the mixing of an air phase and a water phase. The exception is Reykir No. 17 in which the Ne/Ar ratio is slightly less than the ratio for air equilibrated water.

The Kr/Ar and Xe/Ar ratios also lie close to the values for air saturated water at 10°C. Deviation of these ratios from the air saturated water ratios can be explained by equilibration with air at higher temperatures. Estimated recharge temperatures of some of the waters indicate recharge temperatures above 10°C (Table 8.2).

The general pattern for the gases, Ne, Ar, Kr and Xe suggests an atmospheric origin. Let us assume a model of a groundwater initially equilibrated with air which is then partially outgassed. If the outgassing were complete, the inert gas content of the groundwater would be reduced to zero and the inert gas ratios of the exsolved gases would represent the saturation curve for the appropriate air equilibration temperature. Partial outgassing in a single stage would produce products which would lie between the curves for air

and air saturated water. Partial outgassing in several stages could produce significant fractionation, the degree of fractionation depending on the detailed history of the gas and water phases. In Iceland, the groundwater samples were derived by condensation of a high temperature gas/water phase. The groundwaters produced have inert gas contents which are representative of the mixed phase. Their inert gas contents may be explained in terms of partial outgassing as may the gas samples.

Mazor and Wasserburg [160] considered fractional distillation of the inert gases by a Rayleigh process and showed that the following relationships hold for all co-existing rare gas components of atmospheric origin:-

$$\frac{1}{K_{Ar}(T)} \ln(C_{Ar}^{1}/C_{Ar}^{1o}) = \frac{1}{K_{Ne}(T)} \ln(C_{Ne}^{1}/C_{Ne}^{1o}) = \frac{1}{K_{Kr}(T)} \ln(C_{Kr}^{1}/C_{Kr}^{1o})$$

$$= \frac{1}{K_{Xe}(T)} \ln(C_{Xe}^{1}/C_{Xe}^{1o})$$

where C_j^1 is the concentration of species j in the liquid, C_j^{1o} is the original concentration when the liquid was in equilibrium with air, and $K_j(T)$ is the Henry's Law constant at the temperature at which distillation proceeds and is equal to the ratio of the concentrations between the gas and liquid phases.

The preceding equations show that pairs of functions $1/(K_j)$ ln (C_j^1/C_j^{1o}) will plot on a straight line of slope 1. Therefore all gases of atmospheric origin which have evolved by a process such as Rayleigh distillation may be interrelated, regardless of their degree of fractionation. If the temperatures of original equilibration and of distillation can be estimated, it is possible to compare inert gases from different areas. Because of the possible fractionation which may occur after some distillation, the direct ratios of the inert gas components in the gas phase may not be so easily interpreted.

8.2.3. $^{40}Ar/^{36}Ar$ ratios

The $^{40}Ar/^{36}Ar$ ratios are reported in Table 8.4. In most cases, the ratio is close to that in air. The exception is the gas sample from Svartsengi which has a $^{40}Ar/^{36}Ar$ ratio of 327.5, indicating that a significant component of radiogenic ^{40}Ar from the radioactive decay of ^{40}K is present. The Svartsengi gas sample has already been shown to contain a high proportion of radiogenic ^4He indicating a relatively high age. The quartz equilibrium temperature of the groundwater from Svartsengi is 237°C [161]. The long residence time and high equilibration temperature will lead to an efficient release of ^{40}Ar from its site of production in ^{40}K bearing minerals.

It is somewhat surprising that the gas sample from Hveragerdi does not have an enhanced $^{40}Ar/^{36}Ar$ ratio. This sample has a high proportion of radiogenic ^4He and the groundwater from the spring has a high quartz equilibration temperature of 199°C. [162] However, the chemical composition of the Hveragerdi groundwater is very different

Table 8.4. $^{40}Ar/^{36}Ar$ ratios of gas and water samples from Iceland.

Sample	$^{40}Ar/^{36}Ar$
Svartsengi (gas)	322.9
	332.1
Hveragerdi (gas)	295.1
Geysir	296.3
Reykjavic No. 10	292.0
Reykir No. 21	294.1
Reykir No. 17	293.7
Reykir No. 5	299.8
Air	295.5
Air saturated water	295.5

from that of Svartsengi [162]. Hveragerdi groundwater is low in total dissolved solids whereas Svartsengi groundwater is a sodium chloride type brine which is high in total dissolved solids. The $^{40}Ar/^{36}Ar$ enhancement must be a result of special conditions prevailing in the locality of the area from which the Svartsengi (gas) sample was derived.

The origin of the thermal water has been investigated by Arnason [163]. His conclusions based on deuterium and ^{18}O data were that the thermal water is of meteoric origin and it is derived from precipitation deposited in the mountainous interior of the country. It descends to a great depth, whereby becoming heated as a result of the geothermal gradient. From there it flows towards the lower parts of the country, forced by hydrostatic pressure, until it finally escapes through fissures and faults in the rocks of the lowland or at the bottom of the ocean. The gas samples investigated must be derived from the thermal water. The radiogenic ^{4}He and ^{40}Ar become dissolved in the thermal water at depth. When this water outgasses, the gas produced becomes enriched in ^{4}He and ^{40}Ar. Hence the groundwater quartz equilibration temperatures may be used as an indication of the temperature at which the gas samples were derived.

8.3. CONCLUSIONS

The high radiogenic ^{4}He contents of the gas samples from Iceland have been interpreted in terms of the high age of the thermal waters from which the gases are derived. The water samples, which were derived from areas lower in thermal activity showed some evidence for the presence of radiogenic ^{4}He, but at a reduced level compared with the gas samples.

The Ne, Ar, Kr and Xe contents of the gas and water samples have been explained in terms of a Rayleigh distillation process. The water samples from Hvergerdi, Geysir and Reykjavic are undersaturated in these gases relative to air equilibrated water at $10^{o}C$, whereas groundwaters from Reykir contain amounts of these gases close to those expected for air saturated water at $10^{o}C$.

The $^{40}Ar/^{36}Ar$ ratio has been shown to be close to the value in air, 295.5, with the exception of the Svartsengi gas sample. Enhancement of the $^{40}Ar/^{36}Ar$ ratio by radiogenic ^{40}Ar depends on the detailed thermal, chemical and geochemical history of the groundwater/exsolved gas system.

CHAPTER 9

RADON RELEASE FROM ROCKS.

9.1. INTRODUCTION

The loss of ^{222}Rn from uranium minerals was first noted at the beginning of this century in connection with studies of the uranium and thorium decay series. Boltwood [164] obtained values of leakage ranging from 0.7% to 26% of the ^{222}Rn generated in a wide variety of uranium minerals. Lind and Whittemore [165], investigating the radium:uranium ratio in carnotites found that 16 - 50% of the ^{222}Rn generated was released. Føyn [166] found that the percentage release of radon increased with decreasing particle size. More recently, Barretto [167] investigated the activity, release rate and percentage of ^{222}Rn escape for a variety of rocks and minerals. He found a wide range of leakage values ranging from 1 - 20% with the higher release rates being observed for granitic rocks and conglomerates, whereas basic and calcareous rocks showed the lowest values. Accessory minerals, although rich in uranium, showed a very low ^{222}Rn release of less than 1 - 2%. A lack of dependence of ^{222}Rn release on uranium concentrations was shown [167] but a correlation between ^{222}Rn release and weathering was observed.

Equilibrium between ^{238}U and ^{226}Ra, the parent of ^{222}Rn, in a uranium bearing mineral will be established according to the radioactive decay law. Provided that there is no geochemical separation of radium from its parent uranium in the mineral phase, 99% of the equilibrium ^{226}Ra activity will be established in 10,760 years [13]. ^{226}Ra has been assumed to be in radioactive equilibrium with ^{238}U in the samples for which the ^{222}Rn release has been determined. Andrews

and Wood [13] found that this was the case for the Hinton Sand, Midford Sand, Carboniferous Limestone and Old Red Sandstone in Avon. Hence, the ^{226}Ra activity is equal to the ^{238}U activity (in pCi Kg^{-1}) determined by delayed neutron activation analysis. This method was chosen because it was necessary to analyse a large number of samples.

The dependence of ^{222}Rn release on particle size was investigated by determining the amount of ^{222}Rn released into water from rock particles of different sizes by the method described in Chapter 2. The percentage release of ^{222}Rn generated was calculated from the measured ^{238}U content of each particle size. Samples from the Inferior Oolite, Bunter Sandstone, Pennant Sandstone, Cornubian Granite and Swedish Granite were investigated by this method. By comparing the percentage ^{222}Rn release obtained from laboratory experiments, with ^{222}Rn contents of groundwaters it has been possible to discuss the mechanism of ^{222}Rn release into groundwaters from a variety of aquifer types.

9.2. RADON DIFFUSION

^{222}Rn release occurs not only from the porous media of soils and ordinary rocks, but there is also a significant diffusion of ^{222}Rn from the production sites within crystal lattices to the grain surfaces [167]. Rocks show a wide range of ^{222}Rn loss, with granitic rocks contributing more to ^{222}Rn release to the atmosphere than basic and calcareous rocks. The fractional ^{222}Rn release from rocks does

not depend on the parent uranium concentration (Table 9.12). For minerals, xenotime and monazite with high uranium concentrations have a much smaller ^{222}Rn release than apatite or biotite, both with much lower uranium concentrations [167]. It thus appears that the fractional ^{222}Rn release depends partly on the crystal structure. Minerals with severe radiation damage will release a high proportion of their ^{222}Rn whereas minerals with little radiation damage will show a small ^{222}Rn loss. In those minerals with little radiation damage, ^{222}Rn loss is mainly by diffusion through the grain surface and mechanical defects, micro-fissures and dislocations.

The fractional release of ^{222}Rn therefore depends on the total surface area, the temperature, and the nature of the aggregate of mineral grains. For a simple case of isolated, homogeneous, fissure-free grains of spherical shape, the emission is a sum of the contributions of recoil and diffusion in the solid phase. The diffusion coefficient, D, is less than 10^{-22} cm^2 s^{-1} at room temperature, so recoil is a major contributor. The fraction of ^{222}Rn atoms emitted due to recoil, F_r is given by [168]:

$$F_r = \frac{3}{4}\frac{R}{r_o} - \frac{1}{16}\left[\frac{R}{r_o}\right]^3 \qquad \text{for } 2r_o \geq R \qquad 9.1$$

where R = recoil range in the solid

r_o = radius of solid grain.

If $2r_o < R$, every ^{222}Rn atom formed will escape by recoil. R is of the order of 10^{-6} cm (10^{-2} μm) for most minerals. In reality, rocks are composed of a highly irregular aggregate of microcrystals. The

total surface area is high, but the internal fissures are narrow and a certain fraction of the ^{222}Rn atoms ejected into the internal volume decay in the fissures before escaping to the exterior of the mineral. Under these conditions, the observed ^{222}Rn leakage from the mineral as a whole is less than the total ^{222}Rn produced, but it will, however, be proportional to the surface area.

The rate of radon leakage from a mineral increases somewhere between $T^{3/2}$ and T^{2} [168], where T is the temperature difference, ^{o}C. This suggests that the rate determining step is that of gaseous diffusion [169] since the rate of escape from the solid by recoil is essentially temperature independent which at temperatures below the annealing temperature is negligible. However, the diffusion coefficient of radon in air is not negligible ($D = 0.12\ cm^{2}\ s^{-1}$ [168]). Hence the diffusion is essentially immediate once the ^{222}Rn has reached the external volume.

For a given mineral, the uranium concentration, surface area, cross sectional area, internal volume and temperature determine the partial pressure of ^{222}Rn in the internal volume. Since the partial pressure of ^{222}Rn in the external volume is always essentially zero, the effective rate of ^{222}Rn loss from the geometrical surface of the mineral is determined only by the partial pressure of ^{222}Rn in the interior, the temperature and the cross sectional area available to leakage. All three factors will influence the rate of diffusion.

9.3. HYDROLOGIC TRANSPORT OF RADON THROUGH FRACTURED AND POROUS ROCKS

The amount of ^{222}Rn contained in a groundwater depends on the rate of ^{222}Rn release from a unit volume of rock, the volumetric relation between the rock and groundwater, and the time spent by the groundwater in the rock. Stoker and Kruger [12] developed the theoretical basis by which the physical transport can be described.

They assumed (a) a homogeneous, isotropic, porous media, (b) uniformly distributed ^{226}Ra, i.e. homogeneous ^{222}Rn release, (c) steady-state flow conditions, (d) incompressible fluid, and (e) loss of ^{222}Rn from the fluid only by radioactive decay. Their expression for the activity concentration of the ^{222}Rn in the fluid from a linear flow model is given by:

$$C = \frac{E}{\emptyset}\left[1 - e^{\frac{(-\lambda A \emptyset_1 L_1)}{Q}}\right] \qquad 9.2$$

where C = activity concentration of radon in fluid, pCi cm^{-3}

E = the production rate of radon atoms, pCi cm^{-3} radium

$\emptyset_1$ = the fractional porosity of the rock.

λ = the decay constant for radon, s^{-1}

A = the cross sectional area, cm^2

Q = the fluid flow rate, $cm^3\ s^{-1}$

L_1 = length of radium bearing rock, cm

If the fluid flows out through a non-radium bearing rock of length L_2, and porosity $\emptyset_2$, an additional decay factor for transport time through length L_2 is required.

$$C = \frac{E}{\emptyset_1}\left[-e^{\frac{(-\lambda A\emptyset_1 L_1)}{Q}}\right].e^{\frac{(-\lambda A\emptyset_2 L_2)}{Q}} \qquad 9.3$$

Equation 9.3 shows that the maximum concentration of ^{222}Rn approaches $E/\emptyset_1$ when the residence time, $(A\emptyset L/Q)$ in the ^{226}Ra bearing rock is long compared with that in the non-^{226}Ra bearing rock. C should be exponentially dependent on flow rate. For example if there is a significant length of non-radium bearing rock, the decay term would be reduced by an increased flow rate. If the length of the radium bearing rock is relatively short and there is no significant interval for decay, then the concentration would be expected to decrease with increasing flow rate. Or, if the radium bearing rock extends for large distances and there is no significant decay interval, then the concentration would be independent of flow rate.

The result for a radial flow model is qualitatively similar to the linear flow model:

$$C = \frac{E}{\emptyset}\left[1 - e^{-\left[\frac{\lambda \emptyset \pi h}{Q}(r_e^2 - r_w^2)\right]}\right] \qquad 9.4$$

where r_e = effective radius of influence

r_w = radius of non-radium bearing rock

h = rock thickness.

r_e will be related to the permeability of the medium and therefore to the difference in piezometric head required to maintain a given flow rate, Q. For typical values of r_e (300m), a formation thickness of 50m and a porosity of 0.2, the flow rate would have to be in excess

of 400 m^3 hr^{-1} to make the exponential term larger than 0.1. Thus, for relatively low flow rates in a large reservoir, the concentration of radon would be effectively independent of flow rate.

9.4. RADON RELEASE FROM THE INFERIOR OOLITE, BUNTER SANDSTONE AND PENNANT SANDSTONE.

Results for the Inferior Oolite, Bunter Sandstone and Pennant Sandstone are given in Tables 9.1-9.3. The results are represented graphically in Figure 9.1 in which $\log_{10}(Rn)$ is plotted against $\log_{10} d$, where (Rn) is the percentage release of ^{222}Rn generated and d is the average particle diameter. The relationship between ^{222}Rn release and particle size may be written

$$(Rn) = C_1 d^n \qquad 9.5$$

where C_1 and n are constants.
This may be rewritten as

$$\log(Rn) = n \log d + \log C_1$$
$$= n \log d + C_2 \qquad 9.6$$

where C_2 is a constant.
Therefore, by plotting log (Rn) against log d, the value of n can be determined.

If the mechanism of ^{222}Rn release is diffusion through the crystal lattice to the particle-water interface, the amount of ^{222}Rn released should depend on the specific surface area of the particles. This is also true for any contribution by the direct recoil process. The specific surface area is dependent on the particle size and is proportional to $^1/d$. Therefore if the dominant mechanism of ^{222}Rn release is by these processes, n will take the value -1.

Table 9.1 Variation of radon release with particle size for Inferior Oolite, Colmans Quarry, Frome, Somerset.

Sieve size, μm	Average particle diameter, μm	Uranium content $\mu g\ g^{-1}$ rock	Uranium content pCi Kg^{-1} rock	Radon released pCi Kg^{-1} rock	% release of radon generated
2360 - 850	1606	2.64 ± 0.17	874	25.5 ± 1.7	2.9 ± 0.4
850 - 600	726	2.55 ± 0.16	844	25.5 ± 1.7	3.0 ± 0.4
600 - 425	512	2.68 ± 0.18	887	46.3 ± 3.7	5.2 ± 0.8
425 - 300	363	2.88 ± 0.18	953	30.7 ± 2.9	3.2 ± 0.5
300 - 212	256	2.79 ± 0.16	923	30.2 ± 2.1	3.3 ± 0.4
212 - 150	181	2.86 ± 0.17	947	48.1 ± 3.3	5.1 ± 0.6
150 - 106	128	2.89 ± 0.20	957	37.0 ± 2.7	3.9 ± 0.6
106 - 75	91	3.00 ± 0.17	993	62.1 ± 4.2	6.3 ± 0.8
75 - 53	64	3.01 ± 0.24	996	70.7 ± 6.2	7.1 ± 1.2
< 53	26	3.44 ± 0.20	1140	74.3 ± 5.7	6.5 ± 0.9

Table 9.2 Variation of radon release with particle size for Bunter Sandstone, Winterbourne Kingston borehole, Dorset (SY850 975)

Sieve size, μm	Average particle diameter, μm	Uranium content μg g^{-1} rock	Uranium content, pCi Kg^{-1} rock	Radon released pCi Kg^{-1} rock	% release of radon generated
2360 - 850	1606	3.49 ± 0.22	1160	103 ± 8	8.9 ± 1.3
850 - 600	726	1.43 ± 0.15	473	60 ± 6	12.7 ± 2.7
600 - 425	512	1.77 ± 0.16	586	57 ± 4	9.8 ± 1.5
425 - 300	363	1.83 ± 0.15	606	61 ± 4	10.1 ± 1.6
300 - 212	256	1.85 ± 0.15	612	95 ± 7	15.5 ± 2.5
212 - 150	181	2.05 ± 0.17	679	69 ± 6	10.2 ± 1.7
150 - 106	128	2.44 ± 0.17	808	85 ± 5	10.5 ± 1.4
106 - 75	91	4.84 ± 0.30	1600	112 ± 7	7.0 ± 0.9
75 - 53	64	6.78 ± 0.35	2240	187 ± 14	8.4 ± 1.1
< 53	26	7.79 ± 0.33	2580	195 ± 14	7.6 ± 0.9

Table 9.3 Variation of radon release with particle size for Pennant Sandstone,

Uppper Lydbrook Quarry, South Wales

Sieve size, μm	Average particle diameter, μm	Uranium content, $\mu g\ g^{-1}$ rock	Uranium content pCi Kg^{-1} rock	Radon released pCi Kg^{-1} rock	% release of radon generated
> 2360	(4000)	(2.37 ± 0.31)	784	177 ± 13	22.6 ± 4.5
2360 - 850	1606	2.79 ± 0.17	923	197 ± 15	21.3 ± 2.9
850 - 600	726	2.84 ± 0.19	940	180 ± 15	19.1 ± 2.8
600 - 425	512	2.74 ± 0.21	907	175 ± 15	19.3 ± 3.1
425 - 300	363	2.10 ± 0.19	695	170 ± 13	23.0 ± 3.8
300 - 212	256	2.26 ± 0.20	748	165 ± 14	22.1 ± 3.8
212 - 150	181	1.80 ± 0.16	596	153 ± 11	25.7 ± 4.1
150 - 106	128	2.04 ± 0.17	675	149 ± 11	22.1 ± 3.4
106 - 75	91	2.40 ± 0.17	794	175 ± 13	22.0 ± 3.2
75 - 53	64	5.60 ± 0.25	1850	280 ± 22	15.1 ± 1.9
< 53	26	4.45 ± 0.23	1470	364 ± 30	24.7 ± 3.3

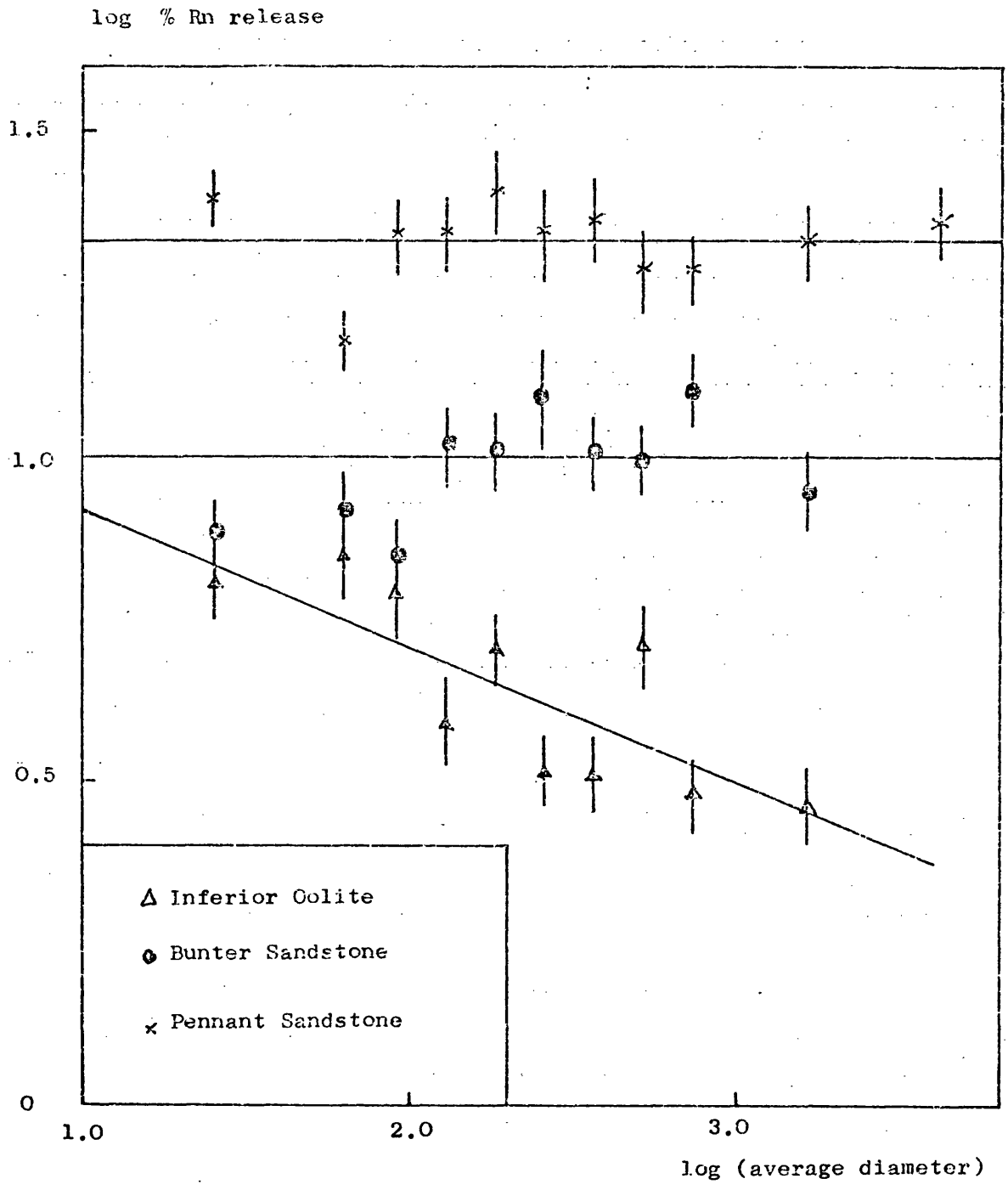

Fig. 9.1. Plot of ^{222}Rn release against average diameter of Inferior Oolite, Bunter Sandstone and Pennant Sandstone rock samples.

The Carboniferous Limestone fragments investigated by Andrews and Wood [13] are polycrystalline aggregates of calcite crystals with many grain boundaries. Crystal imperfections and dislocations may occur even within micro-crystals. Such imperfections and grain boundaries would provide relatively easy diffusion routes. ^{222}Rn release by primary recoil or diffusion into such imperfections, followed by rapid diffusion to the particle surface will depend on the extent to which grain boundaries or imperfections intersect the particle surface. For rock particles composed of uniform grains, the integrated grain boundary length intersecting the surface is proportional to the square root of the specific surface area, and ^{222}Rn release by this mechanism should therefore give n a value of -0.5.

If the rock fragments comprise a number of particles of a much smaller size, such as in the cementing phase of a sandstone, the percentage ^{222}Rn release will be a constant, as the particle size will be effectively constant. The radon release may be proportional to $^{1}/d^{\frac{1}{2}}$ for the basic units which comprise the rock fragment, but d (and $^{1}/d^{\frac{1}{2}}$) will be the same for all fragments. Therefore ^{222}Rn release by this mechanism will give n a value of 0. Values of n have been determined and these are compared with the predicted values of n calculated as above.

9.4.1. Inferior Oolite

From Figure 9.1, the value of n for the Inferior Oolite, Avon is -0.21. This suggests that the mechanism by which ^{222}Rn is released is probably a combination of primary recoil or diffusion into crystal

imperfections in both the bulk ooliths and in the cementing phase. Such a mechanism would lead to a value of -0.5 for n in the bulk ooliths and 0 for n in the cementing phase.

The Lincolnshire Limestone is a member of the Inferior Oolite Series. Limestones of the Inferior Oolite Series vary greatly in character although all were deposited in shallow marine conditions. It is likely, therefore, that the factors affecting the percentage ^{222}Rn release in the Lincolnshire Inferior Oolite will be similar to those in the Inferior Oolite of Avon and n will have a value close to -0.21. The ^{222}Rn contents of groundwaters from the Lincolnshire Limestone have been determined. Statistical analysis shows that the values of the ^{222}Rn content of the groundwater are distributed log normally about a mean value of 127 pCi Kg^{-1} and a median of 96 pCi Kg^{-1} (Figure 5.3).

The ^{222}Rn content of interstitial water is related to the uranium content of the host rock by the equation:

$$[Rn] = 0.33 A \frac{\rho}{\phi} [U][1 - e^{-\lambda t}] \qquad 9.7$$

where $[Rn]$ = ^{222}Rn content of the water (pCi cm^{-3})

$[U]$ = ^{238}U content of the host rock ($\mu g\ g^{-1}$)

ρ = bulk density of the rock (g cm^{-3})

ϕ = fractional porosity

A = fractional efficiency of radon release

λ = decay constant for ^{222}Rn

t = residence time of the interstitial water.

Provided that the residence time of the groundwater is greater than 25 days, the exponential term, $1 - e^{-\lambda t}$ approaches unity, and equation 9.7 becomes:

$$[Rn] = 0.33 A \frac{\rho}{\emptyset} [U] \qquad 9.8$$

The values ρ, $\emptyset$ and $[U]$ have been determined for the Inferior Oolite:

$\rho = 2.80$ g cm^{-3}

$\emptyset = 0.05$

$[U] = 2.87$ g g^{-1}

Substitution into equation 9.8 gives A the value 0.0025 (cf. 0.002 for Carboniferous Limestone [13]). Substituting this value of A into equation 9.5, with n = -0.21 and C_1 = 13.4 gives a value for d of 170 m. This can be interpreted by considering the mechanism of flow in the Lincolnshire Limestone which is a combination of fissure flow and intergranular flow. For fissure flow, the rock particles are massive - of the order of metres in diameter, so it is the fissure flow in the Limestone which dictates the primary mechanism by which ^{222}Rn is released into groundwaters. Naturally there is a large variation in the ^{222}Rn content of groundwaters from different sites. Variation can be explained in terms of different $[U]$, $\emptyset$ and A from equation 9.8 and variation in the relative importance of fissure flow and intergranular flow. These are discussed more thoroughly in the area study of the Lincolnshire Limestone. (Chapter 5).

9.4.2. Bunter Sandstone

The relation between (Rn) and d for the Bunter Sandstone rock sample is given by:-

$$(Rn) = 5.71\ d^{0.10} \qquad 9.9$$

For the Bunter Sandstone, n takes the small positive value of 0.10, that is, the percentage ^{222}Rn release increases with increasing particle size.

The ^{222}Rn contents of groundwaters from the Bunter Sandstone, Nottinghamshire have been determined. Probability plots (Figure 3.3) show that the ^{222}Rn contents are distributed normally about an average of 180 $pCi.Kg^{-1}$. The average primary porosity is 0.3 [170], with a corresponding dry bulk density of 2.15 g cm^{-3}. Substituting these values, together with the average uranium content of 1.87 $\mu g\ g^{-1}$ into equation 9.8 gives a value of 0.04 for A. By substituting (Rn) = 4% into equation 9.5 a value of d of 0.03 μm is obtained.

The Bunter Sandstone (Lower Triassic) is essentially a fluvial red-bed sequence comprising sandstones and conglomerates with occasional thin mudstones. The bulk of the uranium content is likely to occur in the cementing phase. The particles of the cementing phase are small compared with the sandstone particles, and these are essentially responsible for producing the ^{222}Rn contents found in groundwaters of the aquifer. The value 0.03 μm for d is very similar to the value of the recoil range of a ^{222}Rn atom of 0.036 m in glass of composition $Na_2O.CaO\ 6SiO_2$ [101]. It seems unlikely that a particle of this size would release only 4% of the ^{222}Rn generated. The probable explanation is that the average ^{222}Rn content is low because of decay within the aquifer. Also it is likely that n is effectively 0, so the percentage ^{222}Rn release is effectively constant. The average value of (Rn) from the rock samples investigated is 10.1%. This suggests

that the true average radon content should be

$$\frac{10.1}{4} \times 180$$

$$= 453 \text{ pCi Kg}^{-1}$$

^{222}Rn contents in excess of this value are observed for the Bunter Sandstone at Ompton No. 2 and Retford, Clarks No. 2., and these probably better represent the true equilibrium ^{222}Rn content of the groundwaters.

9.4.3. Pennant Sandstone

The situation in the Pennant Sandstone is similar to that in the Bunter Sandstone. The percentage ^{222}Rn release is essentially constant with variation in particle size. The average percentage ^{222}Rn release, however, is 21.5%, which gives A in equation 9.8 a value of 0.215. The porosity and density are 0.22 and 2.25 g cm^{-3} respectively and the average uranium content is 2.37 μg g^{-1}. Substituting these values into equation 9.8 gives a value of 1719 pCi Kg^{-1} for the ^{222}Rn content. The only groundwater sample taken from the Pennant Sandstone was from Hanham in Avon. This had a radon content of 437 pCi Kg, which is of the same order of magnitude as the expected value.

9.5. RADON RELEASE FROM THE CORNUBIAN AND SWEDISH GRANITES

The results of the radon release experiments for the granite samples are given in Tables 9.4 - 9.9. The results are represented graphically in Figure 9.2 which shows that the ^{222}Rn released from a kg of rock increases linearly with the uranium content of the rock. It is important to note also that the uranium content increases with decreasing particle size. This is probably because uranium tends to accompany zirconium into feldspars during magnetic differentiation. These minerals are relatively soft and easily crushed and carry U with them into the small sieve size fraction. The percentage release of ^{222}Rn generated remains essentially constant for a given sample, but because of the increase in uranium content, the ^{222}Rn released increases with decrease in particle size.. The results from Figure 9.2 are summarised in Table 9.10 which lists the calculated percentage ^{222}Rn released from the samples investigated.

The values of fractional ^{222}Rn release (A) are plotted against sample depth in Figure 9.3. The trend is for the fractional ^{222}Rn release to decrease with increasing depth, but it is essentially constant for a given depth. However, the value of A for the deepest Swedish core (832 m) is slightly greater than that for the sample immediately above it (410 m). Clearly this cannot be a surface area effect. It must be the microstructure of the granite which determines the fractional ^{222}Rn release. Weathering plays an important role in ^{222}Rn release. The fractional ^{222}Rn release from weathered granite at the ground surface for both the Swedish and Cornubian granite is much greater than that for the deeper samples.

Table 9.4. Variation of radon release with particle size for Cornubian granite, Ready Mixed Concrete, Penryn, (SW 741 338)

Sieve size, μm	Average particle diameter, μm	Uranium content μg g^{-1} rock	Uranium content p Ci Kg^{-1} rock	Radon released pCi Kg^{-1} rock	% release of radon generated
	(25000)	(13.4 ± 0.4)	(4430)	620 ± 37	13.9 ± 1.2
	(10000)	(13.4 ± 0.4)	(4430)	1030 ± 60	24.3 ± 2.1
> 2360	(4000)	(13.4 ± 0.4)	(4430)	1000 ± 70	22.6 ± 2.1
2360 - 850	1606	11.4 ± 0.3	3760	980 ± 60	26.1 ± 2.5
850 - 600	726	9.6 ± 0.4	3160	1060 ± 70	33.5 ± 3.4
600 - 425	512	10.2 ± 0.3	3380	1010 ± 70	29.9 ± 3.0
425 - 300	362	9.0 ± 0.4	2970	1020 ± 70	34.3 ± 3.8
300 - 212	256	9.0 ± 0.4	2960	1040 ± 70	35.0 ± 3.7
212 - 150	181	13.1 ± 0.5	4330	1280 ± 80	29.5 ± 3.1
150 - 106	128	12.4 ± 0.4	4110	1550 ± 100	37.6 ± 3.7
106 - 75	91	15.9 ± 0.4	5260	1850 ± 120	35.2 ± 3.3
75 - 53	64	22.4 ± 0.5	7410	2470 ± 170	33.4 ± 3.1
< 53	26	26.3 ± 0.6	8720	3690 ± 240	42.3 ± 3.8

Table 9.5 Variation of radon release with particle size for Stripa granite outcrop near Water Table Well 5, Stripa Mine.

Sieve size, μm	Average particle diameter, μm	Uranium content $\mu g\ g^{-1}$ rock	Uranium content pCi Kg^{-1} rock	Radon released pCi Kg^{-1} rock	% release of radon generated
19050 - 12700	15880	(24.4 ± 0.5)	8080	2210 ± 130	27.4 ± 2.2
9525 - 4763	7144	(24.4 ± 0.5)	8080	2850 ± 170	35.3 ± 2.9
3175 - 2360	2768	19.8 ± 0.5	6550	2540 ± 160	38.8 ± 3.3
850 - 600	726	20.5 ± 0.4	6790	2990 ± 200	44.0 ± 3.9
425 - 300	363	21.7 ± 0.4	7180	2870 ± 200	40.0 ± 3.6
212 - 150	181	23.0 ± 0.4	7610	3080 ± 220	40.5 ± 3.6
106 - 75	91	30.6 + 0.5	10100	3640 + 260	36.0 + 3.2
< 53	26	53.8 ± 0.7	17800	6620 ± 450	37.2 ± 3.0

Table 9.6 Variation of radon release with particle size for Stripa granite, Stripa Mine, 338 m level

Sieve size, μm	Average particle diameter, μm	Uranium content $\mu g\ g^{-1}$ rock	Uranium content pCi Kg^{-1} rock	Radon released pCi Kg^{-1} rock	% release of radon generated
> 2360	(4000)	(37.3 ± 0.6)	(12300)	2830 ± 180	22.9 ± 1.8
2360 - 850	1606	28.5 ± 0.5	9400	2910 ± 180	30.9 ± 2.5
850 - 600	726	36.3 ± 0.6	12000	3330 ± 200	27.7 ± 2.1
600 - 425	512	40.2 ± 0.7	13300	3750 ± 230	28.2 ± 2.2
425 - 300	362	42.4 ± 0.8	14000	3820 ± 240	27.2 ± 2.2
300 - 212	256	39.5 ± 0.7	13100	3890 ± 250	29.7 ± 2.4
212 - 150	181	42.3 ± 0.6	14000	4030 ± 260	28.8 ± 2.2
150 - 106	128	57.7 ± 0.9	19100	4460 ± 290	23.4 ± 1.9
106 - 75	91	62.7 ± 0.8	20700	5450 ± 380	26.3 ± 2.2
75 - 53	64	81.8 ± 0.9	27100	7090 ± 460	26.2 ± 2.0
< 53	26	149.1 ± 1.3	49300	10780 ± 670	21.9 ± 1.5

Table 9.7 Variation of radon release with particle size for Stripa granite, Stripa Mine, 345 m level

Sieve size, μm	Average particle diameter, μm	Uranium content μg g^{-1} rock	Uranium content pCi Kg^{-1} rock	Radon released pCi Kg^{-1} rock	% release of radon generated
> 2360	4000	(39.3 ± 0.6)	(13000)	2210 ± 140	17.0 ± 1.3
2360 - 850	1606	42.7 ± 0.6	14100	2240 ± 140	15.9 ± 1.2
850 - 600	726	37.0 ± 0.6	12200	2460 ± 150	20.1 ± 1.6
600 - 425	512	38.2 ± 0.7	12700	2480 ± 160	19.6 ± 1.6
425 - 300	362	42.0 ± 0.6	13900	2550 ± 170	18.3 ± 1.5
300 - 212	256	40.9 ± 0.7	13500	2670 ± 170	19.7 ± 1.5
212 - 150	181	48.6 ± 0.7	16100	2840 ± 190	17.6 ± 1.4
150 - 106	128	45.6 ± 0.7	15100	3210 ± 210	21.3 ± 1.7
106 - 75	91	63.6 ± 0.8	21100	3550 ± 240	16.8 ± 1.3
75 - 53	64	83.8 ± 0.9	27800	4620 ± 300	16.7 ± 1.3
< 53	26	124.0 ± 1.1	41100	6880 ± 450	16.8 ± 1.3

Table 9.8 Variation of radon release with particle size for Stripa granite, Stripa Mine, 410 m level

Sieve size, μm	'Average particle diameter, μm	Uranium content, μg g^{-1} rock	Uranium content pCi Kg^{-1} rock	Radon released pCi Kg^{-1} rock	% release of radon generated
> 2360	(4000)	(39.9 ± 0.7)	(13200)	1510 ± 100	11.4 ± 0.9
2360 - 850	1606	46.3 ± 0.8	15300	1370 ± 90	8.9 ± 0.7
850 - 600	726	43.6 ± 0.6	14400	1610 ± 110	11.2 ± 0.9
600 - 425	512	42.1 ± 0.7	15600	1630 ± 110	10.5 ± 0.9
425 - 300	362	38.3 ± 0.7	12700	1630 ± 110	12.9 ± 1.1
300 - 212	256	45.0 ± 0.8	14900	1780 ± 120	11.9 ± 1.0
212 - 150	181	40.7 ± 0.9	13500	2010 ± 130	15.0 ± 1.3
150 - 106	128	43.4 ± 0.8	13300	2210 ± 150	15.4 ± 1.3
106 - 75	91	62.0 ± 0.9	20500	2350 ± 170	11.4 ± 1.0
75 - 53	64	80.8 ± 1.1	26800	3350 ± 220	12.5 ± 1.0
< 53	26	118.1 ± 1.5	39100	5020 ± 330	12.8 ± 1.0

Table 9.9 Variation of radon release with particle size for Stripa granite, Stripa Mine, 471 m borehole at 410 m level (core sample 831.55 m)

Sieve size, μm	Average particle diameter, μm	Uranium content $\mu g\ g^{-1}$ rock	Uranium content pCi Kg^{-1} rock	Radon released pCi Kg^{-1} rock	% release of radon generated
19050 - 12700	15880	(17.2 ± 0.4)	(5690)	765 ± 50	13.4 ± 1.2
9525 - 4763	7144	(17.2 ± 0.4)	(5690)	1050 ± 70	18.5 ± 1.7
3175 - 2360	2768	14.7 ± 0.3	4870	880 ± 60	18.1 ± 1.7
850 - 600	726	16.0 ± 0.4	5300	1180 ± 80	22.2 ± 2.1
425 - 300	362	14.9 ± 0.4	4930	990 ± 80	20.1 ± 2.1
212 - 150	181	14.8 ± 0.4	4900	1190 ± 80	24.3 ± 2.3
106 - 75	91	16.7 ± 0.4	5530	1240 ± 110	22.4 ± 2.4
< 53	26	33.6 ± 0.6	11100	2430 ± 170	21.9 ± 1.9

Table 9.10 Percentage release of radon generated for granite rock samples.

Sample	(Rn) %
Cornubian granite	32.8
Stripa Mine, ground level	37.0
Stripa Mine, 338 m level	25.6
Stripa Mine, 345 m level	16.7
Stripa Mine, 410 m level	12.0
Stripa Mine, 832 m core	13.8

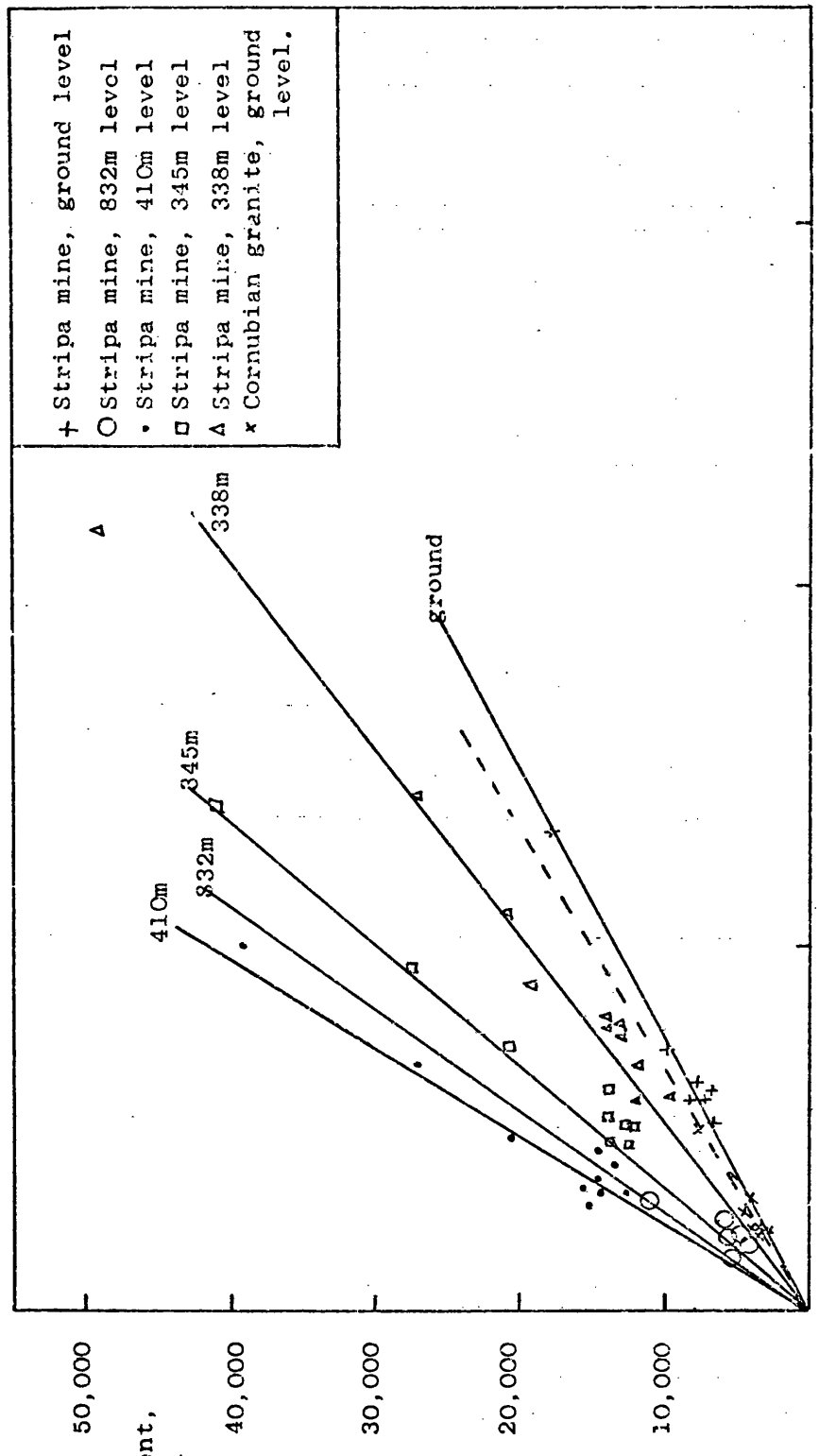

Figure 9.2. Plot of U content against ^{222}Rn release from rock samples from the Cornubian and Stripa granites.

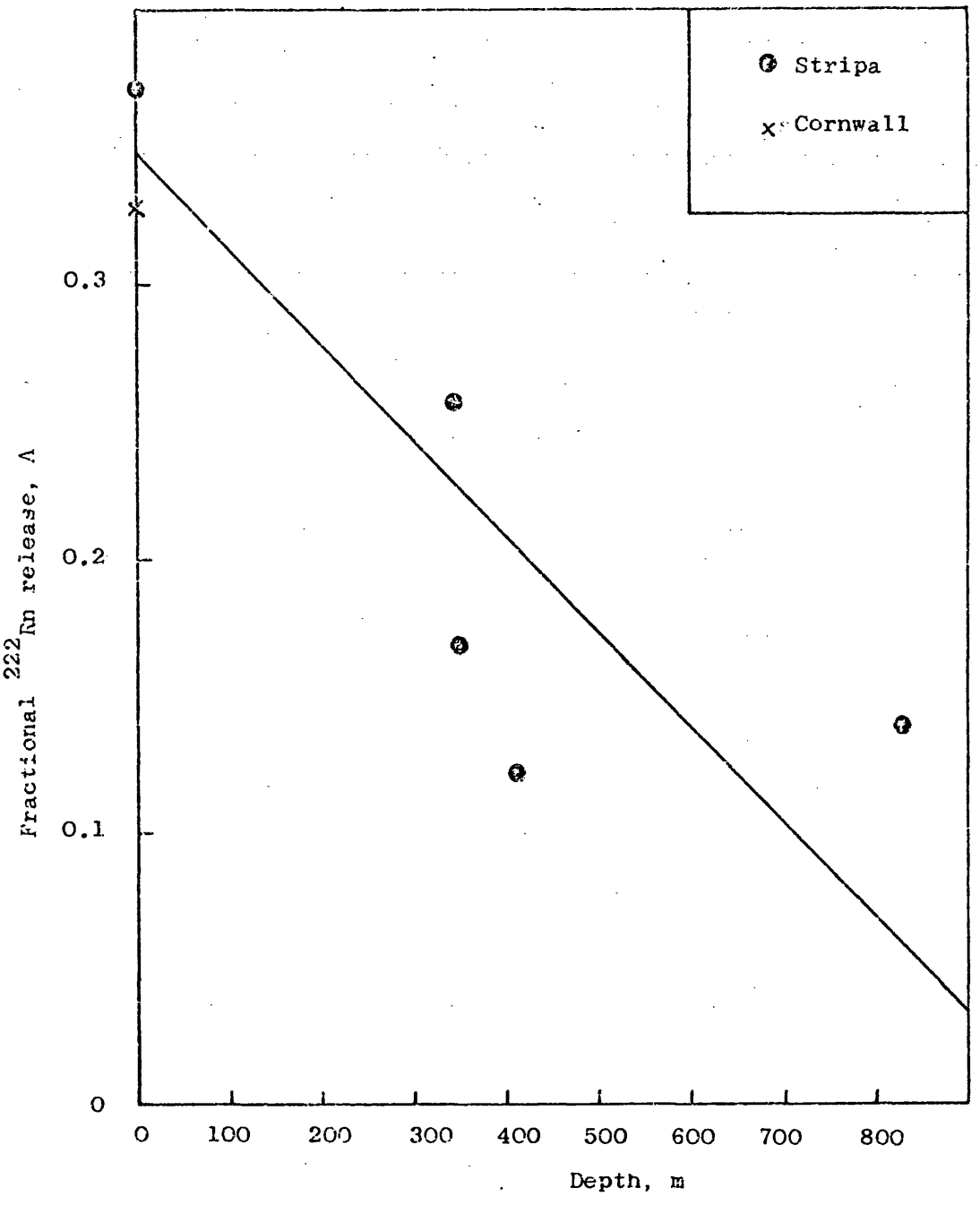

Figure 9.3. Plot of fractional ^{222}Rn release, A, against sample depth of granites from Cornwall and Stripa.

From the values of fractional ^{222}Rn release, A, bulk density, ρ, uranium content, [U], and representative ^{222}Rn content of groundwaters in the respective areas, [Rn], the value of Ø in equation 9.4 may be calculated. Ø is normally called the fractional porosity, but for a granite, this is not necessarily a very meaningful term. Ø may be more correctly termed the ratio of the volume of water to the volume of rock. The calculated values of Ø, and the parameters used to calculate Ø, for the granites studied are given in Table 9.11.

The magnitude of Ø for the outcrop samples from Cornwall is similar to that for the Swedish outcrop samples. However, the value of 0.87 for Ø for the Swedish outcrop granite is greater than the theoretical maximum void space for close packed spheres in a cubic configuration (0.4764 [171]) Fracture porosity in the weathered samples will enhance the microporosity but only by a few percent. The value of 0.8 for Ø is unrealistic. It must arise from a breakdown in equation 9.8 used for calculating Ø:

$$[Rn] = 0.33\ A\ \frac{\rho}{Ø}\ [U]$$

Alternatively, the values of A, ρ and [U] have been overestimated and [Rn] underestimated. The high values of Ø for the outcrop granites reflect the significant amount of weathering which has occurred. The average ^{222}Rn content of the Cornish mine waters is similar to that of the surface waters and this would give a value of Ø closer to those for the Swedish and Cornish outcrop samples than the Swedish mine samples, in which Ø is very low. Therefore the ratio of the volume of water to the volume of rock for the Cornish mines is very high compared with the Swedish mines. The

Table 9.11 Values of Ø for granites and values of the parameters used to calculate Ø

Sample	A	ρ g cm^{-3}	[U] μg g^{-1}	Representative [Rn] pCi cm^{-3}	Ø (calculated)
Cornubian granite	0.328	2.62	13.4	10.5[a]	0.36
Stripa, 0 m	0.370	2.61	24.4	8.94[b]	0.87
Stripa, 338 m	0.256	2.61	37.3	1314[c]	0.0062
Stripa, 345 m	0.167	2.61	39.3	1314[c]	0.0043
Stripa, 410 m	0.120	2.61	39.9	360[d]	0.0114
Stripa, 832 m	0.138	2.61	17.2	685[e]	0.0030

Notes: a Average value for shallow groundwaters of South West England

b Average value for shallow groundwaters in the vicinity of Stripa Mine, Sweden.

c Average value for groundwaters from boreholes at 338 m level, Stripa Mine (M3, R1, R9)

d Value for sampling interval 416-432.4 m, 471 m borehole, 410 m level, Stripa Mine.

e Average of sampling intervals 7865-881 m and 811-838.4 m, 471 m borehole, 410 m level, Stripa Mine.

Table 9.12. Average Uranium contents and fractional radon release for rock particles $<2360\ \mu m$ in diameter.

Sample	Average U content $\mu g\ g^{-1}$	Average Fractional radon release
Inferior Oolite	2.87	0.047
Bunter Sandstone	1.87	0.101
Pennant Sandstone	2.37	0.215
Cornubian Granite	13.4	0.328
Stripa Granite (Outcrop)	24.4	0.370

physical situation corroborates this evidence and the Cornish Mines are very "wet" mines, whereas the Swedish Mines are known as "dry" mines.

The calculated values of Ø for the Swedish Mine samples are around two orders of magnitude less than for the Surface samples. This is a function of the high ^{222}Rn contents, rather than the low values of A used to calculate Ø. In the deep mine samples, the ^{222}Rn content of the water is determined by the small volume of water present compared with the large amount of ^{222}Rn generated. The values of Ø are very similar to the measured porosities of dry granites [172].

In order for the ^{222}Rn generated to be dissolved in the groundwater, it may have to migrate a significant distance through the granite. Barretto [167] studied the mobilization of ^{222}Rn in granitic rocks. His experiments indicated that ^{222}Rn diffuses rapidly through a substantial thickness of solid, fresh granite, although he failed to explain the mechanism by which the ^{222}Rn migrated. A possible explanation is that ^{222}Rn is produced in sites around which radioactive damage has occurred and has a chance of colliding with other particles in the area of damage degrading its 90 keV energy and moving away from its original production site. [167]

The value of Ø is particularly important when considering radioactive waste disposal. Recently, the possibility of using redundant mines in dry granite for storing radioactive waste has been studied. If Ø is large, as in the outcrop sample, Swedish Granite, and in the Cornish Samples, then there is a high probability that the stored

waste will come into contact with water enabling the possibility of transport of soluble radionuclides into the hydrosphere and subsequently into the biosphere. For small values of Ø, such as those found deep within Stripa Mine, there is a two orders of magnitude smaller probability of radioactive waste contaminating the groundwater. It is only the mines with a low Ø which are worth considering as possible repositories for the long-term storage of radioactive waste.

High levels of ^{222}Rn in mine workings have been a constant source of safety problems for many years. An understanding of how the ^{222}Rn is transported to the working areas leads to a possibility of controlling ^{222}Rn levels. Frequently, high levels of ^{222}Rn are found where large volumes of groundwater enter a mine [173]. Therefore, Ø which gives an indication of the volume of water present in a body of rock may prove to be important for such safety work.

9.6. CONCLUSIONS

The percentage release of ^{222}Rn generated into water has been studied for rock samples from oolitic limestone, sandstones and granites. These values have been related to the ^{222}Rn contents of groundwaters and mechanisms have been proposed for the accumulation of ^{222}Rn in groundwaters.

In the Lincolnshire Limestone, ^{222}Rn is generated by primary recoil and diffusion into crystal imperfections in the cementing phase and in the bulk ooliths. Variation in the ^{222}Rn contents of groundwaters from the Lincolnshire Limestone has been explained in terms of variation in

the uranium content, porosity and fractional ^{222}Rn release of the aquifer rock and variation in the relative importance of fissure flow and intergranular flow.

The ^{222}Rn contents of the Bunter and Pennant Sandstones is derived from the ^{226}Ra present in the cementing phase. The small size of the ^{222}Rn generating particles results in an essentially constant fractional release of ^{222}Rn over a wide range of particle sizes. A possible explanation for the low average ^{222}Rn contents of the Bunter Sandstone groundwaters is radioactive decay within the aquifer during transport through the aquifer.

The ^{222}Rn contents of the Cornubian and Swedish granites have been explained in terms of the volume of water to volume of rock ratio and the effect of weathering in the fractional release of ^{222}Rn. Groundwaters from deep within the granite in Stripa Mine have abnormally high ^{222}Rn contents. These are caused by the extremely low "porosities" encountered at depth. The consequences of the findings for ^{222}Rn contents of granite groundwaters have been discussed in terms of radioactive waste disposal and radiological safety in mine workings.

CHAPTER 10

HELIUM IN ROCK CORES

10.1 INTRODUCTION

The maximum estimated abundance of helium in the atmosphere is very much less than its cosmic abundance [58]. The helium content of crustal rocks and the atmosphere would have been much greater were it not for the fact that helium atoms are so light and small that they diffuse readily. In general, sedimentary rocks, especially sandstones, transmit helium more readily than the crystalline metamorphic rocks and non-fractured igneous rocks [174]. Helium may be transported in a porous rock by two mechanisms. Firstly, it may be carried dissolved in groundwater - fluid movement, and secondly by diffusion. Diffusion may occur through the solid or gas phase, but gaseous diffusion will be much more important than diffusion through solids as the diffusion coefficient, D, in solids is small (3.16×10^{-5} m^2 a^{-1} in silica [126].)

Lateral movement of groundwater may result in significant fluid transport of helium and the diffusion contribution may become relatively unimportant. However, in deep rock structures, such as the core samples studied, lateral groundwater movement is slow and diffusion becomes the important mechanism by which helium is transported.

Cores were analysed from five boreholes located in the U.K. In two boreholes, Winterbourne Kingston and Kempsey, it was possible to sample interstitial water which had flowed into the drill stem, in addition to cores. The relationship of the ^4He content of these cores with the ^4He content of the drill stem test samples is considered and related to the residence time of the interstitial water. Subsequently, the variation of the ^4He content of the cores with depth is discussed.

10.2 HELIUM IN WINTERBOURNE KINGSTON AND KEMPSEY CORES AND DRILL STEM TESTS.

The ^4He contents of the core samples from Winterbourne Kingston and Kempsey are given in Table 10.1. ^4He analysis was performed mass spectrometrically by the method described in Chapter 2. Analytical errors arise from ^4He loss during core splitting and result in the measured ^4He contents being lower than the original ^4He contents of the cores. For this reason, the highest measured ^4He contents are taken to be representative of the original ^4He contents. The drill stem test samples were transferred from the drill stem test sample bottle or the drill stand to 1 cm^3 glass tubes, ensuring that no air contamination occurred. The water samples were then analysed for ^4He by the method described for groundwater analysis in Chapter 2. The ^4He contents of the drill stem samples are reported in Table 10.2.

10.2.1. Winterbourne Kingston

The maximum ^4He content of the Winterbourne Kingston cores was found to be 18,400 X 10^{-8} cm^3 STP cm^{-3} interstitial water, on the assumption that all the ^4He dissolved in the water phase. This is much greater than the ^4He content of the drill stem test water samples. However, if it is assumed that helium is uniformly distributed between the water and mineral phases of the core sample and that the helium enters the water saturated pores in proportion to their volume, the volume of helium in the water V_p is given by:

$$V_p = V_{He} \rho$$

where V_{He} = maximum core helium content = 1274 x 10^{-8} cm^3 STP g^{-1} core

ρ = saturated density of core = 2.6 g cm^{-3}

Table 10.1 Helium contents of core samples from Winterbourne Kingston and Kempsey boreholes.

Sample Depth, m	Fractional porosity	Volume of interstitial fluid, cm^3	Total ^4He $cm^3 \times 10^8$	Fluid ^4He content, cm^3 STP cm^{-3} $H_2O \times 10^8$
WINTERBOURNE KINGSTON (TRIASSIC SANDSTONE)				
2316.26	0.16	5.96	109600	18400
		5.62	20500	3650
2318.65		3.29	33800	10300
		4.07	60100	14800
2322.4		4.75	20600	4350
		4.38	32100	7320
KEMPSEY (TRIASSIC SANDSTONE)				
946	0.129	3.42	337	99
		3.83	662	173
KEMPSEY (PERMIAN SANDSTONE)				
1436	0.215	5.01	706	141
		5.99	1720	287

Table 10.2 Helium contents of drill stem test samples from Winterbourne Kingston and Kempsey

Sample	Sampling depth		^4He, cm^3 STP cm^{-3} $H_2O \times 10^8$
WINTERBOURNE KINGSTON			
DST 1	2306 - 2321	(a)	3200 ± 430 *
		(b)	2760 ± 370 *
DST 2	2417 - 2424	(a)	1300 ± 170 *
		(b)	3010 ± 400 *
Average of two highest values			3110 ± 420
KEMPSEY			
DST 1	946	(a)	1770 ± 240 ≠
		(b)	2580 ± 350 ≠
DST 2	1490	(a)	1290 ± 170 *
		(b)	1490 ± 200 *
		(c)	1340 ± 180 ≠
		(d)	1480 ± 200 ≠

* sample taken from drill stem test sample bottle

≠ sample taken from drill standpipe above sample bottle.

This gives V_p a value of 3313 cm^3 STP cm^{-3} H_2O, which is close to the value of 3110 cm^3 STP cm^{-3} H_2O found in the drill stem test water samples. It is likely, therefore, that the helium is uniformly distributed between the water and mineral phases in the Triassic Sandstone, Winterbourne Kingston borehole.

The average ^4He content of the interstitial water is therefore 3213×10^{-8} cm^3 STP cm^{-3} H_2O. This ^4He must be radiogenic in origin, because it is present in an amount far in excess of that derived from air equilibrated water (appendix 4). The total amount of ^4He produced, V(He) (cm^3 STP cm^{-3} H_2O or rock), by radioactive decay of uranium and thorium in an aquifer rock in which there is no preferential solution of ^4He is given by

$$V(He) = \{P_U[U] + P_{Th}[Th]\} t\rho \qquad 10.1$$

where P_U = Helium production rate by uranium decay, cm^3 STP μg^{-1} U yr^{-1}

$[U]$ = Uranium content of rock, $\mu g\ g^{-1}$

P_{Th} = Helium production rate by thorium decay, cm^3 STP μg^{-1} Th yr^{-1}

$[Th]$ = Thorium content of rock, $\mu g\ g^{-1}$

ρ = bulk density of rock, g cm^{-3}

t = age, years

The values of $[U]$ and $[Th]$ have been determined by neutron activation analysis (Chapter 2) and the values of P_U and P_{Th} have been evaluated from the decay constants of U and Th. These values and the value of ρ, measured directly, are as follows:

$P_U = 1.19 \times 10^{-13}$ cm^3 STP μg^{-1} U yr^{-1}

$[U] = 3.4\ \mu g\ g^{-1}$

$P_{Th} = 2.88 \times 10^{-14}$ cm^3 STP μg^{-1} Th yr^{-1}

$[Th] = 18.2\ \mu g\ g^{-1}$

$\rho = 2.15$ g cm^{-3}

Substituting into equation 10.1 gives t a value of 16.1×10^6 years, which is an order of magnitude lower than the formation age.

At Winterbourne Kingston, the ^{4}He contents of cores from the Triassic Sandstone and drill stem tests have shown that ^{4}He is uniformly distributed, volume for volume, between the water and rock phases. This has enabled calculation of a ^{4}He age of the interstitial water. However, it has not been possible to identify the contribution that ^{4}He diffusion from deeper strata has had on the ^{4}He content of the water. Only by determining the diffusion contribution of ^{4}He can a true ^{4}He age be calculated.

10.2.2. Kempsey

The ^{4}He contents of the Kempsey cores are reported in Table 10.1. The maximum ^{4}He contents were found to be 173 and 287 $\times 10^{-8}$ cm^3 STP cm^{-3} interstitial water from depths of 946 and 1486 m respectively, on the assumption that all the ^{4}He was dissolved in the interstitial water. These are very much less than the ^{4}He contents of the drill stem test samples reported in Table 10.2 - 2580 $\times 10^{-8}$ and 1490 $\times 10^{-8}$ cm^3 STP cm^{-3} water at depths of 946 m and 1490 m respectively. The low values obtained for the ^{4}He contents of the core samples were probably caused by loss of ^{4}He between sampling and analysis.

Although every effort was made to seal the samples effectively and to perform the analysis as soon after collection as possible, it is evident that appreciable ^4He has diffused from the Kempsey core samples.

The best values of the ^4He contents of the interstitial water from Kempsey borehole must therefore be taken as those from the drill stem tests - 2580×10^{-8} and 1490×10^{-8} cm^3 STP cm^{-3} H_2O for DST 1 and DST 2 respectively. The values of [U], [Th], ρ and ϕ for the region of the aquifer from which the drill stem test samples were taken have been determined and are as follows:

Aquifer parameter	DST 1	DST 2
[U]	0.66	0.66
[Th]	2.3	2.3
ρ	2.42	2.30
ϕ	0.129	0.215

Substitution of these values into equation 3.2 -

$$^4He \text{ solution rate} = \frac{\rho}{\phi} \left\{ 1.19 \times 10^{-13} [U] + 2.88 \times 10^{-14} [Th] \right\} cm^3 \text{ STP } yr^{-1} cm^{-3} H_2O$$

gives groundwater residence times of 9.5 million years for DST 1 and 9.6 million years for DST 2. These residence times have been calculated assuming that all the ^4He generated dissolves in the interstitial water. They are remarkably similar, considering that the drill stem tests were carried out 544 m apart. If, however, it is assumed that ^4He is uniformly dispersed within the aquifer, the groundwater ages become 74 million years for DST 1 and 45 million years for DST 2. It is unlikely that the deeper of the two samples is the

younger. It is more likely that the groundwaters are of similar age. No information is available on the partitioning of ^4He between the water and rock phases, so any interpretation in terms of groundwater age is rather speculative. Clearly, for calculating groundwater ages at Kempsey, much more data on the ^4He content of the cores and the contribution of ^4He diffusion is necessary.

10.3 HELIUM CONTENTS OF CORES

The ^4He contents of the core samples are presented in Table 10.3. Also shown in Table 10.3 are the ^4He contents per gram of saturated rock sample. The maximum ^4He contents have been taken to be the representative ^4He contents and these are shown in Table 10.4, together with other relevant aquifer parameters which have been determined. The representative ^4He contents of the cores are plotted against sample depth in Figure 10.1. There is a tendency for the ^4He content (cm^3 STP g^{-1} rock) to increase with increasing depth, but the data are rather scattered.

By plotting simply the ^4He contents of the cores against depth, no account has been taken of variation in the radioelement contents of the cores. The normalised ^4He contents shown in Table 10.4 take into account such variations. The normalised ^4He contents were calculated as follows:

$$[\overline{He}] = [He] \left\{ \frac{1.19 \times 10^{-13} [U]_m + 2.88 \times 10^{-14} [Th]_m}{1.19 \times 10^{-13} [U]_s + 2.88 \times 10^{-14} [Th]_s} \right\} \qquad 10.2$$

where $[\overline{He}]$ = normalised ^4He content of rock core, cm^3 STP g^{-1}

$[He]$ = representative ^4He content of rock core, cm^3 STP g^{-1}

Table 10.3 Helium contents of core samples.

Sample Depth, m	Sample weight, g	Total ^4He content $cm^3 \times 10^8$	^4He content per g sample, $cm^3 \times 10^8$
WINTERBOURNE KINGSTON (TRIASSIC SANDSTONE)			
2316.26	86.0	109600	1274
	81.2	20500	253
2318.65	47.6	33800	711
	58.7	60100	1024
2322.4	68.6	20600	301
	63.3	32100	507
SEABARN FARM (UPPER LIASSIC SANDSTONE)			
415.55/47	58.4	284	4.9
	51.8	493	9.5
416.64/.80	69.6	893	12.8
	64.0	834	13.1
SHREWTON (MIDDLE LIASSIC SANDSTONE)			
1193.8-1194.1	68.6	2700	39
	64.3	7630	119
1191.8-1192.0	70.6	4600	65
	58.3	6850	118
1195.8-1195.9	46.5	6650	143
	64.5	8110	126
1196.5-1196.7	46.7	5540	119
	50.6	5690	112
BALLYMACILROY (TRIASSIC SANDSTONE)			
1528	47.6	2160	45
1532	27.9	1360	49
1536	31.3	2290	73
	32.5	1820	56
KEMPSEY (TRIASSIC SANDSTONE)			
946	60.7	337	5.6
	67.9	662	9.8
KEMPSEY (PERMIAN SANDSTONE)			
1486	50.5	706	14
	60.2	1720	29

Table 10.4 Representative ^4He, U and Th contents of cores

Sample	Formation	Approx. sample depth, m	Saturated bulk density (ρ_s) g cm^{-3}	Fractional porosity(Ø)	*U content [U] $\mu g\ g^{-1}$	≠ Th content [Th] $\mu g\ g^{-1}$	Representative ^4He content cm^3 STP g^{-1} rock	Normalised ^4He content
Winterbourne Kingston	Triassic Sandstone	2320	2.31	0.16	3.4	17.9	1274	594
Seabarn Farm	Upper Liassic Sandstone	415	2.33	0.181	3.05	10.7	13.1	8.4
Shrewton	Middle Liassic Sandstone	1195	2.48	0.117	2.34	8.2	143	119
Ballymacilroy	Triassic Sandstone	1530	2.29	0.171	0.83	2.9	73	172
Kempsey	Triassic Sandstone	950	2.42	0.129	0.66	2.3	98	29
	Permian Sandstone	1490	2.30	0.215	0.66	2.3	29	86

* U contents determined by delayed neutron activation analysis

≠ Th content of Winterbourne Kingston determined by neutron activation analysis

Other Th contents calculated assuming Th/U = 3.5 [2]

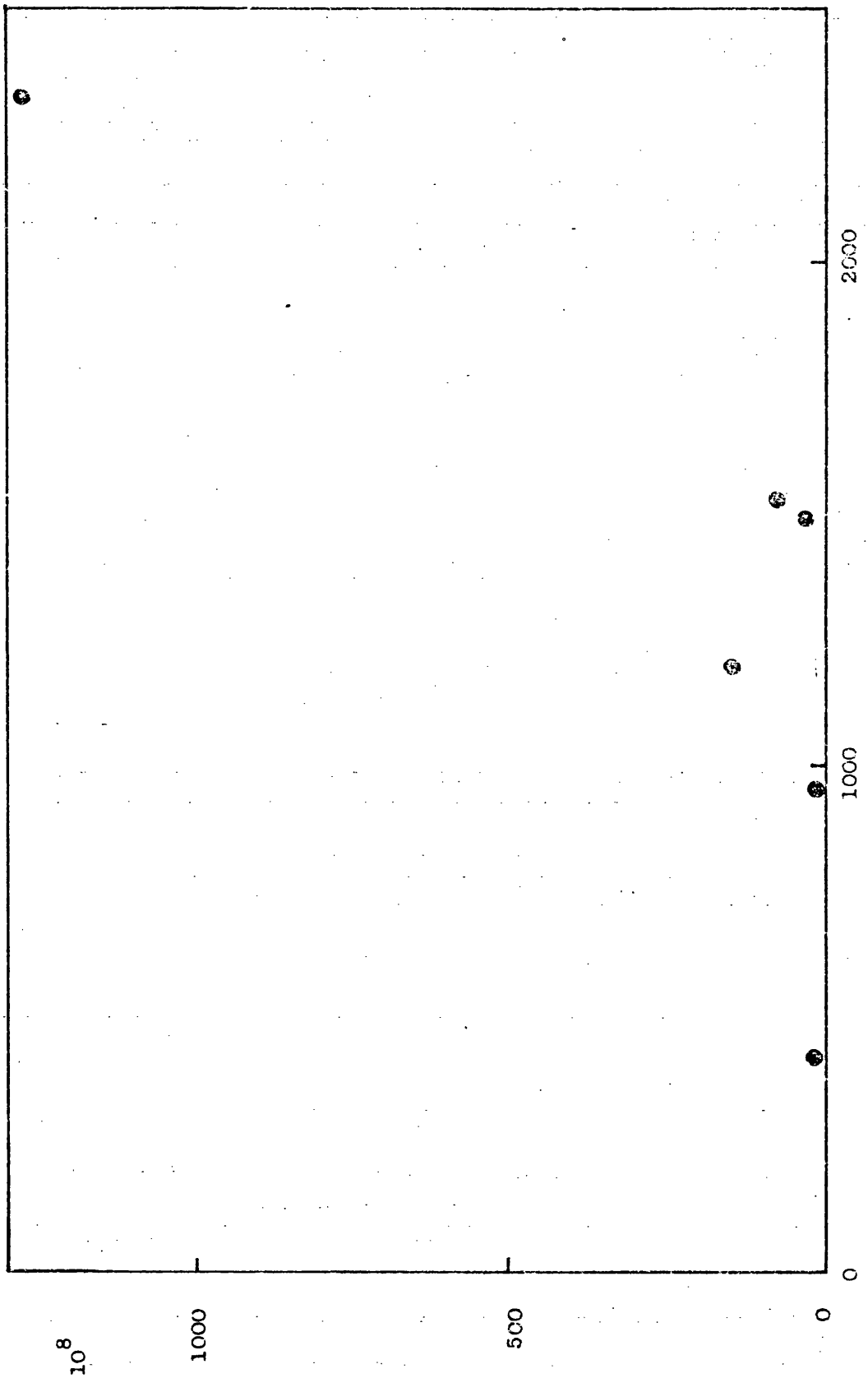

Fig. 10.1 Plot of representative ^{4}He content against depth for core samples

$[U]_m$, $[Th]_m$ = average U and Th contents, respectively, of all the cores studied, $\mu g\ g^{-1}$; $[U]_m = 1.82$, $[Th]_m = 7.4$

$[U]_s$, $[Th]_s$ = U and Th contents, respectively, of each core, $\mu g\ g^{-1}$

1.19×10^{-13}, 2.88×10^{-4} = production rates of He from radioactive decay of natural U and Th respectively, cm^3 STP cm^{-3} yr^{-1} μg^{-1}

Figure 10.2 shows a plot of the normalised ^4He contents against sample depth. It indicates more clearly the increase in ^4He content with depth but the data is still scattered. The shape of the curve is discussed more fully in Section 10.4.4.

10.4 HELIUM DIFFUSION

10.4.1 Helium concentration profiles for a uniform sedimentary layer

Consider the development of the He concentration profile in an ageing sedimentary layer. The layer is considered to be uniform in respect of its uranium and thorium contents and the diffusion coefficient, D, is constant throughout. It is assumed to be sufficiently thick for no diffusive He loss to have occurred at great depth, where the concentration, C, at time t after sedimentation is given by:-

$$C(\infty, t) = Gt \qquad 10.3$$

where G is the He generation rate. He is continuously lost from the upper surface to the atmosphere and hence the He concentration near the surface is always zero:

$$C(o, t) = 0 \qquad 10.4$$

Since the duration of sedimentation is usually short compared with the sediment age, the He content of the newly formed sediment may be taken as zero:

$$C(z, o) = 0 \qquad 10.5$$

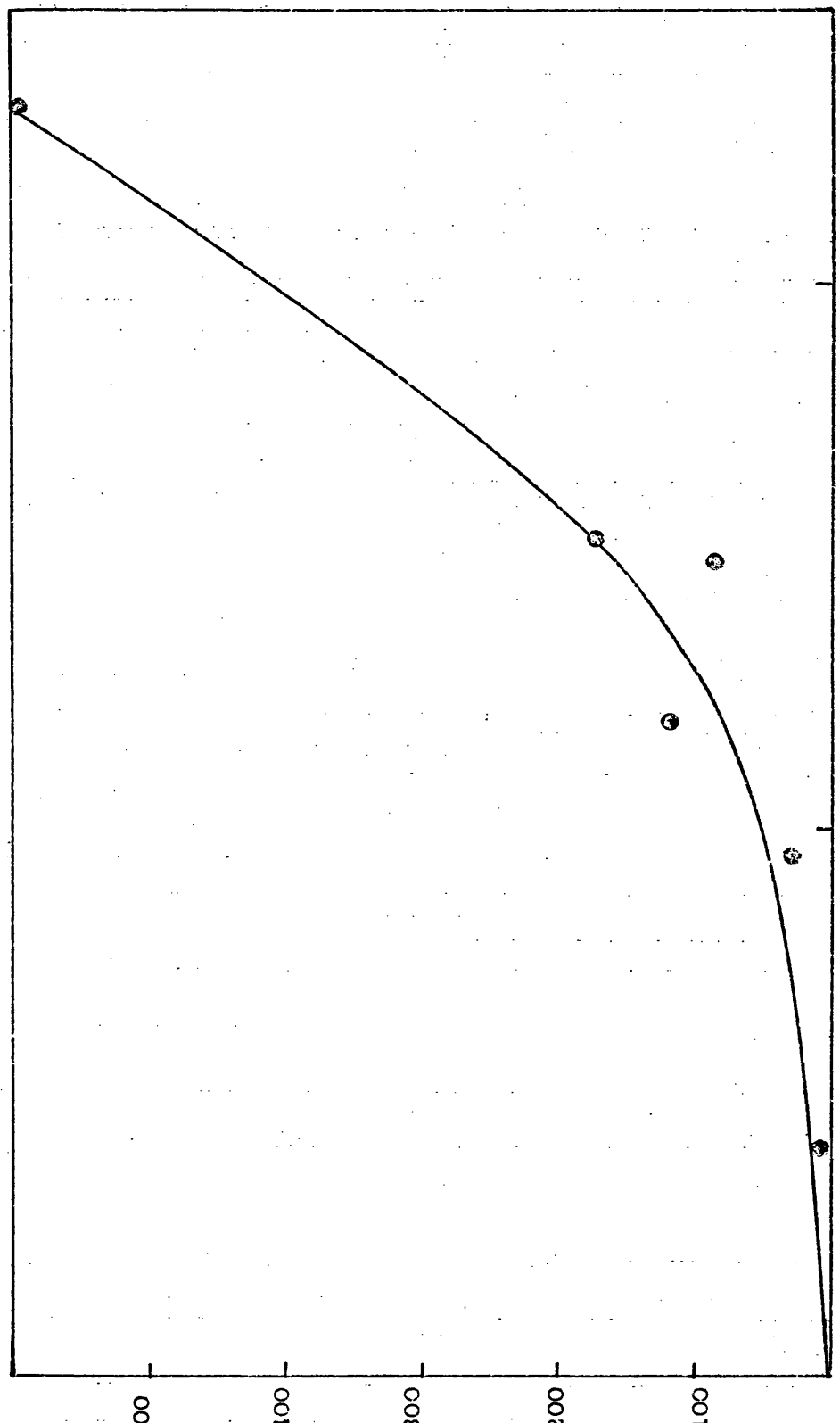

Fig. 10.2. Plot of normalised ^{4}He content against depth for core samples.

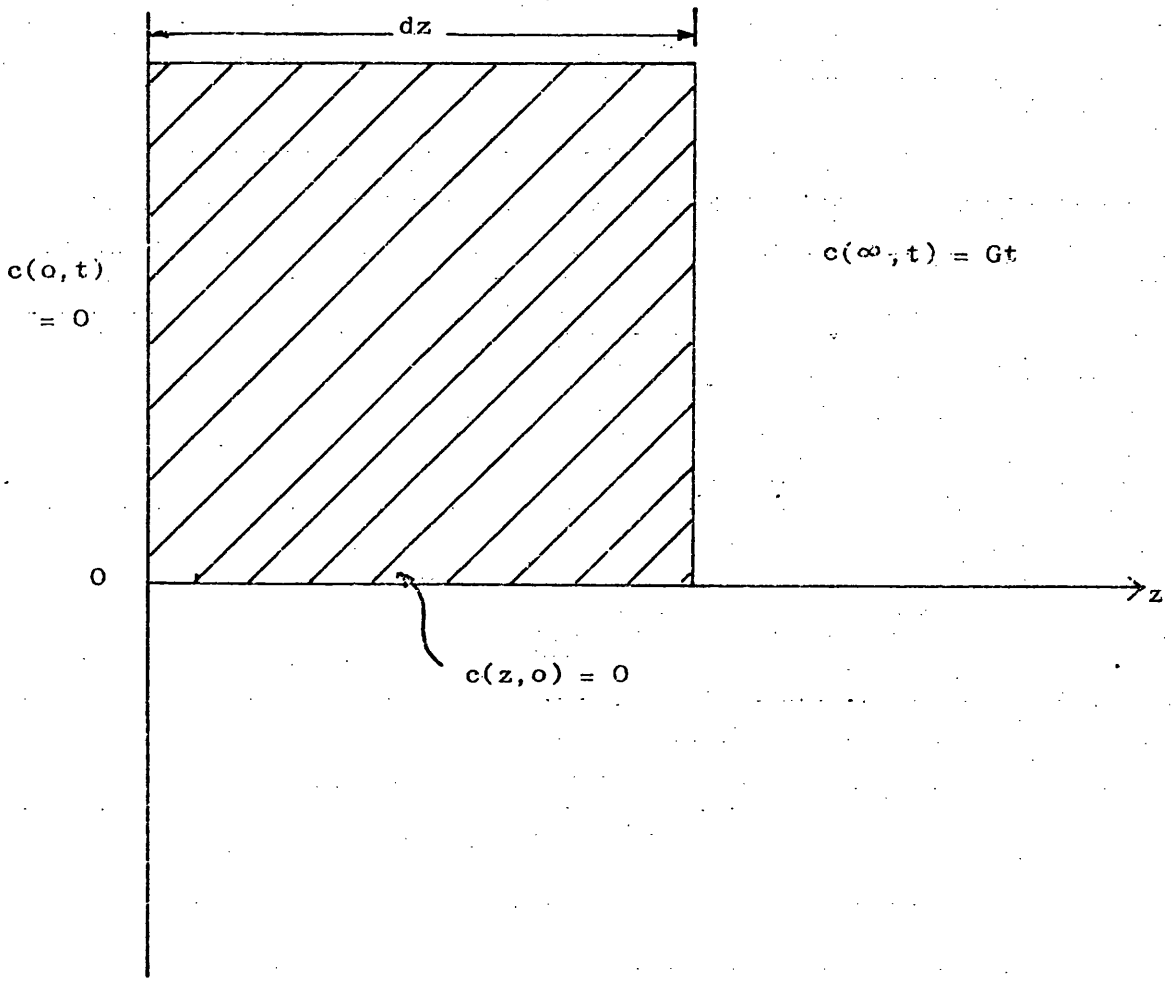

Fig. 10.3. Helium flux through a sedimentary slab of thickness dz

The diffusion equation for such a He generating layer (Figure 10.3) is:

$$\frac{dc}{dt} = G + D\frac{d^2c}{dz^2} \qquad 10.6$$

and the Laplace transform of this equation for boundary condition 10.5 is:

$$p\bar{c} = \frac{G}{p} + D\frac{d^2\bar{c}}{dz^2} \qquad 10.7$$

and on rearranging:

$$D\frac{d^2\bar{c}}{dz^2} - p\bar{c} = -\frac{G}{p} \qquad 10.8$$

the solution of which is:

$$\bar{c} = Ae^{-(P/D)^{\frac{1}{2}}z} + Be^{(P/D)^{\frac{1}{2}}z} + \frac{G}{p^2} \qquad 10.9$$

The transforms of equations 10.3 and 10.4 are:

$$\bar{c}\ (\infty, P) = \frac{G}{p^2} \qquad 10.10$$

and $$\bar{c}\ (o, P) = 0 \qquad 10.11$$

This requires that the constants in equation 10.9 have the values

$A = -G/p^2$ and $B = 0$

Therefore $$\bar{c} = \frac{G}{p^2} - \frac{G}{p^2}e^{-z(P/D)^{\frac{1}{2}}} \qquad 10.12$$

of which the inverse transform is:

$$c = Gt - G\int_o^t \operatorname{erfc}\left\{\frac{z}{2D^{\frac{1}{2}}U}\right\}dU \qquad 10.13$$

or $$c(z,t) = G\int_o^t \operatorname{erf}\left\{\frac{z}{2D^{\frac{1}{2}}U}\right\}dU \qquad 10.14$$

An approximate solution of 10.14 is given by:

$$c(z,\ t) = Gt\left[1 - \exp\left\{\frac{-2}{\sqrt{\pi}} \cdot \frac{z}{(Dt)^{\frac{1}{2}}}\right\}\right] \qquad 10.15$$

Equation 10.15 yields He concentration/depth profiles which are within 5% of the exact solution for all depths. Figure 10.4 shows He concentration/depth profiles calculated for various sediment ages from equation 10.15 for a thick layer of rock which loses He by rapid diffusion into the atmosphere at its surface. The concentration gradient, dc/dz, becomes vanishingly small at depth, for which condition:

$$c(z,\ t) = Gt \qquad 10.16$$

and none of the He generated within the rock at depth is lost by diffusion to the surface. It may be shown that equation 10.15 and 10.16 yield concentrations which agree within 1% at depths greater than $4(Dt)^{\frac{1}{2}}$ and at such depths, the He concentration is determined only by the age of the rock and its radioelement contents.

10.4.2. Helium diffusion into a confined aquifer

Let us now consider the problem of estimating He generation and diffusion in an aquifer which is confined between other sedimentary sequences. (Figure 10.5). The thickness of the overlay is considered to be such that He concentration at the aquifer/overlay interface (a/o) is GT_o, where T_o is the age of the overlay. This requires the overlay thickness to be greater than $4(DT_o)^{\frac{1}{2}}$ which is about 1000m for T_o = 200 million years and $D = 3.16 \times 10^{-4}\ m^2\ a^{-1}$ (about ten times greater than the diffusion coefficient in silica).

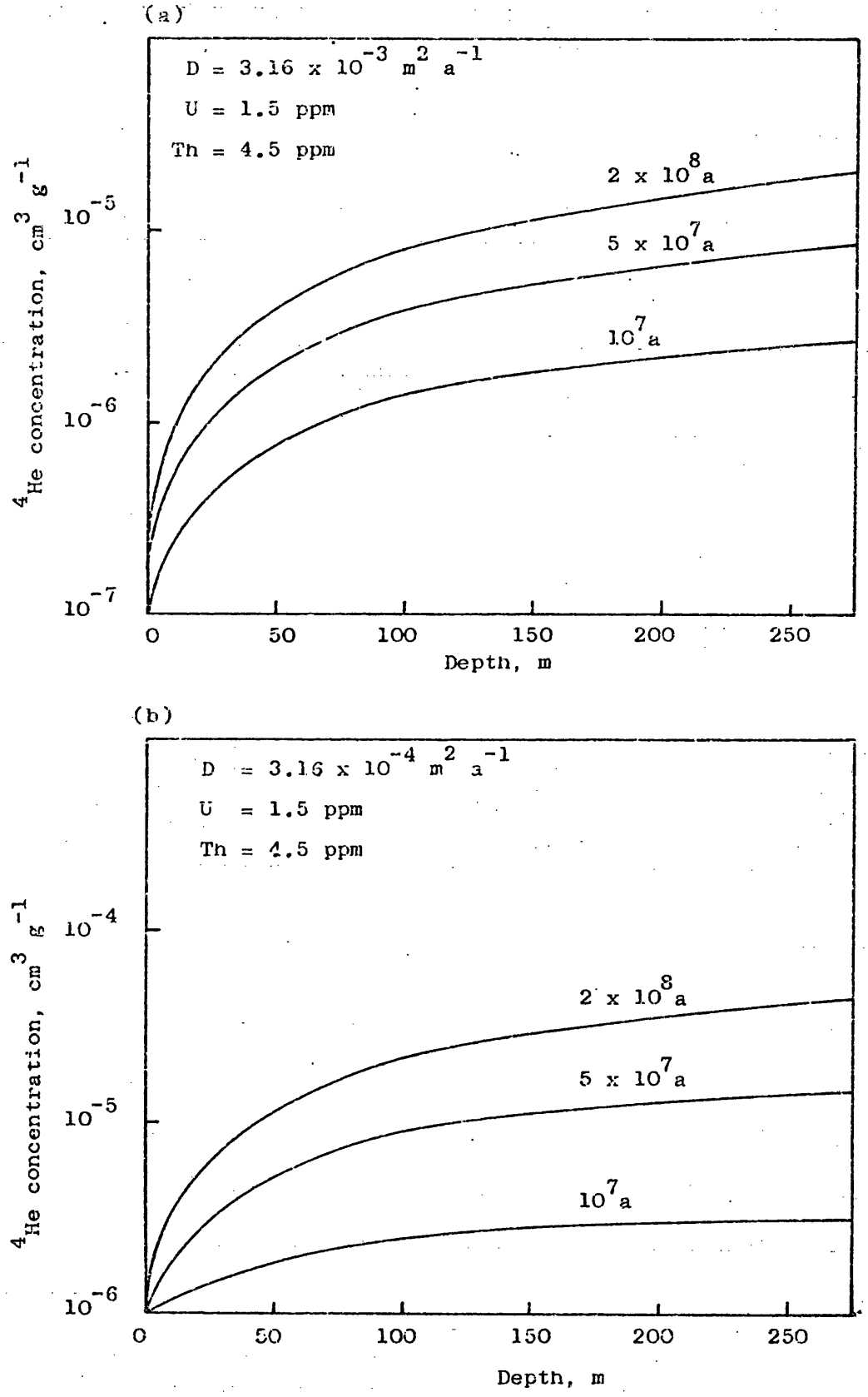

Figure 10.4. Helium generation profiles in a thick sedimentary layer

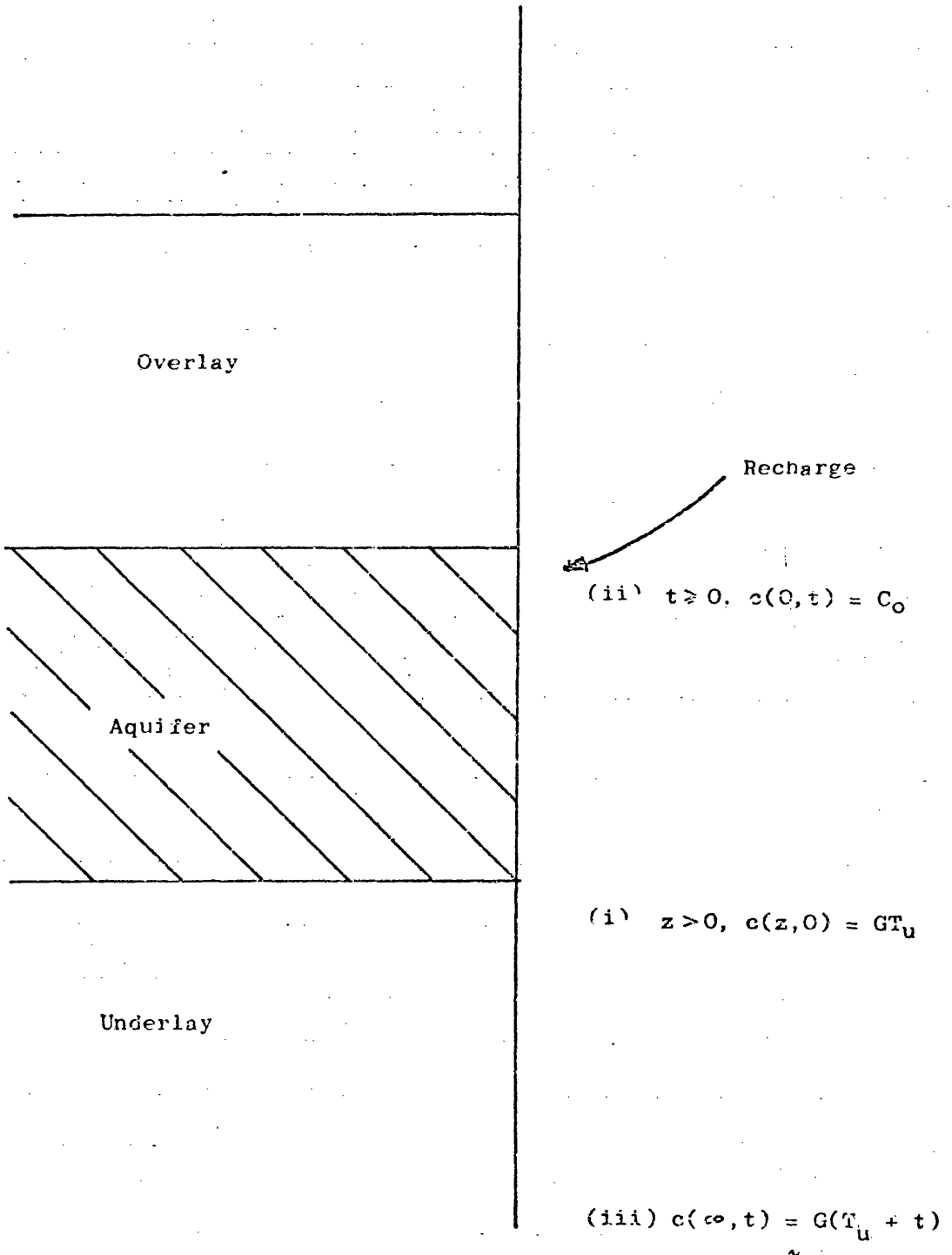

Fig. 10.5. Helium diffusion into a confined aquifer - boundary conditions

The model therefore applies only to very deep aquifers. For such a thick overlay, the He concentration profiles at the o/a and at the aquifer/underlay (a/u) boundaries are symmetrical and the problem may be simplified by at first considering only diffusion into the aquifer from the underlay and for convenience taking $z = o$ at the a/u boundary. The aim is to estimate the He content of the aquifer at times subsequent to $t = o$ at which time it is assumed that the aquifer was instantaneously flushed free of He. This is a necessary simplification but it will be shown later that the concentration gradients at the aquifer interfaces following the incursion of recharge waters are essentially the same as for this model and that flow must continue for a very long time to modify them significantly.

The diffusion equation (10.6) may be applied to diffusion in the underlay, of age T_u, with the following boundary conditions:

(i) for $z > o$, $c(z, o) = GT_u$ 10.17

(ii) for $t \geq o$, $c(o, t) = C_o$ 10.18

where C_o is the He content of the water recharging the aquifer.

(iii) $c(\infty, t) = G(T_u + t) \simeq GT_u$ 10.19

The appropriate Fourier transform of equation 10.6 for these conditions is:

$$-GT_u + P\overline{c} = \frac{G}{P} + D\frac{d^2\overline{c}}{dz^2} \qquad 10.20$$

The resultant concentration gradient is given by:

$$\frac{dc}{dz} = \frac{2}{\sqrt{\pi}} \left\{ \frac{GT_u}{2D^{\frac{1}{2}}t^{\frac{1}{2}}} e^{-\frac{z^2}{4Dt}} - \frac{Co}{2D^{\frac{1}{2}}t^{\frac{1}{2}}} e^{\frac{-z^2}{4Dt}} + G \int_o^t \frac{1}{2D^{\frac{1}{2}}U^{\frac{1}{2}}} e^{\frac{-z^2}{4Du}} du \right\} \qquad 10.21$$

which for $z = o$ yields the concentration gradient at the aquifer interface, which determines the diffusive He flux into the aquifer from the underlay:

$$\left[\frac{dc}{dz}\right]_{z=c} = \frac{2}{\sqrt{\pi}} \left\{ \frac{GT_u - C_o + 2Gt}{2D^{\frac{1}{2}}t^{\frac{1}{2}}} \right\} \qquad 10.22$$

The three terms in the quotient of equation 10.22 correspond to the influence on the concentration gradient of (i) He stored in the underlay prior to the commencement of flow in the aquifer, (ii) the "back-pressure" due to He transported into the aquifer in the recharge water and (iii) He generated in the underlay in time t subsequent to the commencement of flow in the aquifer. It is reasonable to assume that water flow in the aquifer commenced much more recently than the deposition of the sedimentary formations so that $t << T_u$. The quantity of atmospheric He dissolved in the recharge water, C_o, is very small compared with GT_u. The concentration gradient in the underlay at the a/u interface therefore becomes:

$$\left[\frac{dc}{dz}\right]_{z=o} = \frac{GT_u}{\sqrt{\pi} D^{\frac{1}{2}} T_a^{\frac{1}{2}}} \qquad 10.23$$

where T_u is the age of the formation forming the underlay and T_a is the time for which flow has occurred in the aquifer.

10.4.3. The rate of increase of He concentration in a confined aquifer

The low He content recharge water will acquire more He as it moves downdip due to He generation within the aquifer and diffusion into the aquifer at the interfaces with the underlay and overlay. The concentration gradient at the a/u boundary is given by equation 10.23 and the concentration gradient in the overlay at the o/a boundary will be the same for a thick overlay ($4(DT_o)^{\frac{1}{2}}$ m thick). Considering an elementary section of the aquifer (Figure 10.6), of thickness L_a and cross-sectional area δA, the rate of increase of He concentration within it can be evaluated.

The number of He atoms stored within the aquifer element is $C_a L_a \delta A$ where C_a is the mean He concentration in the aquifer. The number of radiogenic He atoms produced in the aquifer in a unit time is $\rho G L_a \delta A$ where G is the He production rate per gram of rock and ρ is the rock dry bulk density. The number of He atoms in the elementary volume also changes due to diffusion from the overlay and underlay, at fluxes of:

$$\delta A\ D_o \left(\frac{dC}{dz}\right)_{o/a} \quad \text{and} \quad \delta A\ D_u \left(\frac{dC}{dz}\right)_{u/a} \quad \text{respectively}$$

The overall rate of change of the He concentration in the aquifer is given by:

$$\frac{d}{dt}\ (C_a\ \delta A L_a) = G L_a\ \delta A + \delta A D_o \left(\frac{dC}{dz}\right)_{o/a} + \delta A D_u \left(\frac{dC}{dz}\right)_{u/a} \qquad 10.24$$

or, dividing by δA

$$\frac{d}{dt}\ (C_a L_a) = G L_a + D_o \left(\frac{dC}{dz}\right)_{o/a} + D_u \left(\frac{dC}{dz}\right)_{u/a} \qquad 10.25$$

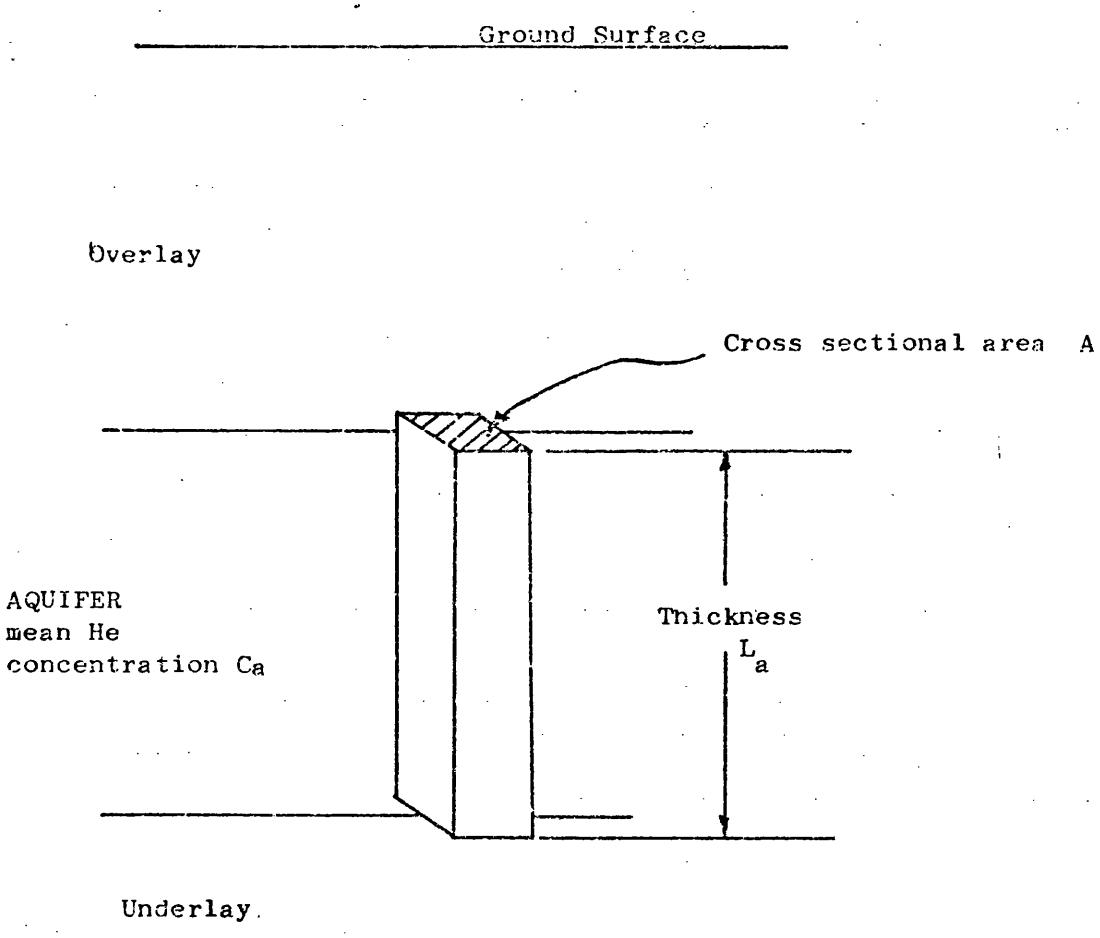

Fig 10 6 Diagram showing an elementary section of a confined aquifer.

and on substituting using equation 10.23:

$$\frac{d}{dt}\ (C_a L_a) = GL_a + \frac{D_o\ G\ T_o}{\sqrt{\pi}\ D_o^{\frac{1}{2}} T_a^{\frac{1}{2}}} + \frac{D_u\ G\ T_u}{\sqrt{\pi}\ D_u^{\frac{1}{2}} T_a^{\frac{1}{2}}} \qquad 10.26$$

where T_a is the time elapsed since flow commenced in the aquifer, T_o and T_u are the ages of the overlying and underlying formations respectively. If the diffusion coefficients in the overlay and underlay are similar ($D_o \simeq D_u$) and the ages of these formations are approximately the same ($T_o \simeq T_u = T_{o/u}$), equation 10.26 simplifies to:

$$\frac{dC_a}{dt} = \frac{G + 2D_{o/u}\ G\ T_{o/u}}{\sqrt{\pi}\ D_{o/u}^{\frac{1}{2}}\ T_a^{\frac{1}{2}}\ L_a} \qquad 10.27$$

or on integration:

$$C_a = Gt\left\{1 + \frac{2(D_{o/u}\ T_{o/u})^{\frac{1}{2}}}{\sqrt{\pi}\ L_a}\left(\frac{T_{o/u}}{T_a}\right)^{\frac{1}{2}}\right\} \qquad 10.28$$

In this equation, t is the time during which He has been accumulating within the aquifer starting from the low concentration present at recharge, that is the groundwater age. This must be distinguished from T_a which is the time for which flow has occurred in the aquifer and which influences the He concentration gradient in the overlay and underlay, close to the aquifer interfaces.

Substituting probable values of the parameters for a 'typical' aquifer into equation 10.28 yields the results below:

for $D = 3.16 \times 10^{-4}\ m^2\ a^{-1}$, $T_{o/u} = 2 \times 10^8$ a,

$(DT_{o/u})^{\frac{1}{2}} = 251$ m

for L_a = 100 m, $T_a = 10^6$ a

$$C_a = Gt \left\{ 1 + \frac{2}{\sqrt{\pi}} \cdot \frac{251}{100} \cdot 200^{\frac{1}{2}} \right\}$$

$$= 41\ Gt$$

Consequently for a given diffusion coefficient for He, age at which the overlay and underlay were deposited, thickness of aquifer and time for which flow has occurred, the concentration of He in an aquifer, C_a, is equal to a constant times the He generation rate times the groundwater age. Therefore, it is possible to calculate the age of a groundwater from the He content of the aquifer in which the water flows.

10.4.4. Application of the He diffusion model to core samples.

The shape of the He concentration profiles with depth in a thick sedimentary layer are shown in Figures 10.4a and b. At shallow depths, the concentration gradient dc/dz, is very high. As the depth increases, dc/dz tends to zero and the ^{4}He concentration c, at any depth $z > z_{max}$ for a sediment age t is given by:

$$c(z, t) = Gt \qquad 10.16$$

where G is the He generation rate by radioactive decay.

The variation of the normalised ^{4}He content of the core samples against depth is shown in Figure 10.2. The shape of the curve is very different to that of the predicted ^{4}He profiles for a uniform, thick sedimentary layer:- initially, dc/dz is zero, and as depth increases, dc/dz increases. Presumably at some depth, greater than 2400 m, dc/dz will tend to zero, but the shape of the initial

part of the curve is difficult to explain. It must be remembered that the strata that have been studied are neither uniform nor homogeneous. There is likely to be significant variability with geographical location. It is evident that significant loss of ^4He occurred from the Kempsey core samples. Loss of ^4He from the other cores would lead to ^4He profiles observed in Figure 10.2. Improved analytical precision and sampling from a single uniform homogeneous sedimentary structure would clarify the diffusion interpretation.

10.4.5. Application of the He diffusion model to the Nottinghamshire Bunter Sandstone aquifer.

The rate of increase of the ^4He concentration in a confined aquifer has been predicted in paragraph 10.4.3:

$$C_a = Gt\left\{1 + 2\,\frac{(D_{o/u}\,T_{o/u})^{\frac{1}{2}}}{\sqrt{\pi}\,L_a}\left(\frac{T_{o/u}}{T_a}\right)^{\frac{1}{2}}\right\} \qquad 10.28$$

The parameters inside the square brackets are essentially constant for a given aquifer and equation 10.28 becomes:

$$C_a = bGt \qquad 10.29$$

where b is a constant,

note G is the He generation rate

and t is the groundwater age.

In the Bunter Sandstone, Nottinghamshire, the following relationship between the ^4He contents of the groundwaters, [He], and their ^{14}C age, t, was observed from the experimental data (Figure 3.5).

$$t \simeq 1.2 \times 10^{11}\,[He]\ (yr) \qquad 10.30$$

The value of G for the Bunter Sandstone can be calculated from the production rates of ^4He, P_u and P_{Th} from natural U and Th decay respectively, and the U and Th contents of the Nottinghamshire Bunter Sandstone, $[U]$ and $[Th]$, as follows (see Chapter 3).

$$G = P_u [U] + P_{Th} [Th] \qquad 10.31$$

where $P_u = 1.19 \times 10^{-13}$ cm^3 STP yr^{-1} μg^{-1}

$P_{Th} = 2.88 \times 10^{-14}$ cm^3 STP yr^{-1} μg^{-1}

$[U] = 1.87$ μg g^{-1}

$[Th] = 8.74$ μg g^{-1}

From equation 10.31, $G = 4.74 \times 10^{-13}$ cm^3 STP yr^{-1} g^{-1}

Substituting the value of G into equation 10.30 gives

$$[He] \text{ (or } C_a) \quad 18 \text{ Gt} \qquad 10.32$$

Equation 10.32 is in the same form as equation 10.29. This indicates that ^4He diffusion occurs from the underlay and overlay into the groundwaters of the Nottinghamshire Bunter Sandstone.

10.5. CONCLUSIONS

Determination of the He content of cores and water samples from drill stem tests has enabled evaluation of the partitioning of the He between the water and rock phases for Winterbourne Kingston and Kempsey. Using this information, the residence time of the interstitial water has been calculated. However, correction for diffusion from the confining strata has not been possible and for this reason the calculated ages are maxima.

The age for Winterbourne Kingston was 15.2 million years and for Kempsey 9.5 million years (assuming that all the ^{4}He is present in the water).

Variation of the He content of cores with depth has been related to the predicted variation of the He contents from a simple diffusion model. The two profiles are very different and have been explained by the non-uniformity and non-homogeneity of the sedimentary structure studied and the imprecision of the analytical techniques.

Variation of the ^{4}He content of groundwaters from the Bunter Sandstone with age fit well the predicted behaviour. The diffusion model in this case is a good description of the aquifer and shows that the ^{4}He content of the water is in part derived by diffusion from the aquifer confining strata.

ACKNOWLEDGEMENTS

I would like to thank in particular my supervisor, Dr. J.N. Andrews, for all his help and encouragement during the past four years and the Natural Environment Research council for the research studentship supporting the work. I would also like to thank Drs. W.M. Edmunds and A.H. Bath and Messrs. W.G. Burgess and N. Walton of the Hydrogeology Unit, Institute of Geological Sciences, and Dr. R.L.F. Kay of the School of Chemistry, University of Bath, for their advice and discussions concerning the work and their assistance with the sampling programmes. I would like to thank Dr. J. Acton of the School of Physics, University of Bath for developing the mathematics of diffusion of ^{4}He used in Chapter 10.

I would like to thank the following Water Authorities for granting permission to sample their public water supply boreholes and for their assistance with the sampling programme:

Anglian Water Authority
Severn Trent Water Authority
Wessex Water Authority

I would also like to thank the management of South Crofty, Wheal Jane, Pendarves and Mount Wellington tin mines for giving permission to sample from their mines and for their assistance with the sampling programme. Bath and Bristol city councils are also thanked for assistance with the sampling programme. Finally I would like to thank Dr. P. Fritz, University of Waterloo, Canada, for financing the Stripa sampling programme, assisting with the sampling and useful discussions on the results.

LIST OF REFERENCES

1. GOLDSCHMIDT, V.M., 1958. Geochemistry. Ed. A. Muir, Oxford University Press.

2. RANKAMA, K. and SAHAMA, Th.G., 1950. Geochemistry. University of Chicago Press, London.

3. EVANS, R.D. and GOODMAN, C., 1941. Radioactivity of rocks. Bull. Geol. Soc. Am., 52: 459.

4. SENFTLE, F.E. and KEEVIL, N.B., 1947. Thorium-uranium ratios in the theory of genesis of lead ores. Trans. Am. Geophys. Union, 28, p372.

5. TOMKEIEFF, S.I., 1946. The geochemistry of uranium. Science Progress, 34, p 696.

6. HABERLANDT, H. and HERNEGGER, F., 1947. Uranbestimmungen an glasopalen und anderen mineralien mit hilfe der fluoreszenzanalyse. Sitzber. Akad. Wiss. Wien, Math. -naturw. klasse, IIa, 155, p 359.

7. LOWDER, W.M. and SOLON, L.R., 1956. Background radiation. U.S. AEC Rept. NYO-4712.

8. BELL, K.G., 1954. Uranium and thorium in sedimentary rocks. In: Nuclear Geology, H. Faul (Ed), Wiley, New York.

9. LARSON, E.S. and PHAIR, G., 1954. The distribution of uranium and thorium in igneous rocks. In: Nuclear Geology, H. Faul (Ed), Wiley, New York.

10. JOLY, J.J., 1910. The amonnt of thorium in sedimentary rocks; II: Arenaceous and argillaceous rocks. Phil. Mag. (6), 20, 353-357.

11. MINAMI, K., 1935. Gehalt an seltenen erden in Europaischen und Japanischen tonschiefern [Rare earth content of European and Japanese shales.] Nachr. Ges. Wiss. Gottingen, math.-physix Kl., Fachgruppen IV, 1, 155-170.

12. STOKER, A and KRUGER, P., 1975. Radon measurements in geothermal systems. Stanford University Technical Report No. SGP-TR-4.

13. ANDREWS, J.N. and WOOD, D.F., 1972. Mechanism of radon release in rock matrices and entry into groundwaters. Trans. Inst. Mining Metallurgy, 81, 198-209.

14. SANDERSON, R.T., 1960. Chemical Periodicity. p.32, Reinhold, New York.

15. MOORE, C.E., 1970. Ionization potentials from optical spectra. NSRDS-NBS 34, U.S. Government Printing Office, Washington, DC.

16. PAULING, L., 1960. The nature of the chemical bond. 3rd Ed., p.514, Cornell University Press, Ithaca, New York.

17. YANNOPOULAS, L.N., EDWARDS R.K. and WAHLBECK, P.G., 1965. The thermodynamics of the Yttrium-Hydrogen System. J. Chem. Phys., 69, 2510.

18. REMY, H., 1956. Treatise on inorganic chemistry, Vol. I, p. 237, Elsevier, New York.

19. WIESNER, 1939. Bestimmung der radiumgehaltes von algen. [Determination of the radium content of algae.] Sitzber. Akad. Wiss. Wien., math-naturw. Kl., Abt. IIa, 147, 521-528.

20. BEERS, R.F. and GOODMAN, C., 1944. Distribution of radioactivity in ancient sediments. Bull. Geol. Soc. Amer., 55, 1229-1253.

21. KARTSEV, A.A., TABASARANSKII, Z.A., SUBBOTA, M.I. and MOGILEVSKII, G.A., 1959. Geochemical methods of prospecting and exploration for petroleum in natural gas. (in Russian) English translation, Univ. Calif. Press.

22. MAZOR, E., 1962. Radon and radium content of some Israeli water sources and a hypothesis on underground reservoirs of brines, oils and gases in the rift valley. Geochim. Cosmochim. Acta, 26, 765-786.

23. TANNER, A.B., 1964. Physical and chemical controls on the distribution of ^{226}Ra and ^{222}Rn in groundwater near Great Salt Lake, Utah. In: Adams and Lowder (Eds), The Natural Radiation Environment, Univ. Chicago Press.

24. KENNY, A.W., CROOKS, R.N. and KERR, J.R.W., 1966. Radium, radon and daughter products in certain drinking waters in Great Britain. J. Inst. Water Eng., 20, 123-134.

25. ANDREWS, J.N. and WOOD, D.F., 1974. Radium-226, radon-222 and lead-210 in Bath thermal springs compared with some environmental waters. Health Physics, 27, 307-310.

26. TANNER, A.B., 1964. Radon migration in the ground: a review. In: Adams and Lowder (Eds), The natural radiation environment, p 161-190, The Univ. Chicago Press.

27. KOVACH, E.M., 1945. Metereological influence upon the radon content of soil gas. Trans. Am. Geophys. Union, 26, 241-248.

28. NORINDER, H., METNIEKS, A. and SIKSNA, R., 1952. Radon content of the air in the soil at Uppsala. Arkiv. Geofysik 1, 571-579.

29. SATTERLEY, J. and MACLENNAN, J.C., 1918. The radioactivity of the natural gases of Canada. Trans. Roy. Soc. Can., Sec.III, 12, 153-160.

30. FAUL, H., GOTT, G.B., MANGER, G.E., MYTTON, J.W. and SAKAKURA, A.Y., 1954. Radon and helium in natural gas. Compt. Rend. 19e Congr. Géol. Intern. Alger., Sec. 9, 339-348.

31. U N, 1958. United Nations comprehensive report of the scientific committee on the effects of atomic radiation.

32. LOCKHART, L.B. Jr., BAUS, R.A., PATTERSON, R.L. Jr., BLIFFORD, I.H. Jr., 1958. Some measurements of the radioactivity of the air during 1957. U.S. Naval Research Lab. Rept. 5208.

33. PANETH, F.A., 1937. Chemical exploration of the stratosphere. Nature, 139, 180.

34. HOLLANDER, J.M., PERLMAN, I. and SEABORG, G.T., 1953. The table of isotopes. Rev. Mod. Phys., 25, 469-651.

35. BOGARD, D.D., 1971. Noble gases in meteorites. U.S. National Report 1967-1971, Fifteenth General Assembly, IUGG.

36. MAZOR, E., HEYMANN, D. and ANDERS, E., 1970. Noble gases in carbonaceous chondrites. Geochim. Cosmochim. Acta, 34, 781-824.

37. FAUL, H., 1954. Nuclear Geology, Wiley, New York.

38. HILL, R.D., 1941. Production of helium-3. Phys, Rev., 69, 671-672.

39. MORRISON, P. and PINE, J., 1955. Radiogenic origin of helium isotopes in rocks. Ann. N.Y. Acad. Sci., 62, 69-92.

40. LIBBY, W.F., 1946. Atmospheric helium-3 and radiocarbon from cosmic radiation. Phys. Rev., 74, 1590-1594.

41. HURLEY, P.M., 1954. The helium age method and the distribution and migration of helium in rocks. In: Nuclear Geology, Faul, H. (Ed), Wiley, New York.

42. HOLMES, A., 1931. Radioactivity and geological time. Physics of the Earth, IV, Nat. Research Council (U.S.) Bull., 80, 124-459.

43. KEEVIL, N.B., 1942. The distribution of helium and radioactivity in rocks, II: Mineral separates from Cape Ann granite. Am. J. Sci., 240, 13-21.

44. GERLING, E.K., 1939. Part taken by close packing of crystals in the diffusion of helium. Compt. rend. acad. sci. U.R.S.S., 24, 274-277.

45. LUPTON, J.E., WEISS, R.F. and CRAIG, H., 1977. Mantle helium in the Red Sea brines. Nature, 266, 244-246.

46. CLARKE, W.B., BEG, M.A. and CRAIG, H., 1969. Excess ^{3}He in the sea: evidence for terrestrial primordial helium. Earth Planet. Sci. Lett., 6, 213.

47. CRAIG, H., CLARKE, W.B. and BEG, M.A., 1975. Excess ^{3}He in deep water of the East Pacific Rise. Earth Planet. Sci. Lett., 26, 125.

48. MAMYRIN, B.A., TOLSTIKHIN, I.N., ANUFRIEV, G.S. and KAMANSKIY, I.L., 1969. Anomalous isotopic composition of helium in volcanic gases D.A.N. SSSR, 184, 1197.

49. MAMYRIN, B.A., TOLSTIKHIN, I.N., ANUFRIEV, G.S. and KAMANSKIY, I.L., 1972. Helium isotopic composition in volcanic gas of Iceland. Geokhimiya, 11, 1396.

50. LUPTON, J.E. and CRAIG, H., 1975. Excess ^{3}He in oceanic basalts: evidence for terrestrial primordial helium. Earth Planet. Sci. Lett. 26, 133.

51. CRAIG, H. and LUPTON, J.E., 1976. Primordial neon, helium and hydrogen in oceanic basalts. Earth Planet. Sci. Lett., 31, 369-385.

52. DYMOND, J. and HOGAN, L. 1973. Noble gas abundance patterns in deep-sea basalts - primordial gases from the mantle. Earth Planet. Sci. Lett., 20, 131.

53. FISHER, D.E., 1974. The planetary primordial component of rare gases in the deep Earth. Geophys. Lett., 1, 161.

54. MACDONALD, G.J.F., 1963. The escape of helium from the Earth's atmosphere. Rev. Geophys. 1, 305-349.

55. BADHWAR, G.D., DENEY, C.L. and KAPLAN, M.F., 1969. Differential energy spectrum of proton, helium nuclei and electron. J. Geophys. Res. 74(3), 744-754.

56. ALDRICH, L.J. and NIER, A.O., 1948. Argon-40 in potassium minerals. Phys. Rev., 74, 876-877.

57. FLEMING, W.H. and THODE, H.G., 1953. Neutron and spontaneous fission in uranium ores. Phys. Rev., 92, 378-382.

58. DAMON, P.E. and KULP, J.L., 1958. Inert gases and the evolution of the atmosphere. Geochim. Cosmochim. Acta, 13, 280-92.

59. SHILLIBEER, H.A. and RUSSELL, R.D., 1955. The argon-40 content of the atmosphere and the age of the Earth. Geochim. Cosmochim. Acta, 8, 16-21.

60. LORD RAYLEIGH, 1939. Nitrogen, argon and neon in the Earth's crust with applications to cosmology. Proc. Roy. Soc. London, A170, 451.

61. WETHERILL, G.W., 1954. Variations in the isotopic abundances of neon and argon extracted from radioactive minerals. Phys. Rev., 96, 679-683.

62. RUSSELL, H.N. and MENZEL, D.H., 1933. The terrestrial abundance of the permanent gases. Proc. Natl. Acad. Sci. U.S., 19, p997.

63. SUESS, H.E., 1949. Abundance of rare gases on Earth and in the Universe. J. Geol., 57, 600-607.

64. MEINZER, O.E., 1923. Occurrence of groundwater in the United States. USGS Water Supply Pap., 489, 1-371.

65. TOLMAN, C.F., 1937. Groundwater. McGraw-Hill, New York.

66. ATKINSON, T.C., 1977. Diffuse flow and conduit flow in limestone terrain in the Mendip Hills, Somerset, Great Britain. J. Hydrol., 35, 93.

67. WILLIAMS, B.P.J., DOWNING, R.A. and LOVELOCK, P.E.R., 1972. Aquifer properties of the Bunter Sandstone in Nottinghamshire, England. Proc. 24th Intl. Geol. Cong., Montreal, Section II, 169.

68. TODD, D.K., 1959. Groundwater hydrology. Wiley, New York.

69. WARD, R.C., 1975. Principles of hydrology, McGraw-Hill, New York, p 183-237.

70. BEAR, J., 1972. Dynamics of fluids in porous media. American Elsevier, New York.

71. WALTON, W.C., 1970. Groundwater resource evaluation. McGraw-Hill, New York.

72. PIPER, A.M., 1944. A graphic procedure in the geochemical interpretation of water analysis. Trans. Am. Geophys. Union, 25, 914-923.

73. TÓTH, J., 1970. A conceptual model of the groundwater regime and the hydrogeological environment. J. Hydrol., 10, 164-176.

74. GARNISH, J.D., 1976. Geothermal energy: the case for research in the United Kingdom. A report prepared for the Department of Energy, Energy Papers Number 9, HMSO, London.

75. EVANS, G.V., OTLET, R.L., DOWNING, R.A., MONKHOUSE, R.A. and RAE, G., 1978. Some problems in the interpretation of isotope measurments in British aquifers. IAEA (UNESCO) Int. Symp. on Isotope Hydrol., Neuherberg, GDR.

76. INGRID, U.O. and KARLÉN, I., 1963. The half-life of ^{14}C and the problems which are encountered in absolute measurements of β-decaying gases. In: Radioactive Dating, IAEA, Vienna.

77. CRAIG, H., 1961. Standard for reporting concentrations of deuterium and oxygen-18 in natural waters. Science, 133, 1833.

78. PAYNE, B.R. and HALEVY, E., 1968. In: Guidebook on nuclear techniques in hydrology, IAEA, Vienna.

79. DAVIS, G.H., 1968. In: Guidebook on nuclear techniques in hydrology, IAEA, Vienna.

80. CRAIG, H., 1966, Isotopic composition of the Red Sea and Salton Sea geothermal brines. Science, 154, 1544-1548.

81. OTLET, R.L., 1979. Tritium concentration of rainfall over the United Kingdom. Personal communication.

82. ANDERSON, E.C. and LIBBY, W.F., 1951, World-wide distribution of natural radiocarbon. Phys. Rev., 81, 64-69.

83. CRAIG, H., 1953. The geochemistry of the stable carbon isotopes. Geochim. Cosmochim. Acta, 3, 53-92.

84. NYDAL, R., 1967. On the transfer of radiocarbon in nature. In: Radioactive dating and methods of low-level counting, IAEA, Vienna.

85. AEGERTER, S.K., LOOSH, H.H. and OESCHGER, H., 1967. Variation in the production of cosmogenic radionuclides. In: Radioactive dating and methods of low-level counting, IAEA, Vienna.

86. FERGUSON, C.W., 1968. Bristlecone pine: science and esthetics. Science, 159, 839-846.

87. PEARSON, F.J. and HANSHAW, B.B., 1970. Sources of dissolved carbonate species in groundwater and their effects on carbon-14 dating. Proc. Symp. Isotop. Hydrol., IAEA, Vienna, 271-286.

88. INGERSON, E. and PEARSON, F.J., 1964. Estimation of age and rate of movement of groundwater by the ^{14}C method. Recent researches in the fields of hydrosphere, atmospheric and nuclear chemistry, Manizen, Tokyo, 263-283.

89. WIGLEY, T.M.L. 1976. Effect of mineral precipitation on isotopic composition and ^{14}C dating of groundwater. Nature, 263, 219-221.

90. REARDON, E.J. and FRITZ, P. 1978. Computer modelling of groundwater ^{13}C and ^{14}C isotope compositions. J. Hydrol., 36, 201-224.

91. PLUMMER, N.L., JONES, B.F. and TRUESDELL, A.H., 1970. WATEQF-F FORTRAN IV Version of WATEQ. U.S. Geol. Surv., Water Res., Invest, 76-13, 61p.

92. MOOK, W.G., 1972. On the reconstruction of the initial ^{14}C of groundwater from the chemical and isotopic composition. Proc. 8th Int. Conf. on Radiocarbon dating, Wellington, p D32-D41.

93. FONTES, J.C. and GARNIER, M.J., 1976. Correction des activites apparent on ^{14}C de cassons dessous-estimation de la vitesse des eaux en nappes captivés. C.R. Réunie Annu. Sci. Terre, Soc. Géol. Fr. Paris (abstr.)

94. HANSHAW, B.B., BACK, W. and RUBIN, M., 1965. Radiocarbon determinations for estimating groundwater flow velocities in central Florida. Science 148, 494-495.

95. KRONFELD, J., GRADSJTAJN, E., MULLER, H.W., RADIN, J., YANIV, A and ZACH, R., 1975. Excess ^{234}U: an aging effect in confined waters. Earth Planet. Sci. Lett., 27, 342-345.

96. OSMOND, J.K., KAUFMAN, M.I. and COWART, J.B., 1974. Mixing volume calculations, sources and aging trends of Floridan aquifer water by uranium isotope methods. Geochim. Cosmochim. Acta, 38, 1083-1100.

97. ANDREWS, J.N. and KAY, R.L.F., 1978. The evolution of enhanced $^{234}U/^{238}U$ activity ratics for dissolved uranium in groundwater dating. Short papers of the 14th Int. Conf., Geochron., Cosmochron., Isotope geol., Colorado, USA, Ed: R.E. Zartman.

98. COWART, J.B. and OSMOND, J.K., 1971. ^{234}U and ^{238}U in the Carrizo Sandstone aquifer of south Texas. IAEA - SM - 182/35, 131-149.

99. KIGOSHI, K., 1971. Alpha-recoil thorium-234: dissolution into water and the uranium-234/uranium-238 disequilibrium in nature. Science, 173, 47-48.

100. OSMOND, J.K. and COWART, J.B., 1976. The theory and uses of natural uranium isotopic variations in hydrology. Atomic Energy Review, 144, 621-679.

101. HECKTER, M., 1934. Radiochemische oberflachenbestimmung an glas. Glastech. Ber., 12, 156-172.

102. DYCK, W. JONASSON, I.R. and HARD, R.F., 1976. Uranium prospecting with ^{222}Rn in frozen terrain. J. Geochem. Expl., 5, 115-127.

103. STOKER, A. and KRUGER, P., 1975. Radon in geothermal reservoirs. Second United Nations Symposium on the development and use of geothermal resources, San Francisco, CA.

104. CHIRKOV, A.M., 1971. ^{222}Rn content in the thermal springs of Kamchatka. Dokl. Acad. Sci. USSR, Earth Sci. Sect., 199, 196-7.

105. ROGERS, A.S., 1956. Applications of radon concentrations to groundwater studies near Salt Lake City and Ogden, Utah. Bull. Geol. Soc. Am., 67, 1781.

106. RUTHERFORD, E., 1906. The mass and velocity of α-particles expelled from radium and actinium. Phil. Mag. (6), 12, 348-371.

107. STRUTT, R.J., 1908. Helium and Radioactivity in rare and common minerals. Proc. Roy. Soc. (London), A80, 572-594.

108. STRUTT, R.J., 1908. The accumulation of helium in geological time. Proc. Roy. Soc. (London), A81, 272-277.

109. KHLOPIN, V.G. and ABIDOV, Sh.A., 1941. Radioactivity and helium content of beryllium, boron and lithium minerals of the USSR. Compt. rend. acad. sci. URSS, 32, 637-640.

110. SCHAEFFER, O.A., 1966. Direct dating of fossils by the He - U method. In: Radioactive dating and methods of low level counting, Monaco, France, Contract AT (30-1) 3029 16p.

111. DAMON, P.E. and GREEN, W.D., 1963. Investigations of the He age dating method by stable isotope dilution technique. Radioactive dating, Vienna, IAEA, 55-71.

112. CLARKE, W.B. and KUGLER, G., 1973. Dissolved helium in groundwater: a possible method for uranium and thorium prospecting. Econ. Geol., 68, 243-251.

113. BULASHEVICH, Yu. P. and BASHORIN, V.N., 1971. Correlation of high helium concentrations in subsurface waters with intersections of disjunctive fractures. Dokl. Acad. Nauk. SSSR, 69, 829-832.

114. NIKONOV, V.F., 1969. Relation of helium to petroleum hydrocarbons Dokl. Acad. Sci. USSR, Earth Sci. Sect., 188, 199-201.

115. ROBERTS, A.A., FRUDMAN, I., DONOVAN, T.J. and DENTON, E.H., 1975. Helium survey, a possible technique for locating geothermal reservoirs. Geophys. Res. Letters, 2, 209-210.

116. MAZOR, E. and FOURNIER, R.O., 1973, More on noble gases in Yellowstone National Park hot waters. Geochim. Cosmochim. Acta, 37, 515-525.

117. MAZOR, E., 1977. Geothermal tracing with atmospheric and radiogenic noble gases. Geothermics, 5, 21-36.

118. MAZOR, E., 1972. Palaeotemperatures and other hydrogeological parameters deduced from noble gases dissolved in groundwaters; Jordon Rift Valley, Israel. Geochim. Cosmochim. Acta, 36, 1321-1336.

119. LUCAS, H.F., 1957. Improved low level alpha scintillation counter for radon. Rev. Sci. Instrum, 28.

120. GALE, N.H., 1967. Development of delayed neutron technique as rapid and precise method for determination of uranium and thorium at trace levels in rocks and minerals, with applications to isotope geochronology. In: Radioactive dating and methods of low level counting. IAEA, Vienna.

121. EDMUNDS, W.M., BATH, A.H. and MILES, D.L., 1980. Hydrogeochemical processes and controls on minor and trace element distribution in a sandstone aquifer. In preparation.

122. LAND, D.H., 1966. Hydrogeology of the Bunter Sandstone in Nottinghamshire Water Supply Pap. Geol. Surv. G.B., Hydrogeol. Rep. No. 1.

123. BATH, A.H., EDMUNDS, W.M. and ANDREWS, J.N., 1978. Palaeoclimatic trends deduced from the hydrochemistry of a triassic sandstone aquifer, U.K. Int. Symp. on Isotope Hydrology, Neuherberg. Pap. IAEA-SM-228/27.

124. FLEISCHER, M. and PARKER, R.L., 1967. Data of geochemistry: composition of the Earth's crust. U.S. Geol. Surv. Prof. Pap. 440-D.

125. ARNOLD, J.H., 1930. A kinetic theory of diffusion in liquid systems. J. Am. Chem. Soc., 52, 3937.

126. SHELBY, J.E., 1972. Helium migration in glass forming oxides. J. Appl. Phys. 43, 3068.

127. van der HAMMEN, T., MAARLEVELD, G.C., VOGEL, J.C. and ZAGWIJN, W.H., 1967. Stratigraph climatic succession and radiocarbon dating of the last glacial in the Netherlands. Geol. Mijnbouw, 46(3), 79.

128. COOPE, G.R., 1977. Fossil Coleopteran assemblages as sensitive indicators of climatic changes during the Devensian (last) cold stage. Philos. Trans. R. Soc. London., Ser. B., 280, 313.

129. HAYS, J.D., IMBRIE, J. and SHACKLETON, N.J., 1976. Variations in the Earth's orbit: pacemaker of the Ice Ages. Science, 194, 1121-1132.

130. SHOTTON, F.W., 1977. The Devensian Stage: its development, limits and substages. Philos. Trans. R. Soc. London., Ser. B., 280, 107.

131. WEST, R.G., 1977. Early and Middle Devensian flora and vegetation. Philos. Trans. R. Soc. London., Ser. B., 280, 229.

132. WATSON, E., 1977. The periglacial environment of Great Britain during the Devensian. Philos. Trans. R. Soc. London., Ser. B., 280, 183.

133. BLACKMAN, G.E., CAESAR, A.A.L., GULLUCK, C.F.W.R., STEERS, J.A. and WORSWICK, G.D.N. (Eds), 1963. The Atlas of Great Britain and N. Ireland. Clarendon, Oxford, p26.

134. DANSGAARD, W., 1964. Stable isotopes in precipitation. Tellus, 16, 436.

135. EDMUNDS, W.M., TAYLOR, B.J. and DOWNING, R.A., 1969. Mineral and thermal waters of the United Kingdom. XXIII Internti Geological Congress, Vol. 18, 139-158.

136. BURGESS, W.G., 1979. Tritium and ^{14}C contents of Norton Malreward groundwater. Personal communication.

137. BURGESS, W.G., EDMUNDS, W.M., ANDREWS, J.N., KAY, R.L.F. and LEE, D.J., 1979. The hydrogeology and hydrochemistry of the thermal water in the Bath - Bristol basin. EEC Contract 084-76-EG (UK).

138. HARRISON, R.K., 1975. With contributions from TRESHAM, A.E., YOUNG, B.R. and LAWSON, R.I. Concretionary concentrations of the rarer elements in permo-triassic redbeds of south-west England. Bull. Geol. Surv. G.B., 52, 1-26.

139. ANDERSON, J., 1977. The origin of the groundwaters derived from the Carboniferous Limestone at Penllyn and Schwyll. Personal Communication.

140. MAZOR, E., and VERHAGEN, B.Th., 1976. Hot springs of Rhodesia: their noble gases isotopic and chemical composition. J. Hydrol., 28, 29-43.

141. EDMUNDS, W.M. 1971. Hydrogeochemistry of groundwaters in the Derbyshire Dome with special reference to trace constituents. NERC. IGS. Report No. 71/7, HMSO.

142. DOWNING, R.A. and WILLIAMS, B.P.J., 1969. The groundwater hydrology of the Lincolnshire Limestone with special reference to groundwater resources. Water Resources Board, Reading, 160p.

143. EDMUNDS, W.M., 1973. Trace element variations across an oxidation-reduction barrier in a limestone aquifer. Proc. Tokyo Symp. Hydrogeochemistry and Biogeochemistry, Vol. 1, Clarke, Washington, DC, 500-526.

144. LAWRENCE, A.R., LLOYD, J.W. and MARSH, J.M., 1976. Hydrochemistry and groundwater mixing in part of the Lincolnshire Limestone aquifer, England. Ground Water, 14(5).

145. DOWNING, R.A., SMITH, D.B., PEARSON, F.J., MONKHOUSE, R.A. and OTLET, R.L., 1976. The age of groundwater in the Lincolnshire Limestone and its relevance to the flow mechanism. J. Hydrol., 33, 201-216.

146. MAZOR, E., KAUFMAN, A. and CARMI, I., 1973. Hammat Gader (Israel): geochemistry of a mixed thermal spring complex. J. Hydrol., 18, 289.

147. DEGRÉMONT, G. 1973. Water treatment handbook. p865.

148. ANGLIAN WATER AUTHORITY 1978. Personal communication.

149. ANDREWS, J.N. and LEE, D.J., 1979. Inert gases in groundwater from the Bunter Sandstone of England as indicators of age and palaeoclimatic trends. J. Hydrol., 41, 233-252.

150. BOTT, M.P.H., DAY, A.A. and MASSON-SMITH, D., 1958. The geological interpretation of gravity and magnetic surveys in Devon and Cornwall. Phil. Trans. R. Soc., 251A, 161-191.

151. BOTT, M.P.H. and SCOTT, P., 1964. Recent geophysical studies in south-west England. In: Present views of some aspects of the geology of Cornwall and Devon, 25-44, Eds. K.F.G. Hosking and G.J. Shrimpton, Royal Geological Society of Cornwall.

152. BOTT, M.P.H., HOLDER, A.P., LONG, R.E. and LUCAS, A.L., 1970. Crustal structure beneath the granites of south-west England. In: Mechanism of igneous intrusion, Eds. G. Newall and N. Rast, Geol. J., Special Issue No. 2, 93-102.

153. HOLDER, A.P. and BOTT, M.P.H., 1971. Crustal structure in the vicinity of south-west England. Geophys. J.R. Astr. Soc., 23, 465-489.

154. TAMMEMAGI, H.Y. and WHEILDON, J., 1974. Terrestrial heat flow and heat generation in south-west England. Geophys. J.R. Astr. Soc., 38, 83-94.

155. ALDERTON, D.M.H. and SHEPPARD, S.M.F., 1977. Chemistry and origin of thermal waters from south-west England. Trans. Inst. Mining Metallurgy, B191-194.

156. BURGESS, W.G.B., 1978. The chemistry of shallow groundwaters from Cornwall, Personal Communication.

157. FRITZ, P., BARKER, J.F., GALE, J.E., ANDREWS, J.N., KAY, R.L.F., LEE, D.J., COWART, J.B., OSMOND, J.K., PAYNE, B.R. and WITHERSPOON, P.K., 1979. Geochemical and isotopic investigations at the Stripa test site (Sweden). Int. Symp. on the Underground Disposal of Radioactive Wastes, IAEA-SM-243/6.

158. ARNÓRSSON, S., JONSSON, J and TOMASSON, J., 1968. General aspects of thermal activity in Iceland. Report of 23rd session Int. Geol. Congr., Czechoslovakia, Academia, Prague, 77-86.

159. BODVARSON, G., 1961. Physical characteristics of natural heat resources in Iceland. U.N. Conference on New Sources of Energy, Vol. 2, Rome.

160. MAZOR, E. and WASSERBURG, G.J., 1965. Helium, neon, argon, krypton and xenon in gas emanations from Yellowstone and Lassen volcanic National Parks. Geochim. Cosmochim. Acta, 29, 443-454.

161. ARNÓRSSON, S., 1978. Major element chemistry of the geothermal sea-water at Reykjanes and Svartsengi, Iceland. Min. Mag., 42, 209-220.

162. ARNÓRSSON, S., GRÖNVOLD, K. and SIGURDSSON, S., 1978. Aquifer chemistry of four high-temperature geothermal systems in Iceland. Geochim. Cosmochim. Acta, 42, 523-536.

163. ARNASON, B., 1977. Hydrothermal systems in Iceland traced by deuterium. Geothermics, 5, 125-151.

164. BOLTWOOD, B.B., 1908. On the radioactivity of uranium minerals. Am. J. Sci., 25, 4th series, 269-298.

165. LIND, S.O. and WHITTEMORE, C.F., 1914. The radium:uranium ratio in carnotites. J. Am. Chem. Soc., 36, 2066-2082.

166. FÖYN, E., 1938 Norske Vid-Akad, Oslo, Skrifter No 4.

167. BARRETTO, P.M.C., 1975. Rn-222 emanation characteristics of rocks and minerals. p129-150 of Radon in uranium mining, Vienna, IAEA. From Panel on radon in uranium mining, Washington, DC, USA. See STI/PUB-391 ; CONF.-7309134.

168. GILETTI, B.J. and KULP, J.L., 1955. Radon leakage from radioactive minerals. Am. Mineralogist, 40, 481-96.

169. JOST, W., 1952. Diffusion in solids, liquids and gases. Academic Press Inc., New York.

170. LOVELOCK, P.E.R., 1977. Aquifer properties of the Permo-Triassic sandstones in the UK. Inst. Geol. Sci. Bull., No. 56.

171. RIDGWAY, K. and TARBUCK, K.J., 1967. The random packing of spheres. Brit. Chem. Eng., 12(3), 384-388.

172. PRICE, M., 1980. Porosities of dry granites. Personal communication, Institute of Hydrology, Oxford.

173. MANAGER, SOUTH CROFTY MINE, CORNWALL, 1978. ^{222}Rn contents of South Crofty mine. Personal Communication.

174. ESFANDIARI, B., 1969. Geochemistry and geology of helium. Norman, Okla.; Univ. Oklahoma, 140p, Thesis.

175. A.E.I., MS10, Operating Instructions.

176. MORRISON, T.J. and JOHNSTONE, N.B., 1954. Solubilities of the inert gases in water. J. Chem. Soc., Part III, 3441-3446.

177. KÖNIG, H., 1963. Über die löslichkeit der edelgase in meerwasser. Z. Naturforsch, 18A, 363-367.

178. WEISS, R.F., 1971. Solubility of helium and neon in water and seawater. J. Chem. Eng. Data, 16, 235-241.

179. BENSON, B.B. and KRAUSE, D.Jr., 1976. Empirical laws for dilute aqueous solutions of non-polar gases. J. Chem. Phys., 64(2), 689-709.

180. DOUGLAS, E., 1964. Solubilities of oxygen, argon and nitrogen in distilled water. J. Phys. Chem., 68, 169.

181. CHEMICAL RUBBER COMPANY, 1965-66. Handbook of chemistry and physics. Vol. 46.

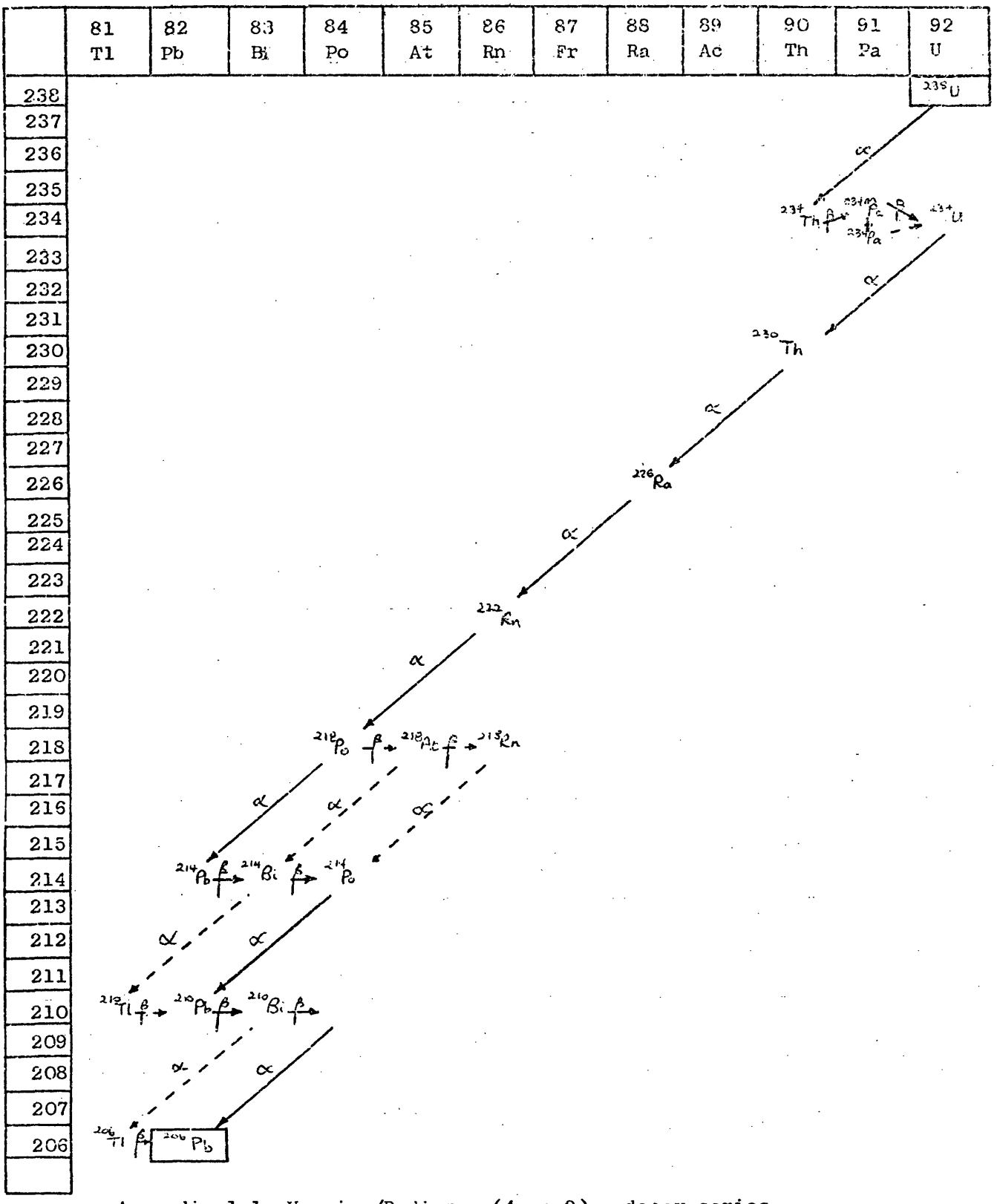

Appendix 1.1 Uranium/Radium - (4n + 2) - decay series.

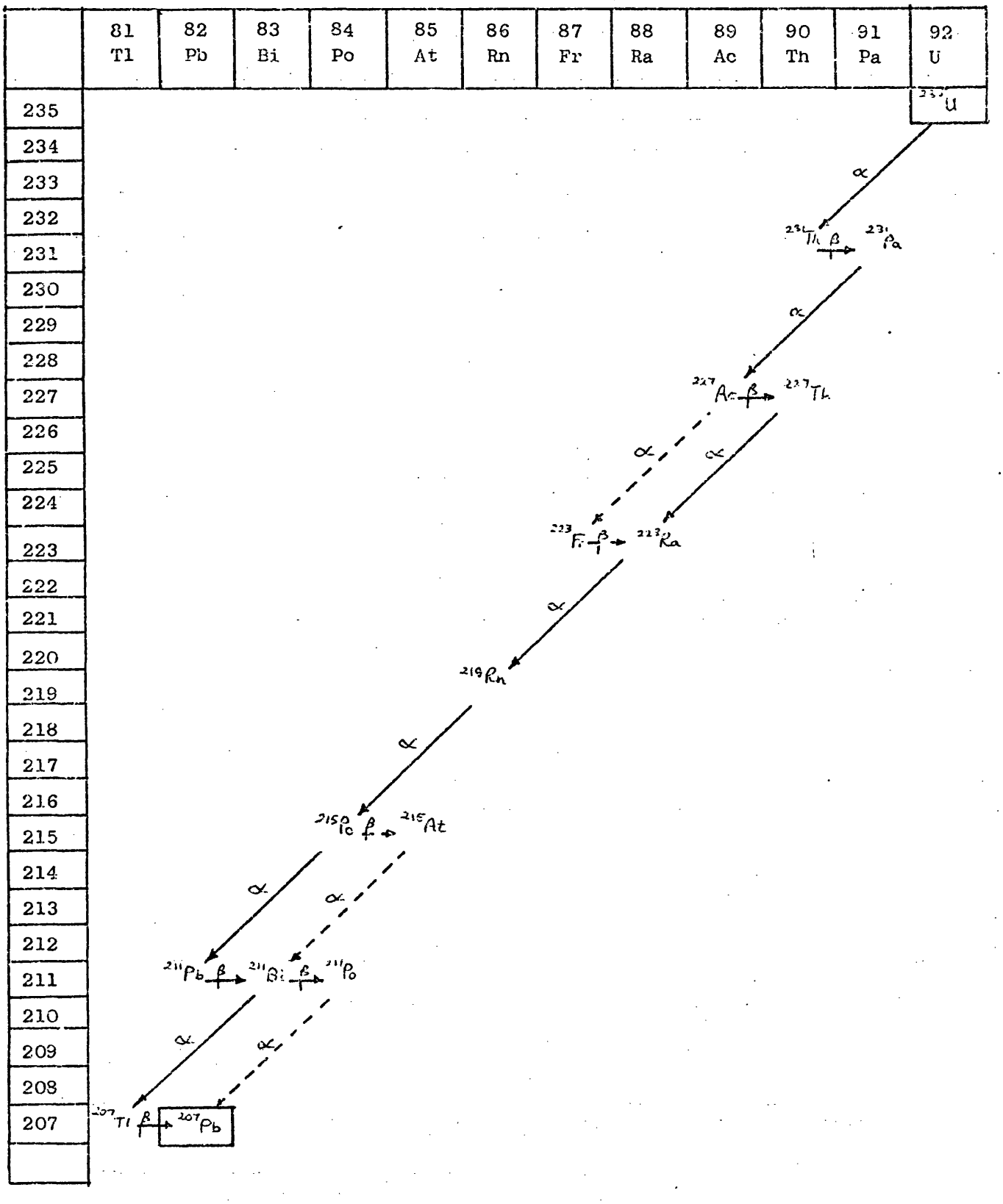

Appendix 1.2 Uranium/Actinium - (4n + 3) - decay series

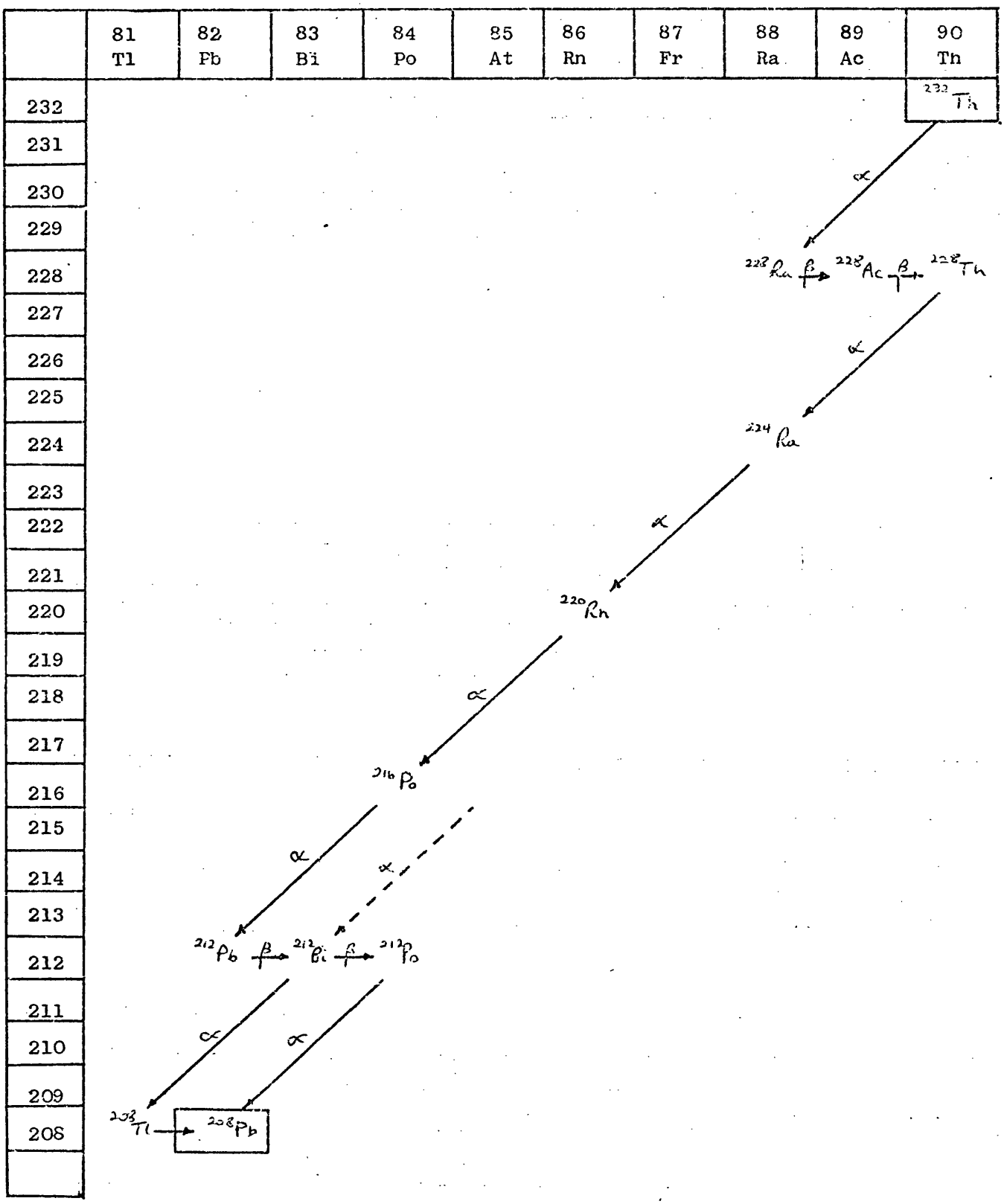

Appendix 1.3. Thorium - (4n) - decay series.

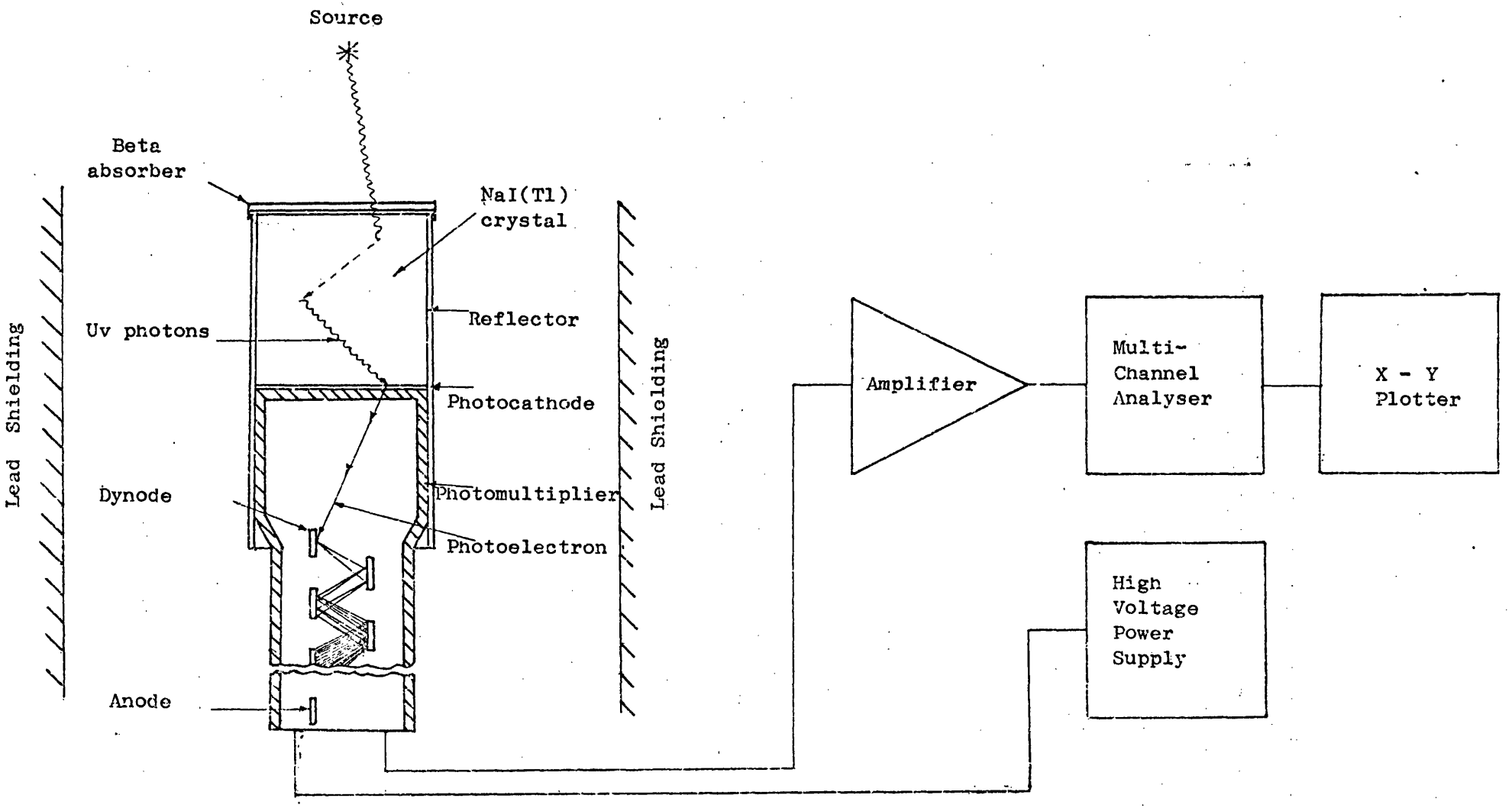

Appendix 2.1.1. Schematic diagram of the NaI(Tl) γ-spectrometer.

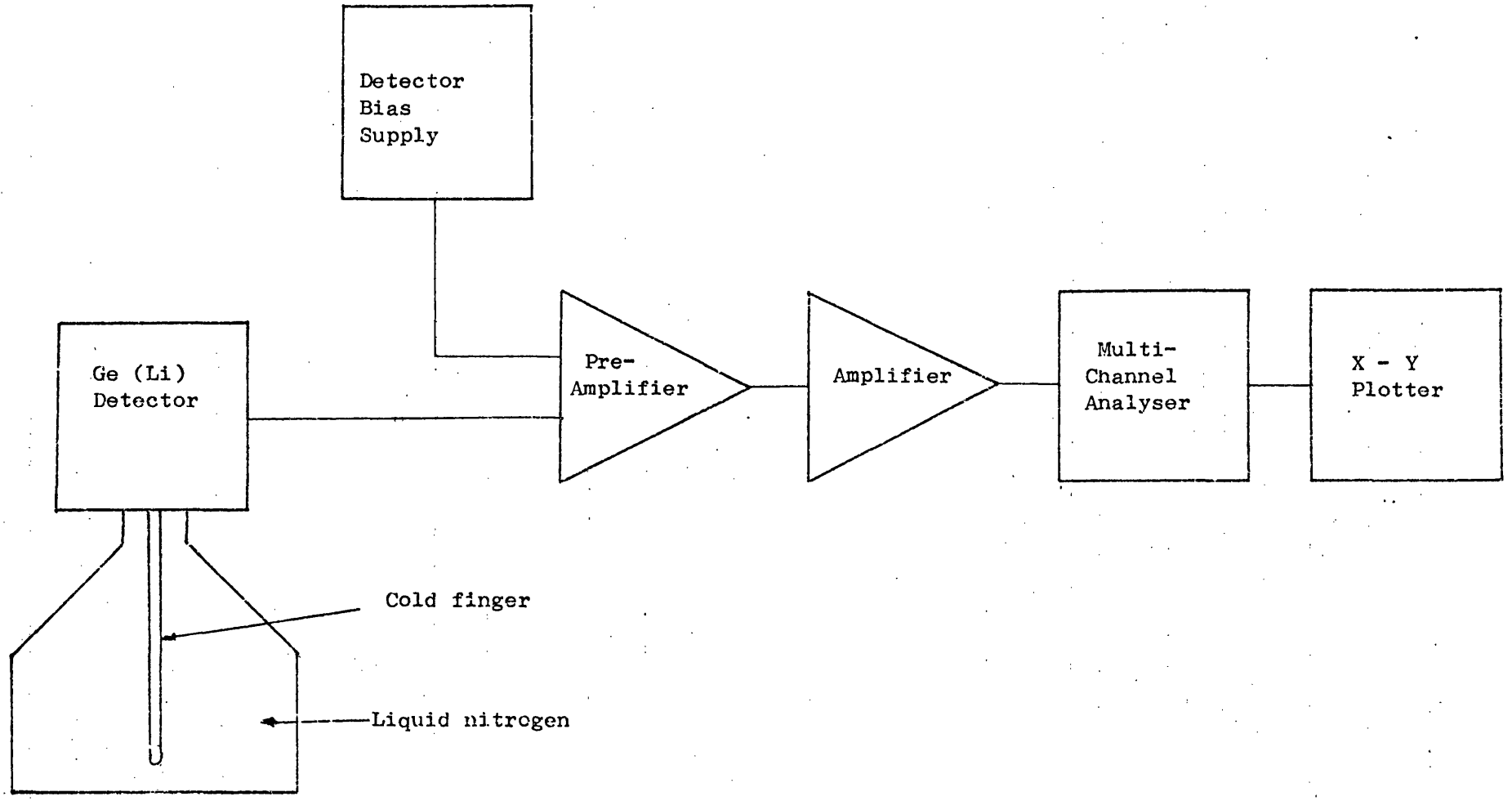

Appendix 2.1.2. Schematic diagram of the Ge(Li) γ-spectrometer.

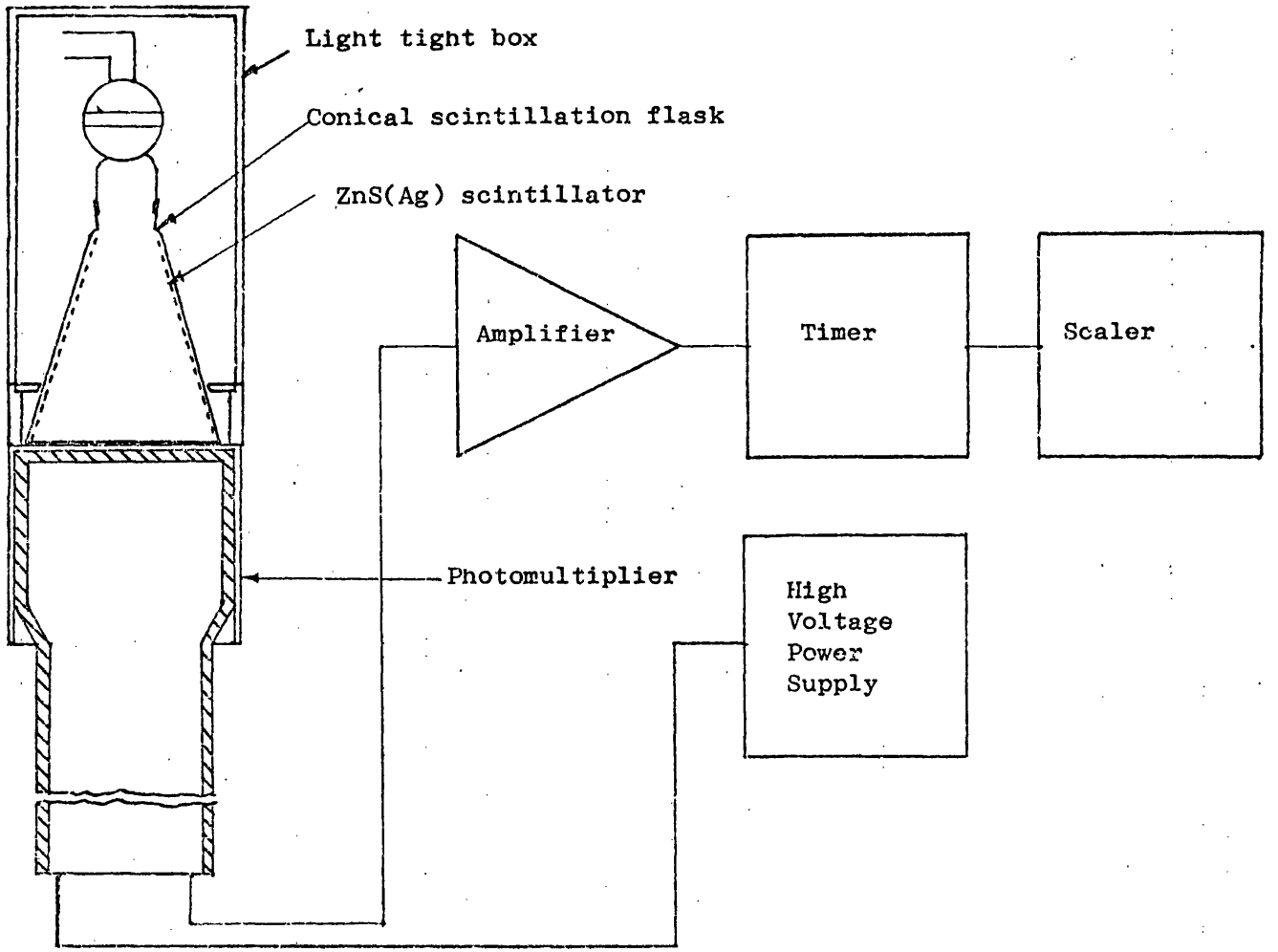

Appendix 2.2. Schematic diagram of the apparatus used for ^{222}Rn determination by α-counting.

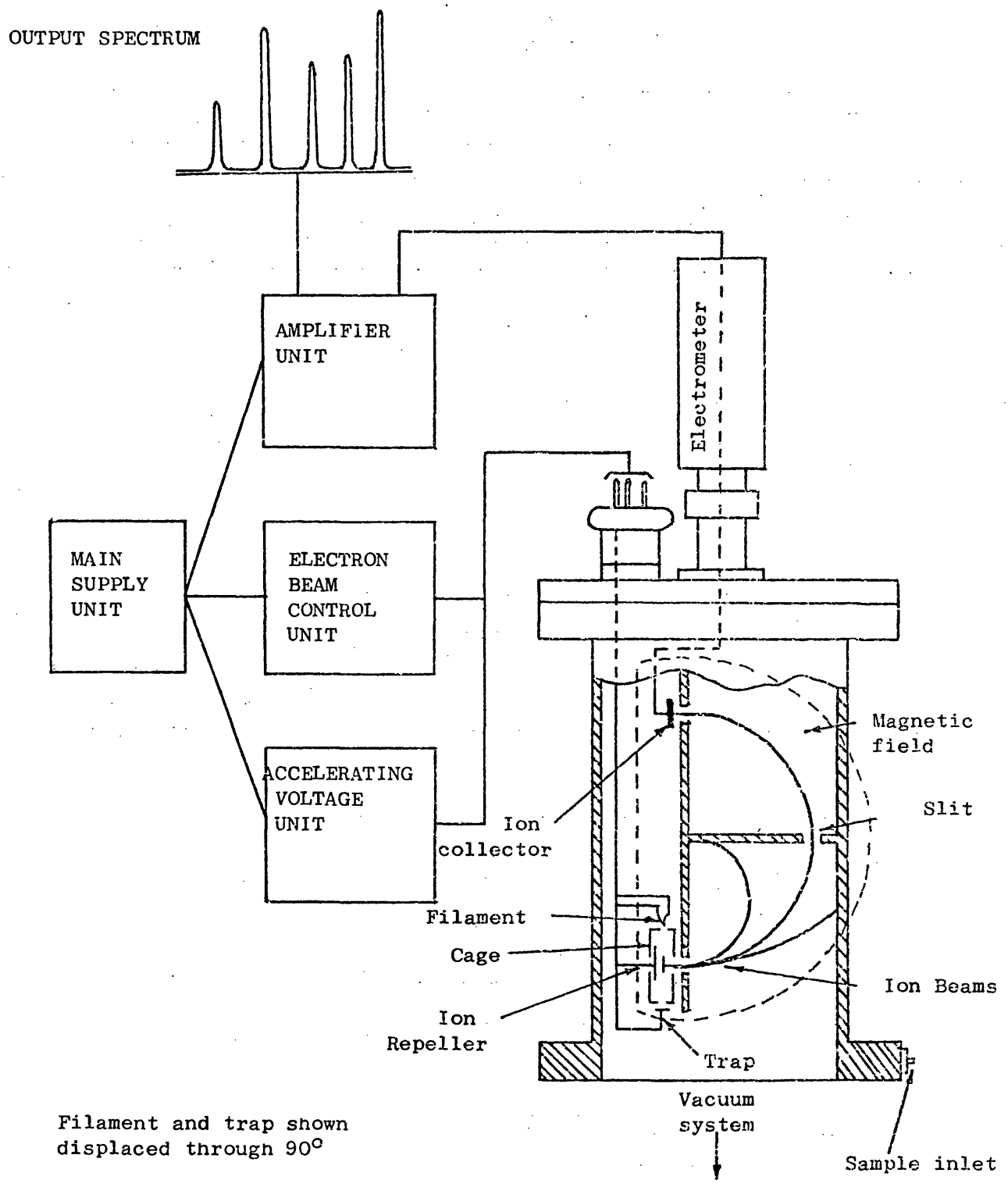

Appendix 3.1. Schematic arrangement of the MS10 Mass Spectrometer.

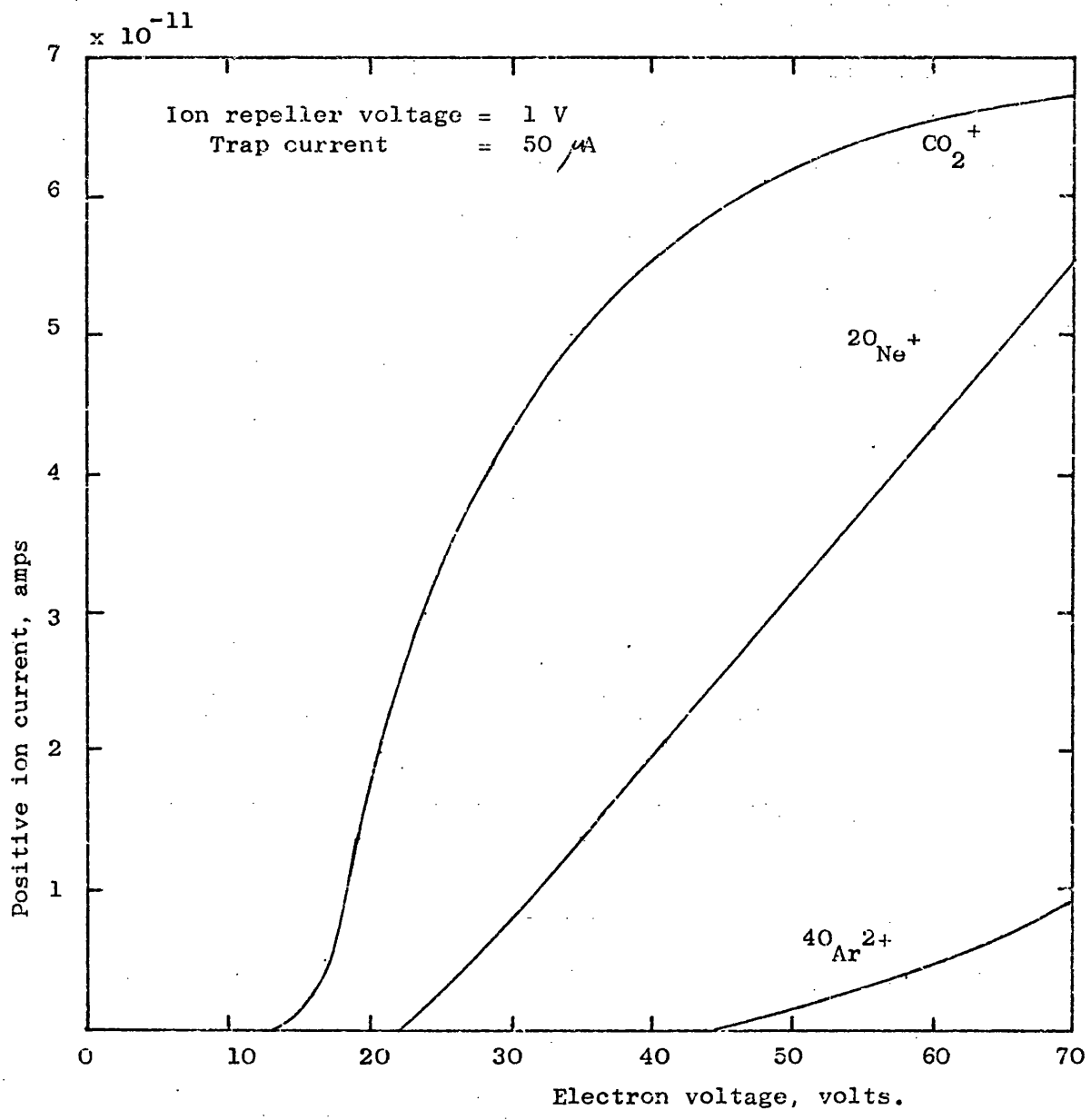

Appendix 3.2. Variation of positive ion current with electron voltage illustrating the difference in ionization potential of $^{40}Ar^{2+}$ and $^{20}Ne^{+}$ 175

Appendix 3.3. Variation in sensitivity (μAmp/torr.) with trap current for the inert gases [175]

Gas	m/e	Trap current				
		10	50	100	150	300
He	40	3.7	17	29	34	40
Ne	20	3.6	14	20	34	58
Ne*	20	0.9	3.6	5.1	8.7	15
Ar	40	16	58	144	280	68
Kr	84	8	40	24	11	-
Xe	-	-	-	-	-	-

All the above sensitivities are for a collector slit width of 0.02" and an electron accelerating voltage of 70V except for Ne* which is for 40V

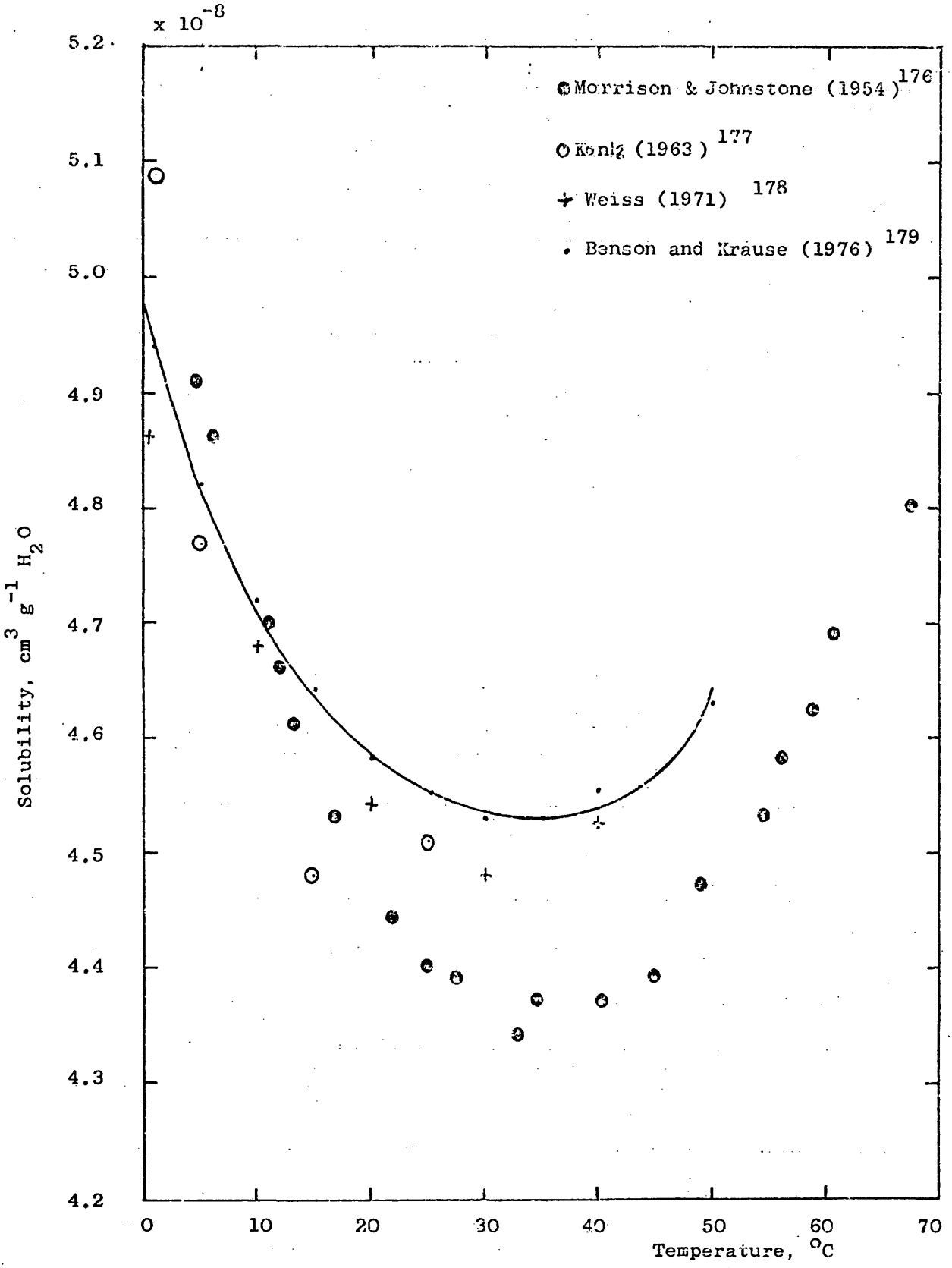

Appendix 4.1. Variation of the fresh water solubility of Ho with temperature at atmospheric partial pressure (5.2×10^{-6} atm.

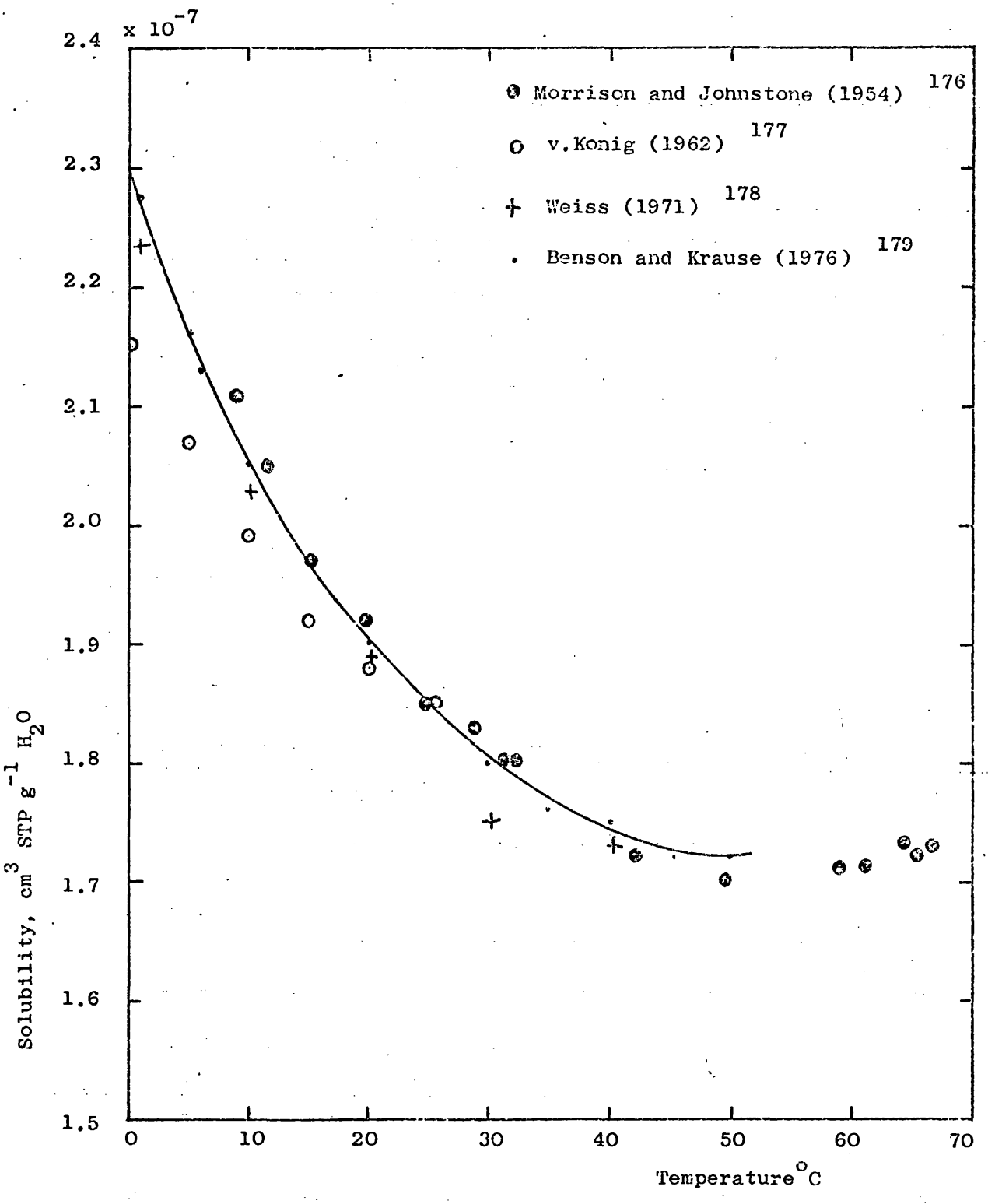

Appendix 4.2. Variation of the fresh water solubility of Ne with temperature at atmospheric partial pressure (1.81×10^{-5} atm.)

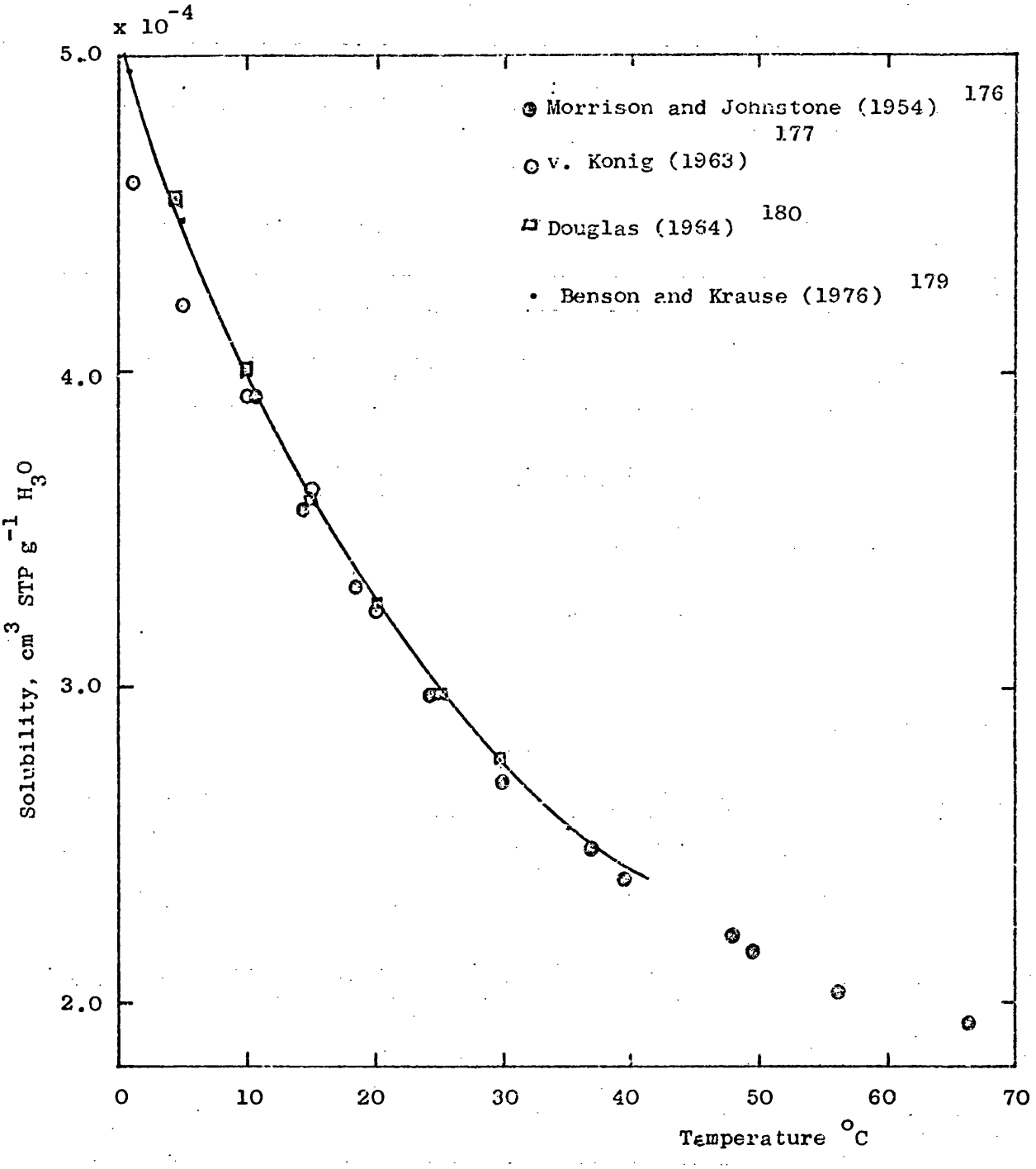

Appendix 4.3 Variation of the fresh water solubility of Ar with temperature at atmospheric partial pressure (9.56×10^{-3} atm.)

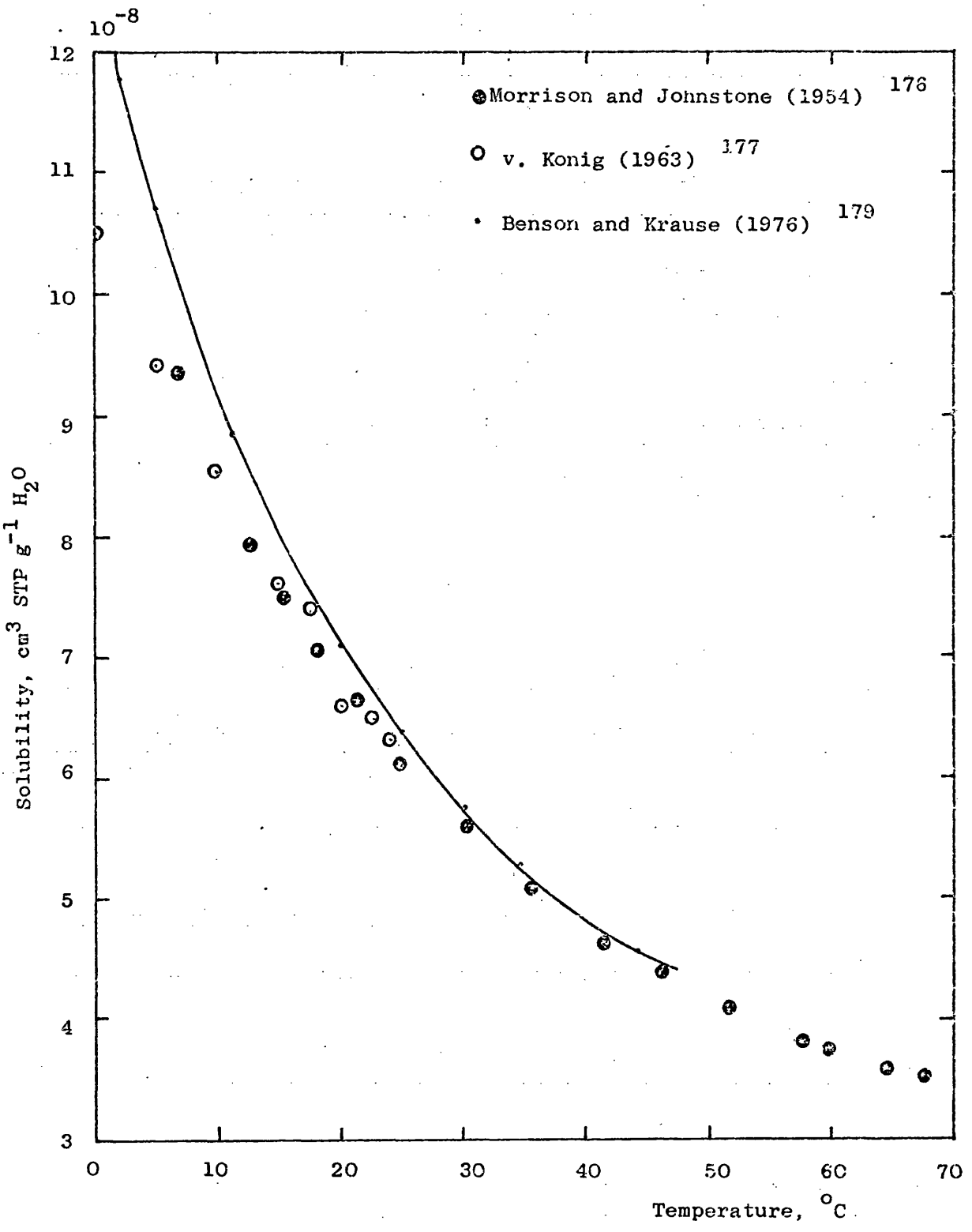

Appendix 4.4 Variation of the fresh water solubility of Kr with temperature at atmospheric partial pressure (1.14×10^{-6} atm.)

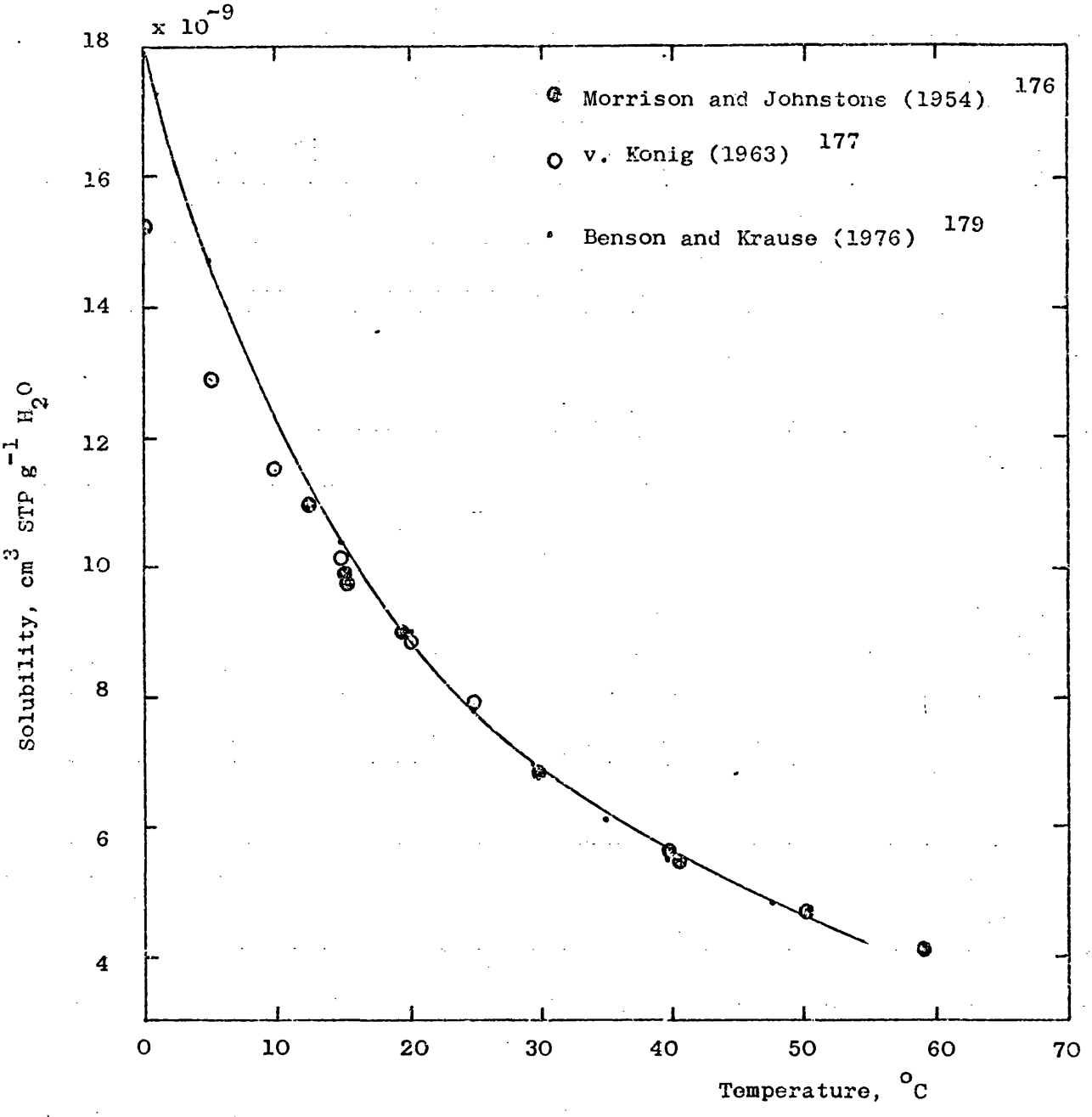

Appendix 4.5. Variation of the fresh water solubility of Xe with temperature at atmospheric partial pressure (8.06×10^{-8} atm.)

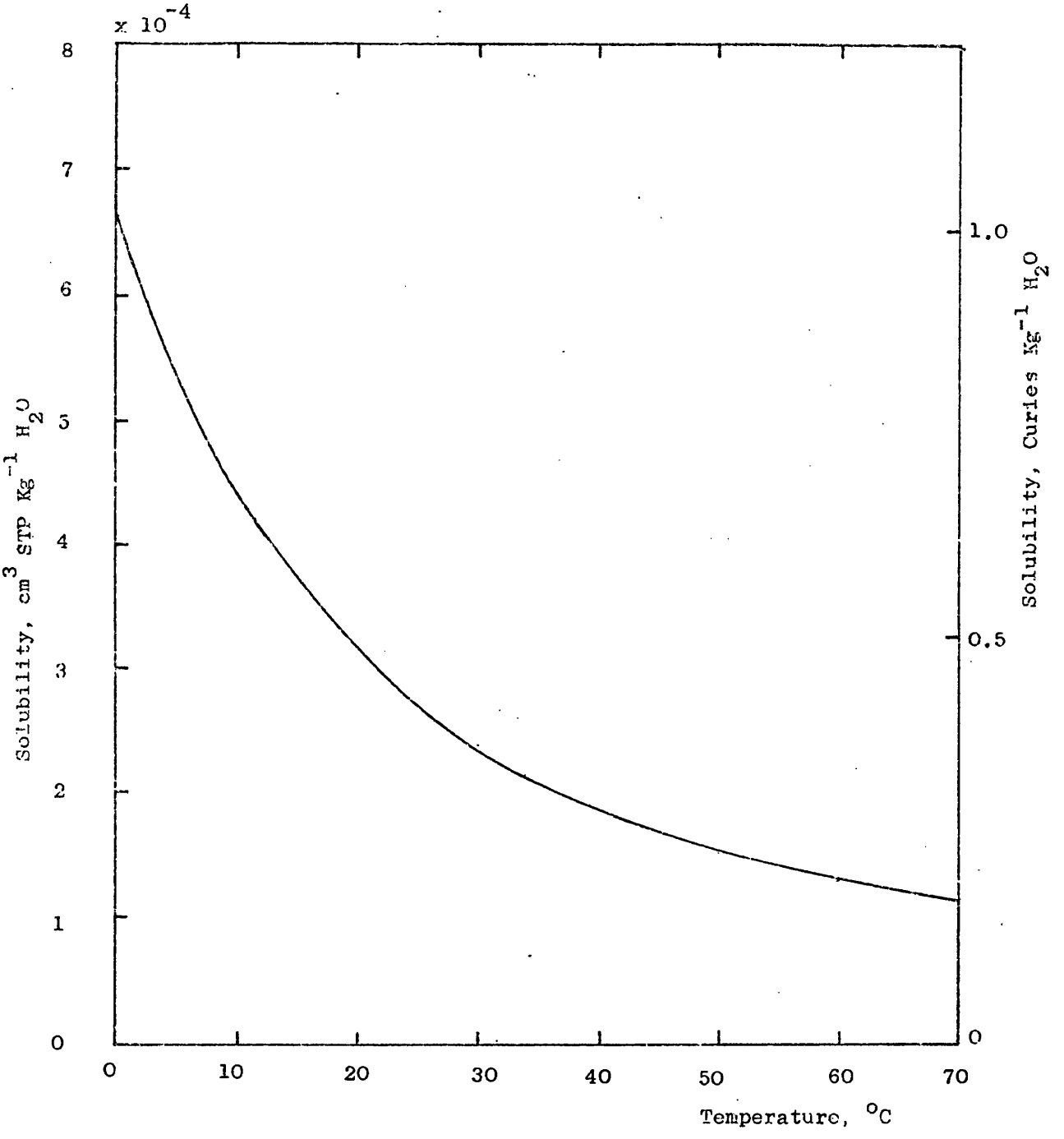

Appendix 4.6 Variation of the fresh water solubility of radon with temperature at one atmosphere partial pressure [181]

APPENDIX 5. Publications

1. Inert gases in groundwater from the Bunter Sandstone of England as indicators of age and palaeoclimatic trends.
John N. Andrews and David J. Lee, 1979 J. Hydrology, 41 233-252

2. Dissolved gases as indicators of groundwater mixing in a Jurassic Limestone aquifer
John N. Andrews and David J. Lee, 1980 Proceedings of the third International Symposium on Water-Rock Interaction, 14-24 July, 1980, Edmonton, Canada.

Journal of Hydrology, 41 (1979) 233—252

[2]

INERT GASES IN GROUNDWATER FROM THE BUNTER SANDSTONE OF ENGLAND AS INDICATORS OF AGE AND PALAEOCLIMATIC TRENDS

JOHN N. ANDREWS and DAVID J. LEE

School of Chemistry, University of Bath, Bath (Great Britain)

(Received September 22, 1978; revised and accepted December 15, 1978)

ABSTRACT

Andrews, J.N. and Lee, D.J., 1979. Inert gases in groundwater from the Bunter Sandstone of England as indicators of age and palaeoclimatic trends. J. Hydrol, 41: 233—252.

A study of the radiogenic and atmospherically derived inert gases in groundwaters from the Bunter Sandstone aquifer of Nottinghamshire, England, is described. The radiogenic gases, ^{222}Rn and ^{4}He, are derived by decay of the radioelements contained in the aquifer. The relationship between radioelement content of the rock and groundwater ^{222}Rn and ^{4}He contents is discussed. An increase in the dissolved ^{4}He content with groundwater age is demonstrated and correlated with ^{14}C ages. Excess ^{4}He ages calculated from average physical properties and radioelement contents of the aquifer rock are greater than the corrected ^{14}C ages and possible explanations for this are discussed.

The dissolved Ar and Kr contents of the groundwaters indicate their temperature of air equilibration in the unsaturated zone at recharge. The recharge temperatures for groundwaters of age greater than $2 \cdot 10^4$ yr. are 5—7°C lower than those for waters recharged in the last 10^4 yr. This is shown to be consistent with the palaeoclimatic record for England during the late Pleistocene.

INTRODUCTION

The geochemistry of groundwaters from the Bunter (Triassic) Sandstone aquifer of Nottinghamshire has been studied to establish the solution—mineral equilibria, redox and exchange reactions which determine the water composition (Edmunds et al., in prep.) and the outline hydrogeology of the area has been described (Land, 1966). The Bunter Sandstone crops out in the west and is overlain towards the east of the region by younger sediments as shown in Fig. 1. The aquifer dips eastwards at a gradient of about 1 in 50 and in the confined part it is sealed by thick overlying marls (Keuper) and underlying mudstones and marls (Permian). The formation thickness ranges from 100 to 300 m and the base lies at a depth of about 500 m below surface in the extreme east of the area from which groundwaters were sampled. Boreholes in both the outcrop and confined parts of the aquifer are used to

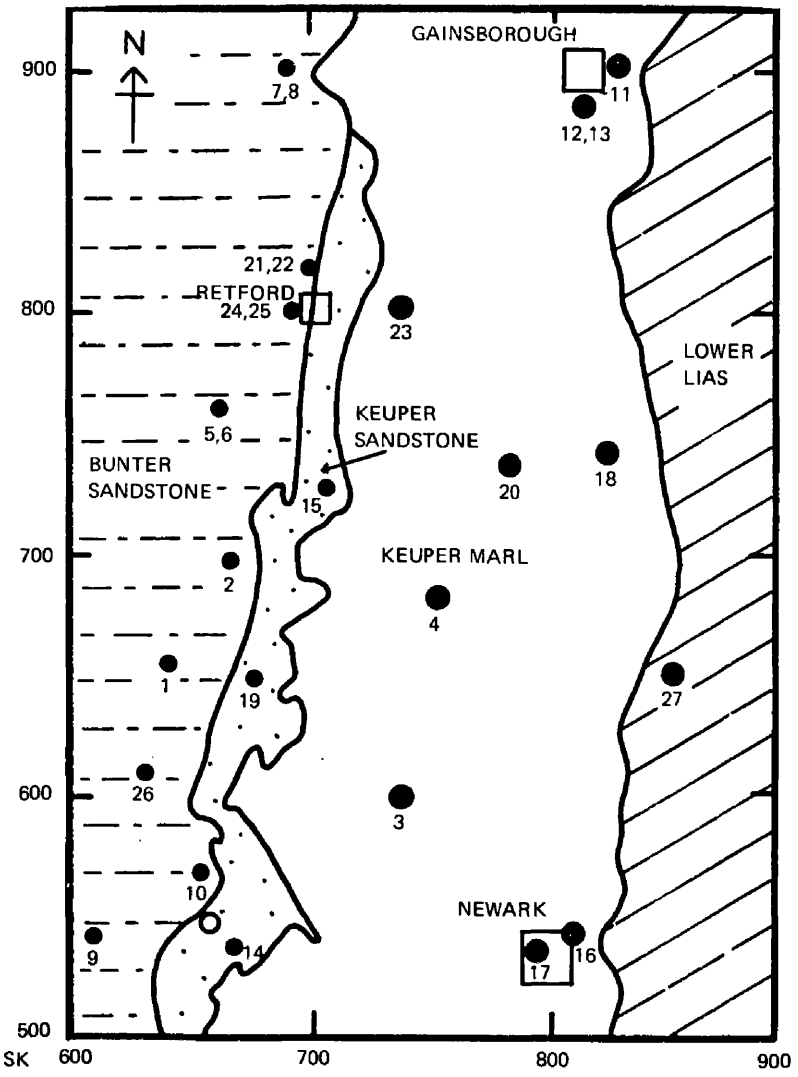

Fig. 1. Location map for sampling sites in Bunter Sandstone showing outcrop geology. (Sites are numbered as in Tables II—IV. Sites indicated by the *larger circles* are in the confined part of the aquifer. The *open circle* is the site of the Newhall borehole.)

provide public water supply in the region. The ^{14}C activity of dissolved bicarbonate in these groundwaters decreases eastwards in the confined aquifer and indicates ages upward of $3 \cdot 10^4$ yr. for water about 30 km from the recharge zone (Bath et al., 1978).

Groundwaters are equilibrated with soil air in the recharge zone and dissolve the stable inert gases in amounts proportional to their solubilities and atmospheric partial pressures. The amounts of such atmosphere derived inert gases in groundwaters are supplemented by radiogenic ^4He arising from decay of U, Th and their daughter products; and by ^{222}Rn which is dissolved as a result of α-recoil on decay of its parent, ^{226}Ra, in mineral surfaces in the aquifer rock (Andrews and Wood, 1972). The radiogenic and atmosphere-derived inert gases have been determined in the Bunter Sandstone groundwaters and their significance is discussed below. The ^{226}Ra in the groundwaters and the radioelement content of the aquifer rock have also been

determined. Variations in the ^{4}He content of the groundwaters are related to the radioelement content of the rock and the west to east groundwater movement and age trend. The stable inert gas contents have enabled palaeo-temperatures to be derived for the soil-air—water equilibration at recharge.

EXPERIMENTAL METHODS

Uranium and thorium analyses

The U and Th contents of Bunter Sandstone core samples from the Newhall Reservoir borehole in the southern part of the aquifer were determined by radioactivation analysis. U was determined by delayed neutron activation analysis (Gale, 1967) at the Atomic Weapons Research Establishment, Aldermaston, under contract. Th was determined by neutron activation based on the 0.31-MeV γ-ray of the 27.0-day half-life ^{233}Pa activation product of ^{232}Th. U and Th were both determined on splits from ca.-250-g core samples which had been crushed to particle size less than 200 μm, using about 5.0 and 0.25 g for the U and Th analyses, respectively. For the Th analyses, the samples were sealed in quartz ampoules and then irradiated in the DIDO reactor at the Atomic Energy Research Establishment, Harwell, in a flux of $6 \cdot 10^{12}$ neutrons cm^{-2} s^{-1} for 2 days. Short-lived radioisotopes were allowed to decay for 2—3 weeks and the 0.31-MeV ^{233}Pa γ-ray was then counted with both NaI(Tl) and Ge(Li) γ-ray spectrometers. The spectrometers were calibrated for the ^{233}Pa γ-ray using Th standards which were irradiated simultaneously with the rock samples.

^{222}Rn and ^{226}Ra determinations

Groundwater samples for Rn and Ra analysis were collected in 20-l glass bottles. Connection to the well head sampling point was made with a rubber hose which was kept below the water surface in the bottle to avoid aeration and consequent ^{222}Rn loss during the collection. ^{222}Rn was determined by outgassing the water samples with ten times their volume of N_2 and adsorbing the ^{222}Rn in the gas stream on a charcoal trap at −80°C. The ^{222}Rn was subsequently desorbed by heating the trap to 200°C whilst under vacuum and was then flushed into an evacuated scintillation flask by slowly admitting a stream of dry air. The scintillation flasks and counting system were calibrated by similarly loading the flasks with ^{222}Rn outgassed from equilibrated ^{226}Ra standard solutions. These solutions were prepared by dissolving a standardised Ra salt (Radiochemical Centre, Amersham) in 0.1 *M* HCl containing some $BaCl_2$ carrier.

The ^{226}Ra contents of the groundwaters were determined on the samples used for ^{222}Rn analysis. Following ^{222}Rn determination, the water samples were further outgassed with ^{222}Rn-free N_2 to ensure that any remaining traces of excess ^{222}Rn were completely removed. The samples were then

stored for a minimum period of 20 days to permit equilibrium between ^{226}Ra and its daughter, ^{222}Rn, to be established. The equilibrium ^{222}Rn was then determined by the same procedure as that used for excess ^{222}Rn determination.

Stable inert gas determinations

Groundwater samples were obtained from sampling points close to the well heads after the wells had been continuously pumped for periods of 12 h or longer to ensure that the samples were representative of the rock—water equilibration in the aquifer. Water from the sampling point was flowed through a glass sample tube in which a 1 cm^3 sample could be isolated between vacuum stopcocks. Connection to the sampling point was made with rubber tubing and the flow was continued until the sample tube was completely free of any air contamination.

For analysis, the tube containing the groundwater sample was sealed with Apiezon® wax to the gas extraction line (Fig. 2) and the system was then evacuated to better than 10^{-5} Torr. A metered volume of isotopically enriched tracers for the inert gases was then admitted to the vacuum system, followed by the water sample. The water was vaporised by warming trap *A* and the water vapor excluded from the remainder of the system by cooling trap *B* with solid CO_2. The gases Ar, Kr and Xe, were then adsorbed on the charcoal trap cooled with liquid N_2. O_2 and N_2 were then removed on the titanium getter heated to 800—900°C by induction. The remaining gases, He and Ne, were then admitted to a 2-in. radius, 180° magnetic deflection mass

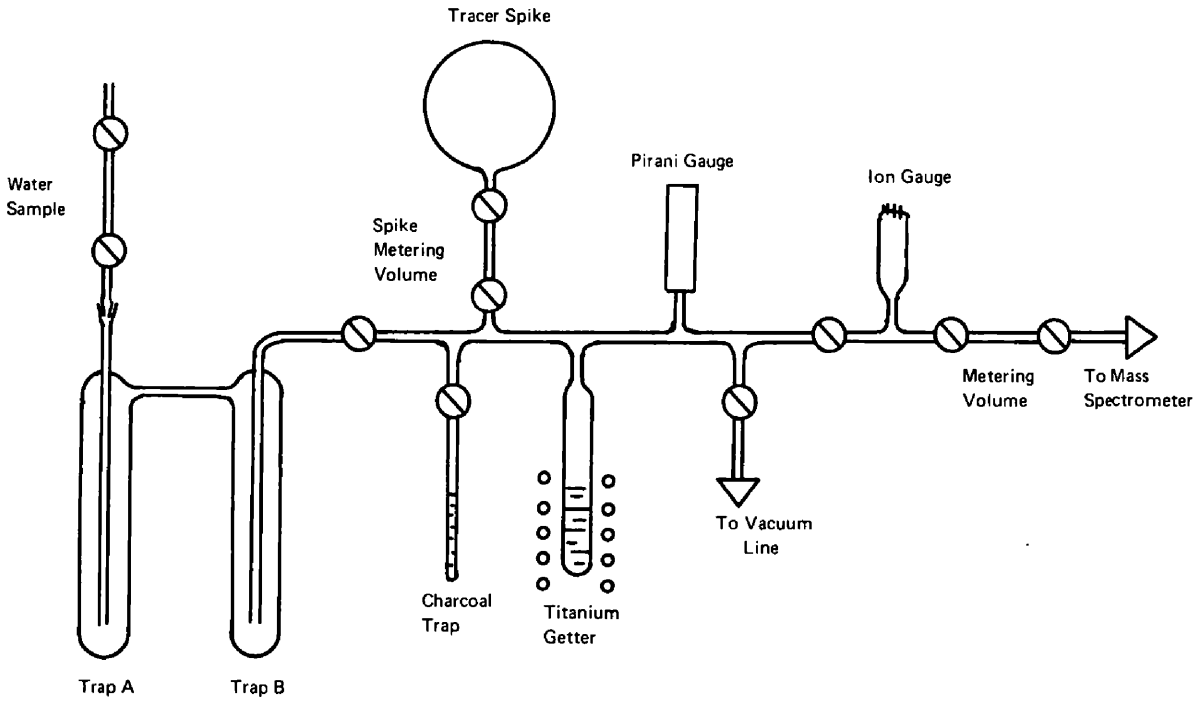

Fig. 2. Schematic diagram of inert-gas extraction line.

spectrometer (Associated Electrical Industries® MS 10) for isotopic ratio analysis. Any residual He and Ne in the extraction line was them pumped away before warming the charcoal trap to −80°C by exchanging the liquid N_2 for a solid CO_2—ethanol refrigerant. The isotopic ratio of the Ar released was then determined by admitting an aliquot of the gas, following removal of N_2 and O_2 by gettering, to the mass spectrometer. Subsequently, the residual Ar in the system was pumped away and Kr and Xe were desorbed from the charcoal trap by heating it to 200°C. The isotopic ratios of these gases were then similarly determined.

The volumes of the inert gases released from the water sample were calculated from the volume of tracer admitted and the change in its isotopic ratios after mixing with the released gases, using the standard relationships for isotopic dilution analysis. The Ne content of water equilibrated with air at 0°C is $2.3 \cdot 10^{-7}$ cm^3 STP/cm^3 H_2O and this is the maximum dissolved Ne content which a groundwater may contain since 0°C is the minimum possible recharge temperature. Samples which contained Ne in excess of this value were considered to contain entrained air in the form of microscopic bubbles. In such cases the inert-gas contents were corrected by subtracting the Ne, Ar and Kr contents of small volumes of air until as close as possible agreement was obtained between the air equilibration temperatures indicated by the corrected contents of these gases. Since the solubility temperature coefficients for these inert gases are different, this procedure leads to a unique solution for the dissolved inert gases in the sample.

RESULTS AND DISCUSSION

Uranium and thorium contents of the Bunter Sandstone

The U and Th contents of core from various depths in the Newhall borehole (Table I) average 1.87 and 8.72 $\mu g\ g^{-1}$, respectively, yielding an average Th/U ratio of 4.7. This value is somewhat higher than the Th/U ratio of 3.5 quoted by Fleischer and Parker (1967) as the average Th/U ratio for various sandstone types. It is also evident from Table I that there is considerable dispersion in the distribution of U and Th at various horizons in the Bunter Sandstone. However, the average U and Th contents of the Newhall borehole cores are the best available estimate for the natural radioelement content of the Bunter Sandstone aquifer.

^{226}Ra and ^{222}Rn contents of groundwaters from the Bunter Sandstone

The ^{226}Ra and ^{222}Rn contents of groundwaters from extraction wells in the locations indicated by Fig. 1, are reported in Table II. The average ^{226}Ra and ^{222}Rn contents are 0.4 and 180 pCi kg^{-1}, respectively. Histograms of the ^{226}Ra and ^{222}Rn distributions are shown in Fig. 3A and C respectively and in Fig. 3B and D probability plots show that these distributions are normal. The

TABLE I

Uranium and thorium contents of core samples from the Newhall borehole (SK 662 546)

Depth (m)	U content ($\mu g\ g^{-1}$)	Th content ($\mu g\ g^{-1}$)	Th/U ratio
6.70	2.12	10.8	5.1
6.95	1.79	11.1	6.2
10.30	2.11	9.0	4.3
39.10	3.47	14.6	4.2
48.40	2.52	9.6	3.8
64.60	1.00	7.7	7.7
65.50*A*	0.98	4.3	4.4
65.50*B*	2.23	7.6	3.4
78.50	1.85	11.4	6.2
135.50	0.93	4.3	4.6
159.40	0.99	4.0	4.0
175.50	1.25	5.5	4.4
186.05	3.04	13.2	4.3
197.00	1.92	9.2	4.8
average	1.87	8.74	4.7

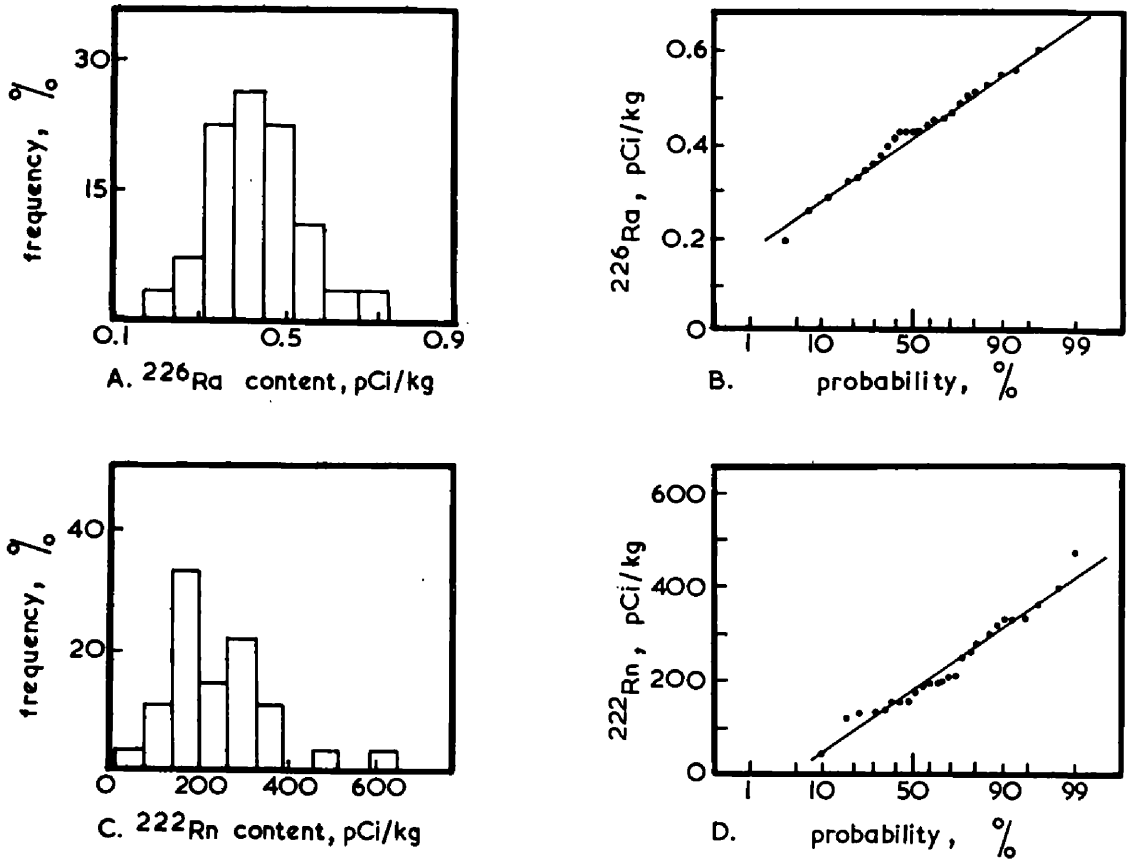

Fig. 3. Histograms of (A) ^{226}Ra distribution and (C) ^{222}Rn distribution in groundwaters from the Bunter Sandstone. Cumulative frequency—probability plots for these distributions are shown in (B) and (D), respectively.

TABLE II

^{226}Ra and ^{222}Rn contents of Bunter Sandstone groundwaters

Site	Location	National Grid reference	^{226}Ra content (pCi kg^{-1})	^{222}Rn content (pCi kg^{-1})
1	Amen Corner, No. 1	SK 642 655	0.36	329
2	Boughton, No. 2	SK 669 697	0.32	282
3	Caunton	SK 739 600	0.44	46
4	Egmanton, B.P.	SK 754 682	0.20	247
5	Elkesley, No. 5	SK 664 760	0.26	133
6	Elkesley, No. 6	SK 664 760	0.33	121
7	Everton, No. 1	SK 692 902	0.52	148
8	Everton, No. 3	SK 694 901	0.60	195
9	Far Baulker, No. 3	SK 612 543	0.38	192
10	Farnsfield	SK 656 568	0.32	266
11	Gainsborough, B.P.	SK 832 902	0.43	330
12	Gainsborough, Humble Carr	SK 818 883	0.43	155
13	Gainsborough, Lea Road No. 3	SK 816 889	0.42	187
14	Halam, No. 1	SK 670 537	0.66	354
15	Markham Clinton, No. 1	SK 711 727	0.35	300
16	Newark, British Gypsum	SK 812 542	0.47	130
17	Newark, Castle Brewery	SK 798 536	0.46	280
18	Newton, No. 2	SK 826 742	0.42	153
19	Ompton, No. 2	SK 678 648	0.53	477
20	Rampton	SK 776 776	0.29	206
21	Retford, Clark's No. 1	SK 703 819	0.46	320
22	Retford, Clark's No. 2	SK 703 819	0.56	608
23	Retford, Grove No. 2	SK 740 803	0.51	211
24	Retford, Ordsall No. 1	SK 695 801	0.55	141
25	Retford, Whisker Hill	SK 692 800	0.49	332
26	Rufford, No. 3	SK 632 610	0.43	392
27	South Scarle	SK 856 650	0.24	191

^{222}Rn contents are considerably in excess of the ^{226}Ra contents, as is generally observed for groundwaters.

The ^{222}Rn content of interstitial water is related to the U content of the host rock by the equation:

$$[\mathrm{Rn}] = 0.33 A \rho \phi^{-1} [\mathrm{U}] [1 - \exp(-\lambda t)] \quad (1)$$

where

[Rn]	=	^{222}Rn content of the water	(pCi cm^{-3})
[U]	=	U content of the host rock	(μg g^{-1})
ρ	=	bulk density of the rock	(g cm^{-3})
ϕ	=	fractional porosity	
A	=	fractional efficiency of ^{222}Rn release	
λ	=	decay constant for ^{222}Rn	
t	=	residence time of the interstitial water	

Provided that the residence time of the pore water is greater than 25 days, and this is certainly the case for the groundwaters under discussion, the exponential term, $[1 - \exp(-\lambda t)]$, approaches unity and the ^{222}Rn content of the water extracted from a well is effectively determined by that part of the aquifer through which it moved during the 25 days immediately prior to extraction. The efficiency of ^{222}Rn release, A, is largely controlled by the extent of the rock—water interface, that is, by the internal surface area of the pore system. Its value can be determined by laboratory experiments in which the efficiency of ^{222}Rn release from sized rock fragments is measured (Andrews and Wood, 1972), or it may be calculated from the average U content of the aquifer rock and the average groundwater ^{222}Rn content. The mode of the ^{222}Rn content distribution for the Bunter Sandstone groundwaters is 180 pCi kg^{-1} and the average primary porosity of the rock is 0.3 (Lovelock, 1977) with a corresponding bulk dry density of 2.15 g cm^{-3}. Substituting these values and the average U content into eq. 1 gives a value of 0.04 for A. This may be compared with a value of 0.03 for the Old Red (Devonian) Sandstone groundwaters from Somerset, England. Higher efficiencies for ^{222}Rn release are found for small grained uncemented sands such as the Midford Sands (Liassic) for which $A = 0.17$. Much lower efficiencies occur for groundwaters from aquifers of much lower primary porosity such as the Carboniferous Limestone ($A = 0.002$).

The variation in the ^{222}Rn contents of the Bunter Sandstone groundwaters may be attributed to aquifer variability around the extraction points. Since the ^{222}Rn content of the water extracted is determined by the rock—water interaction during the last 20 days of its residence in the aquifer, the localised aquifer parameters close to the extraction boreholes will control ^{222}Rn contents. On the assumption that the entire yield is due to intergranular flow, a well which penetrates 100 m into an aquifer of porosity 0.3 can derive all the water required to maintain a flow of 10^4 m^3 day^{-1} for 25 days, from within a radius of about 50 m from the bore. The ^{222}Rn in the extracted water is therefore determined within this distance of the well, although the influence of such extraction rates on the piezometric surface may extend to much greater distances. ^{222}Rn may be transported from greater distances by fissure flow but since ^{222}Rn solution in fissures is small because of the low ratio of rock surface to water, the ^{222}Rn content of water which has travelled long distances by fissure flow is likely to be small and would be even further reduced by decay during transport in the fissure system. The ^{222}Rn content of a groundwater is thus a useful indicator of aquifer variation, the important variables which may influence it being the porosity and grain size distribution of the rock, its radioelement content and the relative importance of intergranular and fissure flow.

Radiogenic ^4He in groundwaters from the Bunter Sandstone

The atmosphere contains 5.239 ± 0.004 ppm He by volume (Glückauf, 1946; Kockarts, 1973). This is mainly radiogenic ^4He with the addition of a

very small quantity of cosmic-ray-produced ^{3}He. He escapes the earth's gravitational field in the upper atmosphere and the amount present in the lower atmosphere represents a balance between crustal outgassing of ^{4}He and loss to space. The rate of production of radiogenic ^{4}He in the earth's crust is $1.02 \cdot 10^{13}$ cm^3 yr.$^{-1}$ based on the crustal model of Shillibeer and Russell (1955) and the average U and Th contents of granitic and basaltic rocks. The total He content of the atmosphere is $2.075 \cdot 10^{19}$ cm^3 so that the minimum residence time for He in the atmosphere is about $2 \cdot 10^6$ yr. if all the crustal He production is released. However, Hurley (1954) showed that many minerals have high He retentions over periods as long as $3 \cdot 10^8$ yr. It is therefore likely that much of the radiogenic ^{4}He in crustal rocks is not rapidly lost by diffusion processes and that the atmospheric He residence time is much longer than the minimum time estimated above.

Naughton et al. (1973) estimated the He flux from the earth's mantle to be $6 \cdot 10^{11}$ cm^3 yr.$^{-1}$. This represents a loss of 17.5% of the He produced in the mantle if a composition similar to peridotites is assumed but is only about 5% of the crustal He production rate. It has recently been shown that mantle-derived He is enriched in ^{3}He in comparison with atmospheric and crustal He (Lupton et al., 1977). Mantle He must therefore be, at least partly, of primordial origin. The presence of primordial He in deep crustal rocks and the retention of radiogenic He in minerals for long periods of time indicate that He loss by diffusion processes is often slow compared with the circulation times of shallow groundwaters. Such groundwaters may therefore be expected to accumulate radiogenic He as they migrate in the pore spaces of an aquifer.

U and Th are generally in equilibrium with their decay products when they are associated with formations more than a few million years old. The ^{4}He production rates for the U and Th series in radioactive equilibrium are $1.19 \cdot 10^{-13}$ cm^3 STP yr.$^{-1}$ μg^{-1} natural U and $2.88 \cdot 10^{-14}$ cm^3 STP yr.$^{-1}$ μg^{-1} natural Th. Assuming that all the ^{4}He generated by radioactive decay in a porous rock is dissolved in the interstitial water, the rate at which the He content of the water increases is given by:

$$^4\text{He solution rate} = \rho \phi^{-1} \{1.19 \cdot 10^{-13} [\text{U}] + 2.88 \cdot 10^{-14} [\text{Th}]\}$$

$$(\text{cm}^3 \text{ STP yr.}^{-1} \text{ cm}^{-3} \text{ H}_2\text{O}) \qquad (2)$$

where [Th] is the Th content of the rock in μg g^{-1} and other symbols have the same meaning as for eq.1. The assumption that all the He generated dissolves in the water is likely to be valid in the case of sandstones since the radioelements are generally concentrated in the cementing phase. The percolating water is in close contact with this phase so that the diffusion path to the water phase is short. Substituting the values for rock density and porosity, and radioelement contents, as discussed earlier for the Bunter Sandstone the following relationship is obtained for the residence time of the

TABLE III

Inert-gas contents and derived palaeotemperatures at recharge for Bunter Sandstone groundwaters

Site	Location	Inert-gas content (cm^3 STP/ cm^3 H_2O)				Paleotemperature (°C)		Collection temperature (°C)
		He ($\times 10^8$)	Ne ($\times 10^7$)	Ar ($\times 10^4$)	Kr ($\times 10^8$)	from Ar	from Kr	
1	Amen Corner, No. 1	4.2	2.09	3.83	9.02	11.9	8.3	9.2
2	Boughton, No. 2	6.2	2.01	4.07	8.71	9.1	9.6	14.3
3	Caunton	3.6	1.84	3.65	7.93	14.0	13.5	10.8
4	Egmanton, B.P.	10.8	2.11	4.07	9.13	9.1	7.9	13.3
5	Elkesley, No. 5	4.3	2.09	4.02	8.68	9.6	9.7	10.0
6	Elkesley, No. 6	4.0	2.09	4.02	8.65	9.6	9.9	10.0
7	Everton, No. 1	4.3	2.07	3.76	8.84	12.7	9.0	10.3
8	Everton, No. 3	4.2	2.05	4.28	9.13	7.2	7.9	10.4
9	Far Baulker, No. 3	4.3	2.09	4.05	8.78	9.3	9.3	9.4
10	Farnsfield	5.1	2.09	4.09	8.70	8.9	9.6	9.6
11	Gainsborough, B.P.	23.7	2.20	4.58	9.85	4.3	4.8	15.8
12	Gainsborough, Humble Carr	27.2	2.18	4.49	10.10	5.1	4.0	17.2
13	Gainsborough, Lea Road No. 3	34.3	2.20	4.52	10.28	4.8	3.4	14.7
14	Halam, No. 1	14.1	2.23	4.15	8.82	8.4	9.1	10.8
15	Markham Clinton, No. 1	4.3	2.09	3.99	8.64	9.9	9.9	12.7
16	Newark, British Gypsum	21.9	2.29	4.86	10.63	1.7	2.2	16.5
17	Newark, Castle Brewery	25.9	2.27	4.78	10.50	2.4	2.7	16.0
18	Newton, No. 2	17.3	2.27	4.72	10.54	3.0	2.5	16.0
19	Ompton, No. 2	7.8	2.12	4.16	9.12	8.3	7.9	10.4
20	Rampton	19.3	2.27	4.68	10.48	3.4	2.7	14.0
21	Retford, Clark's No. 1	7.4	2.09	3.87	8.69	11.4	9.7	10.5
22	Retford, Clark's No. 2	6.5	2.07	3.94	9.14	10.5	7.8	10.7
23	Retford, Grove No. 2	8.4	2.14	4.19	9.13	8.0	7.9	12.7
24	Retford, Ordsall No. 1	3.5	2.09	4.04	8.64	9.4	9.9	11.5
25	Retford, Whisker Hill	4.6	2.08	3.89	8.80	11.1	9.2	10.5
26	Rufford, No. 3	4.9	2.02	3.89	8.74	11.1	9.5	10.3
27	South Scarle	17.6	2.20	4.51	9.96	4.9	4.5	18.8

groundwater:

$$t = 2.95 \cdot 10^{11} \text{ [He]} \quad \text{(yr.)} \tag{3}$$

where [He] is the radiogenic ^{4}He content of the groundwater in excess of that derived from atmosphere equilibration during recharge, expressed in cm^3 STP/cm^3 H_2O. Any contribution to the ^{4}He content due to decay of dissolved U has been neglected since even for an assumed high U concentration of 5 $\mu g\ kg^{-1}$, the ^{4}He generated from this source reaches only 0.01% of that generated within the rock matrix after $5 \cdot 10^4$ yr.

The dissolved inert gas contents of the Bunter Sandstone groundwaters are reported in Table III. The ^{4}He content is plotted against the ^{222}Rn content of the groundwaters in Fig. 4A and it is evident that ^{4}He-rich groundwaters do not correlate with those with high ^{222}Rn contents. The high ^{4}He contents are therefore not due to high radioelement contents or porosity variations in the locality of the extraction boreholes but must arise from a gradual solution of radiogenic ^{4}He as the water moves through a much more extensive part of the aquifer. In Fig. 4B the groundwater ^{4}He content is plotted against the E—W grid reference of the extraction borehole and it may be seen that the high ^{4}He content waters occur in the confined part of the aquifer.

The recharge temperatures of the groundwaters were determined from the inert gases in solution as discussed below. Excess radiogenic ^{4}He contents (the excess of dissolved ^{4}He over the amount dissolved from the atmosphere at the recharge temperature) were then calculated. The excess ^{4}He contents are plotted against the corrected ^{14}C ages (Bath et al., 1978) of the groundwaters in Fig. 5. The excess ^{4}He content increases linearly with increasing groundwater age. Excess radiogenic ^{4}He ages calculated from eq. 3 are compared with the corrected ^{14}C age ranges in Table IV. The ^{4}He ages are generally about double the corrected ^{14}C ages, though the linear correlation with ^{14}C age is goed. ^{4}He ages calculated from eq. 3, however, are very dependent upon both the aquifer radio-element contents and upon its bulk density and average porosity. The radio-element contents used in eq. 3 were determined on core from a single borehole in the southern part of the aquifer and considerable variation was found for samples from various horizons. Clearly, confidence in the numerical factor in eq. 3 can only be improved when much more extensive radio-element analyses for the Bunter Sandstone become available.

It is also possible that part of the calculated ^{4}He age discrepancy arises because of radiogenic ^{4}He diffusion into the aquifer from the upper and lower confining marls. The diffusion coefficient of ^{4}He in water, estimated from the kinetic theory of diffusion in liquids (Arnold, 1930), is of order 10^{-5} $cm^2\ s^{-1}$ whereas in vitreous silica it is of order 10^{-8} $cm^2\ s^{-1}$ (Shelby, 1972). He movement by diffusion will thus be much aided by the presence of water in interconnected pores since the diffusion coefficient in rock-

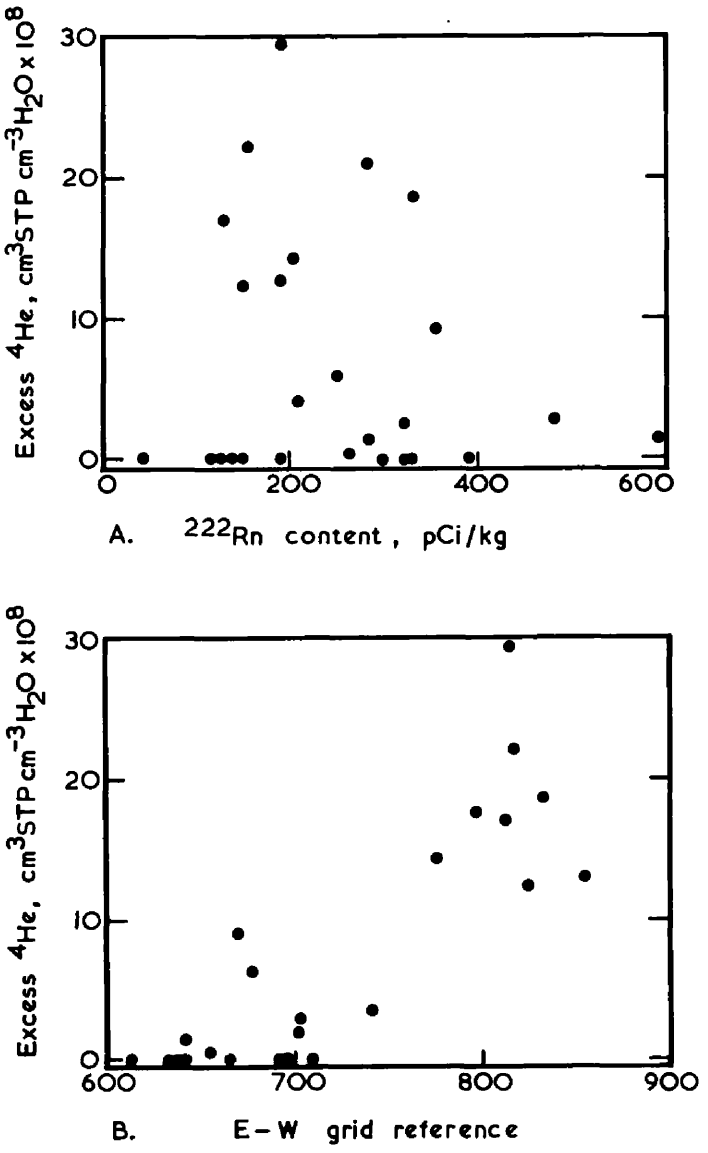

Fig. 4. Excess ^4He contents plotted against ^{222}Rn contents for the Bunter Sandstone groundwaters.
B. Excess ^4He contents plotted against the E—W grid reference of the sample location for Bunter Sandstone groundwaters.

forming silicates is of the same order of magnitude as that in silica. The low-permeability confining marls will therefore act as He diffusion barriers as well as aquifer-confining strata and some of the radiogenic ^4He generated within the marls may diffuse into the aquifer rather than through the marls.

The increase in the ^4He content downdip in the aquifer results in a concentration gradient which would cause ^4He to diffuse updip according to Fick's first law of diffusion:

$$F = -D\,(dC/dX) \tag{4}$$

where F is the rate of He movement in the x-direction, D is the diffusion coefficient of He in water and dC/dx is the He concentration gradient in the

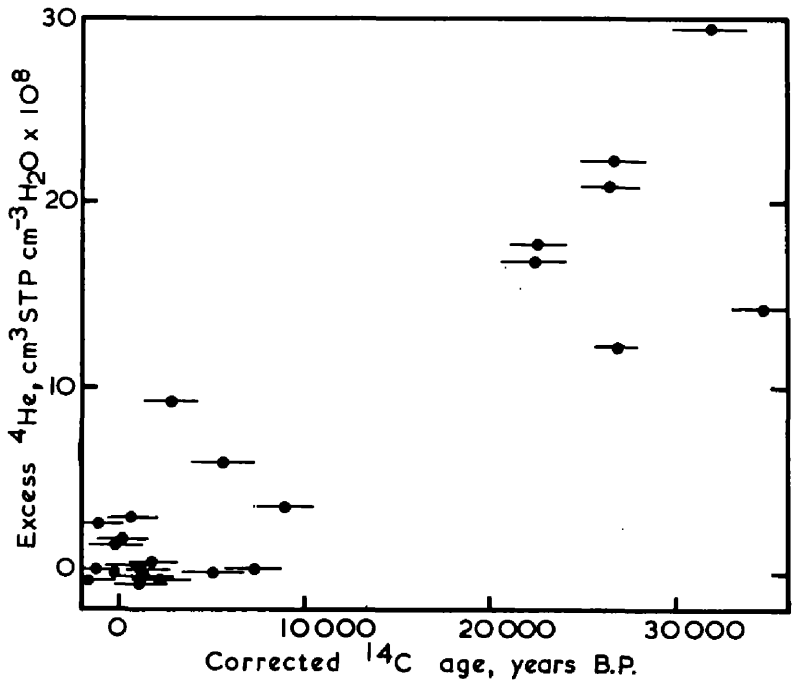

Fig. 5. Excess ^{4}He content of the Bunter Sandstone groundwaters plotted against corrected ^{14}C age ranges.

downdip (x-) direction. From Fig. 4B the He concentration gradient in the downdip direction is $2 \cdot 10^{-13}$ (cm^3 He/cm^3 H_2O) cm^{-1} which yields an updip He diffusion rate of $2 \cdot 10^{-18}$ cm^3 He cm^{-2} s^{-1}. The average rate of water movement downdip, estimated using the ^{14}C ages, is about 40 cm yr.$^{-1}$ and the rate at which He moves downdip due to water transport is about $7 \cdot 10^{-14}$ cm^3 He cm^{-2} s^{-1} in the recharge zone and is greater in the confined zone where the ^{4}He concentration is greater. Since the rate of ^{4}He movement downdip by the transport mechanism greatly exceeds its rate of diffusion in the reverse direction, all the ^{4}He generated in the aquifer will be transported with the groundwater. Any ^{4}He entering the aquifer from the confining marls will similarly be transported and would contribute to enhanced ^{4}He ages.

The rate of upwards diffusion of He may also be shown to be small compared with its rate of transport downdip. In the east of the confined aquifer the base of the Bunter is at 500 m depth and the average vertical ^{4}He concentration gradient, dC/dz, is about $6 \cdot 10^{-12}$ (cm^3 He/cm^3 H_2O) cm^{-1}. This yields an upwards diffusion rate of $6 \cdot 10^{-17}$ cm^3 He cm^{-2} s^{-1} for diffusion through water or $6 \cdot 10^{-20}$ cm^3 He cm^{-2} s^{-1} for diffusion through silicates. The rate of diffusion in the Bunter Sandstone will approximately equal that in water due to the high interconnected porosity of the formation but due to the low permeability of the confining marls the ^{4}He diffusion rate in them will be smaller than in the aquifer. The rate of downdip transport is therefore at least 1000 times as great as the upwards diffusion rate.

It may be concluded that the ^{4}He concentration increases in the confined part of the aquifer with increasing groundwater age. The calculation of groundwater age from excess ^{4}He contents is very dependent upon the aquifer

TABLE IV

Comparison of ^4He ages with corrected ^{14}C age ranges

Site	Location	Excess ^4He (10^8 cm^3 STP/cm^3 H_2O)	^4He age (yr.)	Corrected ^{14}C age (yr.) range*		
				min.	mean	max.
1	Amen Corner, No. 1	0.0	—	−1,800	−100	1,600
2	Boughton, No. 2	1.5	4,400	−1,600	−100	1,400
3	Caunton	0.0	—	5,800	7,350	8,900
4	Egmanton, B.P.	6.0	17,700	4,000	5,650	7,300
5	Elkesley, No. 5	0.0	—	—	—	—
6	Elkesley, No. 6	0.0	—	−3,700	−2,300	−1,000
7	Everton, No. 1	0.0	—	−200	1,250	2,700
8	Everton, No. 3	0.0	—	800	2,450	4,100
9	Far Baulker, No. 3	0.0	—	−2,600	−1,250	100
10	Farnsfield	0.4	1,200	−600	750	2,100
11	Gainsborough, B.P.	18.8	55,450	21,100	22,600	24,100
12	Gainsborough, Humble Carr	22.3	54,800	24,900	26,550	28,200
13	Gainsborough, Lea Road No. 3	29.4	86,700	29,800	31,750	33,700
14	Halam, No. 1	9.3	27,400	1,500	2,900	4,300
15	Markham Clinton, No. 1	0.0	—	3,500	5,150	6,800
16	Newark, British Gypsum	16.9	49,850	20,600	22,400	24,200
17	Newark, Castle Brewery	20.9	61,650	24,900	26,400	27,900
18	Newton, No. 2	12.3	36,300	25,700	26,850	28,000
19	Ompton, No. 2	3.0	8,850	−500	850	2,200
20	Rampton	14.3	42,200	33,000	34,550	36,100
21	Retford, Clark's No. 1	2.7	8,000	−2,900	−1,300	300
22	Retford, Clark's No. 2	1.8	5,300	−1,100	300	1,700
23	Retford, Grove No. 2	3.6	10,600	7,300	8,950	10,600
24	Retford, Ordsall No. 1	0.0	—	40	1,500	3,000
25	Retford, Whisker Hill	0.0	—	500	1,900	3,300
26	Rufford, No. 3	0.2	600	200	1,550	2,900
27	South Scarle	12.7	37,500	—	—	—

*From Bath et al. (1978).

radioelement contents and porosity. Since it is not possible to select single values of these parameters which adequately describe the aquifer and because there is insufficient radioelement concentration data to evaluate the ^4He contribution from the confining marls, the use of ^4He contents to estimate groundwater age must be calibrated against the ^{14}C ages.

Palaeotemperature of recharge derived from inert gas contents

Atmospheric inert gases are equilibrated with water in the soil zone at the time of groundwater recharge. The quantity of dissolved Ar, for example, is given by:

$$[Ar] = s_T P_{Ar} \qquad (cm^3 \text{ STP } cm^{-3} H_2O) \qquad (4)$$

where s_T is the solubility of Ar at 1 atm. pressure and the temperature of recharge, T; and P_{Ar} is the partial pressure of Ar in the atmosphere. Similar relationships apply to the other inert gases. The variation of inert-gas solubilities with temperature has been determined for distilled water (Morrison and Johnstone, 1954; Benson and Krause, 1976). The solubilities in seawater brine are about 20% less than those in pure water (König, 1963) but for low-salinity groundwaters the values will be close to those for distilled water. Recharge temperatures for some thermal waters have been estimated from their inert-gas contents (Mazor, 1972).

Gas solubilities decrease with increasing temperature but any increase in groundwater temperature as the water moves from the soil zone to greater depths in the aquifer will not result in inert-gas exsolution since the increase in hydrostatic pressure maintains the groundwater undersaturated with respect to the gases. It is therefore valid to derive recharge temperatures from inert-gas contents and those for the Bunter Sandstone groundwaters are included in Table III and are plotted against corrected ^{14}C ages in Fig. 6C.

The interruption to recharge indicated by the gap in groundwater ages from about 10^4 to $2 \cdot 10^4$ yr. B.P. may be attributed to the absence of recharge during the last (Devensian) glaciation. The recharge prior to $2 \cdot 10^4$ yr. ago would then have occurred during the climatic improvement in the mid-Pleniglacial interstadials. Palaeotemperature curves for the Pleniglacial are compared with the recharge temperatures derived from inert-gas solubilities in Fig. 6. Both palaeotemperature curves are based on ^{14}C dating of glacial soil horizons and the temperatures derived from pollen counts in the case of The Netherlands (van der Hammen et al., 1967) and from *Coleopteran* assemblages in the case of Britain (Coope, 1977). Although the Pleniglacial interstadials for Britain and continental Europe cannot be precisely correlated, there is broad agreement in the main features of these palaeoclimatic curves. Climatic trends in Britain and Europe would be expected to follow a synchronous pattern as Hays et al. (1976) have shown that glaciation of the northern hemisphere has global effects, ^{18}O enrichment in the Antarctic surface waters, for example, only lagging climatic deterioration by 10^4 yr. due to oceanic

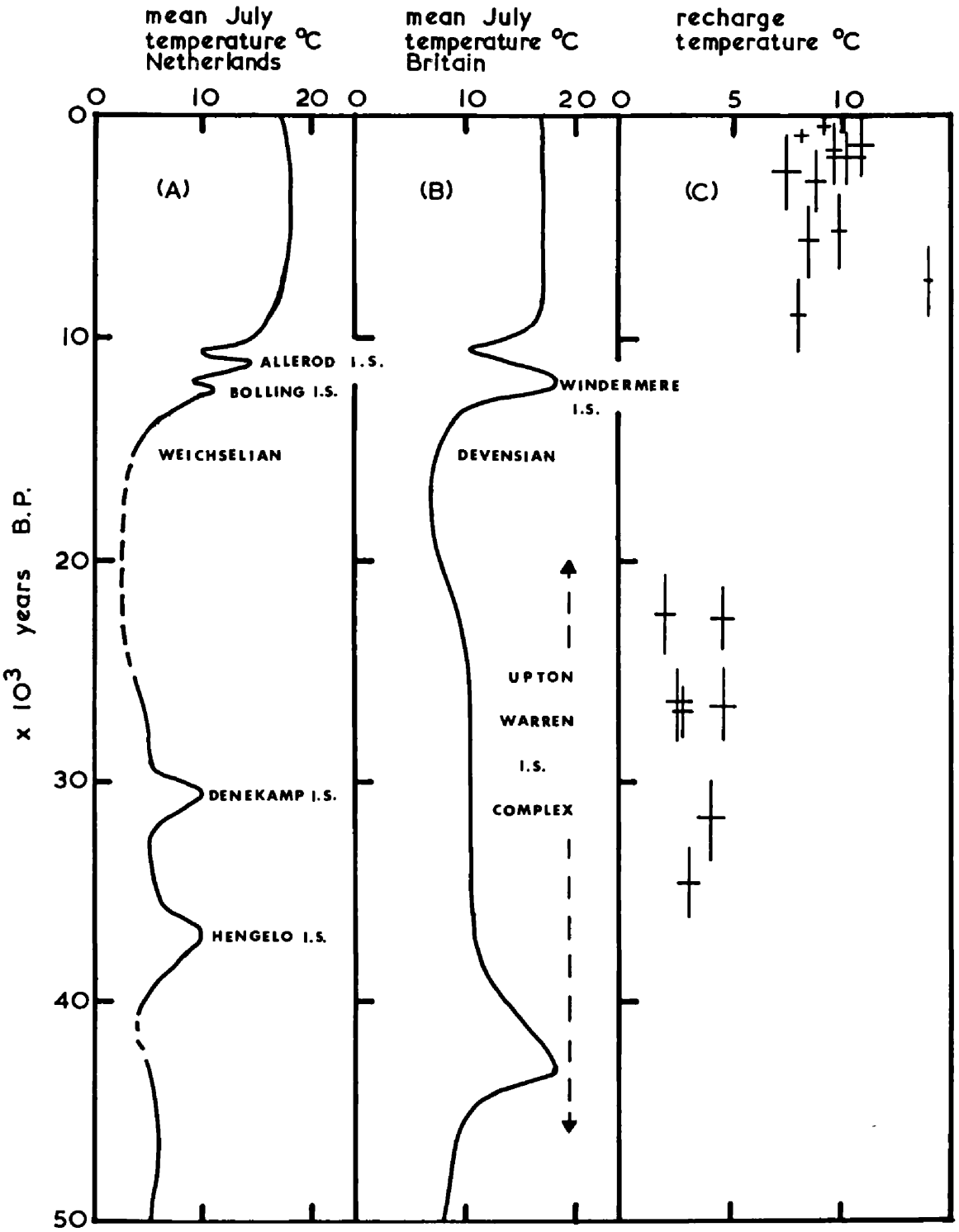

Fig. 6. A. Palaeoclimatic curve for The Netherlands (van der Hammen et al., 1967).
B. Palaeoclimatic curve for Britain (Coope, 1977).
C. Recharge temperatures for the Bunter Sandstone groundwaters plotted against corrected ^{14}C age ranges.

circulation. The climatic improvements following the Devensian glaciation in Britain and the Weichselian glaciation of NW Europe are synchronous and occurred about 14,000 yr. B.P. Climatic deterioration in Britain and The Netherlands following the mid-Pleniglacial interstadials began about 24,000 yr. B.P. In England, "climate deteriorated very rapidly after the Upton Warren Interstadial to become Arctic and eventually to pass to polar desert before the advent of the Late Devensian glaciers" (Shotton, 1977). This glaciation did not cover the southern and central parts of England (West, 1977) but at its maximum advance the climate of central England would have produced a permafrost seal to aquifer recharge. Full polar desert conditions probably existed with mean annual air temperatures at least as low as −16°C (Watson, 1977).

July air temperatures in polar desert/tundra areas in NW America are about 16—21°C higher than mean annual air temperatures (Watson, 1977). If the palaeotemperature curve minimum for the Devensian glaciation (Fig. 6) is reduced by a similar amount the mean annual temperature is about −12°C and corresponds to permafrost conditions. Comparing present-day mean July temperatures and mean annual temperatures for the English Midlands (Blackman et al., 1963) shows that under present climatic conditions mean annual temperatures are about 7°C lower than mean July temperatures. The average annual temperature for the Holocene may therefore be obtained by reducing the July temperatures in Fig. 6B by 7°C, yielding an estimated annual average of about 9°C, in good agreement with the estimated recharge temperatures in this period. Assuming that the July temperatures for the Upton Warren Interstadial may similarly be reduced by about 7°C to yield average annual temperatures, the recharge temperature during the interstadial would have been about 3°C. This is also in good agreement with the recharge temperatures estimated from inert-gas contents.

It may be concluded that the recharge temperature most closely reflects the mean annual temperature. The palaeotemperatures of recharge determined are unsaturated zone temperatures since although rainfall is air equilibrated in the atmosphere, the water must be re-equilibrated with air in the soil zone prior to aquifer recharge. The temperature difference of 5—7°C between the two periods of recharge is in good agreement with the corresponding temperature changes indicated by the climatic record.

A corresponding depletion of the ^{18}O content of recharge during the Upton Warren Interstadial relative to the Holocene recharge has been observed (Bath et al., 1978). The $\delta^{18}O$ decrease corresponds to an air temperature difference of 1—2°C using Dansgaard's (1964) relationship between $\delta^{18}O$ and temperature. A new $\delta^{18}O$—temperature relationship derived for western Europe (Evans et al., 1978) indicates that the observed $\delta^{18}O$ decrease corresponds to a temperature difference between the two recharge periods which is in good agreement with that derived on the basis of inert-gas contents.

CONCLUSIONS

The ^{222}Rn content of a groundwater is dependent upon aquifer characteristics is the locality of the extraction point, even for wells with large extraction rates. The parameters which determine the ^{222}Rn content are the U content of the aquifer rock, its porosity and pore size distribution. The ^{222}Rn content is independent of groundwater residence time provided that this is longer than 25 days. The variability of ^{222}Rn contents for groundwaters from different extraction wells may be used as an indicator of aquifer variability in respect of the parameters which determine the ^{222}Rn content.

The ^{4}He content of groundwater in the confined Bunter Sandstone aquifer generally increases with groundwater age. It is possible, in principle, to calculate the groundwater residence time in the aquifer from its ^{4}He content, the radioelement content of the aquifer rock and its porosity. However, for this purpose it is necessary to select values of these aquifer parameters which adequately represent the average aquifer composition. This requires that extensive radioelement analysis of core material and hydrogeological assessment of the aquifer be carried out. The possibility of ^{4}He generated in the confining strata contributing to the radiogenic ^{4}He in the groundwater must also be considered and radioelement, porosity and permeability measurements on these strata are also necessary to establish the importance of this effect. In the absence of sufficient data to enable ^{4}He ages to be calculated with reasonable certainty, the increase in the ^{4}He content may be correlated with ^{14}C groundwater ages. The ages of groundwaters from the same aquifer which are older than the range of the ^{14}C dating method, may then be determined by extrapolation of the ^{14}C age—^{4}He content relationship.

The atmospheric inert-gas contents of groundwaters from a confined aquifer may be used to establish the ground temperature during recharge. In the case of the Bunter Sandstone groundwaters such derived recharge temperatures have been interpreted in terms of the palaeoclimatic changes for the past $5 \cdot 10^4$ yr.

ACKNOWLEDGEMENTS

This work was supported by a research grant from the Natural Environment Research Council. Drs. W.M. Edmunds and A.H. Bath of the Hydrogeology Unit, Institute of Geological Sciences are thanked for their advice and discussions concerning the work. The Anglian and the Severn Trent Water Authorities are thanked for granting permission to sample their public water supply boreholes and for their assistance with the sampling programme.

A preliminary report on the presence of excess ^{4}He in these groundwaters was presented at the Second International Symposium on Rock—Water Interaction, at Strasbourg, 1977, by one of the authors (J.N.A.).

Dissolved Gases as Indicators of Groundwater Mixing in a Jurassic Limestone Aquifer

John N. Andrews and David J. Lee

School of Chemistry, University of Bath, Bath, BA2 7AY, United Kingdom

The radiogenic ^4He and atmosphere-derived inert gases have been determined in groundwaters from the confined zone of an artesian aquifer in the Lincolnshire Limestone of eastern England. This is a cemented oolitic limestone of Middle Jurassic age with a primary porosity of up to 25 percent but with a fracture porosity of only 0.25 to 0.8 percent (Downing and Williams, 1969). Exploitation of the aquifer for water supply has resulted in an eastwards incursion of rapidly moving fissure water which exchanges with an older interstitially stored water.

The ^4He contents of groundwaters from the artesian zone are plotted in figure 1. Decay of uranium and thorium (and their daughter isotopes) gradually supplements the atmosphere derived ^4He content of the groundwater (4.8×10^{-8} cm^3g^{-1} at 10°C). Such an increase in ^4He content with age has been demonstrated for groundwaters from a Triassic Sandstone in England (Andrews and Lee, 1979) and the maximum ^4He content found was 30×10^{-8} cm^3g^{-1} for a groundwater age of 36,000 years. The ^4He contents of the Lincolnshire Limestone groundwaters are generally much greater, up to 1400×10^{-8} cm^3g^{-1}, implying the presence of a component of considerably greater age. The ^4He isopleths for the aquifer shown in figure 1 may be compared with the chlorinity isopleths given in figure 2. There is a striking similarity between the ^4He and Cl^- distributions in the aquifer.

The general increase in groundwater chlorinity in an easterly direction has been attributed to mixing of the bicarbonate-dominated fissure waters derived at recharge with a high salinity, NaCl-dominated pore water (Lawrence *et al.*, 1976). The flow rate in the fissure system has been estimated as 30 m/day (Downing and Williams, 1969), so that recharge waters from outcrop can move across the whole of the study area in about two years. This rapid movement is confirmed by the presence of tritium in the groundwaters from much of the artesian zone. Groundwater tritium contents decrease eastwards while both chlorinity and ^4He contents increase eastwards. These trends may be explained as a consequence of the progressive exchange of fissure water with the much older interstitially stored water. There is a pronounced eastwards penetration of freshwater just north of Spalding (figures 1 and 2) which is probably a consequence of the high extraction rates of the wells in this area. This eastward movement is much less marked in the south of the study area because of high groundwater extraction from wells between Bourne and Tallington, which intercept the eastward flow.

The relationship between ^4He content and chlorinity is given by:

$$[He] = 1.15 \times 10^{-8} [Cl] \quad (1)$$

where [He] is the ^4He content of the groundwater in cm^3 of He/g of water and [Cl] is the Cl^- content in mg/kg. The residence time, t (years), required for the pore water to accumulate a ^4He content, [He]t, by radioelement decay in the aquifer may be calculated from:

$$[He]t = \rho t (1.19 \times 10^{-13}[U] + 2.88 \times 10^{-14} [Th]) \quad (2)$$

where ρ is the density (g/cm^3), and [U] and [Th] are the uranium and thorium contents ($\mu g/g$) of the limestone. This equation assumes that the helium generated is uniformly distributed between the solid phase and the interstitial fluid in the aquifer. Using radioelement contents and a density typical of the limestone, the age of the groundwater in the east of the study area close to Spalding is 4 million years. It is probable, however, that this is a mixed groundwater with a relatively recent component and a much older, possibly connate, component. If the older component is connate with a chlorinity approaching that of seawater, its ^4He content may be estimated from equation 1. The corresponding age of the connate water, calculated from equation 2, is about 170 million years. Although the estimate of the groundwater ^4He content involved is a considerable extrapolation of equation 1 beyond the range in which it can be verified in the field, this age is within the stratigraphic age range of the limestone, 135 to 190 million years. It suggests that the ancient end member of the mixing sequence is truly connate, a seawater trapped during sedimentation.

The proportion of such connate water in the artesian flow within the study area never exceeds 10 percent and much of the original interstitial fluid in the limestone has evidently been replaced by freshwater in relatively recent times.

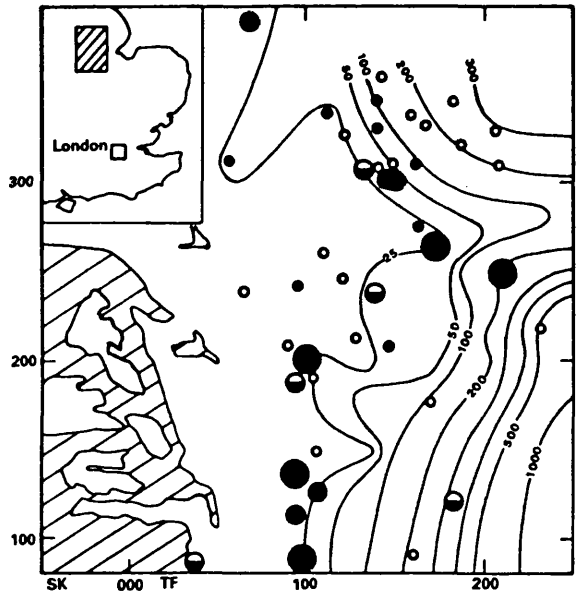

FIGURE 1. Isochlorinity lines (mg Cl^-/kg) for groundwaters in the Lincolnshire Limestone.

LEGEND

Groundwater extraction rates (m^3/day) are indicated as follows: • 500; ○ 500 - 1500; ◒ 1500 - 2500; ● 2500 - 5000 ● 5000 - 10000

The location of the study area is shown in the inset map.

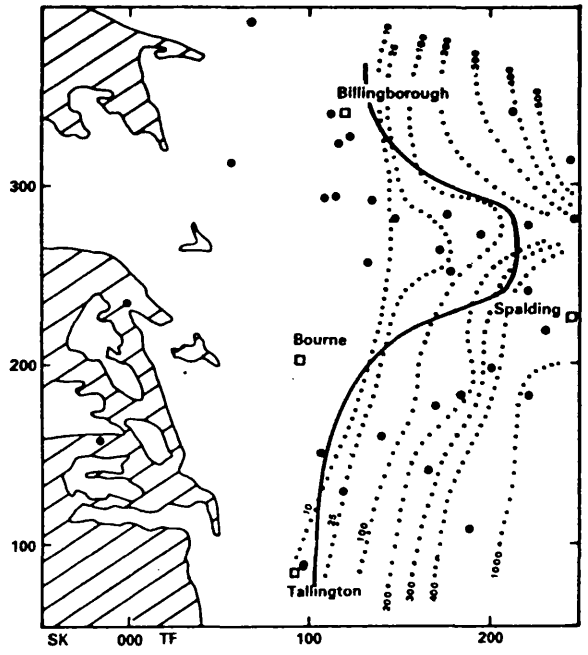

FIGURE 2. ^4He isopleths for groundwaters in the Lincolnshire Limestone. The labels are in units of 10^{-8} cm^3/g. The full line is the 7°C recharge isotherm.

The ^{14}C contents of groundwaters in the southeast of the artesian zone suggest that much of the water now being extracted was recharged in the Pleistocene (Downing *et al.*, 1977). The temperatures prevailing at recharge have been estimated from the amounts of atmospherically derived inert gases dissolved in the groundwaters and a 7°C recharge isotherm has been shown in figure 2. Groundwaters from wells to the west of this isotherm were recharged at an average temperature of 7.6°C which may be compared with the present 30-year average temperature of 7.1°C for September to April, during which most recharge occurs. East of the 7°C isotherm, estimated recharge temperatures average 6°C. Since these groundwaters contain a significant modern component (indicated by the presence of tritium), this lower recharge temperature must be a weighted average of those for the modern and older, low-temperature, component. This low-temperature component must have been recharged under climatic conditions which were significantly colder than the present. Recharge during the most recent (Devensian) glaciation may be excluded since permafrost prevailed in this part of England at that time (Shotton, 1977) but could have occurred during the preceeding Upton Warren Interstadial when temperatures were generally about 6°C lower than post-glacial temperatures (Coope, 1977). Recharge of the nearby Triassic Sandstone aquifer in Nottinghamshire took place during this interstadial at temperatures 5°C to 7°C lower than modern recharge (Andrews and Lee, 1979). The low temperature groundwater component in the Lincolnshire Limestone aquifer was therefore recharged at about 6°C lower than modern recharge, namely, at about 1.6°C. Mixing proportions estimated on the basis of these end-member recharge temperatures (postglacial at 7.6°C and preglacial at 1.6°C) indicate that postglacial recharge accounts for about 70 to 90 percent of the groundwater flow in the southeast of the study area. Significant exchange of the connate interstitial brine with freshwater has occurred during the Pleistocene.

The cooperation of the Anglian Water Authority in the sampling program and in providing analytical data on the major ion chemistry of the waters is gratefully acknowledged. We thank Dr. W.M. Edmunds for his continued interest in the work and the Natural Environment Research Council for its support by research grant GR3/2622.

References

Andrews, J.N. and Lee, D.J. (1979): Inert gases in groundwater from the Bunter Sandstone of England as indicators of age and palaeoclimatic trends; Journal of Hydrology, V. 41, pp. 233-252.

Coope, G.R. (1977): Fossil Coleopteran assemblages as sensitive indicators of climatic change during the Devensian (last) cold stage; Philosophical Transactions of the Royal Society of London, Series B, V. 280, p. 313.

Downing, R.A., Smith, D.B., Pearson, F.J., Monkhouse, R.A., and Otlet, R.L. (1977): The age of groundwater in the Lincolnshire Limestone, England, and its relevance to the flow mechanism; Journal of Hydrology, V. 33, pp. 201-216.

Downing, R.A. and Williams, B.J.P. (1969): The groundwater hydrology of the Lincolnshire Limestone; Publications of the Water Resources Board, Reading, England, 160 pages.

Lawrence, A.R., Lloyd, J.W. and Marsh, J.M. (1976): Hydrochemistry and groundwater mixing in part of the Lincolnshire Limestone aquifer, England; Groundwater, V. 14, pp. 320-327.

Shotton, F.W. (1977): The Devensian Stage; its development, limits and substages; Philosophical Transactions of the Royal Society of London, Series B, V. 280, p. 107.